

BENEATH THE UNDERGROWTH: CAUSES OF NEURAL TUBE DEFECTS AND  
MICROCEPHALY

by

STEPHANIE HERRLINGER

(Under the Direction of Jian-Fu 'Jeff' Chen)

Neurodevelopmental disorders affect one in one thousand births in the United States alone. While genetic and environmental factors drive normal development, they also have the potential to contribute to neurodevelopmental conditions such as microcephaly and neural tube defects (NTDs). This work has examined two of these factors: the RNA-binding protein Lin28, an important post-transcriptional regulator of neural progenitor cell (NPC) behaviors, and the Zika virus, an environmental cause of microcephaly. Lin28 and the Zika virus differentially impact the proliferative capacity of NPCs and the progression of brain development. I have characterized *Lin28a/b* mutant mice to determine Lin28's post-transcriptional regulatory role in NPCs. *Lin28a/b* mutants exhibit NTDs and decreased proliferative capacity. Combining a mouse model of reduced protein synthesis (*Rpl24<sup>Bst/+</sup>*) with *Lin28a/b* mutant and *Lin28aOE<sup>Tg/+</sup>* overexpression, I discovered that Lin28A/B are required to promote protein synthesis during neurulation. Polysome-RNA sequencing studies identified biological mechanisms that were differentially regulated post-transcriptionally in *Lin28a/b* mutants, and showed that Lin28 promotes NPC proliferation in part by promoting ribosome biogenesis and cell cycle. This study has illuminated the importance and complexity of post-

transcriptional regulation in neurodevelopment and suggests that regulators of translation may underlie yet undiscovered causes of NTDs.

To understand how the Zika virus may cause microcephaly in humans, I first developed a model for Zika virus-induced microcephaly in rodents using intracerebral inoculation. In addition to causing microcephaly, massive brain damage, and disrupting NPC proliferation, the Zika virus disrupts the development of the neurovasculature and results in blood brain barrier leakage into the developing parenchyma. I also asked how the Zika virus became associated with causing neurodevelopmental defects only recently, considering it was first detected in 1947. In comparison studies between a 1947 African isolate and a 2016 Mexican isolate of the virus, I found that the African isolate caused more aggressive damage to the developing mouse brain than the more recent Mexican isolate, suggesting that the Zika virus has become less virulent over time. These experiments have identified novel mechanisms for Zika virus-induced neurodevelopmental disruption and provided the field with a better understanding of its virulence and potential therapeutic targets.

**INDEX WORDS:** Neurodevelopment, post-transcriptional regulation, neural progenitor cells, neuroscience, Lin28, RNA-binding proteins, microcephaly, neural tube defects, Zika virus, neurological disorders.

BENEATH THE UNDERGROWTH: CAUSES OF NEURAL TUBE DEFECTS AND  
MICROCEPHALY

by

STEPHANIE A HERRLINGER

B.S., The University of Rochester, 2010

A Dissertation Submitted to the Graduate Faculty of The University of Georgia in Partial  
Fulfillment of the Requirements for the Degree

DOCTOR OF PHILOSOPHY

ATHENS, GEORGIA

2010

© 2018

Stephanie A Herrlinger

All Rights Reserved

BENEATH THE UNDERGROWTH: CAUSES OF NEURAL TUBE DEFECTS AND  
MICROCEPHALY

by

STEPHANIE A HERRLINGER

Major Professor: Jian-Fu Chen

Committee: James Lauderdale  
Jonathan Eggenschwiler  
Philip Holmes  
Douglas Menke

Electronic Version Approved:

Suzanne Barbour  
Dean of the Graduate School  
The University of Georgia  
December 2018

## DEDICATION

To my mom, for 30 years of constant support and encouragement

and

to all the animals whose lives were sacrificed for the advancement of science.

## ACKNOWLEDGEMENTS

These studies would not have been possible without the support and training I received from my pre-doctoral mentor Dr. Jian-Fu (Jeff) Chen. The last five years have yielded the most fruitful and interesting years of my career as a scientist so far, due in no small part to the effort and time Dr. Chen has taken in training me. In addition to my primary mentor, I have received a great deal of support from my thesis committee: Dr. Phil Holmes, Dr. Doug Menke, Dr. Jonathan Eggenschwiler, and especially Dr. Jim Lauderdale, whose constant support throughout these last five years from the earliest stages of my PhD was invaluable.

I must also recognize the support of my family and friends, in particular my mother, who has only been a phone call away every single day of this process, and for whom I would not have made it this far. The unsung heroes of my PhD work are my colleagues and fellow graduate students. In particular, Dr. Qiang (Eric) Shao, Dr. Anastasia Bobilev, Dr. Natale Sciolino, Dr. Emily Trunnell, and Ashley Rasys. These inspiring individuals helped me from everything to setting a high standard for scientific rigor, finding a place to live, and navigating the ins and outs of the UGA PhD program. Their constant support throughout my time at UGA and USC has made me a better, stronger person and inspire me every day to be a better scientist.

This work was supported in part by grant # 2T32GM007103-42 from the National Institute of General Medical Sciences, grant # 1F99NS105187-01 from the National Institute of Neurological Disorders and Stroke, the ARCS foundation, and the Mary Erlanger Graduate Fellowship for Aging Research.

## TABLE OF CONTENTS

	Page
ACKNOWLEDGEMENTS.....	v
LIST OF FIGURES.....	ix
CHAPTER	
1 INTRODUCTION AND LITERATURE REVIEW .....	1
Overview .....	1
Neurulation and Post-Transcriptional Regulation of NPCs.....	2
Microcephaly and the Zika Virus.....	10
References .....	14
2 LIN28-MEDIATED PROMOTION OF TRANSLATION IS CRITICAL FOR NEURAL PROGENITOR CELL MAINTENANCE AND BRAIN DEVELOPMENT IN MICE .....	28
Introduction .....	30
Materials and Methods .....	32
Results .....	38
Discussion .....	58
References .....	66
3 ESTABLISHING MOUSE MODELS FOR ZIKA VIRUS-INDUCED NEUROLOGICAL DISORDERS USING INTRACEREBRAL INJECTION STRATEGIES: EMBRYONIC, NEONATAL, AND ADULT .....	74
Introduction .....	76

	Protocols.....	78
	Representative Results .....	87
	Discussion .....	93
	References .....	95
4	ZIKA VIRUS INFECTION DISRUPTS NEUROVASCULAR DEVELOPMENT AND RESULTS IN POSTNATAL MICROCEPHALY WITH BRAIN DAMAGE .....	100
	Introduction .....	102
	Materials and Methods .....	104
	Results .....	110
	Discussion .....	125
	References .....	133
5	AFRICAN ZIKA VIRUS IS MORE VIRULENT AND CAUSES MORE SEVERE BRAIN DAMAGE WITH POSTNATAL DEATH COMPARED TO ASIAN LINEAGE AND DENGUE VIRUS .....	142
	Introduction.....	144
	Materials and Methods .....	146
	Results .....	151
	Discussion .....	169
	References .....	178
6	DISCUSSION and FUTURE DIRECTIONS .....	185
	The Role of Lin28 in Neurodevelopment .....	185
	Zika Virus Impact on Neurodevelopment .....	188
	Conclusions .....	192

References .....193

## LIST OF FIGURES

	Page
Figure 1.1: Neurulation in the mouse and human.....	4
Figure 2.1: Loss of <i>Lin28a/b</i> results in NTDs and embryonic lethality.....	39
Figure 2.2: <i>Lin28a/b</i> deletion results in reduced proliferation and precocious differentiation in NPCs.....	41
Figure 2.3: <i>Lin28a<sup>-/-</sup>; Rpl24<sup>Bst/+</sup></i> mutants mimic <i>Lin28a/b</i> double knockout phenotypes in neural tube defects (NTDs) and embryonic lethality.....	46
Figure 2.4: Abnormally increased brain size and ratio of apical to intermediate NPCs in <i>Lin28a</i> -overexpressing mice are rescued by <i>Rpl24<sup>Bst/+</sup></i> heterozygosity.....	48
Figure 2.5: Lin28-mediated translation regulation revealed by sucrose density gradient fractionation coupled with RNA-seq analysis.....	51
Figure 2.6: Ribosome biogenesis is defective in <i>Lin28a/b</i> mutant NPCs.....	56
Supplemental Figure: 2.S1: <i>Lin28a</i> expression and TUNEL analysis of <i>Lin28a/b</i> mutants.....	62
Supplemental Figure 2.S2: GO term analysis of dysregulated genes in mutant polysome mRNAs.....	63
Supplemental Figure 2.S3: Decreased mTORC1 signaling in <i>Lin28a/b</i> mutants.....	64
Supplemental Figure 2.S4: <i>Lin28a</i> overexpression results in macrocephaly and altered body sizes.....	65
Figure 3.1: ZIKV causes postnatal microcephaly and growth restriction.....	89
Figure 3.2: ZIKV Embryonic Inoculation at E14.5.....	90

Figure 3.3: Representative histology of P1 inoculation of ZIKV.....	91
Figure 3.4: Adult stage intraventricular injection.....	92
Figure 4.1: ZIKV causes postnatal microcephaly and growth restriction.....	111
Figure 4.2: ZIKV infection results in neuronal loss and cortical thinning.....	114
Figure 4.3: ZIKV infection leads to massive neuronal death and axonal rarefaction....	116
Figure 4.4: Abnormal vasculature and leaky BBB in ZIKV-infected brains.....	119
Figure 4.5: Extensive microglial activation and astrogliosis in ZIKV-infected brain.....	122
Figure 4.6: ZIKV induces dysregulation of genes involved in the immune response...	124
Supplemental Figure 4.S1: ZIKV infection results in microcephaly and growth restriction at P1.....	129
Supplemental Figure 4.S2: ZIKV infection does not cause microcephaly and growth restriction at E16.5.....	130
Supplemental Figure 4.S3: ZIKV infection leads to cell cycle arrest of NPCs.....	131
Supplemental Figure 4.S4: ZIKV causes minor cell death in NPCs.....	132
Figure 5.1: DENV2 causes less severe microcephaly than MEX1-44.....	152
Figure 5.2: MEX1-44 causes more neuron loss and cortical thinning than DENV2 ....	155
Figure 5.3: MEX1-44 causes more severe disruption of NPCs and neuronal death than DENV2 in the developing brain.....	158
Figure 5.4: MR-766 causes more severe brain damage and postnatal death than MEX1-44.....	162
Figure 5.5: More neuron loss in MR-766 infected brains compared with MEX1-44.....	164
Figure 5.6: MR-766 grows faster than MEX1-44 and triggers a similar immune response.....	165
Figure 5.7: MR-766 infection leads to more cell death in NPCs and neurons than	

MEX1-44.....	167
Supplemental Figure 5.S1: DENV2 is sufficient to cause growth restriction at P3.....	173
Supplemental Figure 5.S2: DENV2 infection has minimal impact on NPC proliferation.....	174
Supplemental Figure 5.S3: DENV2 infection leads to increased cell death in neurons and NPCs.....	175
Supplemental Figure 5.S4: MEX1-44, but not DENV2, infection causes NPC cell cycle arrest.....	176
Supplemental Figure 5.S5: DENV2 infects NPCs and is detected in the cortical plate.....	177

# CHAPTER 1

## INTRODUCTION AND LITERATURE REVIEW

“What is perhaps the most intriguing question of all is whether the brain is powerful enough to solve the problem of its own creation.” – Gregor Eichele.

### **1.1. Overview**

Brain development is a complicated and finely-tuned process that is highly vulnerable to disruption and disease. As early neural tissue transitions from a uniform neuroepithelium to a dynamic and heterogeneous cell population of neurons and glia, many regulatory steps must to be taken unperturbed so the brain can develop normally. The earliest disturbances in this process can result in the most devastating consequences of their kind, including neural tube defects (NTDs) where there the neural tube fails to close completely during development and microcephaly which results in a smaller than average head size and life-long disability. NTDs remain the 2<sup>nd</sup> most common birth defect, occurring in 1 in 2000 births annually in the United States, with higher rates in less developed areas (Milunsky, Jick, SS, & al, 1989; Wallingford, Niswander, Shaw, & Finnell, 2013). Similarly, 8 in 10,000 births are affected with microcephaly in the United States alone (Cragan et al., 2016). Both NTDs and microcephaly are multifactorial conditions, with both genetic and environmental factors that frequently contribute in an additive fashion (Harris & Juriloff, 2007; Von der Hagen et al., 2014; C. Geoffrey Woods, Bond, & Enard, 2005). While a large genetic

component is attributed to causing NTDs, few genes implicated in mouse models have been linked to human disease (Rampersaud, Melvin, & Speer, 2006). Many of those identified are transcriptional and epigenetic regulators, while the regulation of protein synthesis has been largely overlooked (Harris & Juriloff, 2007; Wilde, Petersen, & Niswander, 2014). Although the neurodevelopment field has described many of the causative agents behind these conditions, many questions still remain unanswered and new causal agents continue to arise, notably the Zika virus (Cragan et al., 2017; Heymann et al., 2016; Wallingford et al., 2013). It is unclear how and why the Zika virus causes microcephaly, and why it has only recently been associated with neurodevelopmental disorders.

In an effort to provide insight into these conditions and lead the field toward stronger therapeutic outcomes for the treatment and prevention of NTDs and microcephaly, the aims of this dissertation are thus: to 1) examine a post-transcriptional regulator required for neural tube closure and NPC proliferation, the RNA-binding protein Lin28 and 2) investigate the recently infamous agent of neurodevelopmental disruption, the Zika virus, and its capacity to cause microcephaly.

## **1.2. Neurulation and the Post-Transcriptional regulation of NPCs**

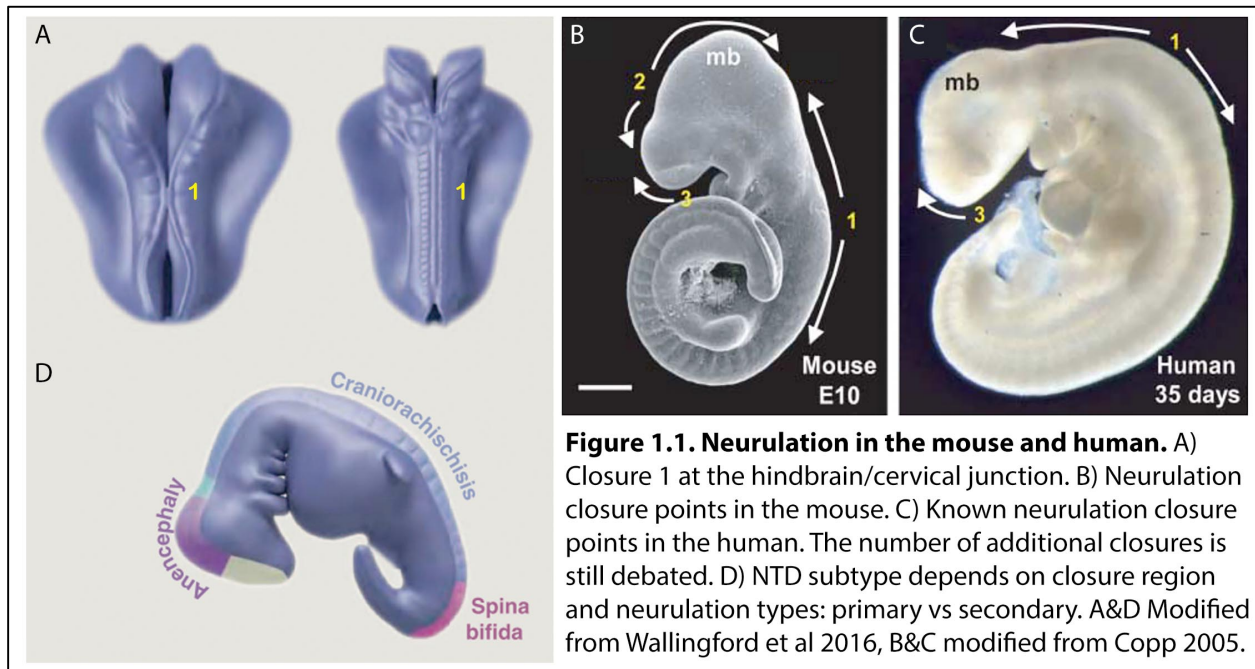
### *1.2.1 Neural Induction (in brief)*

Brain development begins when neural tissue is derived in the early embryo from the ectodermal germ layer (Spemann & Mangold, 1924). The ectoderm gives rise to the epidermis, neural crest, and neural plate. Neural tissue of the central nervous system is completely derived from the neural plate and is differentiated from presumptive

epidermis and neural crest in large part by the level of bone morphogenetic proteins (BMPs) signaling that they receive: high BMPs in the epidermis, mid-levels in the neural crest, and very low levels in the neural plate (Muñoz-Sanjuán & Brivanlou, 2002). These low levels in the neural plate are due in part to the antagonistic effects of follistatin and noggin, signaling molecules secreted from the Spemann organizer, by binding to and inactivating BMPs (Hemmati-Brivanlou, Kelly, & Melton, 1994; Lamb et al., 2014). Pro-neural properties of sonic hedgehog signaling generate ventral neural tube cell types, secreted by both the notochord and floor plate (Cohen, Briscoe, & Blassberg, 2013). The cells of the neural plate are characterized as neural precursors as they express the Sox transcription factors (Sox1, Sox2, Sox3), which in turn prevent BMP signaling and reinforce pro-neural cell fate (Archer, Jin, & Casey, 2011).

### *1.2.2 Neurulation*

Neurulation is the process by which the lateral edges of the neural plate thicken (becoming the neural folds) and fold into one another to fuse dorsally, forming the neural tube. While largely conserved amongst mammals, there exist several distinct mechanisms of neurulation within and between species (Harrington, Hong, & Brewster, 2009). In mice, primary neurulation progresses in discontinuous stages with the neural plate fusing at three separate locations along the anterior-posterior axis of the embryo and subsequently 'zippering' the remaining unfused neural tube closed (Fig. 1.1) (Greene & Copp, 2014; Wallingford et al., 2013). The first closure point (Closure 1) meets at the hindbrain/cervical boundary at embryonic day (E) 8.5 (Fig. 1.1A). Brain formation continues thereafter with two additional closure points, one at the most anterior point of the brain/body axis (Closure 2) and another at the midbrain/hindbrain



boundary (Closure 3) (Fig. 1.1B) (Copp, 2005). Neurulation success requires these closure points to be met in this order for the entirety of the neural tube to close normally (Massarwa & Niswander, 2013). In humans, discontinuous closure points 1 and 3 are conserved but there still remains uncertainty in the field about the existence and locations of additional closure points, with some suggesting that there are upwards of five (Fig. 1.1C) (Bassuk & Kibar, 2009; Copp, 2005; Greene & Copp, 2014). Failure to initiate closure 1 results in Craniorachischisis, where the entire body axis remains open and is typically lethal, albeit rare (Fig. 1.1D); if closure 1 initiation succeeds but fails to ultimately close posteriorly, it results in spina bifida (myelomeningocele) (Fig. 1.1D). A failure of closures 2 and/or 3 in the mouse results in anencephaly, or an open fore/mid/hindbrain, depending on which closure fails (Copp, 2005). A separate

mechanism in the mouse and human to form the most posterior portion of the neural tube is termed secondary neurulation. This form occurs below the sacral level of the tail where an aggregation of mesenchyme coalesces and hollows beneath the surface epidermis as the tail continues to grow (Schoenwolf, 2018). Disruptions in secondary neurulation usually result in closed-skin defects and involve tethering of the spinal cord (Lew & Kothbauer, 2007). Neurulation is accomplished at roughly 3-4 weeks gestation in humans, and E8.5-E9.0 in the mouse (Copp, 2005).

### *1.2.3 Genetic and Environmental Contributors of NTDs*

One of the largest advancements to preventing neural tube defects has been the discovery of the benefits of folic acid supplementation in pregnant women. Antagonists of folic acid (Thiersch, 1952; Warkany, Beaudry, & Hornstein, 1959) and mutations in folic acid metabolism (Molloy, Brody, Mills, Scott, & Kirke, 2009; Shaw et al., 2009) have been implicated in causing NTDs. Folic acid enrichment in pregnant women's diet has been shown to exhibit reduced risk of NTDs in unborn children (Blom, Shaw, den Heijer, & Finnell, 2006; Običan, Finnell, Mills, Shaw, & Scialli, 2010). While folic acid treatment has prevented an estimated 50-75% of NTDs, 1 in 2000 births still result in NTDs in the United States alone suggesting that there are other factors not yet addressed or understood (Blom et al., 2006; Wallingford et al., 2013).

While over 200 genes have been implicated in causing NTDs in mouse models, very few have been linked with causing NTDs in humans (Copp & Greene, 2009). Many of these identified factors are transcriptional and epigenetic regulators, and many exhibit important functions not limited to neural tube development (Harris & Juriloff, 2007). Despite this, it is still believed that there are undiscovered genetic components in NTDs

in humans as evidenced by a 2-5% recurrence risk in siblings, equating to a 50-fold increase from the general population (Rampersaud et al., 2006). This suggests that there are still genetic factors yet not discovered, perhaps associated with largely unexplored biological mechanisms. Disruptions along the process from neural precursor cell fate determination and the last steps of neural tube closure can result in neural tube defects (Greene & Copp, 2014; Wallingford et al., 2013). Studying how these perturbations affect brain development with animal models allow us to better understand the biological processes driving this growth and attempt to prevent and alleviate the burden these disorders cause in affected individuals.

#### *1.2.4 Mechanisms of NTDs: Neural Progenitor Cell Proliferation Disruption*

The neuroepithelial cells of the neural plate divide rapidly and symmetrically prior to neural tube closure, thereafter transitioning into radial glia that will generate both progenitor and post-mitotic daughters that ultimately generate the neurons, astrocytes, and oligodendrocytes of the mature brain (Doe, 2008; Kriegstein & Alvarez-Buylla, 2009). The proliferative capacity required of these progenitors is distinct at different time points in development; for example, proliferation rate has been described with doubling times of 2-7 hours in E5.5-6.5 in mice, and cell doubling time is estimated to be ~10 hours between E8.8 to E11 (Burns & Hassan, 2001). As such, antimitotic agents (Copp, Brook, Peter Estibeiro, Shum, & Cockroft, 1990) and mutations in genes associated with cell cycle progression have been found to cause NTDs in mice (Harris & Juriloff, 2007).

### *1.2.5 RNA-Binding Proteins (RBPs) and Post-Transcriptional Regulation of Brain Development*

Much is known about the transcriptional mechanisms that drive neural tube development, with many transcription factors identified that are required for NPC fate and neural tube specification (Cohen et al., 2013; Englund et al., 2005); conversely, very little is known about genetic regulation at the translational level. Long thought to be a house-keeping process, translation is now known to provide an additional site of tissue-specific regulation in the developing embryo (Kondrashov et al., 2011; Kraushar et al., 2014; Kraushar, Popovitchenko, Volk, & Rasin, 2016; Truitt et al., 2015; S Xue & Barna, 2012; Shifeng Xue et al., 2015). The RBP Hu antigen R (HuR) plays a critical post-transcriptional role in neocortical development by specifying ribosome composition temporally and its functionally related mRNA translation (Kraushar et al., 2014). The dysregulation of protein synthesis is a candidate source of neurological disorder susceptibility or onset. Ribosomopathys have been implicated in the etiology of microcephaly (Brooks et al., 2014) and mutations in genes encoding ribosomal proteins have been associated with NTDs (Wallingford et al., 2013; Wilde et al., 2014). Understanding how translation uniquely contributes to gene expression in NPCs will elucidate new mechanisms and potential therapeutic targets of neurodevelopment and disease.

### *1.2.6 The Post-Transcriptional Regulator Lin28*

The RNA-binding protein Lin28 is a known heterochronic timing regulator discovered as part of a microRNA-mediated pathway that determines the progression of larval stages in the nematode *Caenorhabditis elegans*, specifically important for

developmental timing events in stem cells (Ambros & Moss, 1994; Moss, Lee, & Ambros, 1997). Lin28 is expressed in the cytoplasm of neural progenitor cells in mice and as development progresses this expression decreases and is depleted by birth (D.-H. Yang & Moss, 2003; M. Yang et al., 2015). It uniquely contains two types of RNA-binding domains, a cold shock domain and two zinc-finger domains (Moss & Tang, 2003); the latter are known to target terminal loop GGAG sequences in pre-let-7 miRNA, preventing their maturation at multiple steps (Heo et al., 2009). Lin28 suppression of the miRNA let-7, a known driver of differentiation (Shinoda et al., 2013), is well characterized. As development progresses, let-7 becomes increasingly upregulated, and reciprocally targets the Lin28 transcript, downregulating Lin28 expression and reducing Lin28-mediated inhibition of let-7 maturation (Thornton & Gregory, 2012). However, other work studying Lin28 function suggests that it confers let-7-independent global changes post-transcriptionally.

While the Lin28/let-7 relationship is understood to play a role in developmental timing regulation, there are many studies that implicate let-7-independent functional mechanisms of Lin28 at the post-transcriptional level (Balzer, Heine, Jiang, Lee, & Moss, 2010; Wilbert et al., 2012; M. Yang et al., 2015). The same GGAGA sequence targeted by Lin28 in pre-let-7 is also targeted in the regulation of splicing factors for thousands of mRNA transcripts (Wilbert et al., 2012). Lin28 mediates tissue fate specification in early *Xenopus laevis* development and is critical for neural to glial differentiation switching, despite there being no observable changes in let-7 expression when Lin28 expression is ablated (Balzer et al., 2010; Faas et al., 2013). Work from our previous study identified a relationship between Lin28A and mTOR activity, as read

from mTOR activity-dependent changes in pS6 labeling in the developing ventricular zone, and by directly regulating mTOR pathway-related transcripts without observing altering let-7 expression levels in Lin28A mutants (M. Yang et al., 2015). While Lin28 has been shown to suppress ER-associated translation in stem cells (Cho et al., 2012), it has alternatively been found to be required for and promotes translational efficiency in skeletal myogenesis (Poleskaya et al., 2007). This demonstrates that not only does Lin28 play important let-7 independent roles, but that these functions may differ in a tissue specific manner. This discrepancy of its function in the literature, its spatiotemporal expression in NPCs in neurodevelopment, and its functions as a master translational regulator make Lin28 an excellent candidate to study post-transcriptional regulation within the developing nervous system.

In **Chapter 2**, I focus on the RNA-binding protein Lin28 to further elucidate how translational regulators contribute to NPC behaviors and brain development. There are two homologs of Lin28 (Lin28A and Lin28B) in mammals that contain the same RNA-binding domains (Guo et al., 2006) and exhibit 76% homology overall (M. Yang et al., 2015). In our previous work, we found that loss of Lin28A alone results in microcephaly in mice; however, compound mutants of *Lin28a/b* exhibited further exacerbation of the smaller head size phenotype, suggesting that Lin28A/B exhibit functional redundancy (M. Yang et al., 2015). In my studies I eliminated this redundancy to uncover novel roles of Lin28 in NPCs not yet described (**Chapter 2**).

As we are not able to study NTDs in the developing human, the field establishes model organisms to more specifically probe them, namely in the mouse (Harris & Juriloff, 2007). To this end, I utilized mouse mutant models of *Lin28a/b*.

## **1.3 Microcephaly and the Zika virus**

### *1.3.1 Microcephaly*

A child is diagnosed with microcephaly when they present with a head circumference two standard deviations below the mean (C. Geoffrey Woods, 2004; C. Geoffrey Woods et al., 2005; C G Woods & Basto, 2014) measured from above the brow to the back of the head. Children with microcephaly exhibit a range of symptoms including developmental delay, seizure, intellectual disability, hearing loss, vision problems, and problems with movement and balance, among others, depending on the severity of the disease (Dreher et al., 2014; Lanzieri et al., 2017; Naseer et al., 2017). Roughly half of microcephaly cases are attributed to genetic causes, with the other half to either perinatal or postnatal damage from their environment (Abuelo, 2007; Rita W. Driggers et al., 2016; Miki, Fukui, Takeuchi, & Itoh, 1995; Mlakar et al., 2016; Nicholas et al., 2010; Von der Hagen et al., 2014; C. Geoffrey Woods, 2004; C G Woods & Basto, 2014).

As microcephaly is simply diagnosed by head size (used as a proxy for brain volume) it follows that different types of brain damage or growth malformations result in a similar diagnosis. Primary microcephaly (MCPH, short for microcephaly primary hereditary), also known as autosomal recessive primary microcephaly, is a particular subtype of microcephaly wherein the overall brain organization is maintained without additional damage and typically results from consanguineous marriages (C G Woods & Basto, 2014). Despite its rarity (1.3 to 150 per 100,000 (Kaindl et al., 2010)) 17 genes have been identified to cause MCPH and the most commonly identified have been abnormal spindle-like microcephaly associated (ASPM), which accounts for roughly half

of known MCPH cases and WDR62, which accounts for 10% (Hussain et al., 2013). Mouse genetic studies for ASPM mutants have shown that ASPM is a centrosomal protein localized to the mitotic spindle required for mitotic progression and loss of its function can cause microcephaly in mice (Bond et al., 2002; Pulvers et al., 2010; Zhong, Liu, Zhao, Pfeifer, & Xu, 2005). Likewise, WDR62 is a centrosome protein, and without its function NPCs exhibit significant cell cycle delay and increased apoptosis during brain development, resulting in microcephaly (Chen et al., 2014; Nicholas et al., 2010; Xu, Zhang, Wang, Sun, & Xu, 2014). While these are rare mutations, the lessons we have learned from examining MCPH related genes has illuminated the vulnerability of NPCs, in particular how detrimental the disruption of their proliferative capacity can result in microcephaly and other neurodevelopmental disorders.

### *1.3.2 Zika Virus-induced Microcephaly*

Prior to the Zika virus outbreak in 2015, 8 children in 10,000 births were typically affected with microcephaly in the United States according to the CDC (Cragan et al., 2016). On February 1st of 2016 the World Health Organization declared the Zika Virus a Public Health Emergency of International Concern (PHEIC) due to the alarming increase in cases of microcephaly and Guillain-Barre syndrome found after its known emergence and spread in Latin America in early 2015 (Heymann et al., 2016). Clinical studies examining fetal tissue exposed to the Zika virus during gestation exhibited microcephaly, and affected fetal brain tissue tested positive for the Zika virus (Rita W. Driggers et al., 2016; Mlakar et al., 2016). Therefore, there was an obvious need for the field to identify whether and how the Zika virus directly causes neurodevelopmental defects.

To establish if the Zika virus could cause microcephaly, we developed a mouse model of intracerebral inoculation of the Zika virus at embryonic day (E) 14.5 (**Chapter 3**). This method allowed us to circumvent the typical route of infection and directly ask if and what kind of damage the Zika virus causes during brain development. Our work and others suggest that not only does the Zika virus cause microcephaly and disrupts NPCs (Dang et al., 2016; R.W. Driggers et al., 2017; C. Li et al., 2016; H. Li et al., 2016) (**Chapter 2, Chapter 3**), it disrupts neurovascular development and ultimately causes blood brain barrier leakage (Shao et al., 2016).

### *1.3.3 Distinct associated neurological pathology from two distinct Zika virus lineages and other Flaviviridae family members*

Despite its recent claim to fame, the Zika virus has been around for quite some time. First isolated in Uganda in an infected Rhesus Monkey in 1947 in the Zika forest, the Zika virus has likely had widespread infection of human populations throughout Africa and Asia, and was associated with few symptoms including a mild fever, conjunctivitis, and rash (Dick & Kitchen, 1952; Haddock et al., 2012). In contrast, the Zika virus is currently associated with causing neurological disorders including Guillain-Barres syndrome and microcephaly due to recent outbreaks in French Polynesia in 2008 and in Brazil in 2015 (Cragan et al., 2017; Jaenisch, Rosenberger, Brito, & Brady, 2017; Mlakar et al., 2016; Ramos da Silva & Gao, 2016). The association between neurological disorders and the Zika virus has so far only been associated with the Asian lineage of the Zika virus (Haddock et al., 2012; Heymann et al., 2016). To directly examine the virulence and damage capacity of each lineage, we compared two isolates of the Zika virus from each lineage in side-by-side intracerebral inoculation studies in

**Chapter 5.** We surprisingly found that despite the African lineage never previously being associated with causing birth defects, the African lineage isolate (MR-766) exhibited more aggressive virulence and damage than the Asian lineage isolate (MEX1-44) in mice, ultimately resulting in embryonic lethality of E14.5 infected embryos (Shao et al., 2017).

The Zika virus is a member of the Spondweni serocomplex within the genus *Flavivirus*, family *Flaviviridae* (Fauquet, Mayo, Maniloff, Desselberger, & Ball, 2005). Despite being closely related, other members of the *Flaviviridae* family that co-circulate with the Zika virus in affected areas such as the Dengue virus are frequently co-morbid but have not yet been associated with causing microcephaly (Dupont-Rouzeyrol et al., 2015; Villamil-Gómez et al., 2016). Because of this co-morbidity, it is not clear whether other flaviviruses alone can contribute to causing microcephaly. We asked this question by performing side-by-side comparison studies with the Dengue virus (serotype 2, DENV2) and the Zika virus in our rodent model using intracerebral embryonic brain inoculation (**Chapter 5**) (Shao et al., 2017). In these studies, we show that the Dengue virus is indeed capable of infecting NPCs and gliosis, but only causes a mild reduction in cortical thickness, and pups survive postnatally.

## 1.4 References

- Abuelo, D. (2007). Microcephaly Syndromes. *Seminars in Pediatric Neurology*, 14(3), 118–127. <http://doi.org/10.1016/j.spen.2007.07.003>
- Ambros, V., & Moss, E. G. (1994). Heterochronic genes and the temporal control of *C. elegans* development. *Trends in Genetics : TIG*, 10(4), 123–7. [http://doi.org/10.1016/0168-9525\(94\)90213-5](http://doi.org/10.1016/0168-9525(94)90213-5)
- Archer, T. C., Jin, J., & Casey, E. S. (2011). Interaction of Sox1, Sox2, Sox3 and Oct4 during primary neurogenesis. *Developmental Biology*. <http://doi.org/10.1016/j.ydbio.2010.12.013>
- Balzer, E., Heine, C., Jiang, Q., Lee, V. M., & Moss, E. G. (2010). LIN28 alters cell fate succession and acts independently of the let-7 microRNA during neurogliogenesis in vitro. *Development*, 137(6), 891–900. <http://doi.org/10.1242/dev.042895>
- Bassuk, A. G., & Kibar, Z. (2009). Genetic Basis of Neural Tube Defects. *Seminars in Pediatric Neurology*, 16(3), 101–110. <http://doi.org/https://doi.org/10.1016/j.spen.2009.06.001>
- Blom, H. J., Shaw, G. M., den Heijer, M., & Finnell, R. H. (2006). Neural tube defects and folate: case far from closed. *Nature Reviews Neuroscience*, 7, 724. Retrieved from <http://dx.doi.org/10.1038/nrn1986>
- Bond, J., Roberts, E., Mochida, G. H., Hampshire, D. J., Scott, S., Askham, J. M., ... Geoffrey Woods, C. (2002). ASPM is a major determinant of cerebral cortical size. *Nature Genetics*, 32(2), 316–320. <http://doi.org/10.1038/ng995>

- Brooks, S. S., Wall, A. L., Golzio, C., Reid, D. W., Kondyles, A., Willer, J. R., ... Davis, E. E. (2014). A Novel Ribosomopathy Caused by Dysfunction of X-Linked Microcephaly in Humans, *198*(October), 723–733.  
<http://doi.org/10.1534/genetics.114.168211>
- Burns, J. L., & Hassan, A. B. (2001). Cell survival and proliferation are modified by insulin-like growth factor 2 between days 9 and 10 of mouse gestation. *Development (Cambridge, England)*, *128*(19), 3819–3830.
- Chen, J.-F., Zhang, Y., Wilde, J., Hansen, K. C., Lai, F., & Niswander, L. (2014). Microcephaly disease gene *Wdr62* regulates mitotic progression of embryonic neural stem cells and brain size. *Nat Commun*, *5*.  
<http://doi.org/10.1038/ncomms4885>
- Cho, J., Chang, H., Kwon, S. C., Kim, B., Kim, Y., Choe, J., ... Kim, V. N. (2012). LIN28A is a suppressor of ER-associated translation in embryonic stem cells. *Cell*, *151*(4), 765–77. <http://doi.org/10.1016/j.cell.2012.10.019>
- Cohen, M., Briscoe, J., & Blassberg, R. (2013). Morphogen Interpretation: The Transcriptional Logic Of Neural Tube Patterning. *Current Opinion in Genetics and Development*, *23*(4), 423–428. <http://doi.org/10.1016/j.gde.2013.04.003>
- Copp, A. J. (2005). Neurulation in the cranial region--normal and abnormal. *Journal of Anatomy*, *207*(5), 623–635. <http://doi.org/10.1111/j.1469-7580.2005.00476.x>
- Copp, A. J., Brook, F. A., Peter Estibeiro, J., Shum, A. S. W., & Cockroft, D. L. (1990). The embryonic development of mammalian neural tube defects. *Progress in Neurobiology*, *35*(5), 363–403. <http://doi.org/https://doi.org/10.1016/0301->

0082(90)90037-H

Copp, A. J., & Greene, N. DE. (2009). Genetics and development of neural tube defects. *The Journal of Pathology*, 220(November), 217–230.

<http://doi.org/10.1002/path>

Cragan, J. D., Isenburg, J. L., Parker, S. E., Alverson, C. J., Meyer, R. E., Stallings, E. B., ... Mai, C. T. (2016). Population-based microcephaly surveillance in the United States, 2009 to 2013: An analysis of potential sources of variation. *Birth Defects Research. Part A, Clinical And Molecular Teratology*, 106(11), 972–982.

<http://doi.org/10.1002/bdra.23587>

Cragan, J. D., Mai, C. T., Petersen, E. E., Liberman, R. F., Forestieri, N. E., Stevens, A. C., ... Honein, M. A. (2017). Baseline Prevalence of Birth Defects Associated with Congenital Zika Virus. *Morbidity and Mortality Weekly Report*, 66(8), 219–220.

<http://doi.org/10.15585/mmwr.mm6608a4>

Dang, J., Tiwari, S. K., Lichinchi, G., Qin, Y., Patil, V. S., Eroshkin, A. M., & Rana, T. M.

(2016). Zika Virus Depletes Neural Progenitors in Human Cerebral Organoids through Activation of the Innate Immune Receptor TLR3. *Cell Stem Cell*, 19(2),

258–265. <http://doi.org/10.1016/j.stem.2016.04.014>

Dick, G. W. A., & Kitchen, S. F. (1952). ZIKA VIRUS (I). ISOLATIONS AND SEROLOGICAL SPECIFICITY. *TRANSACTIONS OF THE ROYAL SOCIETY OF TROPICAL MEDICINE AND HYGIENE*, 46(5), 509–520.

Doe, C. Q. (2008). Neural stem cells: balancing self-renewal with differentiation.

*Development*, 135(9), 1575 LP-1587. Retrieved from

<http://dev.biologists.org/content/135/9/1575.abstract>

Dreher, A. M., Arora, N., Fowler, K. B., Novak, Z., Britt, W. J., Boppana, S. B., & Ross, S. A. (2014). Spectrum of Disease and Outcome in Children with Symptomatic Congenital Cytomegalovirus Infection. *Journal of Pediatrics*. Retrieved from <http://proxy-remote.galib.uga.edu/login?url=http://search.ebscohost.com/login.aspx?direct=true&db=edswsc&AN=000333258900038&site=eds-live>

Driggers, R. W., Ho, C.-Y., Korhonen, E. M., Kuivanen, S., Jääskeläinen, A. J., Smura, T., ... Vapalahti, O. (2016). Zika Virus Infection with Prolonged Maternal Viremia and Fetal Brain Abnormalities. *The New England Journal of Medicine*, NEJMoa1601824. <http://doi.org/10.1056/NEJMoa1601824>

Driggers, R. W., Ho, C.-Y., Korhonen, E. M., Kuivanen, S., Jääskeläinen, A. J., Smura, T., ... Vapalahti, O. (2017). Zika Virus Infection With Prolonged Maternal Viremia and Fetal Brain Abnormalities. *Obstetric Anesthesia Digest*. <http://doi.org/10.1097/01.aoa.0000512046.09676.84>

Dupont-Rouzeyrol, M., O'Connor, O., Calvez, E., Daures, M., John, M., Grangeon, J.-P., & Gourinat, A.-C. (2015). Co-infection with Zika and dengue viruses in 2 patients, New Caledonia, 2014.(LETTERS)(Report)(Letter to the editor). *Emerging Infectious Diseases*, 21(2), 381. <http://doi.org/10.3201/eid2102.141553>

Englund, C., Fink, A., Lau, C., Pham, D., Daza, R. a M., Bulfone, A., ... Hevner, R. F. (2005). Pax6, Tbr2, and Tbr1 are expressed sequentially by radial glia, intermediate progenitor cells, and postmitotic neurons in developing neocortex. *The*

*Journal of Neuroscience : The Official Journal of the Society for Neuroscience*,  
25(1), 247–51. <http://doi.org/10.1523/JNEUROSCI.2899-04.2005>

Faas, L., Warrander, F. C., Maguire, R., Ramsbottom, S. a, Quinn, D., Genever, P., & Isaacs, H. V. (2013). Lin28 proteins are required for germ layer specification in *Xenopus*. *Development (Cambridge, England)*, 140, 976–86.  
<http://doi.org/10.1242/dev.089797>

Fauquet, C. M., Mayo, M. A., Maniloff, J., Desselberger, U., & Ball, L. A. B. T.-V. T. (Eds.). (2005). *The Positive Sense Single Stranded RNA Viruses* (pp. 739–1128). San Diego: Academic Press. <http://doi.org/https://doi.org/10.1016/B978-0-12-249951-7.50015-8>

Greene, N. D. E., & Copp, A. J. (2014). Neural Tube Defects. *Annual Review of Neuroscience*, 37(1), 221–242. <http://doi.org/10.1146/annurev-neuro-062012-170354>

Guo, Y., Chen, Y., Ito, H., Watanabe, A., Ge, X., Kodama, T., & Aburatani, H. (2006). Identification and characterization of lin-28 homolog B (LIN28B) in human hepatocellular carcinoma. *Gene*, 384, 51–61.  
<http://doi.org/https://doi.org/10.1016/j.gene.2006.07.011>

Haddow, A. D., Schuh, A. J., Yasuda, C. Y., Kasper, M. R., Heang, V., Huy, R., ... Weaver, S. C. (2012). Genetic characterization of zika virus strains: Geographic expansion of the asian lineage. *PLoS Neglected Tropical Diseases*, 6(2).  
<http://doi.org/10.1371/journal.pntd.0001477>

Harrington, M. J., Hong, E., & Brewster, R. (2009). Comparative analysis of neurulation:

First impressions do not count. *Molecular Reproduction and Development*, 76(10), 954–965. <http://doi.org/10.1002/mrd.21085>

Harris, M. J., & Juriloff, D. M. (2007). Mouse mutants with neural tube closure defects and their role in understanding human neural tube defects. *Birth Defects Research Part A - Clinical and Molecular Teratology*, 79(3), 187–210. <http://doi.org/10.1002/bdra.20333>

Hemmati-Brivanlou, A., Kelly, O. G., & Melton, D. A. (1994). Follistatin, an antagonist of activin, is expressed in the Spemann organizer and displays direct neuralizing activity. *Cell*, 77(2), 283–295. [http://doi.org/https://doi.org/10.1016/0092-8674\(94\)90320-4](http://doi.org/https://doi.org/10.1016/0092-8674(94)90320-4)

Heo, I., Joo, C., Kim, Y.-K., Ha, M., Yoon, M.-J., Cho, J., ... Kim, V. N. (2009). TUT4 in Concert with Lin28 Suppresses MicroRNA Biogenesis through Pre-MicroRNA Uridylation. *Cell*, 138(4), 696–708. <http://doi.org/10.1016/j.cell.2009.08.002>

Heymann, D. L., Hodgson, A., Sall, A. A., Freedman, D. O., Staples, J. E., Althabe, F., ... Menon, K. U. (2016). Zika virus and microcephaly: Why is this situation a PHEIC? *The Lancet*, 387(10020), 719–721. [http://doi.org/10.1016/S0140-6736\(16\)00320-2](http://doi.org/10.1016/S0140-6736(16)00320-2)

Hussain, S., Bakhtiar, M., Farooq, M., Anjum, I., Janzen, E., Toliat, R., ... Hansen, L. (2013). Genetic heterogeneity in Pakistani microcephaly families. *Clinical Genetics*, 83(1), 446–451. <http://doi.org/10.1111/cge.12955>

Jaenisch, T., Rosenberger, D., Brito, C., & Brady, O. (2017). Risk of microcephaly after Zika virus infection in Brazil , 2015 to 2016, 95(3), 191–198.

- Kaindl, A. M., Passemard, S., Kumar, P., Kraemer, N., Issa, L., Zwirner, A., ... Gressens, P. (2010). Many roads lead to primary autosomal recessive microcephaly. *Progress in Neurobiology*, *90*(3), 363–383.  
<http://doi.org/10.1016/j.pneurobio.2009.11.002>
- Kondrashov, N., Pusic, A., Stumpf, C. R., Shimizu, K., Hsieh, A. C., Xue, S., ... Barna, M. (2011). Ribosome-mediated specificity in Hox mRNA translation and vertebrate tissue patterning. *Cell*, *145*(3), 383–397. <http://doi.org/10.1016/j.cell.2011.03.028>
- Kraushar, M. L., Popovitchenko, T., Volk, N. L., & Rasin, M.-R. (2016). The frontier of RNA metamorphosis and ribosome signature in neocortical development. *International Journal of Developmental Neuroscience*, *55*, 131–139.  
<http://doi.org/https://doi.org/10.1016/j.ijdevneu.2016.02.003>
- Kraushar, M. L., Thompson, K., Wijeratne, H. R. S., Viljetic, B., Sakers, K., Marson, J. W., ... Rasin, M.-R. (2014). Temporally defined neocortical translation and polysome assembly are determined by the RNA-binding protein Hu antigen R. *Proceedings of the National Academy of Sciences of the United States of America*, *111*(36), E3815-24. <http://doi.org/10.1073/pnas.1408305111>
- Kriegstein, A., & Alvarez-Buylla, A. (2009). The Glial Nature of Embryonic and Adult Neural Stem Cells. *Annual Review of Neuroscience*, *32*(1), 149–184.  
<http://doi.org/10.1146/annurev.neuro.051508.135600>
- Lamb, T. M., Knecht, A. K., Smith, W. C., Stachel, S. E., Aris, N., Stahl, N., ... Economides, A. N. (2014). Neural Secreted by the Induction Polypeptide Noggin, *262*(5134), 713–718.

- Lanzieri, T. M., Leung, J., Caviness, A. C., Chung, W., Flores, M., Blum, P., ...  
Demmler-Harrison, G. (2017). Long-term outcomes of children with symptomatic congenital cytomegalovirus disease. *Journal of Perinatology: Official Journal Of The California Perinatal Association*. <http://doi.org/10.1038/jp.2017.41>
- Lew, S. M., & Kothbauer, K. F. (2007). Tethered Cord Syndrome: An Updated Review. *Pediatric Neurosurgery*, 43(3), 236–248. <http://doi.org/10.1159/000098836>
- Li, C., Xu, D., Ye, Q., Hong, S., Jiang, Y., Liu, X., ... Xu, Z. (2016). Zika Virus Disrupts Neural Progenitor Development and Leads to Microcephaly in Mice. *Cell Stem Cell*, 19(5), 672. <http://doi.org/10.1016/j.stem.2016.10.017>
- Li, H., Saucedo-Cuevas, L., Regla-Nava, J. A., Chai, G., Sheets, N., Tang, W., ... Gleeson, J. G. (2016). Zika Virus Infects Neural Progenitors in the Adult Mouse Brain and Alters Proliferation. *Cell Stem Cell* (Vol. 19). Retrieved from <http://www.sciencedirect.com/science/article/pii/S1934590916302521>
- Massarwa, R., & Niswander, L. (2013). In toto live imaging of mouse morphogenesis and new insights into neural tube closure. *Development (Cambridge, England)*, 140(1), 226–36. <http://doi.org/10.1242/dev.085001>
- Miki, T., Fukui, Y., Takeuchi, Y., & Itoh, M. (1995). A quantitative study of the effects of prenatal X-irradiation on the development of cerebral cortex in rats. *Neuroscience Research*, 23, 241–247.
- Milunsky, A., Jick, H., SS, J., & al, et. (1989). Multivitamin/folic acid supplementation in early pregnancy reduces the prevalence of neural tube defects. *JAMA*, 262(20), 2847–2852. Retrieved from <http://dx.doi.org/10.1001/jama.1989.03430200091032>

- Mlakar, J. . J., Korva, M. M. . M., Tul, N. N. . N., Popović, M. M. ., Poljšak-Prijatelj, M. M. ., Mraz, J. J. . J., ... Avšič Županc, T. (2016). Zika Virus Associated with Microcephaly. *New England Journal of Medicine*, 374(10), 951–958. <http://doi.org/10.1056/NEJMoa1600651>
- Molloy, A. M., Brody, L. C., Mills, J. L., Scott, J. M., & Kirke, P. N. (2009). The search for genetic polymorphisms in the homocysteine/folate pathway that contribute to the etiology of human neural tube defects. *Birth Defects Research Part A: Clinical and Molecular Teratology*, 85(4), 285–294. <http://doi.org/10.1002/bdra.20566>
- Moss, E. G., Lee, R. C., & Ambros, V. (1997). The cold shock domain protein LIN-28 controls developmental timing in *C. elegans* and is regulated by the lin-4 RNA. *Cell*, 88(5), 637–646. [http://doi.org/10.1016/S0092-8674\(00\)81906-6](http://doi.org/10.1016/S0092-8674(00)81906-6)
- Moss, E. G., & Tang, L. (2003). Conservation of the heterochronic regulator Lin-28, its developmental expression and microRNA complementary sites. *Developmental Biology*, 258(2), 432–442. [http://doi.org/10.1016/S0012-1606\(03\)00126-X](http://doi.org/10.1016/S0012-1606(03)00126-X)
- Muñoz-Sanjuán, I., & Brivanlou, A. H. (2002). Neural Induction, the Default Model and Embryonic Stem Cells. *Nature Reviews Neuroscience*, 3(4), 271–280. <http://doi.org/10.1038/nrn786>
- Naseer, M. I., Rasool, M., Sogaty, S., Chaudhary, R. A., Mansour, M., Chaudhary, A. G., ... Al-qahtani, M. H. (2017). A novel WDR62 mutation causes primary microcephaly in a large consanguineous Saudi family. *Annals of Saudi Medicine*, 37(2). <http://doi.org/10.5144/0256-4947.2017.148>
- Nicholas, A. K., Khurshid, M., Désir, J., Carvalho, O. P., Cox, J. J., Thornton, G., ...

- Woods, C. G. (2010). WDR62 is associated with the spindle pole and is mutated in human microcephaly. *Nature Genetics*, 42(11), 1010–4.  
<http://doi.org/10.1038/ng.682>
- Običan, S. G., Finnell, R. H., Mills, J. L., Shaw, G. M., & Scialli, A. R. (2010). Folic acid in early pregnancy: a public health success story. *The FASEB Journal*, 24(11), 4167–4174. <http://doi.org/10.1096/fj.10-165084>
- Poleskaya, A., Cuvellier, S., Naguibneva, I., Duquet, A., Moss, E. G., & Harel-Bellan, A. (2007). Lin-28 binds IGF-2 mRNA and participates in skeletal myogenesis by increasing translation efficiency. *Genes and Development*, 21(9), 1125–1138.  
<http://doi.org/10.1101/gad.415007>
- Pulvers, J. N., Bryk, J., Fish, J. L., Wilsch-Bräuninger, M., Arai, Y., Schreier, D., ... Huttner, W. B. (2010). Mutations in mouse *Aspm* (abnormal spindle-like microcephaly associated) cause not only microcephaly but also major defects in the germline. *Proceedings of the National Academy of Sciences of the United States of America*, 107(38), 16595–600. <http://doi.org/10.1073/pnas.1010494107>
- Ramos da Silva, S., & Gao, S. J. (2016). Zika virus: An update on epidemiology, pathology, molecular biology, and animal model. *Journal of Medical Virology*.  
<http://doi.org/10.1002/jmv.24563>
- Rampersaud, E., Melvin, E., & Speer, M. (2006). Nonsyndromic neural tube defects: genetic basis and genetic investigations. In D. Wyszynski (Ed.), *Neural Tube Defects: From Origin to Treatment* (pp. 165–175). Oxford University Press.
- Schoenwolf, G. C. (2018). Histological and ultrastructural studies of secondary

neurulation in mouse embryos. *American Journal of Anatomy*, 169(4), 361–376.

<http://doi.org/10.1002/aja.1001690402>

Shao, Q., Herrlinger, S., Yang, S.-L., Lai, F., Moore, J. M. J. M., Brindley, M. A. M. A., & Chen, J.-F. J.-F. (2016). Zika virus infection disrupts neurovascular development and results in postnatal microcephaly with brain damage. *Development (Cambridge, England)*, 143(22), 4127–4136. <http://doi.org/10.1242/dev.143768>

Shao, Q., Herrlinger, S., Zhu, Y.-N., Yang, M., Goodfellow, F., Stice, S. L. S. L., ... Chen, J.-F. J.-F. (2017). The African Zika virus MR-766 is more virulent and causes more severe brain damage than current Asian lineage and Dengue virus. *Development*, 144(22). <http://doi.org/10.1242/dev.156752>

Shaw, G. M., Lu, W., Zhu, H., Yang, W., Briggs, F. B. S., Carmichael, S. L., ... Finnell, R. H. (2009). 118 SNPs of folate-related genes and risks of spina bifida and conotruncal heart defects. *BMC Medical Genetics*, 10(1), 49. <http://doi.org/10.1186/1471-2350-10-49>

Shinoda, G., Shyh-Chang, N., Soysa, T. Y., Zhu, H., Seligson, M. T., Shah, S. P., ... Daley, G. Q. (2013). Fetal deficiency of lin28 programs life-long aberrations in growth and glucose metabolism. *Stem Cells*, 31(8), 1563–1573. <http://doi.org/10.1002/stem.1423>

Spemann, H., & Mangold, H. (1924). über Induktion von Embryonalanlagen durch Implantation artfremder Organisatoren. *Archiv Für Mikroskopische Anatomie Und Entwicklungsmechanik*, 100(3), 599–638. <http://doi.org/10.1007/BF02108133>

Thiersch, J. B. (1952). Therapeutic Abortions with a Folic Acid Antagonist, 4-

Aminopteroylglutamic Acid (4-Amino P. G. A.) Administered by the Oral Route.

*American Journal of Obstetrics & Gynecology*, 63(6), 1298–1304.

[http://doi.org/10.1016/S0002-9378\(16\)38924-4](http://doi.org/10.1016/S0002-9378(16)38924-4)

Thornton, J. E., & Gregory, R. I. (2012). How does Lin28 let-7 control development and disease? *Trends in Cell Biology*, 22(9), 474–82.

<http://doi.org/10.1016/j.tcb.2012.06.001>

Truitt, M. L., Conn, C. S., Shi, Z., Seo, Y., Barna, M., Truitt, M. L., ... Coady, A. M. (2015). Differential Requirements for eIF4E Dose in Normal Development and Cancer Article Differential Requirements for eIF4E Dose in Normal Development and Cancer. *Cell*, 162(1), 59–71. <http://doi.org/10.1016/j.cell.2015.05.049>

Villamil-Gómez, W. E., Rodríguez-Morales, A. J., Uribe-García, A. M., González-Arismendy, E., Castellanos, J. E., Calvo, E. P., ... Musso, D. (2016). Zika, dengue, and chikungunya co-infection in a pregnant woman from Colombia. *International Journal of Infectious Diseases*, 51, 135–138.

<http://doi.org/10.1016/j.ijid.2016.07.017>

Von der Hagen, M., Pivarcsi, M., Liebe, J., von Bernuth, H., Didonato, N., Hennermann, J. B., ... Kaindl, A. M. (2014). Diagnostic approach to microcephaly in childhood: A two-center study and review of the literature. *Developmental Medicine and Child Neurology*, 56(8), 732–741. <http://doi.org/10.1111/dmcn.12425>

Wallingford, J. B., Niswander, L. A., Shaw, G. M., & Finnell, R. H. (2013). The Continuing Challenge of Understanding, Preventing, and Treating Neural Tube Defects. *Science*, 339(6123), 1047–1055. <http://doi.org/10.1038/nrn1986>

- Warkany, J., Beaudry, P., & Hornstein, S. (1959). Attempted abortion with aminopterin (4-amino-pteroylglutamic acid): Malformations of the child. *A.M.A. Journal of Diseases of Children*, *97*(3), 274–281. Retrieved from <http://dx.doi.org/10.1001/archpedi.1959.02070010276003>
- Wilbert, M. L., Huelga, S. C., Kapeli, K., Stark, T. J., Liang, T. Y., Chen, S. X., ... Yeo, G. W. (2012). LIN28 Binds Messenger RNAs at GGAGA Motifs and Regulates Splicing Factor Abundance. *Molecular Cell*, *48*(2), 195–206. <http://doi.org/http://dx.doi.org/10.1016/j.molcel.2012.08.004>
- Wilde, J. J., Petersen, J. R., & Niswander, L. (2014). Genetic, Epigenetic, and Environmental Contributions to Neural Tube Closure. *Annual Review of Genetics*, *48*(1), 583–611. <http://doi.org/10.1146/annurev-genet-120213-092208>
- Woods, C. G. (2004). Human microcephaly. *Current Opinion in Neurobiology*, *14*, 112–117. <http://doi.org/10.1016/j.conb.2004.01.003>
- Woods, C. G., & Basto, R. (2014). Microcephaly. *Current Biology*, *24*(23), R1109–R1111. <http://doi.org/http://dx.doi.org/10.1016/j.cub.2014.09.063>
- Woods, C. G., Bond, J., & Enard, W. (2005). Autosomal Recessive Primary Microcephaly (MCPH): A Review of Clinical, Molecular, and Evolutionary Findings. *The American Journal of Human Genetics*, *76*(5), 717–728. <http://doi.org/10.1086/429930>
- Xu, D., Zhang, F., Wang, Y., Sun, Y., & Xu, Z. (2014). Microcephaly-Associated Protein WDR62 Regulates Neurogenesis through JNK1 in the Developing Neocortex. *Cell Reports*, *6*(1), 104–116. <http://doi.org/http://dx.doi.org/10.1016/j.celrep.2013.12.016>

- Xue, S., & Barna, M. (2012). Specialized ribosomes: a new frontier in gene regulation and organismal biology. *Nat Rev Mol Cell Biol*, 13(6), 355–369.  
<http://doi.org/10.1038/nrm3359>
- Xue, S., Tian, S., Fujii, K., Kladwang, W., Das, R., & Barna, M. (2015). RNA regulons in Hox 5' UTRs confer ribosome specificity to gene regulation. *Nature*, 517(7532), 33–8. <http://doi.org/10.1038/nature14010>
- Yang, D.-H., & Moss, E. G. (2003). Temporally regulated expression of Lin-28 in diverse tissues of the developing mouse. *Gene Expression Patterns*, 3(6), 719–726.  
[http://doi.org/10.1016/S1567-133X\(03\)00140-6](http://doi.org/10.1016/S1567-133X(03)00140-6)
- Yang, M., Yang, S.-L., Herrlinger, S., Liang, C., Dzieciatkowska, M., Hansen, K. C., ... Chen, J.-F. (2015). Lin28 promotes the proliferative capacity of neural progenitor cells in brain development. *Development*, 142(9), 1616–1627.  
<http://doi.org/10.1242/dev.120543>
- Zhong, X., Liu, L., Zhao, A., Pfeifer, G. P., & Xu, X. (2005). The abnormal spindle-like, microcephaly-associated (ASPM) gene encodes a centrosomal protein. *Cell Cycle*, 4(9), 1227–1229. <http://doi.org/10.4161/cc.4.9.2029>

## CHAPTER 2

# LIN28-MEDIATED PROMOTION OF PROTEIN SYNTHESIS IS CRITICAL FOR NEURAL PROGENITOR CELL MAINTENANCE AND BRAIN DEVELOPMENT IN MICE<sup>1</sup>

---

<sup>1</sup>Stephanie Herrlinger, Qiang Shao, Mei Yang, Qing Chang, Gustavo Martinez, Yang Liu, Xiaohan Pan, Hang Yin, Li-Wei Xie, Jian-Fu Chen. 2018. Submitted to *Development*, 11/16/2018.

## Abstract

Neural progenitor cells (NPCs) undergo rapid proliferation during neurulation in early development. This rapid growth generates a high demand for mRNA translation in a timing-dependent manner, but its underlying mechanism and functional importance remain largely unknown. Lin28 is an RNA-binding protein with two paralogs, Lin28a and Lin28b, in mammals. We previously reported that Lin28a deletion led to microcephaly. Here we found that Lin28a/b double knockout (dKO) caused reduced proliferation and precocious differentiation of NPCs leading to neural tube defects (NTDs) in mice. We used ribosomal protein 24 hypomorphic mice (Rpl24Bst/+) as a genetic tool to dampen global protein synthesis. In support of the importance of Lin28-mediated translation promotion, Lin28a<sup>-/-</sup>;Rpl24Bst/+ compound mutants exhibited NTDs resembling those seen in Lin28a/b dKO mice. Furthermore, increased NPC numbers and brain sizes in Lin28a-overexpressing mice were rescued by Rpl24Bst/+ heterozygosity. Mechanistically, RNA-sequencing of polysome sucrose gradient fractions revealed a reduced translation of genes involved in the regulation of cell cycle, ribosome biogenesis, and translation in mutants. Lin28a localizes in the nucleoli of NPCs. Ribosome biogenesis was reduced in Lin28a/b mutants and increased in Lin28a-overexpressing NPCs. Given Lin28's specific expression in early development, our data suggest that Lin28-mediated promotion of translation is essential for NPC maintenance and early brain development.

## Introduction

The disruption of the highly complex regulation of neural progenitor cell (NPC) proliferation and growth during neurulation leads to neural tube defects (NTDs) (Greene & Copp, 2014; Wallingford, Niswander, Shaw, & Finnell, 2013). The proliferation rate is high during early mammalian development, with doubling times of 2-7 hours at embryonic day (E) 5.5-6.5 in mice. Extrapolating from the accumulation of cell numbers, cell doubling time is estimated to be ~10 hours between E8.8 to E11.4 (Burns & Hassan, 2001). A high level of transcriptional output is required for the fast proliferation of the epiblast in early development (Guzman-Ayala et al., 2014). The global protein synthesis rate and mRNA-specific translation are under precise regulation in distinct cell types at different developmental stages (Buszczak, Signer, & Morrison, 2014; Shi & Barna, 2015). The fast proliferation and growth of NPCs in early development generate a high, temporally specific demand for protein synthesis, including mRNA translation and ribosome biogenesis. However, neither the impact nor the mechanisms driving protein synthesis have been explored as extensively as transcriptional regulation in development. How the protein synthesis of rapidly expanding NPCs is temporally regulated in early brain development remains largely unknown.

RNA-binding proteins (RBPs) are capable of mediating coordinated steps of translation. In embryonic stem (ES) cells, hundreds of RBPs have been identified and reported to modulate ES cell self-renewal and pluripotency by regulating post-transcriptional processes including translational control (Kwon et al., 2013; Ye & Blelloch, 2014). The RBP Hu antigen R (HuR) has been found to play a critical role in post-transcriptionally regulating neocortical development by dictating the temporal

specificity of ribosome composition and functionally related mRNA translation (Kraushar et al., 2014). Loss of function of the RBP FMRP causes Fragile X syndrome, the most common form of inherited intellectual disability. FMRP directly binds to the ribosome and stalls ribosomal translocation on mRNAs encoding proteins involved in synaptic function and autism (Chen, Sharma, Shi, Agrawal, & Joseph, 2014; Darnell et al., 2011). Neurulation is a developmental process that occurs after implantation and before neuronal differentiation. RBPs might temporally modulate translation machinery to meet the increased demand for protein synthesis and mRNA translation specificity during rapid NPC expansion in neurulation.

The RBP Lin28 was first discovered to be a critical heterochronic regulator of cell fate in *Caenorhabditis elegans* larvae (Moss, Lee, & Ambros, 1997). Lin28 contains two types of RNA binding domains, namely a cold shock domain (CSD) and two CCHC zinc finger domains. Previous studies have established the importance of Lin28's functions in a wide range of biological processes and disease conditions, including its roles in ES self-renewal, reprogramming of induced pluripotent stem cells (iPSCs), various cancers, and diabetes, among others (Shyh-Chang & Daley, 2013; Thornton & Gregory, 2012). In ES cells, Lin28a associates with ribosomes at the endoplasmic reticulum (ER) and represses the translation of a subset of specific mRNAs destined for the ER (Cho et al., 2012). On the other hand, Lin28a acts as a "translational enhancer" and promotes translational efficiency in skeletal muscle precursor cells (Poleskaya et al., 2007), suggesting that Lin28's action mechanism is context dependent. The in vivo functions of Lin28 in early mammalian embryos are less studied. Whether Lin28 promotes or inhibits protein synthesis in NPCs and brain development remains unknown.

We previously reported that Lin28 is highly enriched in the developing neural tube and exhibits a temporal pattern of expression that decreases as brain development progresses (Balzer, Heine, Jiang, Lee, & Moss, 2010; M. Yang et al., 2015). Lin28a promotes the proliferative capacity of NPCs in the developing neocortex after neural tube closure (M. Yang et al., 2015), leaving its potential functions in neurulation unknown. Using Lin28a and Lin28b double knockout (dKO) mice, here we report that Lin28a/b control the balance of proliferation and differentiation of NPCs in early embryo development, and their disruption results in NTDs. By employing ribosomal protein hypomorphic mice (Rpl24Bst/+) as a genetic tool to dampen global protein synthesis (Barna et al., 2008), our mouse genetic studies demonstrated that Lin28 promotes, rather than inhibits, protein synthesis in the developing brain; Lin28-mediated promotion of protein synthesis is essential for proper NPC behaviors and neural tube closure. This is further supported by studies in neuroepithelial tissues using sucrose density-gradient ultracentrifugation and fractionation coupled with RNA sequencing (RNAseq) and bioinformatic analysis. Specifically, Lin28 is expressed in both the cytoplasm and the nucleolus, and it promotes ribosome biogenesis, mTORC1 signaling, and translation of genes involved in the cell cycle, ribosome biogenesis, and mRNA translation.

## Materials and Methods

### Ethics Statement

All animals were used according to animal use protocols granted by the University of Georgia (Approval # A2016 08-010-Y1-A1) and University of Southern California (Approval # 20718) Institutes of Animal Care and Use Committees (IACUC).

## Mouse models

Lin28a<sup>-/-</sup> knockout mice and Lin28a transgenic mice were described in our previous publication (M. Yang et al., 2015). The Lin28b<sup>-/-</sup> mice were kindly provided by the Dr. George Daley laboratory and were described in published studies (Shinoda et al., 2013). Hypomorphic allele Rpl24Bst/+ (C57BLKS-Rpl24Bst/J, stock # 00516) and Nestin-Cre mice (B6.Cg-Tg(Nes-cre)1Kln/J, stock # 003771) were purchased from Jackson Laboratories.

## Histology and immunohistochemistry of embryonic tissue

These experiments were performed according to published procedures (Shao et al., 2017). Briefly, embryos were dissected at various stages in development, as noted in the text for each individual experiment (E8.5, E9.5, E11.5, E13.5, E18.5). Dissected embryos at earlier stages (E8.5-E13.5) remained intact and were fixed in 4% paraformaldehyde for 1 hour at room temperature, washed 3 times in 1x PBS and incubated overnight in 25% sucrose. Embryos were transferred to a 50% OCT; 50%, 25% sucrose solution for 45 min prior to freezing. Fixed embryos were sectioned to a thickness of 12  $\mu$ m using a cryostat. E18.5 embryonic brain tissue was dissected from the body, and followed the above mentioned fixation steps thereafter. The secondary antibodies used were Alexa 488 and Alexa 555 conjugated to specific IgG types (Invitrogen Molecular Probes). Primary antibodies were used at concentrations depicted in Supplemental Table 1. All the experiments have been repeated at least three times, and representative images are shown in the individual figures.

### BrdU pulse labeling experiments

BrdU labeling was performed as described previously (Shao et al., 2016; S.-L. Yang et al., 2015). Briefly, pregnant dams with stage E11.5 embryos were injected intraperitoneally with BrdU at 10 mg/kg body weight 30 min prior to dissection of the embryos. Immediately after dissection, embryos were fixed in 4% PFA for 1 hr at RT, subsequently washed in 1x PBS 3x 5 min, and incubated overnight in 25% sucrose. The next day, OCT embedded tissues were then sectioned and stained IHC, with antigen retrieval.

### Nucleolar size analyses

FIJI (Fiji Is Just ImageJ) was utilized with the analyze particles toolbox. The nucleoli from z-stack images taken every 1  $\mu\text{m}$  of 12  $\mu\text{m}$  thick sections immunolabeled for Nucleophosmin (B23) were subjected to area image analysis.

### Polysome fractionation and polysome isolation

Fractionation protocol has been adapted and modified from previous work (Kondrashov et al., 2011; Kraushar et al., 2014). Two technical replicates were performed using neural tube tissues from E11.5 or E12.5 embryos with control or Lin28a<sup>-/-</sup>;b<sup>-/-</sup> genotypes.

*Sucrose Gradients:* The day before fractionation, two sucrose gradient solutions were prepared (17% and 51% sucrose) in DEPC-treated water (50 mM NaCl, 50 mM Tris-HCl pH 7.4, and 10 mM MgCl<sub>2</sub>). On the day of fractionation, smaller aliquots were allocated for the sucrose gradients and 20 mM DTT and 100  $\mu\text{g}/\text{mL}$  Cycloheximide was added to

the aliquots. To generate the gradient, 8.5 mL of 51% sucrose solution was added to a Beckman Coulter Polypropylene Tube (cat# 331372). 2.5 mL of 17% sucrose was added on top of the dense layer while holding the tube nearly parallel to the ground so as to minimally disturb the higher density sucrose layer. The tube was then covered with parafilm and carefully laid on the bench for 1 hr at RT.

*Sample Preparation and Fractionation:* Prior to fractionation experiments stage E11.5, embryonic brain tissue was dissected and immediately flash frozen by liquid nitrogen and stored at -80 °C. The remaining embryonic tissue was used to confirm genotyping. On the day of fractionation, 7 samples were pooled together per genotype in 250 µl Polysome Buffer (20 mM Tris-HCl pH 7.4, 100 mM NaCl, 10mM MgCl<sub>2</sub>, 1 tablet EDTA-free protease inhibitor, 20 mM DTT, 1% Triton-X100, 1 µg/mL Heparin, and 100 µg/mL Cycloheximide) for 30 min with pipetting every 5 min to homogenize the tissue. Lysate was cleared by centrifugation for 20 min at 14,000xg at 4° C. Supernatant was collected and RNA concentration was measured using NanoDrop 2000 (ThermoFisher). 55 µL of supernatant was stored separately at -80 ° C for total RNA reference sample. The remaining supernatant was carefully applied to the sucrose gradients and ultracentrifuged at 39,000 RPM for 160 min at 4° C (SW40 rotor). Gradients were then applied to a tube piercer connected to a Foxy Automated Fractionator and Isco UA-6 UV Detector that measures absorbance at 252 nm. Fractions were collected and their RNA concentration measured prior to RNA extraction from sucrose gradients.

*Sucrose extraction and RNA isolation.* The high concentration of sucrose in the fractions interferes with the phase separation required in standard Trizol extraction of RNA. To address this issue, we utilized and adapted an existing published protocol for sucrose

extraction from gradient fractions (Clancy et al., 2007). In brief, three volumes of 100% EtOH were added to each fraction and mixed immediately, and the lysate was precipitated overnight at -80° C. The following day, the precipitate was spun at 16,000xg for 20 min (at 4° C) and supernatant was removed. The resulting pellet was dried by spinning and removal of remaining supernatant. 1 mL of Trizol was added to the pellet and vortexed to dissolve the pellet. After waiting for 5 min for nucleoprotein complexes to dissociate, RNA was then isolated using standard Trizol extraction (Life Biotechnologies).

#### High-throughput sequencing

Genomic DNA and ribosomal RNA were removed with Turbo DNA-free kit and RiboMinus Eukaryote Kit (Life Technologies), respectively. The resulting RNA fractions were subjected to strand-specific library preparation using NEBNext Ultra Directional RNA Library Prep Kit for Illumina (New England Biolabs). Sequencing was performed on a Nextseq500 (Illumina).

#### RNA-seq assembly and gene enrichment analysis

Raw RNAseq reads in fastq format were passed through FASTQC to verify quality. The low quality reads were removed with Fastx-toolkit. The high quality reads were mapped to the mouse genome (GRCm38/mm10) by TopHat (PMID:19289445) at the optional setting of -G mouse\_mRNA.gtf and assembled against mRNA annotation by HTSeq. Differential expression analysis was performed between Lin28a/b dKO and control groups using the R package DESeq2 (Love, Huber, & Anders, 2014). Genes were

considered significant if the P-value was  $<0.05$ . This methodology was applied for the subgroup analysis on the Lin28a/b dKO/control (poly) groups and the Lin28a/b dKO/control (total) groups. Heatmaps were generated using the R package pheatmap based on read counts of significant differential expressed genes. Volcano plots were generated using the R package ggplot2 based on up and down regulated significant differential expressed genes. The list of genes with significant changes were then separated into four groups according to their log<sub>2</sub> fold change ( $> 1.5$ ,  $>1.25$ ,  $<-1.5$ ,  $<-1.25$ ). Gene Ontology (GO) and Kyoto Encyclopedia of Genes and Genomes (KEGG) analysis were performed by using R package clusterProfiler for the differentially expressed genes (Yu, Wang, Han, & He, 2012). The P values were corrected for multiple comparisons using the Benjamini-Hochberg method.

#### Western blot analysis

Samples for Western blot analyses were prepared from isolated E11.5 neocortex. For individual studies, the densitometry of individual blot signals from three independent western blot experiments were quantified using Image J software. The individual values for each blot signal was normalized to respective controls followed by the statistical analysis among different samples (Student's t-test). The antibodies used and their concentrations are described in Supplemental Table 1.

#### Quantitation and statistical analysis

Statistics were run in GraphPad PRISM © 7.0 software for all ANOVA and Student's t-tests. Analyses with 2 dependent variables were performed with 2-way ANOVA with

Bonferroni posthoc analyses. Data in all graphs are represented as mean  $\pm$  SEM. \*:  $p \leq 0.05$ , \*\*:  $p \leq 0.01$ , \*\*\*:  $p \leq 0.001$ , ns: not significant.

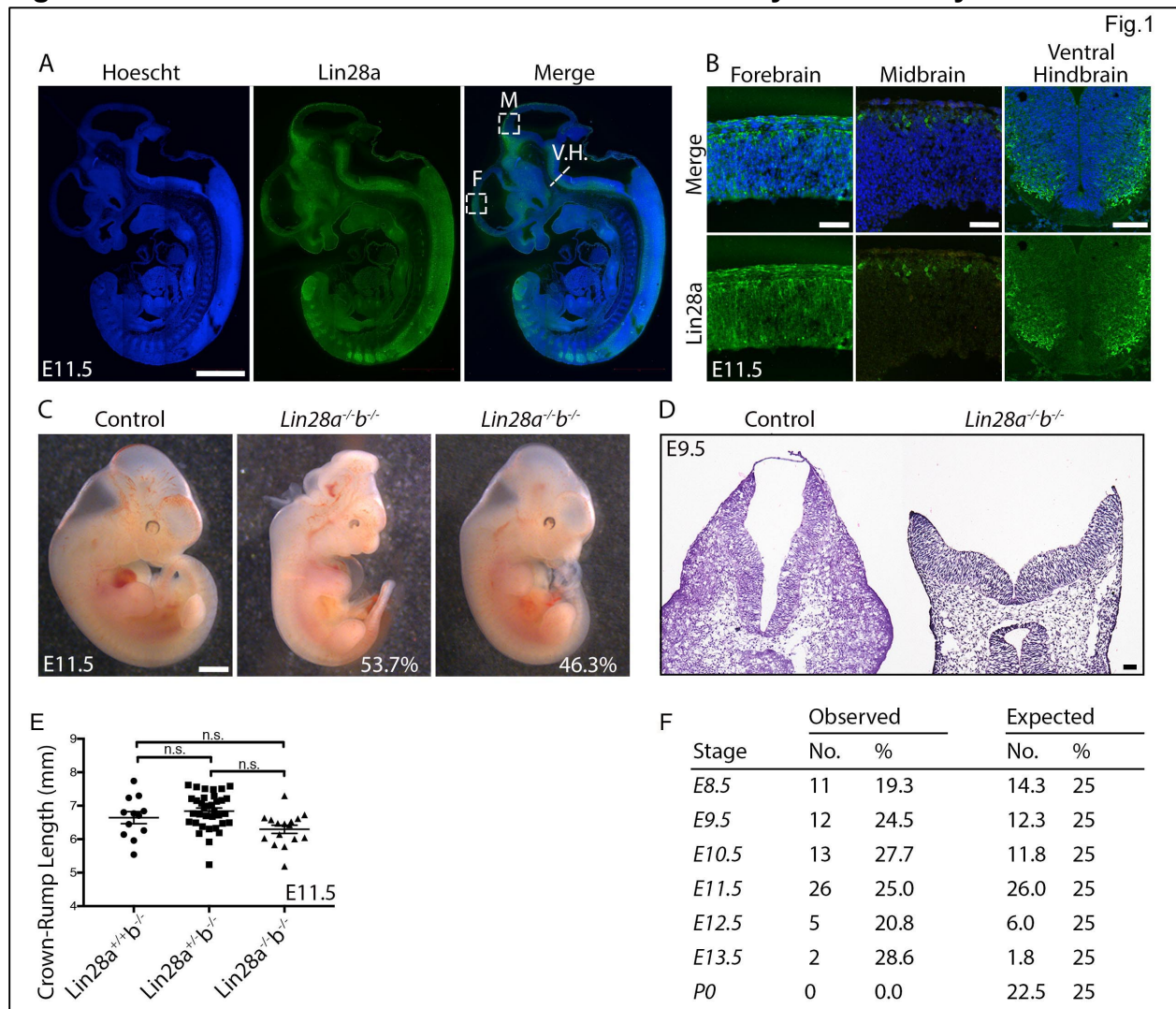
## Results

### Loss of Lin28a/b results in NTDs and embryonic lethality.

Lin28A protein is ubiquitously expressed in NPCs in the E9.5 neural tube (Fig. S1A). While highly expressed throughout the neural tube at E11.5 (Fig. 1A), Lin28A expression displays an increasingly dynamic pattern in NPC populations of the forebrain, midbrain, and ventral hindbrain (Fig. 1B). Together with the temporal expression pattern of Lin28A from our previous studies (M. Yang et al., 2015), these results revealed Lin28A's spatiotemporal expression pattern with high and low expression levels at early and late developmental stages, respectively.

To investigate Lin28's function in the developing brain, we generated compound *Lin28a<sup>-/-</sup>b<sup>-/-</sup>* mutants. For all following analyses in this study, *Lin28a<sup>-/-</sup>b<sup>-/-</sup>* mutants were evaluated against *Lin28b<sup>-/-</sup>* single knockout littermate controls. We did not detect morphological or developmental defects in *Lin28b<sup>-/-</sup>* mutant mice, which is consistent with published studies (Shinoda et al., 2013). Litters were evaluated at various early embryonic stages (E8.5-E13.5) as well as postnatal day 0 (P0). *Lin28a/b* dKO mice failed to close the neural tube with partial penetrance (Fig. 1C, middle panel, 53.7% penetrance, n=41 embryos), primarily in the midbrain/hindbrain regions (Fig. 1D). In contrast, *Lin28a<sup>-/-</sup>b<sup>-/-</sup>* embryos and mice did not exhibit any apparently abnormal

**Figure 2.1. Loss of *Lin28a/b* results in NTDs and embryonic lethality.**



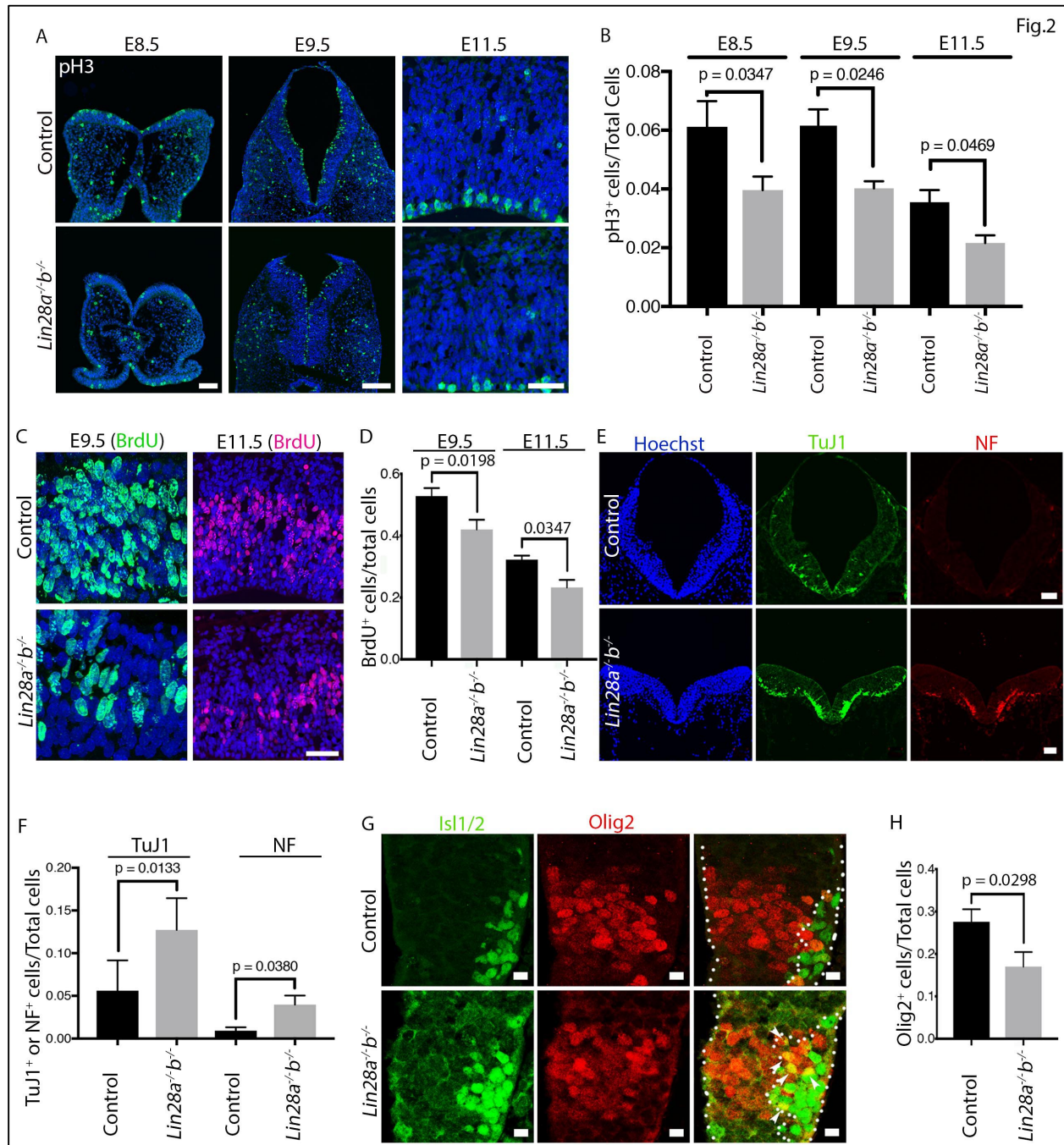
(A) Confocal microscopy images of E11.5 wild-type embryo sectioned sagittally show *Lin28a* expression across the entire neural tube. Indicated areas demonstrate zoomed in images in B: Forebrain (F), Midbrain (M), and Ventral Hindbrain (V.H.). Scale bar: 1 mm. (B) Confocal microscopy images show zoomed in areas indicated in A, right panel. Right panels show coronal section of the ventral hindbrain. Scale bars from left to right; 50  $\mu$ m, 50  $\mu$ m, 100  $\mu$ m. (C) Bright field images of E11.5 *Lin28a/b* double mutant embryos with (middle panel) or without (right panel) NTDs. (Controls include *Lin28a*<sup>+/+</sup>*b*<sup>-/-</sup>: n = 102 and *Lin28a*<sup>+/-</sup>*b*<sup>-/-</sup>: n = 207; *Lin28a*<sup>-/-</sup>*b*<sup>-/-</sup>: n = 41). Scale bar: 1 mm. (D) H&E staining of comparable hindbrain sections of E9.5 embryos. Scale bar: 50  $\mu$ m. (E) E11.5 *Lin28a/b* mutant embryos do not exhibit a significant decrease in crown/rump ratio compared with littermate controls. *Lin28a*<sup>-/-</sup>*b*<sup>-/-</sup> (n=16) embryos from 9 different litters were measured, *Lin28a*<sup>+/-</sup>*b*<sup>-/-</sup> (n=35) and *Lin28a*<sup>+/+</sup>*b*<sup>-/-</sup> (n=12) littermates serve as controls. N.s. represents not significant. (F) Numbers of compound mutant embryos recovered alive from indicated developmental stages. Parents were *Lin28a*<sup>+/-</sup>*b*<sup>-/-</sup> x *Lin28a*<sup>+/-</sup>*b*<sup>-/-</sup>. Ratios of actual and expected *Lin28a*<sup>-/-</sup>*b*<sup>-/-</sup> double mutant embryos are listed on the right.

phenotype, whereas *Lin28a*<sup>-/-</sup> and *Lin28a*<sup>-/-</sup>;*b*<sup>+/-</sup> displayed microcephaly without influence on animal survival. In addition to NTDs, *Lin28a/b* double mutants also exhibited other consistent phenotypes including smaller head size, a straight-backed appearance of the spinal column, shorter tail length (Fig. 1C, middle and far right panel). Despite these defects, crown-rump lengths were not significantly decreased in *Lin28a/b* double mutants compared to controls (Fig. 1E) at E11.5. *Lin28a/b* dKO mice were not reliably recovered after E13.5, and could not survive postnatally (Fig. 1F). Together, these observations suggest that loss of *Lin28a/b* results in NTDs and embryonic lethality in mice.

#### *Lin28a/b* depletion leads to reduced proliferation and precocious differentiation of NPCs.

NPCs proliferate rapidly before and during neural tube closure (Burns & Hassan, 2001). The presence of NTDs and smaller brain sizes suggested loss of NPCs in *Lin28a/b* dKO mice. To examine NPC proliferation, we performed immunohistochemical (IHC) staining using antibodies against phospho-histone3 (pH3), a marker for mitotic cells. We examined stages E8.5, E9.5, and E11.5 in the hindbrain region, where NTDs occur in mutant embryos (Fig. 1C-1D). As reported in previous studies (S.-L. Yang et al., 2015), pH3+ NPCs form a nearly continuous line at the ventricular surface of the neuroepithelium at early stages of brain development (Fig. 2A). *Lin28a/b* mutant embryos exhibit a reduction in the density of pH3+ labeled NPCs at both E8.5 (prior to neural tube closure) and E9.5 (after neural tube closure) (Fig. 2A-2B). This decrease in pH3+ cells could be due to reduced proliferation or cell cycle arrest at mitosis. To distinguish these two possibilities, we investigated NPC G1/S phase transition. Labeling with bromodeoxyuridine (BrdU) was performed for 30 min to mark NPCs in S-phase. At

**Figure 2.2. *Lin28a/b* deletion results in reduced proliferation and precocious differentiation in NPCs.**



(A) Confocal micrographs of phospho-histone3 (pH3, green) IHC in E8.5 (left panels), E9.5 (middle panels), and E11.5 (right panels) of comparable coronal hindbrain sections. Hoechst stains nuclei (blue). Scale bar: 50  $\mu$ m (leftmost); 100  $\mu$ m (middle); 50  $\mu$ m (rightmost). (B) Quantification of the ratio of pH3<sup>+</sup> cells/Hoechst<sup>+</sup> cells in neuroepithelium of E8.5 and E9.5 hindbrain sections, or in ventricular zone (VZ) of E11.5 cerebral cortex. (E8.5:  $p = 0.0347$ , E9.5:  $p = 0.0246$ , E11.5:  $p = 0.0469$ ; Student's t-test). ( $n \geq 3$  sections from individual 3 litters). (C) Confocal micrographs of E9.5 (green) and E11.5 (red) coronal hindbrain sections stained with antibodies for BrdU

after a 0.5 hr pulse prior to dissection. Hoechst stains nuclei (blue). Scale bar: 25  $\mu\text{m}$  (leftmost and middle panels); 50  $\mu\text{m}$  (rightmost). (D) Quantification of ratio of BrdU<sup>+</sup> cells/Hoechst<sup>+</sup> cells in hindbrain sections (E9.5) or in VZ of cerebral cortex (E11.5). (E9.5:  $p = 0.0198$ , E11.5:  $p = 0.0347$ ; Student's t-test). ( $n = 3$  sections from individual 3 embryos). (E) Confocal micrographs from E9.5 hindbrain sections stained with NF (Neurofilament, red) and Tuj1 (green). Hoechst stains nuclei (blue). Scale bar: 50  $\mu\text{m}$ . (F) Quantification of ratio of NF<sup>+</sup> cells/Hoechst<sup>+</sup> cells and Tuj1<sup>+</sup> cells /Hoechst<sup>+</sup> cells from E. (NF:  $p = 0.0380$ , Tuj1:  $p = 0.0133$ ; Student's t-test). ( $n \geq 3$  sections from 3 individual embryos). (G) Confocal micrographs from E9.5 spinal cord sections stained with Olig2 (red) and Isl1/2 (green). Hoechst stains nuclei (blue). White dots outline the neuroepithelial cells, and white arrowheads indicate Olig2- and Isl1/2- double-positive cells in mutant neuroepithelium. Scale bar: 20  $\mu\text{m}$ . (H) Quantification of ratio of Olig2<sup>+</sup> cells/Hoechst<sup>+</sup> cells in the E9.5 hindbrain area depicted in images (right panels) in G. ( $p = 0.0298$ ; Student's t-test). ( $n \geq 3$  sections from 3 individual embryos).

both E9.5 and E11.5, there was a significant decrease in the percentage of BrdU+ cells out of total NPCs in the ventricular zone/subventricular zone (VZ/SVZ) of mutant brains (Fig. 2C-2D). Altogether, these data suggest that *Lin28a/b* are required to maintain NPC proliferation in the early neural tube.

NPC proliferation is coupled with neural differentiation in the developing embryo (Doe, 2008). We therefore investigated NPC differentiation by using  $\beta$ III-Tubulin (Tuj1) and Neurofilament (NF) to label differentiating neurons in the hindbrain of neural tube. Tuj1- and NF-positive cells were hardly detectable in the wild type neural tube at E9.5 (Fig. 2E). In contrast, there was a dramatic increase in both Tuj1- and NF-positive cells in mutants (Fig. 2E-2F), suggesting a precocious neural differentiation. These results raised the possibility that prematurely differentiated cells were generated at the cost of NPCs in the mutant neuroepithelium. To test this hypothesis, we examined motor neuron progenitors and motor neurons, which are labeled by Olig2 and Isl1/2 in the ventral spinal cord (Jessell, 2000). There was a mutually exclusive distribution of Olig2 and Isl1/2 positive cells in wild type spinal cords (Fig. 2G). In contrast, Olig2 and Isl1/2 double positive cells were frequently detected in mutants (white arrowheads in Fig. 2G). The ratio of Olig2+ cells to the total cells within the anterior spinal cord was significantly decreased in *Lin28a/b* dKO embryos (Fig. 2H). Together, these results suggest precocious differentiation of NPCs in the mutant neural tube.

Programmed cell death occurs in normal embryonic brain development (Kuan, Roth, Flavell, & Rakic, 2000); abnormal cell death has been associated with NTDs (Copp, 2005). To determine whether abnormal apoptosis could be contributing to the

NTDs in *Lin28a/b* dKO mice, we performed TUNEL analyses. No significant changes in TUNEL+ cells were detected between mutants and controls at E9.5, a stage at which NTDs can be detected in mutants (Fig. S1B-1C,  $p = 0.4525$ ). Therefore, abnormal apoptosis is not an early causative event for NTDs in *Lin28a/b* dKO mice, despite its potential involvement in embryonic lethality at later stages. Together, these data suggest that *Lin28a/b* deletion causes the reduced proliferation and precocious differentiation of NPCs, which could contribute to NTDs in mutant embryos.

*Lin28a<sup>-/-</sup>;Rpl24<sup>Bst/+</sup>* mutants mimic *Lin28a/b* dKO phenotypes in NTDs and embryonic lethality.

To elucidate Lin28's functional mechanisms we focused on mRNA translation and utilized the *Rpl24<sup>Bst/+</sup>* (Belly Spot & Tail, ribosomal protein large subunit 24) mouse model. *Rpl24<sup>Bst/+</sup>* mice contain a hypomorphic allele of ribosomal protein L24, and has been utilized as a genetic tool for reducing global protein synthesis (Barna et al., 2008; Signer, Magee, Salic, & Morrison, 2014). In ES cells, Lin28A inhibits the translation of a subset of mRNAs destined for the ER (Cho et al., 2012). In contrast, Lin28A functions as a "translation enhancer" to promote mRNA translation efficiency in skeletal muscle precursor cells (Polesskaya et al., 2007). These studies suggest that Lin28A regulates mRNA translation in a cell type-dependent manner. We employed mouse genetic approaches to investigate the mechanism and functional significance of Lin28-mediated translation regulation. If Lin28 inhibits translation, a global reduction of protein synthesis by *Rpl24<sup>Bst/+</sup>* should rescue the microcephaly defect in *Lin28a<sup>-/-</sup>* mutant mice. However, if Lin28a promotes translation, further reducing protein synthesis by *Rpl24<sup>Bst/+</sup>* in the

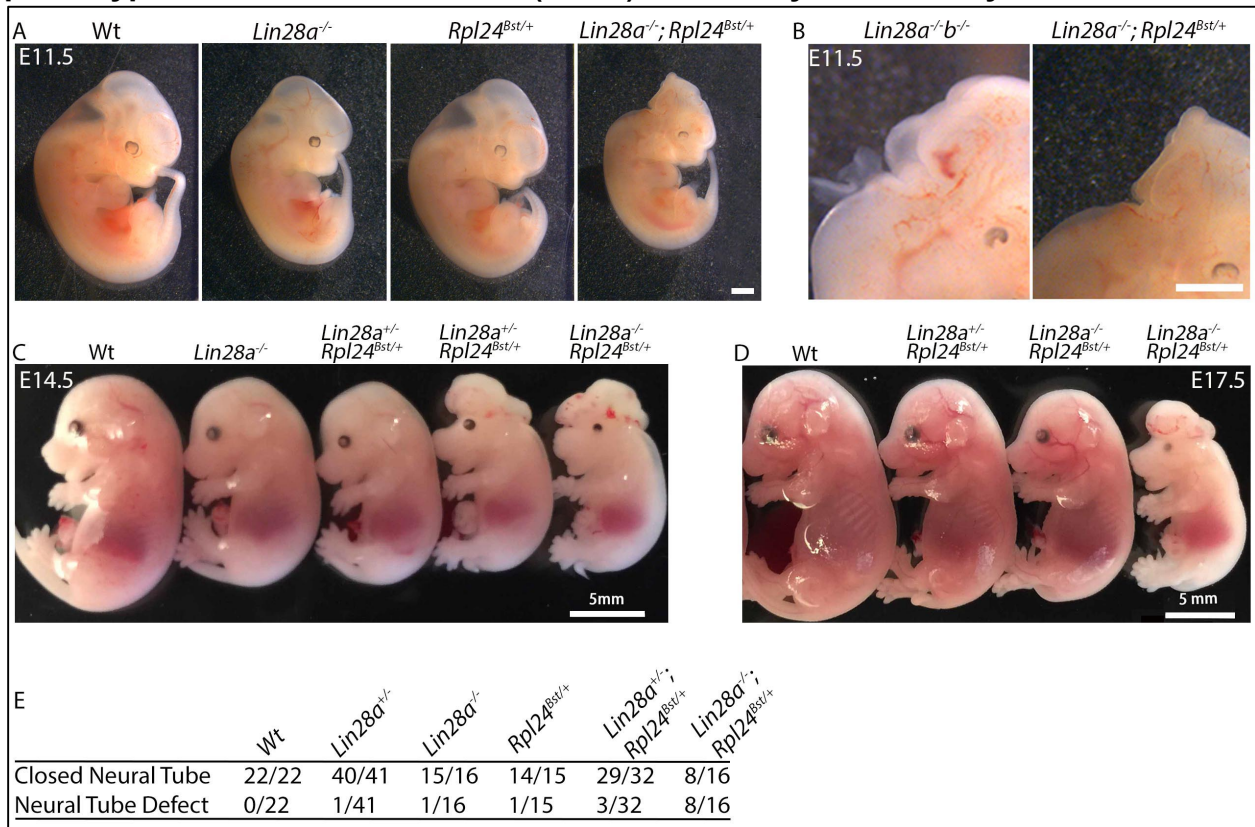
background of *Lin28a*<sup>-/-</sup> will exacerbate its microcephaly defect and potentially cause NTDs and embryonic lethality.

We crossed *Lin28a*<sup>+/-</sup>;*Rpl24*<sup>Bst/+</sup> and *Lin28a*<sup>+/-</sup> mice to generate *Lin28a*<sup>-/-</sup>;*Rpl24*<sup>Bst/+</sup> embryos and their littermate controls. We analyzed progeny embryos at various stages including E11.5, E14.5 and E17.5. *Lin28a*<sup>-/-</sup>;*Rpl24*<sup>Bst/+</sup> embryos exhibited an open NTD at E11.5 (Fig. 3A, far right panel), whereas *Lin28a*<sup>-/-</sup> and *Rpl24*<sup>Bst/+</sup> embryos do not. Interestingly, this defect closely mimicked the midbrain/hindbrain NTDs in *Lin28a/b* mutant embryos (Fig. 3B). The neural tube failed to close in the midbrain/hindbrain of affected embryos, resulting in exencephaly of the compound mutant embryos as development progressed to E14.5 (Fig. 3C) and E17.5 (Fig. 3D). NTDs in *Lin28a*<sup>-/-</sup>;*Rpl24*<sup>Bst/+</sup> embryos occurred with 50% penetrance (8/16 *Lin28a*<sup>-/-</sup>;*Rpl24*<sup>Bst/+</sup> embryos), which was much higher than we found in individual *Lin28a*<sup>-/-</sup> (1/16) or *Rpl24*<sup>Bst/+</sup> (1/15) knockout mice (Fig. 3E). Occasionally, loss of a single copy of *Lin28a* in the background of *Rpl24*<sup>Bst/+</sup> also results in NTDs (Fig. 3C, second right most, and 3/32 *Lin28a*<sup>+/-</sup>;*Rpl24*<sup>Bst/+</sup> in Fig. 3E). Together, these genetic studies demonstrate that *Lin28a/b* promote, rather than inhibit, protein synthesis in the developing brain, and *Lin28*-mediated promotion of protein synthesis is essential for neural tube closure.

Abnormally increased brain size and ratio of apical to intermediate NPCs in *Lin28a*-overexpressing mice is rescued by *Rpl24*<sup>Bst/+</sup> heterozygosity

The above studies suggested that *Lin28*-mediated protein synthesis is required for early brain development. Next we investigated whether *Lin28*-mediated promotion of protein synthesis is sufficient to alter NPC behaviors and drive brain development.

**Figure 2.3. *Lin28a*<sup>-/-</sup>; *Rpl24*<sup>Bst/+</sup> mutants mimic *Lin28a/b* double knockout phenotypes in neural tube defects (NTDs) and embryonic lethality.**

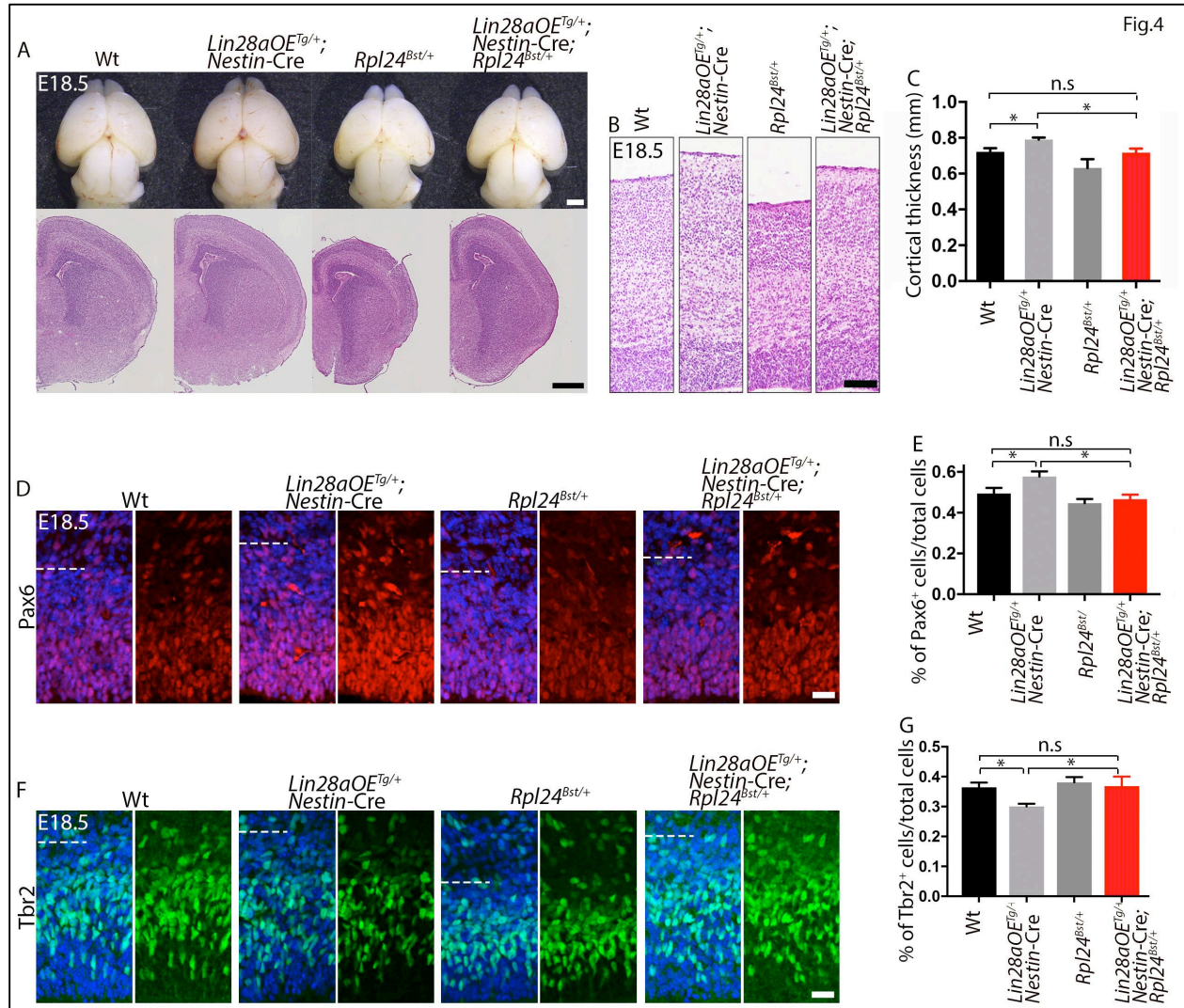


(A) E11.5 *Lin28a*<sup>-/-</sup>; *Rpl24*<sup>Bst/+</sup> mutant embryos exhibit NTDs compared to littermate controls. Scale bar: 1 mm. (B) *Lin28a*<sup>-/-</sup>; *Rpl24*<sup>Bst/+</sup> mutant embryos exhibit NTDs in the hindbrain (right panel), similar to *Lin28a/b* mutant embryos (left panel). Scale bar: 1 mm. (C) E14.5 *Lin28a*<sup>-/-</sup>; *Rpl24*<sup>Bst/+</sup> or *Lin28a*<sup>+/-</sup>; *Rpl24*<sup>Bst/+</sup> mutant embryos exhibit exencephaly in comparison to littermate controls. Scale bar: 3 mm. (D) *Lin28a*<sup>-/-</sup>; *Rpl24*<sup>Bst/+</sup> mutant embryos exhibit exencephaly at E17.5. Scale bar: 3 mm. (E) NTD penetrance for all genotypes generated from crossing between *Lin28a*<sup>+/-</sup>; *Rpl24*<sup>Bst/+</sup> males with *Lin28a*<sup>+/-</sup> females.

Using *Nestin-Cre* mice, we previously found that NPC-specific overexpression of Lin28a is able to promote Pax6-positive apical NPCs and reduce Tbr2-positive intermediate NPCs, resulting in an abnormally increased ratio of apical NPCs to intermediate NPCs and ultimately enlarged brain size (M. Yang et al., 2015). To determine to what extent the effect of Lin28a overexpression is mediated by increased protein synthesis, we generated *Lin28OE<sup>Tg/+</sup>;Nestin-Cre;Rpl24<sup>Bst/+</sup>* compound mice. Embryos were collected at E18.5 (n ≥ 9 per genotype). While *Lin28OE<sup>Tg/+</sup>;Nestin-Cre* mice exhibit enlarged brain sizes, *Lin28OE<sup>Tg/+</sup>;Nestin-Cre; Rpl24<sup>Bst/+</sup>* mice display brain sizes comparable to wild-type controls (Fig. 4A). We performed hematoxylin and eosin (H&E) staining to examine cortical thickness followed by statistical analyses. Cortical thickness was significantly increased in Lin28a-overexpressing mice, which is consistent with our previous publication (M. Yang et al., 2015). The increased cortical thickness of Lin28a-overexpressing brains was rescued by *Rpl24<sup>Bst/+</sup>* (Fig. 4B-4C), suggesting that protein synthesis is a major mediator of Lin28a's function in promoting brain growth.

To determine whether *Rpl24<sup>Bst/+</sup>* rescued the disrupted balance between apical NPCs and intermediate NPCs in Lin28a-overexpressing brains (S.-L. Yang et al., 2015), we performed IHC staining with Pax6 to label apical NPCs and Tbr2 to label intermediate NPCs in the VZ/SVZ of the developing brains. Lin28a overexpression resulted in an increase in the percentage of Pax6-labeled apical NPCs, which was rescued by *Rpl24<sup>Bst/+</sup>* heterozygosity (Fig. 4D-4E). Similarly, the decreased Tbr2-positive intermediate NPCs in Lin28a-overexpressing brains was also rescued by *Rpl24<sup>Bst/+</sup>*-mediated dampening of protein synthesis. By manipulating protein synthesis in the Lin28a loss- and gain-of-function mouse models, these mouse genetic studies

**Figure 2.4. Abnormally increased brain size and ratio of apical to intermediate NPCs in *Lin28a*-overexpressing mice are rescued by *Rpl24*<sup>Bst/+</sup> heterozygosity.**



(A) Dorsal views of E18.5 embryonic brains (top panels) and H&E staining of coronal sections (bottom panels) from Wt, *Lin28aOE*<sup>Tg/+</sup>; *Nestin-Cre*, *Rpl24*<sup>Bst/+</sup>, and *Lin28aOE*<sup>Tg/+</sup>; *Nestin-Cre*; *Rpl24*<sup>Bst/+</sup> littermate. Scale bar: 1 mm (top panels). Scale bar: 500  $\mu$ m (bottom panels). (B) Columns of cortices from E18.5 brain sections stained with H & E. Scale bar: 100  $\mu$ m. (C) Quantification of cortical thickness length from H&E sections represented in B. ANOVA analyses were performed with Bonferroni posthoc multiple comparison analysis, \* $p < 0.05$ , n.s represents not significant, and  $n \geq 3$  sections per genotype from  $n = 3$  litters. (D) Confocal micrographs of caudal neocortical coronal sections stained with antibodies against Pax6 (red). Areas underneath the white lines represent ventricular and sub-ventricular zone (VZ/SVZ). Hoechst stains nuclei (blue). Scale bar: 20  $\mu$ m. (E) Quantification for the ratios of Pax6<sup>+</sup> cells/Hoechst<sup>+</sup> cells in the E18.5 VZ/SVZ areas from experiments D. 2-way ANOVA analyses were performed with Bonferroni posthoc multiple comparison analysis, \* $p < 0.05$ , n.s represents not significant, and  $n \geq 3$  sections per genotype from  $n = 3$  litters. (F) Confocal micrographs of the VZ/SVZ from E18.5 brain sections stained with antibodies against Tbr2 (green).

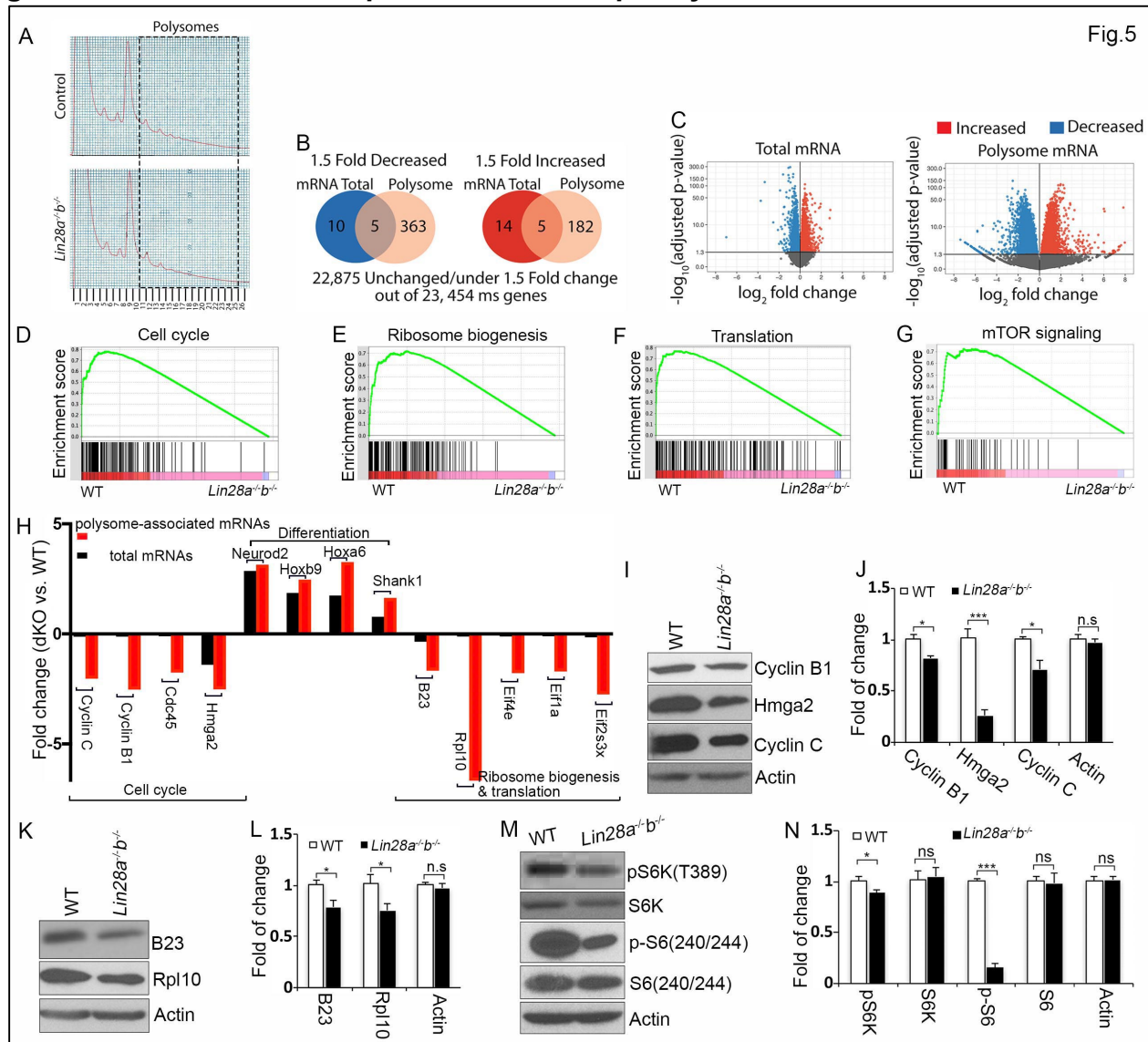
Areas underneath the white lines represent VZ/SVZ. Hoechst stains nuclei (blue). Scale bar: 20  $\mu\text{m}$ . (G) Quantification of the ratios of Tbr2<sup>+</sup> cells/Hoechst<sup>+</sup> cells in the E18.5 VZ/SVZ areas from experiments F. 2-way ANOVA analyses were performed with Bonferroni posthoc multiple comparison analysis, \*p < 0.05, n.s represents not significant, and n  $\geq$  6 sections per genotype from n = 2 litters.

demonstrate that Lin28-mediated promotion of protein synthesis is necessary and sufficient to modulate NPC proliferation and cell fate.

Lin28 regulates mRNA translation revealed by sucrose density gradient fractionation coupled with RNA sequencing

Having established that Lin28 promotes protein synthesis on a global level, we attempted to determine whether Lin28 promotes gene-specific mRNA translation. We performed sucrose density gradient ultracentrifugation and fractionation using control and Lin28a/b dKO E11.5 neuroepithelial tissue (Fig 5A). E11.5 was selected as the time point for this experiment based on the availability of sufficient materials and on the phenotypic characterization described above. We pooled equivalent polysome fractions (fractions #11-#25), verified by consistent polysome profiles and post-fractionation RNA concentrations (Fig. 5A). These samples were then used for RNA isolation followed by RNA sequencing (RNA-Seq) and bioinformatic analyses. Total mRNAs from corresponding brain tissues were directly used for RNA-Seq and bioinformatics analyses. Using a threshold of a 1.5-fold change in transcript abundance, we examined changes in total mRNA expression levels between wild type and mutants. Only 15 genes were decreased and 19 were increased at the total mRNA level (Fig. 5B). In contrast, when we examined changes in mRNA levels from polysome fractions, 368 genes were significantly decreased in the mutant polysome fractions, and 187 genes were found to be significantly increased (Fig. 5B). Individual mRNA expression level changes are depicted in volcano plots, in which blue and red colorized dots represent decreased or increased gene expression levels, while gray dots indicate unchanged genes. Again, the aberrations in transcript abundance between control and *Lin28a/b*

**Figure 2.5. Lin28-mediated translation regulation revealed by sucrose density gradient fractionation coupled with RNA-seq analysis.**



(A) Fractions containing polysomes from control and *Lin28a/b* mutant cortical tissues were illustrated through polysome profiling studies, and corresponding fractions (#11-#25) were confirmed by measuring RNA concentration. (B) RNA-seq and bioinformatics analyses of total RNAs or RNAs from polysome fractions derived from E11.5 embryonic brains. Venn diagrams show total and polysome-associated mRNAs that change in abundance in *Lin28a/b* double mutants compared to controls. Only 1.5 fold increased or decreased mRNA expression in mutants compared to controls are considered in the analyses. (C) Volcano plots show gene-expression levels relative to controls from bioinformatic study; blue dots represent transcripts significantly decreased; red dots represent transcripts significantly increased; and grey dots represent statistically unchanged levels. (D-G) Gene set enrichment analysis (GSEA) of polysome-associated mRNAs for gene sets involved in cell cycle (D), ribosome biogenesis (E), translation (F), and mTORC1 signaling (G). Each line represents a single gene in the gene set. (H)

Analysis of RNA-Seq data from total mRNAs and polysome-associated mRNAs reveals translational regulation of genes involved in cell cycle, neural differentiation, ribosome biogenesis and translation. (I, K, M) Western blot analyses of the expression of proteins as indicated using cortical tissues from E11.5 *Lin28a/b* mutant and control embryos. I, K, and M emphasize on proteins involved in the regulation of cell cycle, ribosome biogenesis, and mTORC1 signaling, respectively. (J, L, N) Quantification of western blot data from 3 independent experiments (\*:  $p \leq 0.05$ , \*\*\*:  $p \leq 0.001$ , ns: not significant; Student's t-test).

mutants was much more pronounced in polysome mRNAs compared to total mRNAs (Fig. 5C). Therefore, the majority of significant changes in transcript abundance occurred within the polysome-associated mRNAs in comparison to total mRNAs. Together, these results indicate that loss of Lin28a/b function results in gene expression changes at the translational level.

To determine the pathways in which these dysregulated genes are involved, we performed gene ontology (GO) and Kyoto Encyclopedia of Genes and Genomes (KEGG) analyses. The most significantly decreased biological pathways included GO terms related to ribosome biogenesis and protein synthesis in mutants (Fig. S2A, Suppl. Table 3). Meanwhile, increased cellular components in mutants included neurotransmitter complexes and the postsynapse, indicating that genes important for neuronal differentiation were upregulated (Fig. S2B). These results are consistent with the precocious differentiation phenotype observed in Lin28a<sup>-/-</sup>b<sup>-/-</sup> mutants. Gene set enrichment analysis (GSEA) suggested that Lin28a/b deletion results in down-regulation of genes involved in the regulation of cell cycle, ribosome biogenesis, mTORC1 signaling, and translation (Fig. 5D-5G). To validate our RNA-Seq data, we re-analyzed those top dysregulated genes with published biological significance in brain development. We found that genes related to the cell cycle and protein synthesis were substantially reduced in polysome-associated mRNA but not in total mRNA measurement (Fig. 5H), suggesting their translational dysregulation. Western blot analysis confirmed down-regulation of protein levels of genes involved in the cell cycle (Fig. 5I-5J) and ribosome biogenesis (Fig. 5K-5L).

Mammalian target of rapamycin complex 1 (mTORC1) is a master regulator of protein synthesis (Laplante & Sabatini, 2012). Our previous studies showed that Lin28a is associated with mRNAs encoding components of mTORC1 signaling (M. Yang et al., 2015). Therefore, we examined mTORC1 activation. S6-kinase (S6K) is phosphorylated by mTORC1, and Ribosomal Protein S6 (S6) is phosphorylated in turn by S6K, initiating protein translation (Ferrari, Regina Bandi, Hofsteenge, Russian, & Thomas, 1991; Fingar et al., 2004). Western blot results showed that the expression levels of pS6K and pS6 240/244 were significantly reduced in mutants compared to controls (Fig. 5M-5N). To examine mTORC1 signaling in vivo, we performed IHC on hindbrain regions of the neural tube. Both pS6 240/244 and pS6 235/236 signal intensities were reduced in E11.5 but not E9.5 mutant neuroepithelium (Fig. S3). Altogether, these data suggest that Lin28a/b enhance mTORC1 signaling and promote translation of genes involved in the cell cycle and ribosome biogenesis.

#### Lin28 is expressed in nucleoli and promotes ribosome biogenesis in NPCs

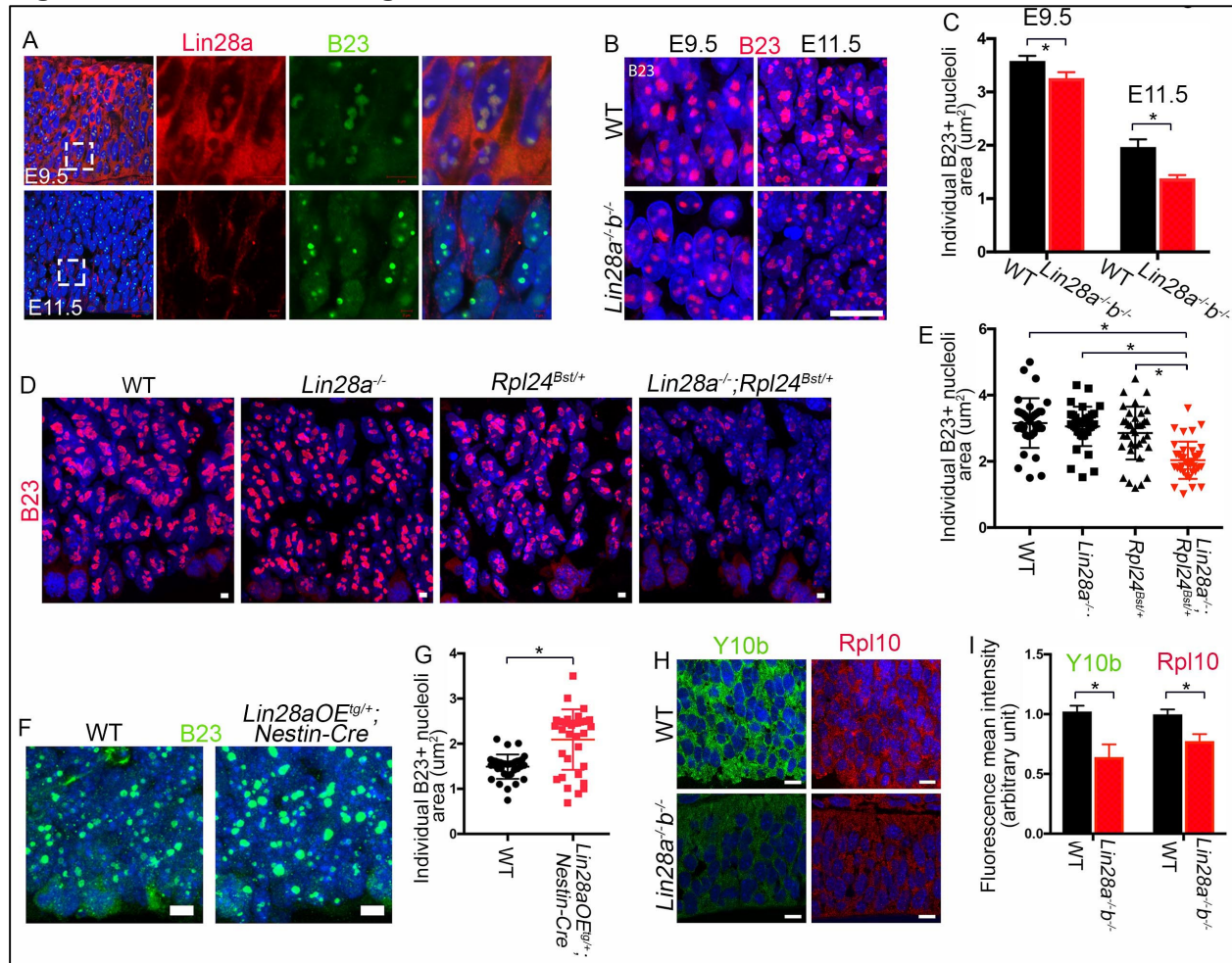
RNA-Seq data revealed that genes with decreased expression in Lin28a/b mutant polysomes are linked with various pathways related to ribosome biogenesis, including 5.8S ribosome maturation, ribonucleoprotein complex biogenesis, and rRNA processing (Fig. S2A, Suppl. Table 3). Western blotting confirmed the downregulation of proteins involved in ribosome biogenesis (Fig. 5K-5L). Previous studies showed that Lin28 localizes to both the nucleolar precursor body (NPB) and mature nucleolus in ES cells and mouse preimplantation embryos (Vogt, Meglicki, Hartung, Borsuk, & Behr, 2012). Therefore, these results provoked us to examine the nucleolus, the site of ribosome biogenesis. In addition to the cytoplasm, Lin28a is also highly enriched in the

nucleoli, labeled by Nucleophosmin (also known as Npm1 or B23), of NPCs during early brain development (Fig. 6A). As development progresses, Lin28a's nucleolar localization is eliminated at E13.5, whereas its cytoplasmic expression can be detected at this stage (Fig. 6A).

The nucleolus is the site of ribosomal RNA transcription and initial ribosome subunit assembly. Nucleolar size is indicative of ribosome biogenesis and growth (Baker, 2013; Derenzini et al., 2000), and is proportional to the rapidity of cell proliferation in cancer cells (Derenzini et al., 2000). Lin28a's localization in nucleoli paired with reduced ribosome protein expression and proliferation in mutant NPCs prompted us to examine nucleolar size in *Lin28a/b* mutant neural tubes. Using B23 to label nucleoli, we found that average nucleolar size was significantly decreased in NPCs at both E9.5 and E11.5 in the mutant neural tube (Fig. 6B-6C), whereas nucleolar numbers appeared normal. In addition to serving as a nucleolar marker, B23 protein has endonuclease activities required for appropriate ribosomal RNA maturation (Savkur & Olson, 1998). Reduced B23 expression is correlated with reduced rRNA transcription (Murano, Okuwaki, Hisaoka, & Nagata, 2008). Western blotting confirmed that the B23 protein level was significantly reduced in *Lin28a/b* mutant neural tube tissues (Fig. 5K-5L). Overall, these data indicate that ribosome biogenesis is defective in mutant NPCs.

Next we examined nucleolus size in *Lin28a*<sup>-/-</sup>, *Rpl24*<sup>Bst/+</sup>, and compound mutant neural tubes. *Lin28a*<sup>-/-</sup>; *Rpl24*<sup>Bst/+</sup> compound mutants exhibited a significant decrease in individual B23-positive nucleolar area compared to *Lin28a*<sup>-/-</sup> and *Rpl24*<sup>Bst/+</sup> mutants (Fig. 6D-6E). These results suggest that Lin28a and Rpl24 function together to promote protein synthesis, at least in part, through regulation of protein synthesis. Conversely,

**Figure 2.6. Ribosome biogenesis is defective in *Lin28a/b* mutant NPCs.**



(A) Confocal images of hindbrain sections stained with antibodies against Nucleophosmin (B23, green) and Lin28a (red). Hoechst stains nuclei (blue). Middle and right panels are enlargement of white boxed areas in leftmost panels. Scale bars: 20  $\mu\text{m}$  (leftmost panels); 5  $\mu\text{m}$  (middle and right panels). (B) Confocal images of E9.5 or E11.5 hindbrain coronal sections stained with antibodies against Nucleophosmin (B23, red). Hoechst stains nuclei (blue). Scale bar: 10  $\mu\text{m}$ . (C) Quantification of nucleoli mean area from images represented in B. (\* $p \leq 0.05$ , Student's t-test). (n  $\geq 3$  sections per genotype from n = 3 litters). (D) Confocal images of E9.5 hindbrain coronal sections from different mutants as indicated. Sections were stained with antibodies against Nucleophosmin (B23, red). Hoechst stains nuclei (blue). Scale bar: 2  $\mu\text{m}$ . (E) Quantification of individual B23-positive nucleoli area from images represented in D. (n=3 and 36 individual nucleoli were counted for each experiment, \* $p \leq 0.05$ , Student's t-test). (F) Confocal images of coronal sections of E18.5 cerebral cortex with genotypes as indicated. Sections were stained with antibodies against Nucleophosmin (B23, green). Hoechst stains nuclei (blue). Scale bar: 5  $\mu\text{m}$ . (G) Quantification of individual B23-positive nucleoli areas from images represented in F. (n=3, and 35 individual nucleoli in each experiment, \* $p \leq 0.05$ , Student's t-test). (H) Confocal images of E9.5 hindbrain sections stained with antibodies against Y10b (green) and Rpl10 (red). Hoechst stains nuclei (blue). Scale bar: 10  $\mu\text{m}$ .

(I) Quantification of fluorescence mean intensity for Y10b and Rpl10 signal as depicted in H. (n=3 of 3 sections each were analyzed, \*p ≤ 0.05, Student's t-test).

we found a substantial increase in nucleolar size in Lin28a-overexpressing NPCs (Fig. 6F-6G). These results suggest that Lin28a is sufficient to promote nucleolar size enhancement and ribosome biogenesis. Monoclonal anti-rRNA antibody Y10b specifically labels the 28S subunit of rRNA and serves as a marker of mature ribosomal integrity (Garden, Hartlage-Rübsamen, Rubel, & Bothwell, 1995; Lerner, Lerner, Janeway, & Steitz, 1981). We observed significantly reduced Y10b immunoreactivity in dKO neuroepithelium compared to controls (Fig. 6H-6I). The expression of ribosomal protein Rpl10, a key protein in assembling the 60S ribosomal subunit (Ferreira-Cerca, Pöll, Gleizes, Tschochner, & Milkereit, 2005), was also reduced in mutant neuroepithelium (Fig. 6H-6I, 5K-5L). Together, these results suggest that ribosomal biogenesis is defective in NPCs, which could contribute to the deficits in protein synthesis and NTDs in Lin28a/b mutants.

### Discussion

This study revealed that Lin28 acts in the cytoplasm and nucleolus to promote mTORC1 signaling, mRNA translation, and ribosome biogenesis, which collectively enhance protein synthesis. Given Lin28's specific enrichment in early development, our mouse genetic studies demonstrated that Lin28-mediated temporal promotion of protein synthesis is essential for NPC maintenance and early brain development.

One of the key discoveries presented here is that Lin28 promotes, rather than inhibits, protein synthesis in NPCs and early brain development in vivo. Lin28a's role in translation regulation remains unclear. Lin28a could inhibit the translation of a subset of mRNAs destined for the ER in ES cells (Cho et al., 2012). On the other hand, Lin28a

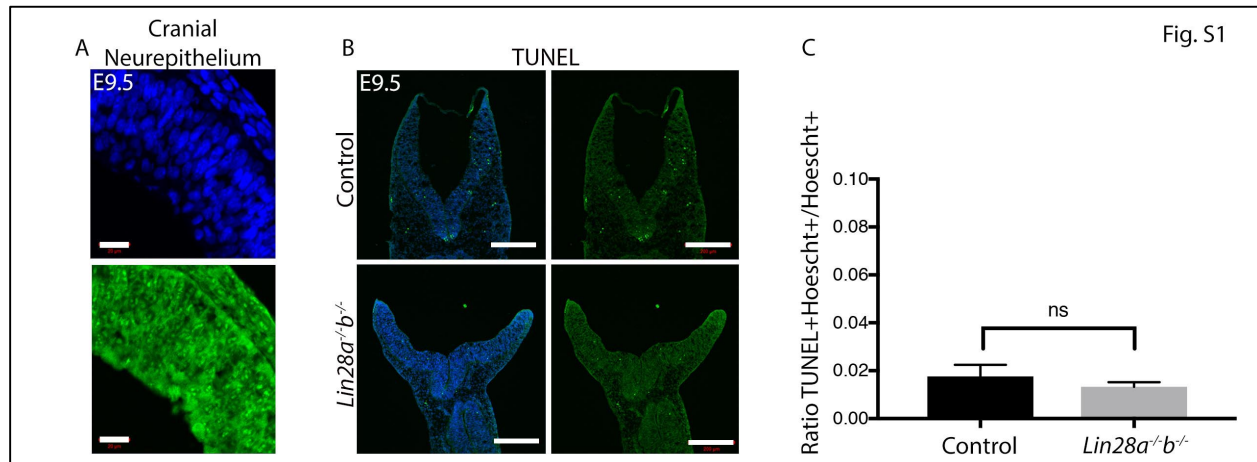
acts as a 'translational enhancer' in muscle precursor cells (Poleskaya et al., 2007). We previously found that Lin28a is linked with mTORC1 signaling and mRNA translation in the developing brain (M. Yang et al., 2015). However, these correlation studies could not determine the causative relationship between Lin28 and translation promotion or its functional significance, which thus constituted the main focus of the present work. Our previous studies showed that Lin28a depletion alone causes mild microcephaly without an impact on animal survival (M. Yang et al., 2015). Here we showed that further dampening global protein synthesis by Rpl24Bst/+ in the background of Lin28a<sup>-/-</sup> leads to NTDs and embryonic lethality, which resemble the phenotypes of Lin28a/b dKO mice and are more severe than those seen in Lin28a single knockout mice. These results provide the genetic evidence that Lin28 promotes protein synthesis in the developing brain. Our polysome fractionation paired with RNA-sequencing studies further support the notion that Lin28 promotes mRNA translation of specific genes involved in the cell cycle, ribosome biogenesis, and translation. While it appears that our RNA-Seq analysis of polysome-associated mRNAs did not identify all mRNAs dysregulated at total mRNA levels, most of these genes were indeed found to be dysregulated, but at lower fold levels than the 1.5 fold used in our analyses. Further more comprehensive validation of RNA-Seq data is necessary to confirm specific genes regulated by Lin28 at the translational level.

The second discovery presented here is that Lin28-mediated protein synthesis is essential for NPC maintenance and early brain development. Previous research has not characterized Lin28a/b dKO embryonic phenotypes. Although Lin28's involvement in translational regulation has been reported in cultured cells (Cho et al., 2012; Poleskaya

et al., 2007; Shyh-Chang et al., 2013), the biological significance of Lin28-mediated translation is unknown on the organismic level. We found that Lin28a/b dKO mice exhibited reduced proliferation and precocious differentiation of NPCs, leading to NTDs. Decreasing protein synthesis by Rpl24Bst/+ in the background of Lin28a-/- further exacerbated the phenotypes seen in Lin28a-/- and led to NTDs, which resembled the phenotypes of Lin28a/b dKO mice. These results indicate that Lin28a/b's regulation of neural tube closure, at least in part, functions through promoting protein synthesis. Furthermore, the abnormally increased brain size and ratio of apical to intermediate NPCs in Lin28a-overexpressing mice were rescued by Rpl24Bst/+ heterozygosity. These results suggest that Lin28-mediated promotion of protein synthesis is sufficient to promote proliferation, alter NPC cell fate, and drive brain growth. RBPs can modulate cell fate and pluripotency in ES cells via regulating mRNA translation (Ye & Blelloch, 2014). Changes in rRNA transcription influence proliferation and cell fate in ovarian germline stem cells (GSCs) (Zhang, Shalaby, & Buszczak, 2014). Together with these discoveries, our studies emphasize that protein synthesis is tightly linked with the proliferation and cell fate of stem/progenitor cells. It is important to investigate whether, at late stages, Rpl24Bst/+ heterozygosity can rescue macrocephaly in Lin28a-overexpressing mice. Unfortunately, NPC-specific overexpression of Lin28a led to variable postnatal phenotypes including reduced body size and postnatal death (Fig. S4). Rpl24Bst/+ heterozygous mice had a reduced body size and exhibited enhanced apoptosis and mitotic arrest in the cerebral cortex at later developmental stages. These complications prevented us from further long-term investigation.

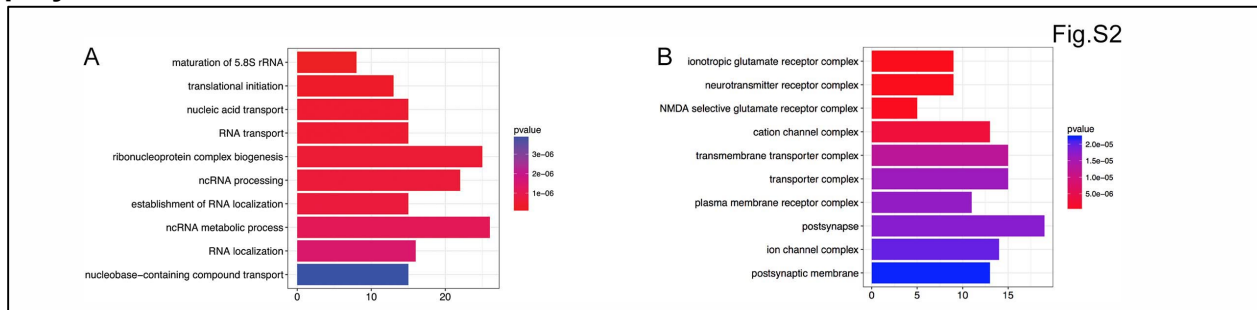
Our studies identify ribosome biogenesis as a novel action mechanism of Lin28 in promoting protein synthesis. First, Lin28a expression is enriched in the nucleoli, where ribosome biogenesis occurs, in NPCs during early development. Nucleolar size is indicative of ribosome biogenesis (Baker, 2013; Montanaro, Treré, & Derenzini, 2008), and is proportional to the rapidity of cell proliferation (Derenzini et al., 2000). Second, nucleolar size was significantly reduced in Lin28a/b mutant NPCs, and conversely was increased in Lin28a-overexpressing NPCs. Lin28a<sup>-/-</sup>;Rpl24Bst<sup>+/+</sup> mutants exhibited a reduction in individual nucleolar area compared to Lin28a<sup>-/-</sup> and Rpl24Bst<sup>+/+</sup> mutants. These data suggest that Lin28a and Rpl24 functionally interact to regulate ribosome biogenesis. Third, ribosomal integrity is defective in Lin28a/b mutant neuroepithelium, as revealed by reduced expression of Y10b and Rpl10. Together, these results suggest that Lin28 is necessary and sufficient to modulate nucleolar size and ribosome biogenesis, disruption of which may contribute to protein synthesis reduction in Lin28a/b mutant neuroepithelium. It is well established that Lin28 represses Let-7 (Hagan, Piskounova, & Gregory, 2009; Piskounova et al., 2011). However, it is technically challenging to determine whether and to what extent knocking out Let-7 can rescue Lin28a/b mutant phenotypes because there are more than ten Let-7 loci in the mouse genome (Lee, Han, Kwon, & Lee, 2016; Roush & Slack, 2008). Lin28 promotes mTORC1 signaling, a master regulator of protein synthesis (Laplante & Sabatini, 2012). Future study should dampen mTORC1 activity to determine to what extent Lin28-mediated promotion of protein synthesis proceeds through mTORC1 signaling.

**Supplemental Figure 2.S1. Lin28a expression and TUNEL analysis of Lin28a/b mutants.**



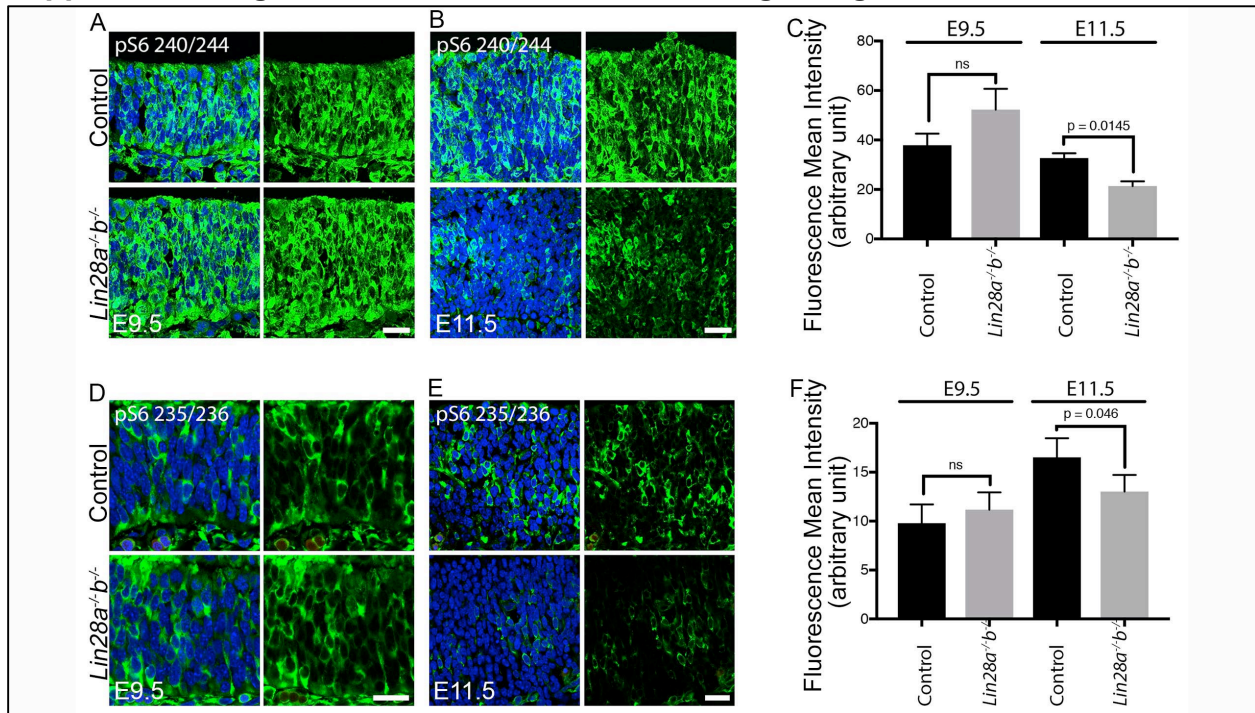
(A) Representative confocal images of E9.5 hindbrain sections stained with antibodies against Lin28a (green). Hoechst stains nuclei (blue). Scale bar: 20  $\mu\text{m}$  (B) TUNEL analyses identify no change in apoptosis between control and *Lin28a/b* mutant hindbrain. Scale bar: 200  $\mu\text{m}$ . (C) Quantification of the percentage of TUNEL<sup>+</sup> cells out of total cells in experiment B. ( $p = 0.4525$ ; Student's t-test). ( $n = 3$  sections from  $n = 3$  somite-matched control and *Lin28a/b* mutant sections).

**Supplemental Figure 2.S2. GO term analysis of dysregulated genes in mutant polysome mRNAs.**



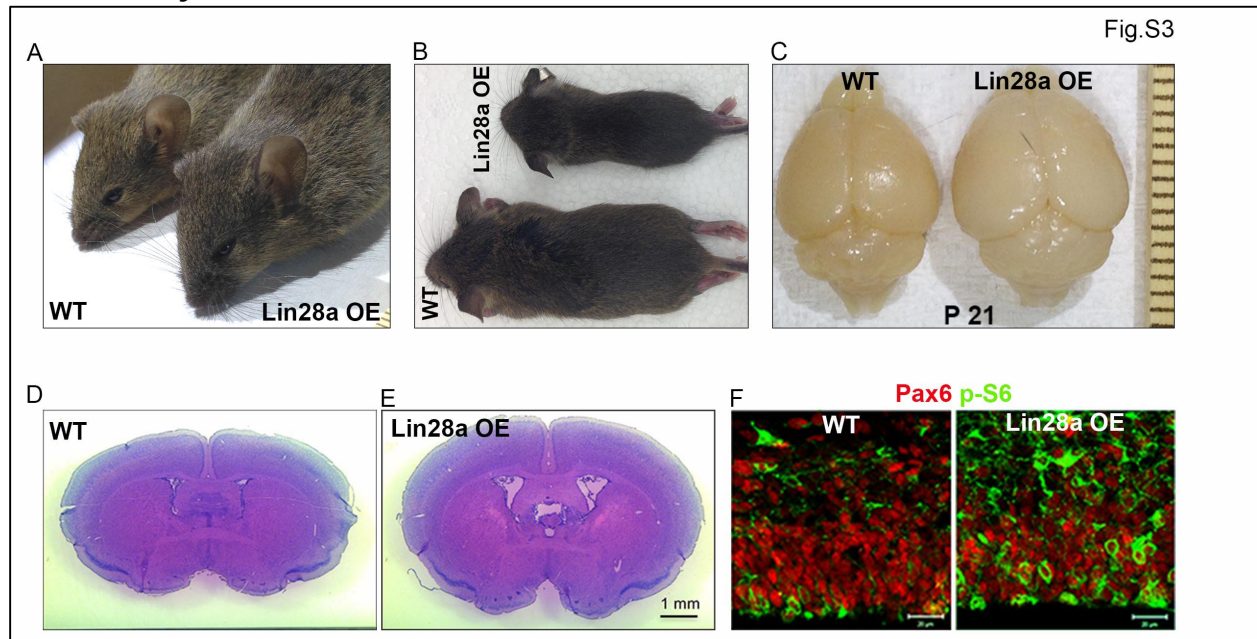
(A) GO term analysis for biological pathways from genes decreased by at least 1.5 fold.  
 (B) GO term analysis for cellular components from genes increased by at least 1.5 fold.

**Supplemental Figure 2.S3. Decreased mTORC1 signaling in *Lin28a/b* mutants.**



(A, B) Confocal images of coronal sections stained with antibodies against pS6 240/244 (green) from hindbrain areas of E9.5 (A) or E11.5 (B) embryos. Hoechst stains nuclei (blue). Scale bar: 25  $\mu$ m. (C) Quantification of fluorescence mean intensity of pS6 240/244 staining from experiments A, B from whole neuroepithelium in hindbrain sections (E9.5: ns represents not significant; E11.5:  $p = 0.0145$ , Student's t-test;  $n \geq 3$  sections per genotype from  $n = 3$  litters). (D) Confocal images of coronal sections stained with antibodies against pS6 235/236 (green) from hindbrain areas of E9.5 (D) or E11.5 (E) embryos. Hoechst stains nuclei (blue). Scale bar: 25  $\mu$ m. (F) Quantification of fluorescence mean intensity of pS6 235/236 staining from experiments D, E from whole neocortex in hindbrain sections (E9.5: ns represents not significant; E11.5:  $p = 0.046$ , Student's t-test;  $n \geq 3$  sections per genotype from  $n = 3$  litters).

**Supplemental Figure 2.S4. Lin28a overexpression results in macrocephaly and altered body sizes.**



(A, B) Nestin-Cre directed Lin28a overexpression (Lin28a OE) in NPCs resulted in enlarged (A) or decreased (B) body sizes. (C) Dorsal view of postnatal 21 (P21) Wt and Lin28a overexpression mouse brains. (D, E) H&E staining of adult coronal mouse brain sections. (F) Confocal images of coronal sections stained with antibodies against pS6 (green) and Pax6 (red) in Wt and Lin28a overexpression cerebral cortex.

## References

- Baker, N. E. (2013). Developmental Regulation of Nucleolus Size during *Drosophila* Eye Differentiation. *PLOS ONE*, 8(3), e58266. Retrieved from <https://doi.org/10.1371/journal.pone.0058266>
- Balzer, E., Heine, C., Jiang, Q., Lee, V. M., & Moss, E. G. (2010). LIN28 alters cell fate succession and acts independently of the let-7 microRNA during neurogliogenesis in vitro. *Development*, 137(6), 891–900. <http://doi.org/10.1242/dev.042895>
- Barna, M., Pusic, A., Zollo, O., Costa, M., Kondrashov, N., Rego, E., ... Ruggero, D. (2008). Suppression of Myc oncogenic activity by ribosomal protein haploinsufficiency. *Nature*, 456, 971. Retrieved from <http://dx.doi.org/10.1038/nature07449>
- Burns, J. L., & Hassan, A. B. (2001). Cell survival and proliferation are modified by insulin-like growth factor 2 between days 9 and 10 of mouse gestation. *Development (Cambridge, England)*, 128(19), 3819–3830.
- Buszczak, M., Signer, R. A. J., & Morrison, S. J. (2014). Cellular differences in protein synthesis regulate tissue homeostasis. *Cell*, 159(2), 242–251. <http://doi.org/10.1016/j.cell.2014.09.016>
- Chen, E., Sharma, M. R., Shi, X., Agrawal, R. K., & Joseph, S. (2014). Fragile X Mental Retardation Protein Regulates Translation by Binding Directly to the Ribosome. *Molecular Cell*, 54(3), 407–417. <http://doi.org/10.1016/j.molcel.2014.03.023>
- Cho, J., Chang, H., Kwon, S. C., Kim, B., Kim, Y., Choe, J., ... Kim, V. N. (2012).

- LIN28A is a suppressor of ER-associated translation in embryonic stem cells. *Cell*, 151(4), 765–77. <http://doi.org/10.1016/j.cell.2012.10.019>
- Clancy, J. L., Nusch, M., Humphreys, D. T., Westman, B. J., Beilharz, T. H., & Preiss, T. (2007). Methods to Analyze MicroRNA-Mediated Control of mRNA Translation. *Methods in Enzymology*, 431(07), 83–111. [http://doi.org/10.1016/S0076-6879\(07\)31006-9](http://doi.org/10.1016/S0076-6879(07)31006-9)
- Copp, A. J. (2005). Neurulation in the cranial region--normal and abnormal. *Journal of Anatomy*, 207(5), 623–635. <http://doi.org/10.1111/j.1469-7580.2005.00476.x>
- Darnell, J. C., Van Driesche, S. J., Zhang, C., Hung, K. Y. S., Mele, A., Fraser, C. E., ... Darnell, R. B. (2011). FMRP Stalls Ribosomal Translocation on mRNAs Linked to Synaptic Function and Autism. *Cell*, 146(2), 247–261. <http://doi.org/10.1016/j.cell.2011.06.013>
- Derenzini, M., Trerè, D., Pession, A., Govoni, M., Sirri, V., & Chieco, P. (2000). Nucleolar size indicates the rapidity of cell proliferation in cancer tissues. *Journal of Pathology*, 191(2), 181–186. [http://doi.org/10.1002/\(SICI\)1096-9896\(200006\)191:2<181::AID-PATH607>3.0.CO;2-V](http://doi.org/10.1002/(SICI)1096-9896(200006)191:2<181::AID-PATH607>3.0.CO;2-V)
- Doe, C. Q. (2008). Neural stem cells: balancing self-renewal with differentiation. *Development*, 135(9), 1575 LP-1587. Retrieved from <http://dev.biologists.org/content/135/9/1575.abstract>
- Ferrari, S., Regina Bandi, H., Hofsteenge, J., Russian, B. M., & Thomas, G. (1991). Mitogen-activated 70K S6 kinase: Identification of in vitro 40 S ribosomal S6 phosphorylation sites. *Journal of Biological Chemistry*, 266(33), 22770–22773.

- Ferreira-Cerca, S., Pöll, G., Gleizes, P.-E., Tschochner, H., & Milkereit, P. (2005). Roles of Eukaryotic Ribosomal Proteins in Maturation and Transport of Pre-18S rRNA and Ribosome Function. *Molecular Cell*, 20(2), 263–275.  
<http://doi.org/10.1016/j.molcel.2005.09.005>
- Fingar, D. C., Richardson, C. J., Tee, A. R., Cheatham, L., Tsou, C., & Blenis, J. (2004). mTOR Controls Cell Cycle Progression through Its Cell Growth Effectors S6K1 and 4E-BP1 / Eukaryotic Translation Initiation Factor 4E mTOR Controls Cell Cycle Progression through Its Cell Growth Effectors S6K1 and 4E-BP1 / Eukaryotic Translation Initiation. *Molecular and Cellular Biology*, 24(1), 200–216.  
<http://doi.org/10.1128/MCB.24.1.200>
- Garden, G. A., Hartlage-Rübsamen, M., Rubel, E. W., & Bothwell, M. A. (1995). Protein Masking of a Ribosomal RNA Epitope Is an Early Event in Afferent Deprivation-Induced Neuronal Death. *Molecular and Cellular Neuroscience*, 6(3), 293–310.  
<http://doi.org/https://doi.org/10.1006/mcne.1995.1023>
- Greene, N. D. E., & Copp, A. J. (2014). Neural Tube Defects. *Annual Review of Neuroscience*, 37(1), 221–242. <http://doi.org/10.1146/annurev-neuro-062012-170354>
- Guzman-Ayala, M., Sachs, M., Koh, F. M., Onodera, C., Bulut-Karslioglu, A., Lin, C.-J., ... Ramalho-Santos, M. (2014). Chd1 is essential for the high transcriptional output and rapid growth of the mouse epiblast. *Development (Cambridge, England)*, 118–127. <http://doi.org/10.1242/dev.114843>
- Hagan, J. P., Piskounova, E., & Gregory, R. I. (2009). Lin28 recruits the TUTase

- Zcchc11 to inhibit let-7 maturation in mouse embryonic stem cells. *Nature Structural & Molecular Biology*, 16, 1021. Retrieved from <http://dx.doi.org/10.1038/nsmb.1676>
- Jessell, T. M. (2000). Neuronal specification in the spinal cord: inductive signals and transcriptional codes. *Nature Reviews Genetics*, 1, 20. Retrieved from <http://dx.doi.org/10.1038/35049541>
- Kondrashov, N., Pusic, A., Stumpf, C. R., Shimizu, K., Hsieh, A. C., Xue, S., ... Barna, M. (2011). Ribosome-mediated specificity in Hox mRNA translation and vertebrate tissue patterning. *Cell*, 145(3), 383–397. <http://doi.org/10.1016/j.cell.2011.03.028>
- Kraushar, M. L., Thompson, K., Wijeratne, H. R. S., Viljetic, B., Sakers, K., Marson, J. W., ... Rasin, M.-R. (2014). Temporally defined neocortical translation and polysome assembly are determined by the RNA-binding protein Hu antigen R. *Proceedings of the National Academy of Sciences of the United States of America*, 111(36), E3815-24. <http://doi.org/10.1073/pnas.1408305111>
- Kuan, C.-Y., Roth, K. A., Flavell, R. A., & Rakic, P. (2000). Mechanisms of programmed cell death in the developing brain. *Trends in Neurosciences*, 23(7), 291–297. [http://doi.org/10.1016/S0166-2236\(00\)01581-2](http://doi.org/10.1016/S0166-2236(00)01581-2)
- Kwon, S. C., Yi, H., Eichelbaum, K., Föhr, S., Fischer, B., You, K. T., ... Kim, V. N. (2013). The RNA-binding protein repertoire of embryonic stem cells. *Nature Structural & Molecular Biology*, 20, 1122. Retrieved from <http://dx.doi.org/10.1038/nsmb.2638>
- Laplanche, M., & Sabatini, D. M. (2012). mTOR signaling in growth control and disease.

*Cell*, 149(2), 274–293. <http://doi.org/10.1016/j.cell.2012.03.017>

Lee, H., Han, S., Kwon, C. S., & Lee, D. (2016). Biogenesis and regulation of the let-7 miRNAs and their functional implications. *Protein & Cell*, 7(2), 100–113. <http://doi.org/10.1007/s13238-015-0212-y>

Lerner, E. A., Lerner, M. R., Janeway, C. A., & Steitz, J. A. (1981). Monoclonal antibodies to nucleic acid-containing cellular constituents: probes for molecular biology and autoimmune disease. *Proceedings of the National Academy of Sciences of the United States of America*, 78(5), 2737–2741. Retrieved from <http://www.ncbi.nlm.nih.gov/pmc/articles/PMC319432/>

Love, M. I., Huber, W., & Anders, S. (2014). Moderated estimation of fold change and dispersion for RNA-seq data with DESeq2. *Genome Biology*, 15(12), 550. <http://doi.org/10.1186/s13059-014-0550-8>

Montanaro, L., Treré, D., & Derenzini, M. (2008). Nucleolus, Ribosomes, and Cancer. *The American Journal of Pathology*, 173(2), 301–310. <http://doi.org/10.2353/ajpath.2008.070752>

Moss, E. G., Lee, R. C., & Ambros, V. (1997). The cold shock domain protein LIN-28 controls developmental timing in *C. elegans* and is regulated by the lin-4 RNA. *Cell*, 88(5), 637–646. [http://doi.org/10.1016/S0092-8674\(00\)81906-6](http://doi.org/10.1016/S0092-8674(00)81906-6)

Murano, K., Okuwaki, M., Hisaoka, M., & Nagata, K. (2008). Transcription Regulation of the rRNA Gene by a Multifunctional Nucleolar Protein, B23/Nucleophosmin, through Its Histone Chaperone Activity. *Molecular and Cellular Biology*, 28(10), 3114–3126. <http://doi.org/10.1128/MCB.02078-07>

- Piskounova, E., Polytarchou, C., Thornton, J. E., LaPierre, R. J., Pothoulakis, C., Hagan, J. P., ... Gregory, R. I. (2011). Lin28A and Lin28B Inhibit let-7 MicroRNA Biogenesis by Distinct Mechanisms. *Cell*, *147*(5), 1066–1079.  
<http://doi.org/https://doi.org/10.1016/j.cell.2011.10.039>
- Poleskaya, A., Cuvellier, S., Naguibneva, I., Duquet, A., Moss, E. G., & Harel-Bellan, A. (2007). Lin-28 binds IGF-2 mRNA and participates in skeletal myogenesis by increasing translation efficiency. *Genes and Development*, *21*(9), 1125–1138.  
<http://doi.org/10.1101/gad.415007>
- Roush, S., & Slack, F. J. (2008). The let-7 family of microRNAs. *Trends in Cell Biology*, *18*(10), 505–516. <http://doi.org/https://doi.org/10.1016/j.tcb.2008.07.007>
- Savkur, R. S., & Olson, M. O. J. (1998). Preferential cleavage in pre-ribosomal RNA by protein B23 endoribonuclease. *Nucleic Acids Research*, *26*(19), 4508–4515.  
<http://doi.org/10.1093/nar/26.19.4508>
- Shao, Q., Herrlinger, S., Yang, S.-L., Lai, F., Moore, J. M. J. M., Brindley, M. A. M. A., & Chen, J.-F. J.-F. (2016). Zika virus infection disrupts neurovascular development and results in postnatal microcephaly with brain damage. *Development (Cambridge, England)*, *143*(22), 4127–4136. <http://doi.org/10.1242/dev.143768>
- Shao, Q., Herrlinger, S., Zhu, Y.-N., Yang, M., Goodfellow, F., Stice, S. L. S. L., ... Chen, J.-F. J.-F. (2017). The African Zika virus MR-766 is more virulent and causes more severe brain damage than current Asian lineage and Dengue virus. *Development*, *144*(22). <http://doi.org/10.1242/dev.156752>
- Shi, Z., & Barna, M. (2015). Translating the Genome in Time and Space: Specialized

Ribosomes, RNA Regulons, and RNA-Binding Proteins. *Annual Review of Cell and Developmental Biology*, 31(1), 31–54. <http://doi.org/10.1146/annurev-cellbio-100814-125346>

Shinoda, G., Shyh-Chang, N., Soysa, T. Y., Zhu, H., Seligson, M. T., Shah, S. P., ... Daley, G. Q. (2013). Fetal deficiency of lin28 programs life-long aberrations in growth and glucose metabolism. *Stem Cells*, 31(8), 1563–1573. <http://doi.org/10.1002/stem.1423>

Shyh-Chang, N., & Daley, G. Q. (2013). Lin28: Primal regulator of growth and metabolism in stem cells. *Cell Stem Cell*, 12(4), 395–406. <http://doi.org/10.1016/j.stem.2013.03.005>

Shyh-Chang, N., Zhu, H., Yvanka de Soysa, T., Shinoda, G., Seligson, M. T., Tsanov, K. M., ... Daley, G. Q. (2013). Lin28 enhances tissue repair by reprogramming cellular metabolism. *Cell*, 155(4), 778–92. <http://doi.org/10.1016/j.cell.2013.09.059>

Signer, R. A. J., Magee, J. A., Salic, A., & Morrison, S. J. (2014). Haematopoietic stem cells require a highly regulated protein synthesis rate. *Nature*, 508(7498), 49–54. <http://doi.org/10.1038/nature13035>

Thornton, J. E., & Gregory, R. I. (2012). How does Lin28 let-7 control development and disease? *Trends in Cell Biology*, 22(9), 474–82. <http://doi.org/10.1016/j.tcb.2012.06.001>

Vogt, E. J., Meglicki, M., Hartung, K. I., Borsuk, E., & Behr, R. (2012). Importance of the pluripotency factor LIN28 in the mammalian nucleolus during early embryonic development. *Development*, 139(24), 4514–4523.

<http://doi.org/10.1242/dev.083279>

Wallingford, J. B., Niswander, L. A., Shaw, G. M., & Finnell, R. H. (2013). The Continuing Challenge of Understanding, Preventing, and Treating Neural Tube Defects. *Science*, 339(6123), 1047–1055. <http://doi.org/10.1038/nrn1986>

Yang, M., Yang, S.-L., Herrlinger, S., Liang, C., Dzieciatkowska, M., Hansen, K. C., ... Chen, J.-F. (2015). Lin28 promotes the proliferative capacity of neural progenitor cells in brain development. *Development*, 142(9), 1616–1627. <http://doi.org/10.1242/dev.120543>

Yang, S.-L., Yang, M., Herrlinger, S., Liang, C., Lai, F., & Chen, J.-F. J.-F. (2015). MiR-302/367 regulate neural progenitor proliferation, differentiation timing, and survival in neurulation. *Developmental Biology*, 408(1), 140–150. <http://doi.org/10.1016/j.ydbio.2015.09.020>

Ye, J., & Blelloch, R. (2014). Regulation of pluripotency by RNA binding proteins. *Cell Stem Cell*, 15(3), 271–280. <http://doi.org/10.1016/j.stem.2014.08.010>

Yu, G., Wang, L.-G., Han, Y., & He, Q.-Y. (2012). clusterProfiler: an R Package for Comparing Biological Themes Among Gene Clusters. *OMICS: A Journal of Integrative Biology*, 16(5), 284–287. <http://doi.org/10.1089/omi.2011.0118>

Zhang, Q., Shalaby, N. A., & Buszczak, M. (2014). Changes in rRNA Transcription Influence Proliferation and Cell Fate-Science2014.pdf, 343(January), 298–302.

CHAPTER 3  
ESTABLISHING MOUSE MODELS FOR ZIKA VIRUS-INDUCED NEUROLOGICAL  
DISORDERS USING INTRACEREBRAL INJECTION STRATEGIES: EMBRYONIC,  
NEONATAL, AND ADULT<sup>1</sup>

---

<sup>1</sup>Stephanie A. Herrlinger, Qiang Shao, Li Ma, Melinda Brindley, Jian-Fu Chen. 2018. *Journal of Visualized Experiments (JoVE)*. (134), e56486, doi:10.3791/56486. Reprinted here with permission of the publisher. URL: <https://www.jove.com/video/56486>

## Abstract

The Zika virus (ZIKV) is a flavivirus currently endemic in North, Central, and South America. It is now established that the ZIKV can cause microcephaly and additional brain abnormalities. However, the mechanism underlying the pathogenesis of ZIKV in the developing brain remains unclear. Intracerebral surgical methods are frequently used in neuroscience research to address questions about both normal and abnormal brain development and brain function. This protocol utilizes classical surgical techniques and describes methods that allow one to model ZIKV- associated human neurological disease in the mouse nervous system. While direct brain inoculation does not model the normal mode of virus transmission, the method allows investigators to ask targeted questions concerning the consequence after ZIKV infection of the developing brain. This protocol describes embryonic, neonatal, and adult stages of intraventricular inoculation of ZIKV. Once mastered, this method can become a straightforward and reproducible technique that only takes a few hours to perform.

## Introduction

Microcephaly is a condition resulting from defective brain development characterized by smaller than average head size in newborns. Children with microcephaly exhibit a range of symptoms which can include developmental delay, seizure, intellectual disability, hearing loss, vision problems, and problems with movement and balance, among others, depending on the severity of the disease and cause (Dreher et al., 2014; Lanzieri et al., 2017; Naseer et al., 2017). This condition is multifactorial in nature, with genetic, infectious agent, and environmental factors linked to causing microcephaly (Abuelo, 2007; Herrlinger, Shao, Ma, Brindley, & Chen, 2018; C. Li et al., 2016; Miki, Fukui, Takeuchi, & Itoh, 1995; Nicholas et al., 2010; Pulvers et al., 2010). Prior to the 2015 - 2016 ZIKV outbreak, 8 children out of 10,000 births were diagnosed with microcephaly in the United States according to the CDC (Cragan et al., 2016). On February 1<sup>st</sup> of 2016 the World Health Organization declared the Zika virus a Public Health Emergency of International Concern due to the alarming increase in microcephaly diagnoses associated with ZIKV infection in mothers (Cragan et al., 2017; Mlakar et al., 2016). A recent study from the CDC on ZIKV cases in the United States suggests that maternal ZIKV infection results in a 20-fold increased risk for a child to develop microcephaly compared to uninfected individuals, and 4% of ZIKV infected mothers from the USA have resulted in children with microcephaly (Cragan et al., 2017). The rate of microcephaly-associated birth defects during pregnancy from ZIKV infection in Brazil have been reported to have affected up to 17% of babies in infected mothers, indicating that other factors in Latin America may be contributing to the increased risk (Jaenisch, Rosenberger, Brito, & Brady, 2017). While we know that the ZIKV can cause

microcephaly and pathogenesis in the neural progenitor cell (NPC) population (Clancy, Darlington, & Finlay, 2001; C. Li et al., 2016; Qiang Shao et al., 2016) the complete pathogenesis of ZIKV in the developing brain remains elusive. It is important to develop animal models to further investigate the disease mechanisms underlying the brain abnormalities associated with ZIKV infection.

To directly study the effect that the ZIKV has on brain development, we first developed a mouse model using intracerebral inoculation of embryonic day 14.5 (E14.5) brain with ZIKV (Qiang Shao et al., 2016). This stage was chosen as it is considered representative of the end of the first trimester in human gestation (Clancy et al., 2001). Pups can survive up to postnatal day 5 (P5) with this embryonic intracerebral injection method (~ 1  $\mu$ L of  $1.7 \times 10^6$  tissue culture infective dose (TCID<sub>50</sub>/mL)). These postnatal pups exhibit a range of phenotypes similarly observed in infected human infants including enlarged ventricles, neuronal loss, axonal rarefaction, astrogliosis, and microglial activation (Driggers et al., 2016; Mlakar et al., 2016). A newborn mouse brain is relatively immature, akin to the developmental stage of the human brain at mid-gestation (Semple, Blomgren, Gimlin, Ferriero, & Noble-Haeusslein, 2013), and mouse brain development includes a major postnatal component. To study later gestation stage infections, a method for postnatal infection is also described. Neonates infected with ZIKV at P1 are able to survive up to 13 days post-injection. Blood-borne adult stage infection has been described in the mouse previously (H. Li et al., 2016) but requires the use of the interferon (IFN) regulatory factor (IRF) transcription factors IRF-3, -5, -7 triple knockout strain. This protocol describes a method of inoculating ZIKV intraventricularly to circumvent disabling the antiviral response of the murine model in the adult. While

this circumvents the murine immune system, this route of injection does not directly mimic the typical route of infection. To address this discrepancy directly, the experimenter can perform an intrauterine infection of ZIKV instead of the intracranial route. Adopted from previous work<sup>18</sup>, we have briefly described this technique in this embryonic infection protocol.

The Zika virus strains implemented with this technique include the Mexican isolate MEX1-44 (Goodfellow et al., 2016; Qiang Shao et al., 2016) and the African isolate MR-766 isolated in 1947 (Dick & Kitchen, 1952). Zika MEX1-44 was isolated in Chiapas, Mexico in January of 2016 from an infected *Aedes aegypti* mosquito. We obtained this virus with permission through the University of Texas Medical Branch at Galveston (UTMB). In addition, the Dengue virus serotype 2 (DENV2) was inoculated using this technique in a comparison study. DENV2, strain S16803 (sequence GenBank GU289914), was isolated from a patient sample from Thailand in 1974 and passaged in C6/36 cells. The virus was passaged twice in Vero cells by the World Reference Center for Emerging Viruses and Arboviruses (WRCEVA) before mouse injections. This demonstrates that this technique works equally well for diverse strains of ZIKV and other flaviviruses that may have an impact on brain development.

### Protocols

All animal use protocols follow the animal care guidelines of the University of Southern California and the University of Georgia. Euthanasia methods for pregnant dams and adults are performed according to approved protocols: carbon dioxide

asphyxiation, followed by cervical dislocation as a secondary method to ensure euthanasia. Neonatal pups are euthanized by decapitation.

Caution: The following protocol involves handling a pathogenic virus. Proper precaution should be taken while handling the virus. All protocols must be approved by the appropriate institutional committee prior to use.

### **1. Embryonic Intracerebral Inoculation of Zika Virus**

1. For timed pregnant mating, consider noon of the day after mating as E0.5. Pair mice at the end of the day and check plugs in the early morning to reduce variability of mating time.
2. Prepare the glass needle prior to surgery. Pull the needle and cut at 1/3 its length, then sharpen at a 45° angle using a micropipette grinder with a water drip until the pore is sized to 50 - 70 µm. Check needle tips under a stereoscope for quality and breakage.
3. Keep the virus aliquot on ice. Just prior to surgery, load the ZIKV injection mix into the prepared glass injection needle. Assemble the gas-tight injection syringe (50 µL volume), luer-lock attachment, and tubing, and saturate the assembled syringe with the tubing with mineral oil. Once saturated, attach the needle, and draw ~ 6 - 7 µL ZIKV into the needle (~ 1 µL is  $1.7 \times 10^6$  TCID<sub>50</sub>/mL).
4. Inject pregnant C57BL/6J or 129S1/SvImJ mice with embryonic day E14.5 embryos (for intracranial injection) or E10.5 embryos (for intrauterine injection) with ketamine hydrochloride (80-100 mg/kg) and xylazine (5-10 mg/kg) diluted in sterile saline solution intraperitoneally to induce anesthesia in the mother.

Alternatively, anesthetize mothers with monitored isoflurane isoflurane provided by inhalation, with waste gas scavenging, if appropriate. Inject buprenorphine-SR (0.5-1.0mg/kg) subcutaneously to induce analgesia.

5. Pinch test anesthetized mothers on the toe tip or tail and then lay them supine on an animal-approved heating pad (thermal pad of 100 x 200 2.5 mm). The toe pinch forceps are not sterile and are not used to handle tissue in surgery. Alternatively, gloved hands may be used to test the toe pinch withdrawal reflex. NOTE: Refer to your institutional veterinary staff for the preferred perioperative heating method. A cover was placed between this heating pad and the animal.
6. Add ophthalmic ointment to the eyes.
7. Shave the surface of the abdomen and sterilize with iodine and alcohol three times. Alternate the iodine and alcohol wipes; wipe in a circular motion away from the surgical site.
8. Drape the skin surrounding the surgical site with sterile cloths to avoid contamination of the incision and the instruments. NOTE: The drape opening should not be larger than the prepared surgical site; no hair should be seen in the drape opening.
9. Pinch the mother's skin away from her abdomen with forceps and cut the lower abdomen in a 1 - 1.5 cm line at the medial sagittal line with sterile surgical scissors. This cuts into the skin and further into the abdominal cavity so that the

embryos are now exposed. NOTE: Surgical scissors are used to incise the skin and peritoneal layer. Sterile instruments and gloves are used for each surgery.

10. Cut a slit in the middle of a small sterile gauze and apply on top of the surgical opening. Hydrate with sterile saline. Pull the embryos through the slit to rest on the sterile gauze, with care to not remove more than 4 - 5 embryos focusing on one uterine horn at one time.

11. Hydrate the embryos with sterile saline prior to and throughout the inoculation to ensure they do not dry out. Keep track of which embryos are injected and their location within the uterine horn. Individual embryos are thus treated as separate experiments, as embryos do not change position while developing *in utero*.

(Continue to step 1.15 for intrauterine injection).

12. Gently place a spatula under the head of the embryo. Illuminate the embryos well with a lamp to visualize the head and skull sutures. NOTE: Aseptic technique is followed, including sterile surgical gloves and instruments. After non-sterile items (such as the lamp) are manipulated, gloves should be replaced with new sterile gloves prior to handling sterile instruments and areas.

13. Position the head by manipulating the embryo with both the lamp (behind the head for visibility) and free fingers until the head of the embryo is pushed up directly against the uterine wall and held in place with the non-dominant hand. NOTE: Positioning the embryo is a critical part and the technique that takes the most practice. Too much finger pressure can damage the embryonic

membranes leading to lethality and not enough pressure can make the injection difficult.

14. Use the blood vessels running along the skull suture as a guide. Inject ZIKV virus (~ 1  $\mu\text{L}$ ,  $1.7 \times 10^6$  TCID<sub>50</sub>/mL Mexican isolate MEX1-44) into the lateral ventricles of E14.5 embryo brains with the assembled syringe and needle. Use control media as a sham injection.
15. To improve retention of the pregnancy, avoid viral injection of the two embryos next to the ovaries and the two embryos next to the upper vagina (**Figure 3.1A**). Overall, no more than 6 embryos are injected per litter to reduce the time of the surgery and prevent embryo loss.
16. Place the injected embryos back into the pregnant dams, and fill the abdominal cavity with ~ 0.5 mL sterile saline. To close, first suture both the abdominal peritoneal muscle and then secondly suture the external skin layer with 4.0 sterile sutures. It is preferable to use interrupted sutures; there is possibility of wound dehiscence if the mouse chews the suture.
17. Place the mouse in a cage partially resting on a heating pad to allow the mouse to escape to a non-heated area if needed. Monitor the mothers while they recover (1 - 2 h) from anesthesia. Develop the embryos after surgery for varied times according to individual experiments.

#### 18. Intrauterine injection

- (1) With one uterine horn and embryos exposed, use a 1 mL syringe and 27G needle to inject 100  $\mu\text{L}$  Zika virus ( $10^6$  TCID<sub>50</sub> units suspended in 100  $\mu\text{L}$  DMEM), or control medium, into the intrauterine space or into the placental

tissue. Note which embryos have been injected for embryonic-stage dissections. See previously published work for more details (Oliveira Melo et al., 2016).

- (2) Place injected embryos back into the pregnant dams, and fill the abdominal cavity with ~ 0.5 mL sterile saline. To close, first suture the abdominal peritoneal muscle and then secondly suture the external skin layer with 4.0 sterile sutures. It is preferable to use interrupted sutures; there is possibility of wound dehiscence if the mouse chews the suture.
- (3) Place the mouse in a cage partially resting on a heating pad to allow the mouse to escape to a non-heated area if needed. Monitor the mothers while they recover (1 - 2 h) from anesthesia. Develop the embryos after surgery for varied times according to individual experiments.

## **2. Neonatal Intracerebral Inoculation of Zika Virus: P0/P1**

1. Ensure that the gas-tight injection syringes (10  $\mu$ L volume) and needles are not clogged. Clean and test by loading three 20 mL disposable syringes with 26-gauge needles: one with saline, one with 70% ethanol, and one with air to clear the solutions. Sterilize with 10% bleach if previously used for virus injection.
2. Keep virus on ice. Load the syringe by filling it with saline to reduce dead volume in the syringe, and draw 0.75  $\mu$ L of air to separate the saline solution from the injection material.

3. Set up a warmed humidified recovery chamber for injected pups. Using a heating block, place a closeable container (such as an empty tip box) with a sterile gauze and humidify with saline. Preheat it prior to starting injections.
4. Set up the microinjector including the pump and the controller. Determine the device type code for the specific syringe (*i.e.*, for a 10  $\mu$ L syringe, the device type is "D"). Determine the speed of injection.
5. Collect the postnatal day 0 or 1 pups (P0/P1) near the surgical setup. Load the injection syringe with virus. Disinfect the pup head mount with 70% EtOH.
6. Wrap the pups in a thin layer of gauze and bury them completely in ice to achieve an anesthetic state. Pups are cryoanesthetized for 5 min. Ensure that the pups are sufficiently anesthetized for injection by performing a tail/toe pinch without response. This roughly yields 15 min of an anesthetic state.
7. Place the pup on head mount, sterilize the surface of the head with iodine and, ethanol (three times) and then wipe dry with a sterile wipe (isopropanol or 70% EtOH).
8. Mark lambda with a black marker and record the coordinates at lambda using the stereotaxic instrument. Measure the distance from lambda to the edge of the eye and beginning from the stereotaxic coordinates of lambda calculate the 2/5 distance from lambda to the eye (for both hemispheres if you are injecting both).
9. Re-check the anesthetic depth prior to creating a hole for the injection site. Use a 26-gauge needle to carefully and superficially puncture the scalp and skull at the injection location (the skull is very soft in neonates) to create an opening for the injection needle.

10. Lower the injection needle into the punctured location, and once the needle has just breached the skin, calculate a 1 mm depth for the injection site (lateral ventricle) using the stereotaxic instrument.
11. Once the needle is lowered to the injection depth, program the microinjector to inject: 1  $\mu$ L of virus, at a rate of 10 nL/s, injecting approximately 1  $\mu$ L over 1.5 min ( $\sim$  1  $\mu$ l  $3.4 \times 10^5$  TCID<sub>50</sub>/mL ZIKV).
12. When the injection finishes, wait 30 s, and retract the needle in 0.5 mm increments by rotating the screw (dorsally), waiting 30 s after each increment.  
NOTE: This reduces leakage of injected virus.
13. Once removed, either quickly load the needle and syringe with more virus (different viruses or mock controls should be loaded into separate syringes/needles) or remove the pup from the head mount to the pre-warmed humidified chamber. Monitor the pup every few minutes to gauge recovery. Replace the pups with its litter.

### **3. Adult Intracerebral Inoculation of Zika Virus**

1. Inject adult mice intraperitoneally with ketamine hydrochloride (80-100 mg/kg) and xylazine (5-10 mg/kg) diluted in sterile saline to induce anesthesia. Inject buprenorphine-SR (0.5-1.0mg/kg) subcutaneously to induce analgesia. Toe/tail pinch the mouse to ensure its anesthetic state, and subsequently mount it on the stereotaxic instrument (with a heating pad) to immobilize the head during surgery.

2. Add ophthalmic ointment to the eyes to prevent the eyes of the mouse from drying out during surgery. Shave the scalp starting behind the eyes to the beginning of the ears. Sterilize the exposed skin with iodine and 70% EtOH three times. Alternate the iodine and alcohol wipes; wipe in a circular motion away from the surgical site.
3. Re-check the anesthetic depth prior to incising the skin. Using a scalpel, make a 0.5 cm incision along the medial sagittal line of the head in the sterilized location, exposing bregma. Using a rolling motion with a cotton-tipped applicator, clear the surface of the skull of meningeal tissues, while simultaneously pushing the skin away from the injection sites.
4. Starting from bregma, align the surgical drill bit and identify the injection sites using the following coordinates: AP -0.5 mm, ML: +/-1.5 mm. Using the control foot pedal, drill into skull slowly as to only drill bone until a hole has been cleared for the needle.
5. Replace the drill with the microinjector pump and gas-tight syringe (10  $\mu$ L volume) on the stereotaxic. Leaving a small air bubble between the saline solution and the virus, draw ~ 4-5  $\mu$ L of virus. Determine the device type code for the specific syringe volume (ie, D for 10  $\mu$ L volume syringe). Lower the needle to DV: -1.5 mm from the brain surface. To inject 1  $\mu$ L of virus, program a rate of 10 nL/s, injecting approximately 1  $\mu$ L over 1.5 min.
6. When the injection finishes, wait 30 s, and remove the needle in 0.5 mm increments, waiting 30 s after each turn. This reduces backflow and leakage of the injected virus.

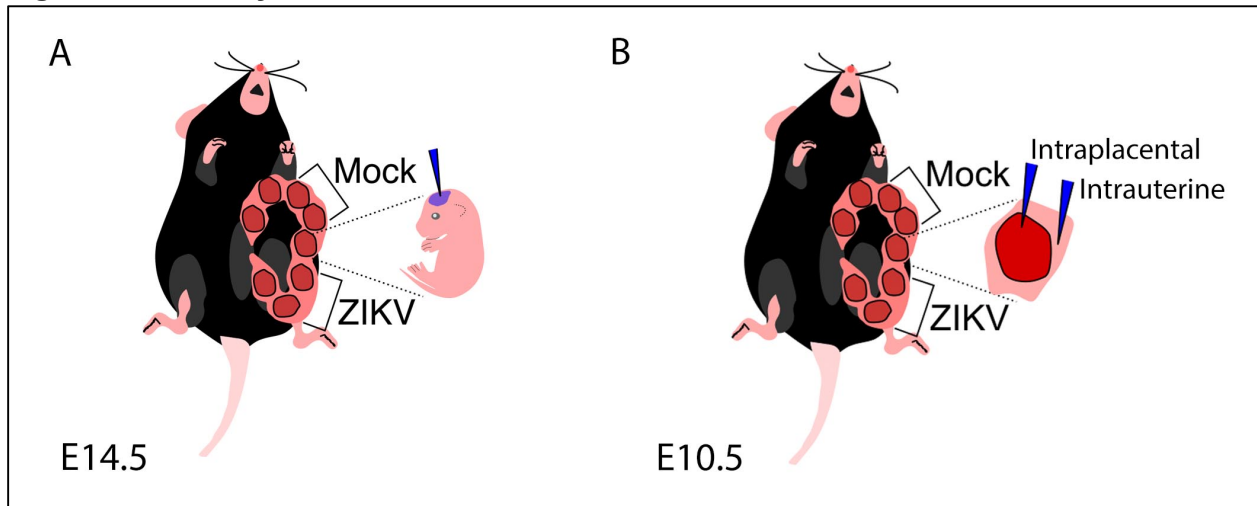
7. When the injection(s) are finished, use forceps to loosen the skin and recover the exposed skull. Suture the scalp back together using 4.0 sutures and remove the mouse from the stereotaxic instrument. Place the mouse in a cage partially resting on a heating pad to allow the mouse to escape to a non-heated area if needed and monitor while they recover (1 - 2 h) from anesthesia.

### Representative Results

Representative images of our injection methods for the ZIKV inoculation of embryonic brain are shown in diagrams depicting intracerebral injections (**Figure 3.1A**) and intrauterine and intraplacental injections (**Figure 3.1B**), illustrating the way the pregnant dam and embryos should be viewed and oriented for surgery (embryonic inoculation protocol). **Figure 3.2A** exhibits ZIKV (MEX1-44) infection (immunostained with the antibody against flavivirus group antigen, green) in the E18.5 cerebral cortex. Pax6 (red) labels NPCs in the developing cortex. ZIKV was inoculated into E14.5 embryonic brains. Using the TCID<sub>50</sub> assay from tissue samples (Qiang Shao et al., 2016), our growth curve analyses show that the ZIKV can efficiently replicate and grow in the developing brains (**Figure 3.2B, 3.2C**), as published (Qiang Shao et al., 2016). **Figure 3.2D** shows successful infection with DENV2 in the developing cortex using the embryonic inoculation method. DENV2 is detected using an antibody against flavivirus group antigen (green). **Figure 3.2E** demonstrates infection with a different strain of ZIKV, the African lineage (MR-766). **Figure 3.2F** demonstrates a representative infection for the alternative-route, intraplacental inoculation of ZIKV-Asia (MEX1-44) at stage E10.5.

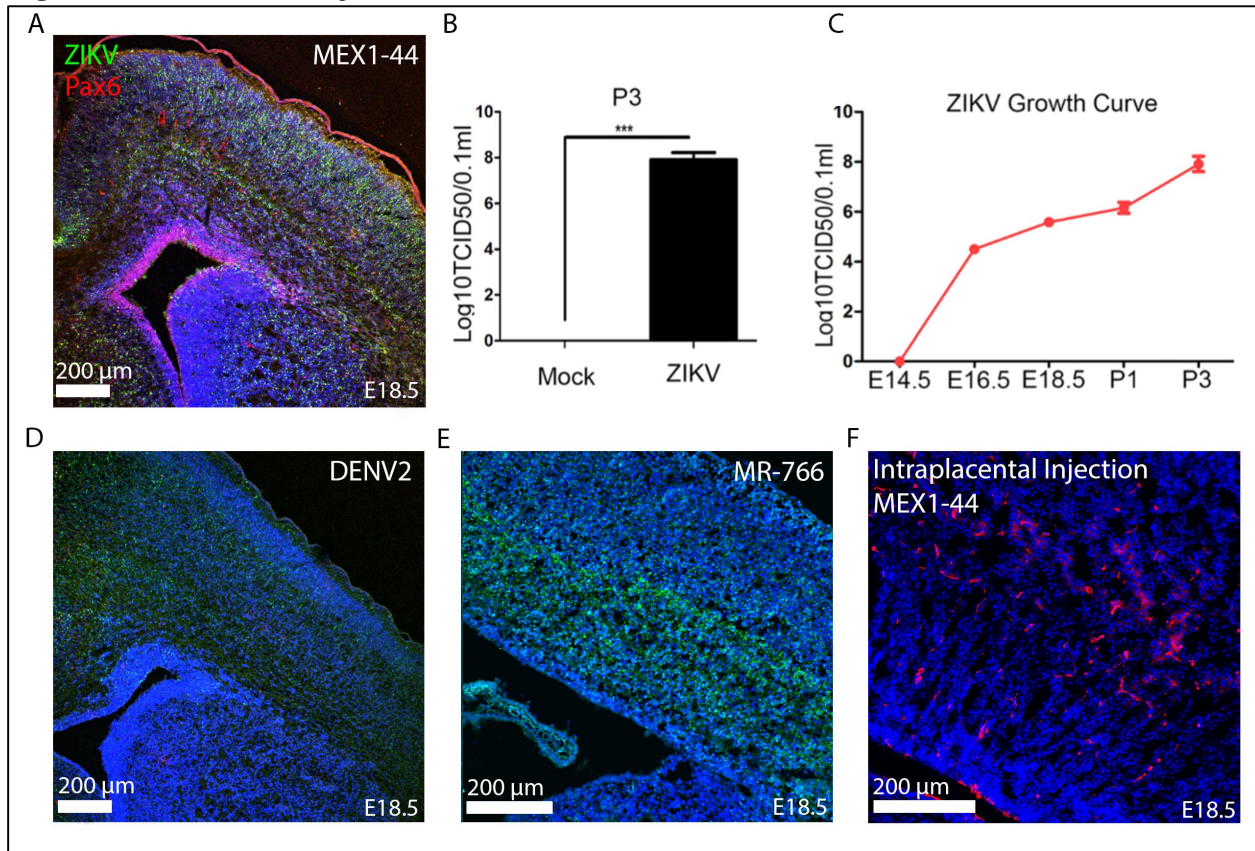
**Figure 3.3A** is a diagram depicting the landmarks used to identify the location of injection into the lateral ventricles for ZIKV inoculation of the P0/1 pups. **Figure 3.3B** shows the ZIKV (MEX1-44) infection at P13 cerebral cortex after P0/1 injection. ZIKV (MEX1-44) is detected using antibody against flavivirus group antigen (red). **Figure 3.4** shows the fluorescent beads (red) that were used to practice injection location, and lateral ventricle injection success in adults.

**Figure 3.1: Embryonic inoculation of the ZIKV.**



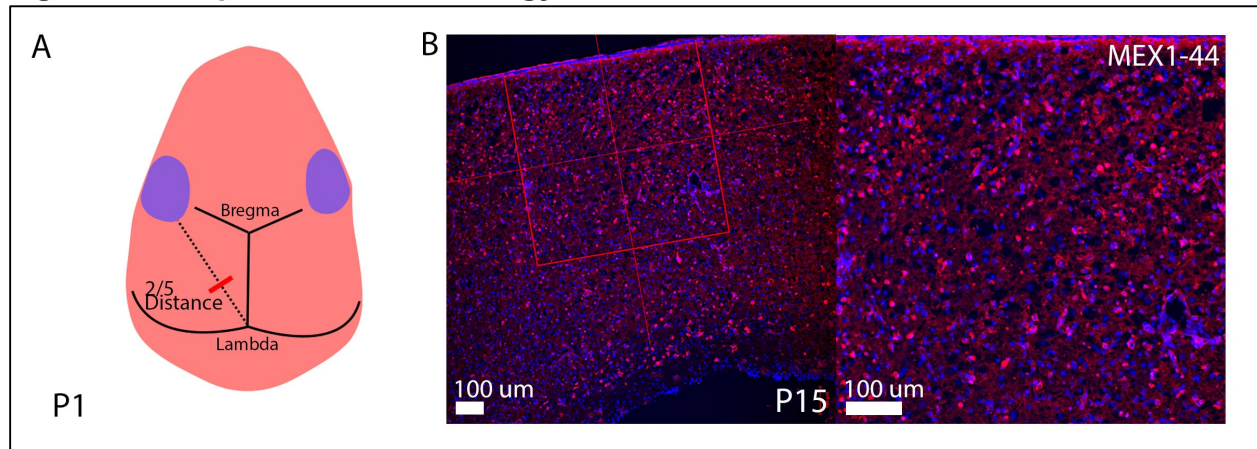
(A) Diagram representing exposure of one uterine horn, with a note to avoid injection of embryos adjacent to vagina and the most lateral embryo along the horn. (B) Diagram representing exposure of one uterine horn, depicting the location of intraplacental and intrauterine injections. These diagrams have been modified from their original publication (Qiang Shao et al., 2017).

**Figure 3.2: ZIKV Embryonic Inoculation at E14.5.**



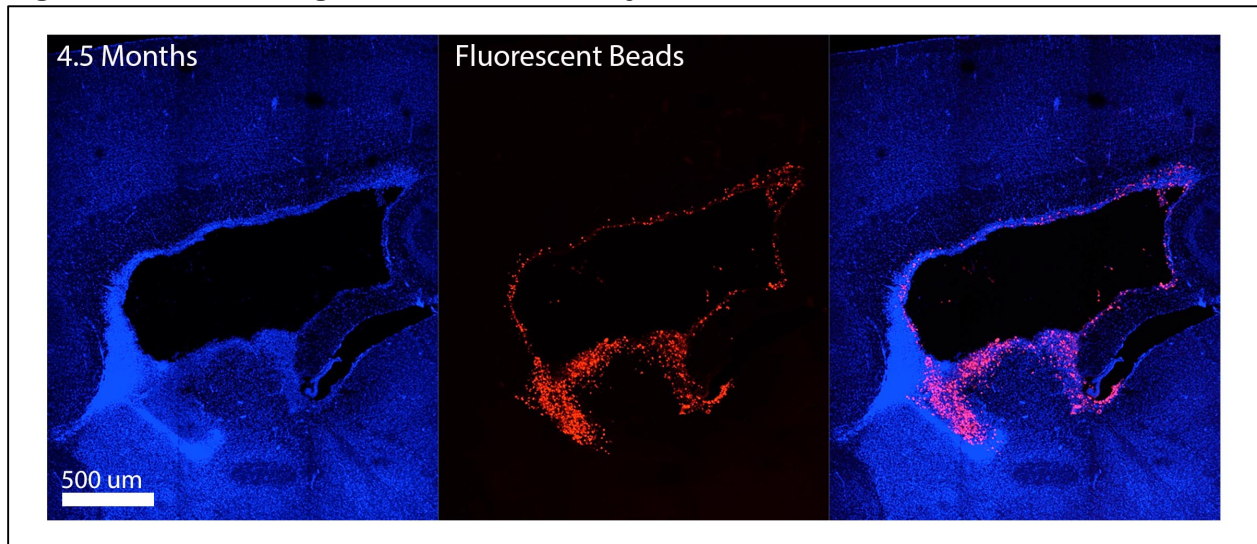
(A) At E18.5 the embryonic brain is infected with ZIKV-Asia (MEX1-44) across all layers of the developing neocortex (scale bar is 200  $\mu$ m). Neural progenitor cells are immunolabeled with Pax6 (red) and ZIKV via flavivirus antigen (green). (B) TCID<sub>50</sub> results from Postnatal Day 3 (P3) brain tissue inoculated at E14.5 with ZIKV-Asia (MEX1-44). Error bars indicate s.e.m. of three independent measurements with one mock and one ZIKV-infected brain in each measurement (\*\*\*)  $p < 0.0001$ , Student's t-test (Qiang Shao et al., 2016). (C) TCID<sub>50</sub> results describing typical increased growth curve of ZIKV viremia in infected fetal brain tissue. Error bars indicate the s.e.m. of three independent measurements with one mock and one ZIKV-Asia (MEX1-44) infected brain in each measurement. Analysis of variance (ANOVA) detects a significant increase in viral titer as development proceeds (Qiang Shao et al., 2016). (D) Dengue virus (DENV2) infected representative histology (E14.5 embryos inoculated with  $\sim 1 \mu$ L of  $3.4 \times 10^5$  TCID<sub>50</sub>/mL, scale bar is 200  $\mu$ m) and (E) ZIKV-Africa (MR766) infected representative histology (scale bar 200  $\mu$ m). (F) ZIKV-Asia (MEX1-44) infected representative histology from the intraplacental injection strategy (scale bar is 200  $\mu$ m). In all images, Hoechst stains nuclei. These figures have been modified from their original publication (Q. Shao et al., 2016).

**Figure 3.3: Representative histology of P1 inoculation of ZIKV.**



(A) Diagram demonstrating the method to determine the injection location into the lateral ventricles of P1 pups. (B) Representative coronal cryosections immunostained for flavivirus group antigen with low (on left, scale bar is 100  $\mu\text{m}$ ) and high (on right, scale bar is 50  $\mu\text{m}$ ) magnification of P1 inoculation of ZIKV at P15 ( $\sim 1 \mu\text{l}$   $3.4 \times 10^5$  TCID<sub>50</sub>/mL ZIKV). Hoechst stains nuclei.

**Figure 3.4: Adult stage intraventricular injection.**



Adult mouse injected with fluorescent beads was sacrificed shortly after surgery to determine the injection location success (scale bar is 200  $\mu\text{m}$ ). Sagittal cryosection could be viewed immediately after sectioning as beads do not require further staining. Hoechst stains nuclei.

## Discussion

Described here is a method for intracerebral inoculation of the ZIKV at embryonic, neonatal, and adult stages for the investigation of ZIKV- induced damages in brain development. While straightforward, there are a few considerations that investigators should take to ensure the quality of the study and the safety of those involved.

DENV is closely related to ZIKV in the flavivirus genus. DENV has not been causally linked with pediatric brain disorders in humans. DENV2 can successfully infect and replicate in the developing brain using the embryonic inoculation method (~ 1  $\mu$ L of  $3.4 \times 10^5$  TCID<sub>50</sub>/mL) (**Figure 3.2D**). Therefore, in addition to uninfected Vero cell media (mock), DENV infection can be used as a negative control in order to study ZIKV-specific pathogenesis in the developing brain. It is important to avoid virus leakage *in utero*, which can result in unwanted contamination of other embryos. Therefore, it is necessary to verify infected and non-infected individuals through isolating brain tissue from each embryo followed by qRT-PCR or the TCID<sub>50</sub> assay. A dye may be added to the viral medium to visually confirm the injection, but test to ensure that the dye does not cause damage itself.

Mouse strains exhibit growth variability, and therefore P1 injection locations need to be verified for each mouse line. Perform a mock neonate injection with fluorescent beads to visualize the injection site. This preliminary study will inform whether the injection reaches the ventricle or goes too deep into the brain tissue. For ideal results, pups can be sacrificed shortly after injection to identify the location of the fluorescent beads in the ventricle. The entire head of the pup can be fixed overnight, embedded,

and cryosectioned to observe the precise injection location. Injection with the oil-saturated syringe requires experience and it is recommended to practice using sham injections with dye onto parafilm to verify that the injection volume is accurate.

Biosafety measures are critical in these studies to avoid accidental infection of laboratory personnel working with the virus. Biosafety approvals must be made in advance at the facility where the work is being completed. ZIKV is considered a Biosafety Level 2 (BSL2) pathogen by the United States Centers for Disease Control and Prevention. All individuals working with the virus or working in areas where the virus is being handled should be aware and familiarized with biosafety protocols for their institution. All tools and surfaces exposed to the ZIKV or DENV2 should be disinfected with 10% bleach to destroy remaining viral particles after use. Women who are pregnant or are attempting to conceive are recommended to not interact with research areas exposed to ZIKV or DENV2. All tissue used for histology are fixed in 4% PFA to inactivate the viruses for analysis. Storing and culturing the virus should be done in Vero cells in a hood designated for BSL2 work. Stock viruses and tissue titration can be quantified using the TCID50 protocol.

### Acknowledgements

The authors would like to acknowledge Dr. Abdellatif Benraiss at the University of Rochester for his mentorship and discussions relevant to learning the adult surgical and neonate techniques. The authors would also like to acknowledge Dr. James Lauderdale at UGA for the use of his stereotaxic equipment and discussions related to setting up the methodology for this technique, and the Advancement for Research College

Scientists (ARCS) foundation for their support and our NIH support (NINDS grants R01NS096176-02, R01NS097231-01, & F99NS105187-01).

### References

- Abuelo, D. (2007). Microcephaly Syndromes. *Seminars in Pediatric Neurology*, 14(3), 118–127. <http://doi.org/10.1016/j.spen.2007.07.003>
- Clancy, B., Darlington, R. B., & Finlay, B. L. (2001). Translating developmental time across mammalian species. *Neuroscience*, 105(1), 7–17. [http://doi.org/10.1016/S0306-4522\(01\)00171-3](http://doi.org/10.1016/S0306-4522(01)00171-3)
- Cragan, J. D., Isenburg, J. L., Parker, S. E., Alverson, C. J., Meyer, R. E., Stallings, E. B., ... Mai, C. T. (2016). Population-based microcephaly surveillance in the United States, 2009 to 2013: An analysis of potential sources of variation. *Birth Defects Research. Part A, Clinical And Molecular Teratology*, 106(11), 972–982. <http://doi.org/10.1002/bdra.23587>
- Cragan, J. D., Mai, C. T., Petersen, E. E., Liberman, R. F., Forestieri, N. E., Stevens, A. C., ... Honein, M. A. (2017). Baseline Prevalence of Birth Defects Associated with Congenital Zika Virus. *Morbidity and Mortality Weekly Report*, 66(8), 219–220. <http://doi.org/10.15585/mmwr.mm6608a4>
- Dick, G. W. A., & Kitchen, S. F. (1952). ZIKA VIRUS (I). ISOLATIONS AND SEROLOGICAL SPECIFICITY. *TRANSACTIONS OF THE ROYAL SOCIETY OF*

*TROPICAL MEDICINE AND HYGIENE*, 46(5), 509–520.

Dreher, A. M., Arora, N., Fowler, K. B., Novak, Z., Britt, W. J., Boppana, S. B., & Ross, S. A. (2014). Spectrum of Disease and Outcome in Children with Symptomatic Congenital Cytomegalovirus Infection. *Journal of Pediatrics*. Retrieved from <http://proxy-remote.galib.uga.edu/login?url=http://search.ebscohost.com/login.aspx?direct=true&db=edswsc&AN=000333258900038&site=eds-live>

Driggers, R. W., Ho, C.-Y., Korhonen, E. M., Kuivanen, S., Jääskeläinen, A. J., Smura, T., ... Vapalahti, O. (2016). Zika Virus Infection with Prolonged Maternal Viremia and Fetal Brain Abnormalities. *The New England Journal of Medicine*, NEJMoa1601824. <http://doi.org/10.1056/NEJMoa1601824>

Goodfellow, F., Tesla, B., Simchick, G., Hodge, T., Zhao, Q., Brindley, M. A., & Stice, S. L. (2016). Zika Virus Induced Mortality and Microcephaly in Chicken Embryos. *Stem Cells and Development*, 25(22), 1–27. <http://doi.org/10.1089/scd.2016.0231>

Herrlinger, S. A., Shao, Q., Ma, L., Brindley, M., & Chen, J.-F. (2018). Establishing mouse models for Zika virus-induced neurological disorders using intracerebral injection strategies: Embryonic, neonatal, and adult. *Journal of Visualized Experiments*, 2018(134). <http://doi.org/10.3791/56486>

Jaenisch, T., Rosenberger, D., Brito, C., & Brady, O. (2017). Risk of microcephaly after Zika virus infection in Brazil, 2015 to 2016, 95(3), 191–198.

Lanzieri, T. M., Leung, J., Caviness, A. C., Chung, W., Flores, M., Blum, P., ... Demmler-Harrison, G. (2017). Long-term outcomes of children with symptomatic

congenital cytomegalovirus disease. *Journal of Perinatology: Official Journal Of The California Perinatal Association*. <http://doi.org/10.1038/jp.2017.41>

Li, C., Xu, D., Ye, Q., Hong, S., Jiang, Y., Liu, X., ... Xu, Z. (2016). Zika Virus Disrupts Neural Progenitor Development and Leads to Microcephaly in Mice. *Cell Stem Cell*, 19(5), 672. <http://doi.org/10.1016/j.stem.2016.10.017>

Li, H., Saucedo-Cuevas, L., Regla-Nava, J. A., Chai, G., Sheets, N., Tang, W., ... Gleeson, J. G. (2016). Zika Virus Infects Neural Progenitors in the Adult Mouse Brain and Alters Proliferation. *Cell Stem Cell* (Vol. 19). Retrieved from <http://www.sciencedirect.com/science/article/pii/S1934590916302521>

Miki, T., Fukui, Y., Takeuchi, Y., & Itoh, M. (1995). A quantitative study of the effects of prenatal X-irradiation on the development of cerebral cortex in rats. *Neuroscience Research*, 23, 241–247.

Mlakar, J. . J., Korva, M. M. . M., Tul, N. N. . N., Popović, M. M. ., Poljšak-Prijatelj, M. M. ., Mraz, J. J. . J., ... Avšič Županc, T. (2016). Zika Virus Associated with Microcephaly. *New England Journal of Medicine*, 374(10), 951–958. <http://doi.org/10.1056/NEJMoa1600651>

Naseer, M. I., Rasool, M., Sogaty, S., Chaudhary, R. A., Mansour, M., Chaudhary, A. G., ... Al-qahtani, M. H. (2017). A novel WDR62 mutation causes primary microcephaly in a large consanguineous Saudi family. *Annals of Saudi Medicine*, 37(2). <http://doi.org/10.5144/0256-4947.2017.148>

Nicholas, A. K., Khurshid, M., Désir, J., Carvalho, O. P., Cox, J. J., Thornton, G., ... Woods, C. G. (2010). WDR62 is associated with the spindle pole and is mutated in

human microcephaly. *Nature Genetics*, 42(11), 1010–4.

<http://doi.org/10.1038/ng.682>

Oliveira Melo, A. S., Malinger, G., Ximenes, R., Szejnfeld, P. O., Alves Sampaio, S., & Bispo de Filippis, A. M. (2016). Zika virus intrauterine infection causes fetal brain abnormality and microcephaly: tip of the iceberg? *Ultrasound in Obstetrics & Gynecology*, 47(1), 6–7. <http://doi.org/10.1002/uog.15831>

Pulvers, J. N., Bryk, J., Fish, J. L., Wilsch-Bräuninger, M., Arai, Y., Schreier, D., ... Huttner, W. B. (2010). Mutations in mouse *Aspm* (abnormal spindle-like microcephaly associated) cause not only microcephaly but also major defects in the germline. *Proceedings of the National Academy of Sciences of the United States of America*, 107(38), 16595–600. <http://doi.org/10.1073/pnas.1010494107>

Semple, B. D., Blomgren, K., Gimlin, K., Ferriero, D. M., & Noble-Haeusslein, L. J. (2013). Brain development in rodents and humans: Identifying benchmarks of maturation and vulnerability to injury across species. *Progress in Neurobiology*, 106, 1–16. <http://doi.org/10.1016/j.pneurobio.2013.04.001>

Shao, Q., Herrlinger, S., Yang, S.-L., Lai, F., Moore, J. M., Brindley, M. A., & Chen, J.-F. (2016). Zika virus infection disrupts neurovascular development and results in postnatal microcephaly with brain damage. *Development (Cambridge)*, 143(22). <http://doi.org/10.1242/dev.143768>

Shao, Q., Herrlinger, S., Yang, S.-L., Lai, F., Moore, J. M. J. M., Brindley, M. A. M. A., & Chen, J.-F. J.-F. (2016). Zika virus infection disrupts neurovascular development and results in postnatal microcephaly with brain damage. *Development*

*(Cambridge, England)*, 143(22), 4127–4136. <http://doi.org/10.1242/dev.143768>

Shao, Q., Herrlinger, S., Zhu, Y.-N., Yang, M., Goodfellow, F., Stice, S. L. S. L., ...

Chen, J.-F. J.-F. (2017). The African Zika virus MR-766 is more virulent and causes more severe brain damage than current Asian lineage and Dengue virus.

*Development*, 144(22). <http://doi.org/10.1242/dev.156752>

## CHAPTER 4

# ZIKA VIRUS INFECTION DISRUPTS NEUROVASCULAR DEVELOPMENT AND RESULTS IN POSTNATAL MICROCEPHALY WITH BRAIN DAMAGE<sup>1</sup>

---

<sup>1</sup> Stephanie Herrlinger\*, Qiang Shao\*, Si-Lu Yang, Fan Lai, Julie M. Moore, Melinda A. Brindley, and Jian-Fu Chen. 2016. *Development*. 143: 4127-4136. \*co-first authorship. Reprinted here with permission of the publisher. URL: <http://dev.biologists.org/content/early/2016/10/08/dev.143768>

## Abstract

Zika virus (ZIKV) infection of pregnant women can result in fetal brain abnormalities. It has been established that ZIKV disrupts neural progenitor cells (NPCs) and leads to embryonic microcephaly. However, the fate of other cell types in the developing brain and their contributions to ZIKV-associated brain abnormalities remain largely unknown. Using intracerebral inoculation of embryonic mouse brains, we found that ZIKV infection leads to postnatal growth restriction including microcephaly. In addition to cell cycle arrest and apoptosis of NPCs, ZIKV infection causes massive neuronal death and axonal rarefaction, which phenocopy fetal brain abnormalities in humans. Importantly, ZIKV infection leads to abnormal vascular density and diameter in the developing brain, resulting in a leaky blood–brain barrier (BBB). Massive neuronal death and BBB leakage indicate brain damage, which is further supported by extensive microglial activation and astrogliosis in virally infected brains. Global gene analyses reveal dysregulation of genes associated with immune responses in virus- infected brains. Thus, our data suggest that ZIKV triggers a strong immune response and disrupts neurovascular development, resulting in postnatal microcephaly with extensive brain damage.

## Introduction

The Zika virus (ZIKV) outbreak reported in 2015 in South and Central America has quickly reached pandemic status as it spreads through 66 countries (Ramos da Silva & Gao, 2016; Saiz et al., 2016). A major concern associated with ZIKV infection is the severe abnormalities in babies born to mothers infected with ZIKV, including microcephaly, CNS injury, fetal growth restriction, and stillbirth, among others (Brasil et al., 2016; Marris et al., 2016). In 2015, the Brazilian Ministry of Health reported a 20-fold increase in reported neonatal microcephaly, which is now attributed to ZIKV infection. On 1 February 2016, the World Health Organization announced that ZIKV-associated microcephaly and other neurological disorders are a public health emergency of international concern (PHEIC) (Heymann et al., 2016; Marris et al., 2016). Therefore, there is an urgent need for improved understanding of ZIKV pathogenesis in the developing brain.

Emerging evidence suggests a causative relationship between ZIKV infection and microcephaly. An increase of the number of cases of fetal microcephaly coincides with the ZIKV outbreak, and ZIKV has been detected in the amniotic fluid of infected pregnant woman as well as in microcephalic brain tissues (Brasil et al., 2016; Calvet et al., 2016; R.W. Driggers et al., 2017; Mlakar et al., 2016; Oliveira Melo et al., 2016). Precise control of neural progenitor cell (NPC) self-renewal and differentiation is essential for brain development, disruption of which is sufficient to cause microcephaly (Kriegstein & Alvarez-Buylla, 2009; Manzini & Walsh, 2011; Nigg & Raff, 2009). Indeed, it has been reported that ZIKV infects human NPCs and impairs their growth (Corbin, Nery, & Fishell, 2001; Dang et al., 2016; Garcez et al., 2016; Qian et al., 2016; Tang et

al., 2016), which could lead to smaller brain size. Recent studies show that ZIKV infection disrupts NPCs and leads to embryonic microcephaly and growth restriction in mice (Cugola et al., 2016; H. Li et al., 2016; Miner et al., 2016). However, current approaches to model ZIKV infection in rodents results in lethality during pregnancy, although human babies survive and display microcephaly. In addition, a newly born mouse brain is relatively immature, akin to the developmental stage of the human brain at mid- gestation (Semple, Blomgren, Gimlin, Ferriero, & Noble-Haeusslein, 2013), and mouse brain development includes a major postnatal component. Thus, it has been suggested that examination of neurodevelopmental defects of ZIKV in mice requires postnatal analysis (Miner et al., 2016). Hence, despite considerable rapid progress, fundamental questions remain regarding ZIKV-associated fetal brain abnormalities. It remains unknown whether ZIKV infection in mice can be used to study postnatal microcephaly. Although microcephaly has been the predominant focus a wide spectrum of fetal brain abnormalities are described in humans including neuronal loss, axonal rarefaction, astrogliosis, and microglial activation (Rita W. Driggers et al., 2016; Mlakar et al., 2016). So far, there are no reported animal models that recapitulate these fetal brain abnormalities associated with ZIKV. Most importantly, NPC disruption is considered to be the major cause of microcephaly (Nigg & Raff, 2009; Thornton & Woods, 2009), and NPC abnormalities are suggested to be the cause of ZIKV-induced embryonic microcephaly (C. Li et al., 2016). However, it remains unknown whether other cell types, including differentiated neurons and vascular cells, are also damaged in the developing brain, contributing to the brain abnormalities associated with ZIKV infection.

To fill in these knowledge gaps, we established a mouse model of fetal brain abnormalities associated with human ZIKV infection. Our mouse model exhibits massive neuronal death, in addition to cell cycle arrest and apoptosis of NPCs, as well as global growth restriction. Interestingly, our model survives birth, allowing us to study postnatal microcephaly and leading to the discovery of neuronal loss and axonal rarefaction, which phenocopy fetal brain abnormalities reported in humans (Rita W. Driggers et al., 2016; Mlakar et al., 2016). Most notably, ZIKV infection leads to abnormal vascular density and diameter in brains, resulting in a leaky blood–brain barrier (BBB). Extensive microglial activation and astrogliosis were detected in virally infected brains, which is further supported by dysregulation of genes associated with the immune response in the developing brain after ZIKV infection. Thus, our data suggest that ZIKV triggers a strong immune response, disrupts NPCs and neurovascular development, and leads to postnatal microcephaly with extensive brain damage.

## Materials and Methods

### Ethics statement

All animals were handled according to protocols approved by the Institutional Animal Care and Use Committee (IACUC) at the University of Georgia Athens (UGA). All of the experiments related to ZIKV were conducted by the following protocols approved by the UGA Institutional Biosafety Committee.

### ZIKV virus (Mexican isolate MEX1-44)

Zika MEX1-44 was isolated in Chiapas, Mexico in January 2016 from an infected *Aedes aegypti* mosquito. The virus was passaged by the World Reference Center for Emerging Viruses and Arboviruses (WRCEVA) four times in Vero cells. We obtained this virus with permission through the University of Texas Medical Branch at Galveston (UTMB). We then amplified the stock an additional two passages in Vero cells, so the virus used in the experiments had been passaged six times in Vero cells from the time it was isolated from the mosquito. We have sequenced the virus (passage 5) and found that the sequence of ZIKV-MEX1-44 is 99% identical at the nucleotide level to the sequence of the ZIKV strain from Brazil (ZIKV PE243/2015).

### Viral inoculation of embryonic brains

For timed pregnant mating, noon of the day after mating was considered E0.5. Pregnant C57BL/6J or 129S1/SvImJ mice with E14.5 embryos were treated with ketamine hydrochloride and xylazine to induce anesthesia. ZIKV virus ( $\sim 1 \mu\text{l } 1.7 \times 10^6$  TCID<sub>50</sub>/ml Mexican isolate MEX1-44) was injected into the lateral ventricles of E14.5 embryo brains. Control media was used as a sham injection. To improve retention of the pregnancy, we avoided viral injection of the two embryos next to the ovaries and the two embryos next to the upper vagina. Injected embryos were placed back to pregnant dams and allowed to develop after surgery for varied times according to individual experiments.

## Viruses and titration

Vero cells (African green monkey kidney epithelial cells) were obtained from ATCC. Vero cells were maintained in Dulbecco's modified Eagle's medium (DMEM) supplemented with penicillin/streptomycin and 10% fetal bovine serum at 37°C with 5% CO<sub>2</sub>. ZIKV stocks were propagated on Vero cells after inoculating at a multiplicity of infection of 0.01 and harvesting supernatants at 96 h and 120 h post-infection. The viral titer of ZIKV for brains and other organs were determined as 50% tissue culture infectious doses (TCID<sub>50</sub>) on Vero cells. Briefly, tissues were homogenized in ten volumes PBS and centrifuged at 3000 rpm (845 g) for 10 min. The supernatant was serially diluted tenfold in DMEM. A 100 µl aliquot of each diluted sample (10 dilutions in total) was added to 96-well plates, containing a monolayer of Vero cells. Cells were cultured for 96-120 h at 37°C in a tissue culture incubator. Cytopathic effect of endpoint dilutions was monitored.

## Quantitative real-time PCR of ZIKV RNA

Total RNA was extracted with TRIzol (Invitrogen). Then, 1 µg RNA was reverse transcribed into cDNA utilizing SuperScript III first-strand synthesis for RT-PCR (Invitrogen) in a 20 µl reaction system. The cDNA was analyzed by qRT-PCR with Master mix (Taqman). The primers and probe specific for Zika virus have been previously described (Lanciotti et al., 2008). qRT-PCR was conducted under the following cycling conditions: 95°C for 10 min for pre-denaturation, followed by 40 cycles of 95°C for 15 s and 60°C for 1 min. The last step was conducted at 95°C for 15 s, 60°C for 15 s, and 95°C for 15 sec, which is necessary to acquire a melting curve for the PCR

products to confirm the specificity of amplification. The relative mRNA abundances were analyzed utilizing the  $2^{-\Delta\Delta C_t}$  method with Gapdh as a reference and plotted as fold changes compared with the mock-treated samples. Specific ZIKV primers and probes were: ZIKV-1086 GCCCAACACAAG; ZIKV- 1162c CCACTAACGTTCTTTTGCAGACAT; ZIKV-1107-FAM AGCCTACCTTGACAAGCAGTCAGACACTCAA.

#### Mouse brain phenotype analysis

Histological processing, TUNEL assay, and immunohistochemical labeling of cryosections were performed as described previously (J.-F. Chen et al., 2014). Coronal sections of the cerebral cortex from different stages of embryos as indicated in the figure and text were used. The primary antibodies used are listed in Table S2. The secondary antibodies used were Alexa 488 and Alexa 555 conjugated to specific IgG types (Invitrogen Molecular Probes). All the experiments have been repeated at least three times, and representative images are shown in the individual figures.

#### CldU labeling study

After ZIKV inoculation of E14.5 brains, pregnant dams with E17.5 embryos were injected intraperitoneally with CldU at 10 mg/kg body weight. The animals were sacrificed 2 h after the injection. The brains were dissected out and fixed in 4% paraformaldehyde (PFA) overnight. Subsequently, the brains were stored in 30% sucrose for 16 h and embedded in Tissue-Tek O.C.T. Compound (Sakura). Cortical

coronal sections were prepared for immunohistochemical staining using antibodies against CldU (Abcam, ab6326, 1:200).

### Cell cycle length analysis

Cell cycle kinetics were determined by a dual-labeling approach as described previously (Martynoga, Morrison, Price, & Mason, 2005; Siegenthaler, Tremper-Wells, & Miller, 2008). On E17.5, the pregnant mouse was injected with CldU (10 mg/ml, Sigma; 100  $\mu$ l per 100 g body weight) at a time designated as T=0 h, such that all cells at S phase from the beginning of the experiment were labeled with CldU. At T=1.5 h, the pregnant mouse was injected with EdU (1 mg/ml, Invitrogen; 100  $\mu$ l for per 100 g body weight) to label all cells in S phase. The animal was killed at T=2 h and its embryos were collected immediately. Embryo sections were immunostained using an anti-CldU antibody (Abcam, ab6326, 1:200) and Click-iT EdU Alexa Fluor 555 Imaging Kit (Life Technologies, C10338). Images were obtained with a Zeiss LSM 710 inverted confocal microscope. The length of S phase ( $T_s$ ) and total length of cell cycle ( $T_c$ ) were determined based on the relative number of cells that incorporated one or both of CldU and EdU (Martynoga et al., 2005). The ratio of the length of any one period of the cell cycle to that of another period is equal to the ratio of the number of cells in the first period to the number in the second period (Nowakowski, Lewin, & Miller, 1989). So  $T_s$  was calculated as the interval between both injections ( $T_i=1.5$  h) divided by the quotient of the density of CldU+EdU<sup>-</sup> cells ( $L_{cells}$ , i.e. cells that have been in but left S phase before EdU injection) and CldU+EdU<sup>+</sup> cells ( $S_{cells}$ , i.e. cells remaining in S phase at the end of the experiment), i.e.  $T_i/T_s=L_{cells}/S_{cells}$ . Using the same logic, the total cell

cycle length can be calculated as below:  $T_s/T_c = S_{cells}/P_{cells}$  where  $P_{cells}$  is estimated by counting the total numbers of cells in the assessed area.

#### Postnatal BBB permeability assay

This method was based on the well-established adult BBB dye-injection permeabilization assay, with modifications to perform on P0 pups (Ben-Zvi et al., 2014). In brief, P0 pups were deeply anesthetized and 10  $\mu$ l of 10 mg/ml 10kDa dextran tetramethylrhodamine (D3312, Molecular Probes) was injected into the left ventricle using a Hamilton syringe. After allowing for 5 min of circulation, brains were dissected without perfusion in order to avoid damage or washout of the dye, and fixed in 4% PFA overnight. Brains were then rinsed 3 $\times$ 5 min in PBS and cryopreserved in 25% sucrose for overnight. Brains were embedded coronally in Tissue-Tek O.C.T. Compound (Sakura) and sectioned at 25  $\mu$ m. Sections were stained with PECAM antibody (550274, BD Biosciences, 1:200) to visualize the blood vessels against the distribution of the dye.

#### RNA isolation and high-throughput sequencing

Total RNAs were extracted from two mock and two ZIKV-infected E17.5 brains using TRIzol reagent (Life Technologies). Genomic DNA and ribosomal RNA was removed with Turbo DNA-free kit and RiboMinus Eukaryote Kit (Life Technologies). The resulting RNA fractions were subjected to strand-specific library preparation using NEBNext Ultra Directional RNA Library Prep Kit for Illumina (New England Biolabs). Sequencing was performed on a Nextseq500 (Illumina).

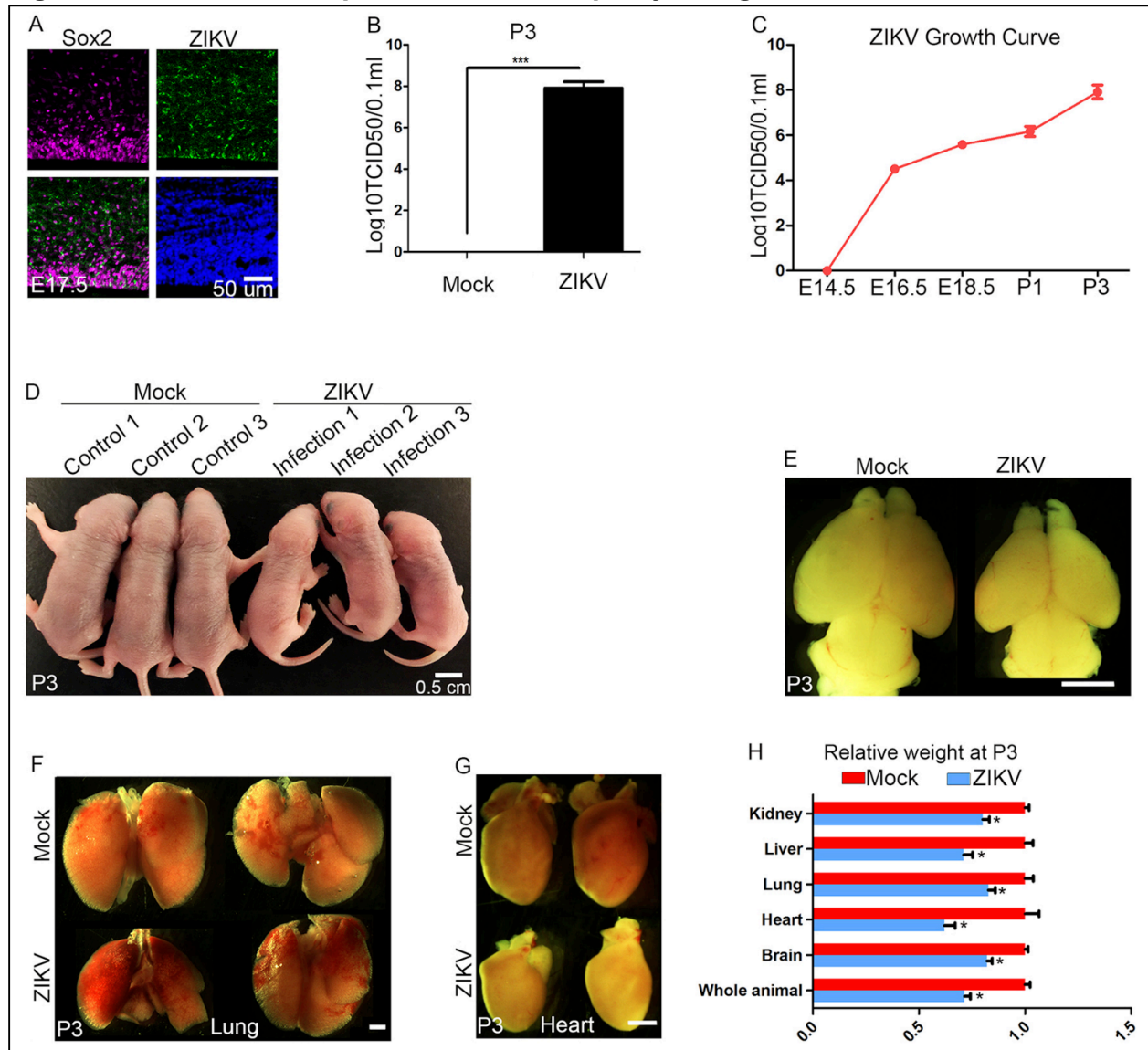
## Results

### ZIKV causes postnatal microcephaly and growth restriction

To investigate whether ZIKV can infect NPCs in developing mouse brains, we injected ~1  $\mu$ l of  $1.7 \times 10^6$  TCID<sub>50</sub>/ml ZIKV virus (Mexican isolate MEX1-44) into the cerebral ventricles of embryonic day (E) 14.5 mouse brains. Zika MEX1-44 belongs to the Asian lineage, and was isolated in Chiapas, Mexico from an infected *Aedes aegypti* mosquito. The virus was passaged six times in Vero cells before inoculation of embryonic mouse brains. We sequenced the virus (passage 5), and found that the sequence of ZIKV-MEX1-44 is 99% identical at the nucleotide level to the sequence of the ZIKV strain isolated in Brazil (ZIKV PE243/2015).

Staining E17.5 cerebral cortex with antibodies against a Flavivirus group antigen reveals ZIKV infection (ZIKV, green) of NPCs labeled by Sox2 (Fig. 4.1A). We also detected ZIKV in Pax6- positive apical NPCs and newly formed neurons labeled by TuJ1 (Tubb3) (data not shown). We measured viral titers at different stages after intracerebral inoculation of E14.5 embryonic brains. The ZIKV growth curve shows that ZIKV can effectively replicate in mouse brains from developmental to postnatal stages (Fig. 4.1B,C). Pups can survive until postnatal day (P) 3, and a lower titer ZIKV infection ( $3.4 \times 10^5$  TCID<sub>50</sub>/ml) allowed recovery of P5 living pups. At P3, ZIKV-infected pups had a significantly smaller body (Fig. 4.1D,H) and brain (Fig. 4.1E,H) compared with controls. Previous studies on microcephaly genes suggest that NPCs are selectively vulnerable to genetic or environmental disturbances, resulting in smaller brains yet normal size of other organs (Gruber et al., 2011; Nigg & Raff, 2009; Thornton & Woods, 2009). To investigate whether the brain is selectively smaller after ZIKV infection, we dissected

**Figure 4.1. ZIKV causes postnatal microcephaly and growth restriction.**



(A) Confocal imaging of infected E17.5 cerebral cortex stained with antibodies against Sox2 (labeling NPCs; magenta) and Flavivirus group antigen (ZIKV; green). Hoechst stains nuclei (blue). Scale bar: 50  $\mu$ m. (B) Viral titers in P3 pup brains were determined using the TCID<sub>50</sub> assay. A significantly higher titer of ZIKV ( $1 \times 10^{9.5}$  TCID<sub>50</sub>/ml) was detected in P3 pup brains compared with mock controls. Error bars indicate s.e.m. of three independent measurements with one mock and one ZIKV-infected brain in each measurement (\*\**P*<0.0001, Student's t-test). (C) Viral titers were determined in brains at different stages using the TCID<sub>50</sub> assay. Error bars indicate the s.e.m. of three independent measurements with one mock and one ZIKV-infected brain in each measurement. Analysis of variance (ANOVA) detects a significant increase in viral titer as development proceeds. (D) Dorsal views of P3 pups. ZIKV ( $\sim 1 \mu$ l  $1.7 \times 10^6$  TCID<sub>50</sub>/ml) was injected into cerebral ventricles of E14.5 brains followed by analyses at P3. Scale bar: 0.5 cm. (E) ZIKV-infected brains are smaller than controls at P3. Scale bar: 2 mm. (F,G) Dorsal views of P3 hearts and lungs after ZIKV intracerebral inoculation of E14.5

mouse brains. Scale bar: 1 mm. (H) Relative weights of different organs from control or ZIKV-infected pups at P3. Error bars indicate the s.e.m. of six independent experiments with one mock and one ZIKV-infected brain in each experiment (\* $P < 0.01$ , Student's t-test).

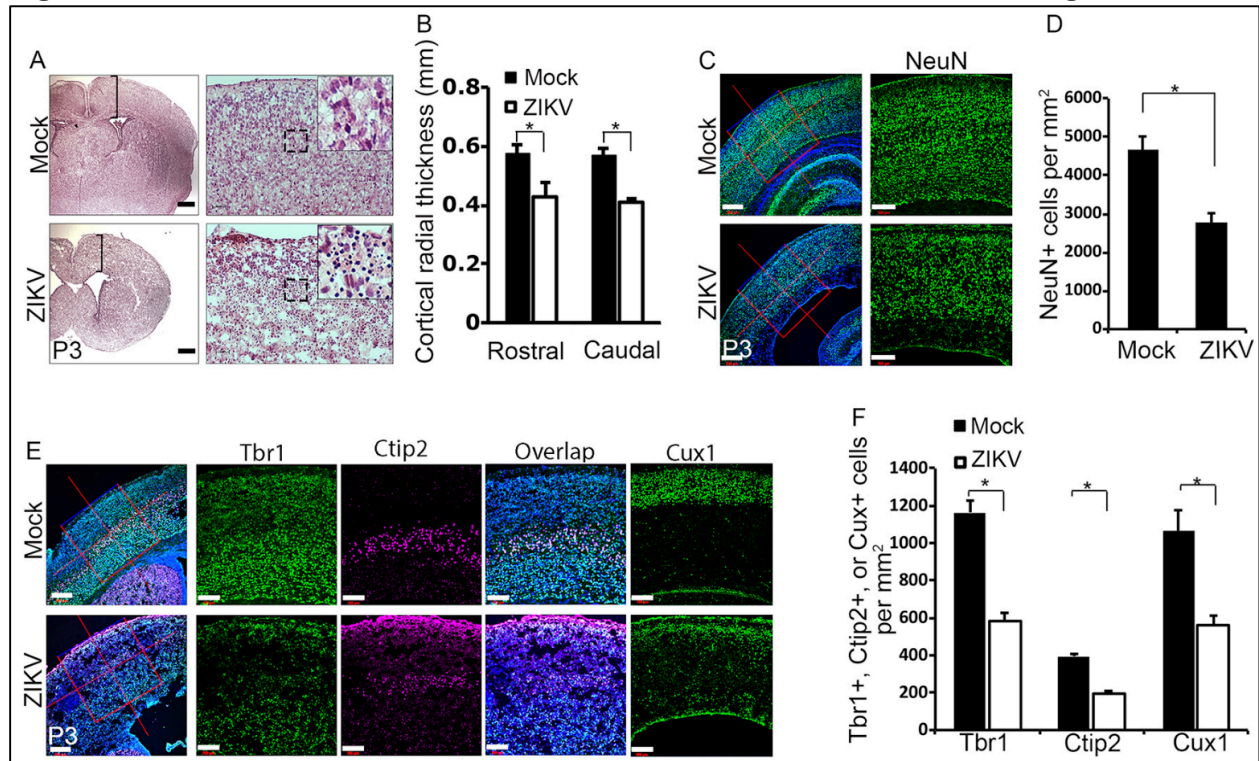
and weighed different organs, including brain, heart, lung, liver and kidney (Fig. 4.1F-H). Experimental results showed that individual organ masses are decreased in addition to total body weight (Fig. 4.1H). ZIKV-induced growth restriction can be observed as early as P1 for the brain and other organs compared with P1 controls (Fig. S1). Together, these results suggest that ZIKV infection is sufficient to cause postnatal microcephaly and growth restriction in mice.

#### ZIKV infection results in neuronal loss and cortical thinning

We focused our studies on brain development as microcephaly is a prominent fetal brain abnormality associated with ZIKV infection (Rita W. Driggers et al., 2016; Mlakar et al., 2016; Oliveira Melo et al., 2016). As expected, cortical radial thickness is significantly reduced in ZIKV-infected brains compared with controls (Fig. 4.2A,B). Hematoxylin and Eosin (H&E) staining shows dead cell accumulation in ZIKV-infected brains, indicated by the presence of dark puncta (Fig. 4.2A, black box). Next, we measured total neuronal cell numbers using antibodies against NeuN (Rbfox3), a neuron-specific nuclear protein (Mullen, Buck, & Smith, 1992). We found a drastic decrease in total number of neurons after ZIKV infection compared with controls (Fig. 4.2C,D). These results suggest that embryonic infection of ZIKV causes a significant neuronal loss in postnatal brains.

The cerebral cortex is composed of a six-layer structure generated through the well-described 'inside-out' mechanism of corticogenesis. Neurons born earlier reside in deeper layers, whereas later-born neurons migrate over existing layers to form the more superficial layers (Angevine & Sidman, 1961; Marín & Rubenstein, 2003). To determine

**Figure 4.2. ZIKV infection results in neuronal loss and cortical thinning.**



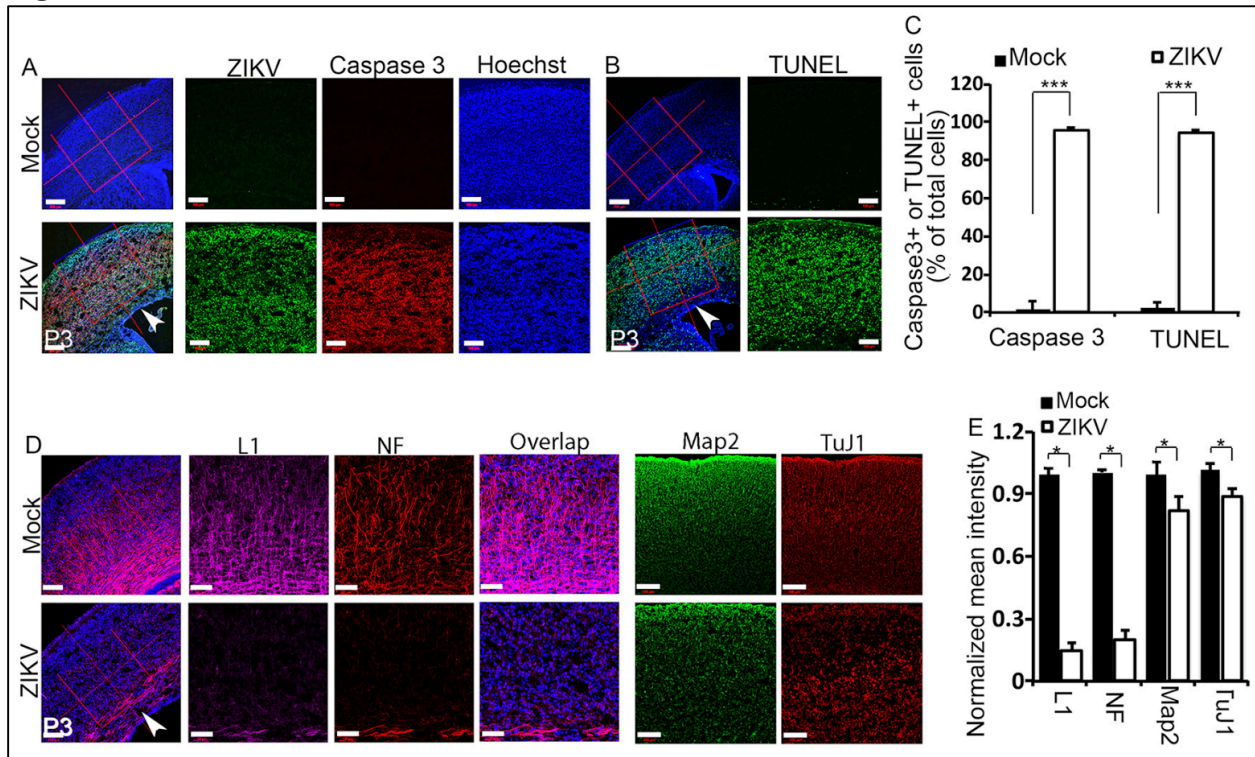
(A) Coronal sections of P3 cerebral cortex stained with H&E. Scale bars: 0.2 mm (left panels); 50  $\mu$ m (right panels). Black brackets indicate the measurement of cortical radial thickness. Black boxed areas are enlarged in insets and show a substantial number of dead cells indicated by dark staining in ZIKV-infected brains. (B) Quantification of cortical radial thickness from the experiment shown in A. Error bars indicate s.e.m. of nine sections from three independent experiments. \* $P < 0.05$  (Student's t-test). (C) Confocal imaging of P3 cerebral cortex stained with antibodies against NeuN (green). Hoechst stains nuclei (blue). Right panels are enlargements of the regions outlined by red boxes in left panels. Scale bars: 200  $\mu$ m (left panels); 100  $\mu$ m (right panels). (D) Quantification of NeuN-positive cells per  $\text{mm}^2$  in a  $3.385 \times 10^5 \mu\text{m}^2$  boxed area of P3 cerebral cortex from the experiment shown in C. Error bars indicate s.e.m. of nine sections from three independent experiments. \* $P < 0.05$  (Student's t-test). (E) Confocal microscope images of coronal sections from P3 cortex stained with antibodies against Tbr1 (green), Ctip2 (magenta) and Cux1 (green). Hoechst stains nuclei (blue). Right panels are enlargements of the regions outlined by red boxes in left panels. Scale bars: 200  $\mu$ m (left panels); 100  $\mu$ m (right panels). (F) Quantification of percentage of Tbr1-, Ctip2- and Cux1-positive cells per  $\text{mm}^2$  in a  $5.274 \times 10^5 \mu\text{m}^2$  boxed area of P3 cerebral cortex from the experiment shown in E. Error bars indicate s.e.m. of nine sections from three independent experiments (\* $P < 0.05$ , Student's t-test).

whether cortical lamination is disrupted and which layer(s) of neurons were affected in ZIKV-infected brains, we examined the well-established layer markers Tbr1 and Ctip2 (Bcl11b) to label layers V-VI, and Cux1 to label layers II-IV (Hevner et al., 2001; Nieto et al., 2004). The overall organization of cortical layers appears to be normal in ZIKV-infected brains compared with controls (Fig. 4.2E). However, viral infection results in a significant decrease in total Tbr1-, Ctip2- and Cux1-labeled neurons (Fig. 4.2E,F). Together, these data indicate that the cytoarchitecture of the cortex is largely preserved after ZIKV infection, suggesting that radial migration and lamination are not severely disrupted in the developing brain.

#### ZIKV infection leads to massive neuronal death and axonal rarefaction

Extensive neuronal cell death is detected in human fetal brains infected with ZIKV (Rita W. Driggers et al., 2016; Mlakar et al., 2016). Our H&E staining also suggests cell death in ZIKV-infected mouse brains (Fig. 4.2A). To identify the causes of cortical thinning and postnatal microcephaly associated with ZIKV, we first examined cell death. We stained P3 cerebral cortex using antibodies against activated caspase 3 and found that there is a drastic increase in caspase 3-positive cells in cerebral cortex after ZIKV infection (Fig. 4.3A, red; Fig. 4.3C). ZIKV was abundant throughout the cerebral cortex of P3 brains (Fig. 4.3A, green). Terminal deoxynucleotidyl transferase dUTP nick end labeling (TUNEL) staining further confirmed the dramatic increase of apoptotic cells in the virally infected cerebral cortex (Fig. 4.3B, green; Fig. 4.3C). Together, these results suggest that ZIKV infection results in extensive neuronal death in the P3 cerebral cortex, which could lead to the smaller brain phenotype.

**Figure 4.3. ZIKV infection leads to massive neuronal death and axonal rarefaction.**



(A) Confocal imaging of P3 cerebral cortex stained with antibodies against cleaved caspase 3 (red) and Flavivirus group antigen (ZIKV, green). Hoechst stains nuclei (blue). Right panels are enlargements of the regions outlined by red boxes in left panels. White arrowhead indicates the ventricular zone (VZ) with fewer viruses detected. Scale bars: 200  $\mu\text{m}$  (left panels); 100  $\mu\text{m}$  (right panels). (B) TUNEL staining (green) on coronal sections of P3 cortex reveals extensive apoptotic cell labeling in the ZIKV-infected cortex compared with controls. Hoechst stains nuclei (blue). Right panels are enlargements of the regions outlined by red boxes in left panels. White arrowhead indicates the ventricular zone (VZ) with less viruses detected. Scale bars: 200  $\mu\text{m}$  (left panels); 100  $\mu\text{m}$  (right panels). (C) Quantification of percentage of caspase-3- and TUNEL-positive cells out of total cells in a  $5.625 \times 10^5 \mu\text{m}^2$  boxed area in the experiments shown in A and B. Error bars indicate s.e.m. of nine sections from three independent experiments.  $***P < 0.001$  (Student's t-test). (D) Confocal microscope images of coronal sections from P3 cortex stained with antibodies against L1 (magenta; labels axons), NF (neurofilament; red; labels mature neurons), Map2 (green; labels dendrites) and TuJ1 (red; labels newly generated neurons). Hoechst stains nuclei (blue). Right panels are enlargements of the regions outlined by red boxes in left panels. Note the drastically reduced L1 and NF staining indicated by white arrowhead in ZIKV-infected cerebral cortex. Scale bars: 200  $\mu\text{m}$  (left panels); 100  $\mu\text{m}$  (right panels). (E) Quantification of relative signal intensities from L1, NF, Map2 and TuJ1 staining using ImageJ. Error bars indicate s.e.m. of nine sections from three independent experiments ( $*P < 0.05$ , Student's t-test).

To determine whether axons are impaired by ZIKV infection, we used L1 (L1cam) to label callosal axons and found that there is dramatic axon reduction in virally infected brains (Fig. 4.3D, magenta; Fig. 4.3E). Similarly, callosal axons labeled with antibodies for neurofilament (NF) were nearly absent from ZIKV-infected P3 cerebral cortex (Fig. 4.3D, red; Fig. 4.3E), which suggests a corpus callosum defect (Fig. 4.3D, white arrowhead). By contrast, staining with the dendritic marker Map2 revealed a relatively minor reduction of dendrites in the cortex compared with axons in ZIKV-infected brains (Fig. 4.3D, green; Fig. 4.3E). These results suggest that axons are more severely affected than dendrites in the developing brain. Next, we used antibodies against TuJ1 to label newly generated neurons. We found a relatively minor reduction in newly generated neurons in virally infected brains (Fig. 4.3D,E). Together, these results suggest that ZIKV infection leads to massive neuronal death and axonal rarefaction.

#### Cell cycle arrest and apoptosis in ZIKV-infected NPCs

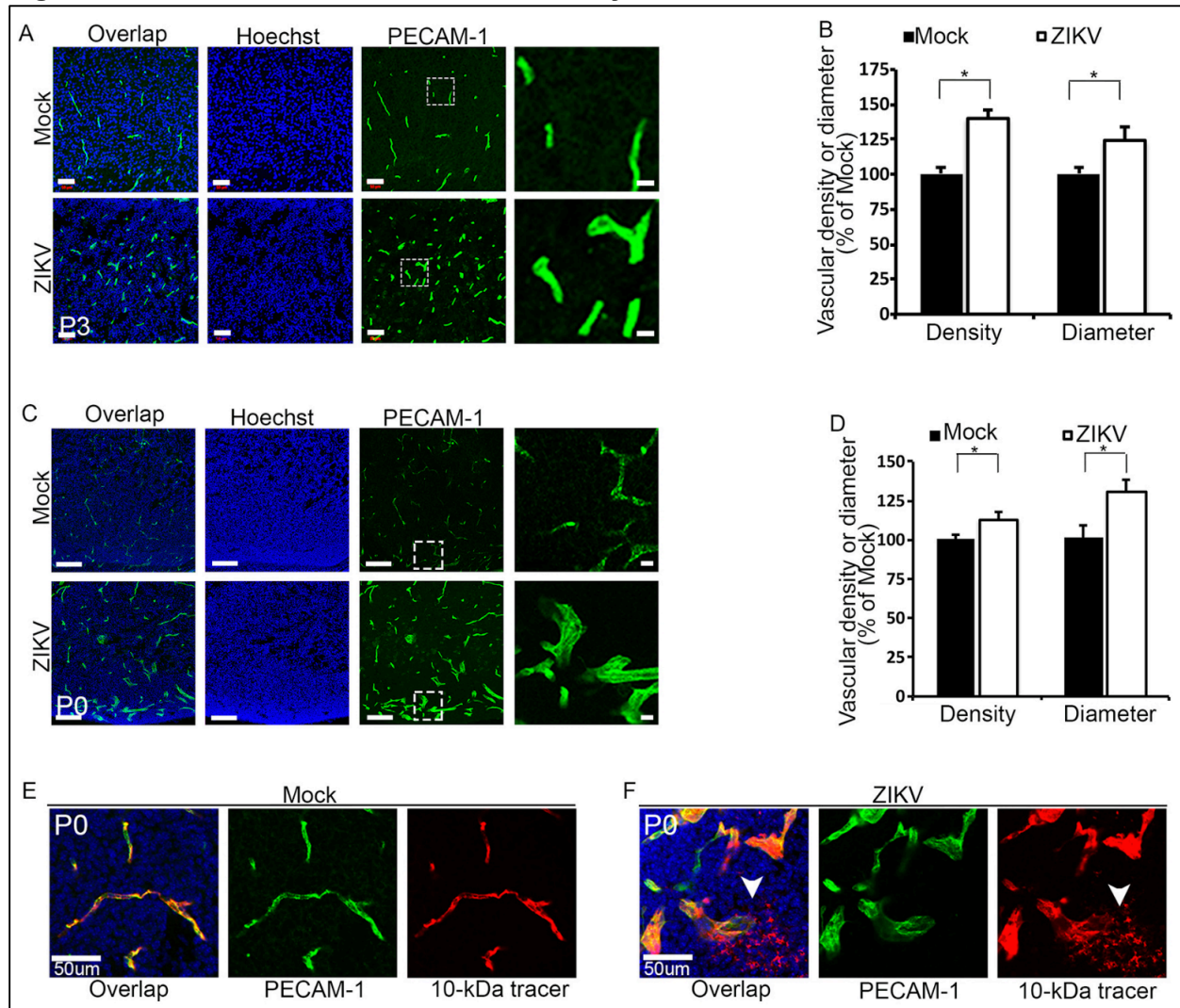
ZIKV infects human NPCs and causes their cell cycle arrest (Dang et al., 2016; Garcez et al., 2016; Qian et al., 2016; Tang et al., 2016). Next, we examined NPCs in ZIKV-infected embryonic brains. We did not detect significant growth reduction or microcephaly in E16.5 embryos after ZIKV inoculation at E14.5 (Fig. 4.S2A,B) and ZIKV was not detected in the cerebral cortex sections of E16.5 brains (Fig. 4.S2C). Therefore, we focused on NPCs located at the ventricular zone and subventricular zone (VZ/SVZ) of the E17.5 cerebral cortex.

Phosphorylation of histone H3 (p-H3) is tightly correlated with chromosome condensation and serves as a marker for mitosis. We found that p-H3-positive cells are significantly reduced in ZIKV- infected brains compared with controls (Fig. 4.S3A,B).

Next, we used Ki67 (Mki67) to label all cycling cells and found that there is a slight but significant increase in Ki67-positive cells in virally infected brains compared with controls (Fig. 4.S3A,C). Cell proliferation can be measured with the thymidine analog 5-chloro-2'-deoxyuridine (CldU) following its incorporation into newly synthesized DNA and its subsequent detection with antibodies against CldU. We performed CldU pulse experiments and found that there is a significant decrease in CldU-positive cells in the virally infected brains (Fig. 4.S3D,E). Finally, we measured cell cycle length. Control NPCs exhibit a cell cycle length of around 20 h in E17.5 embryonic brains, which is consistent with published studies (Siegenthaler et al., 2008). However, virally infected NPCs display an extended cell cycle length of around 30 h (Fig. 4.S3F). Together, these results suggest that there is a cell cycle arrest of NPCs after ZIKV infection in the developing brain.

To examine NPC survival, we used Pax6 to label apical neural progenitor cells, and Tbr2 (Eomes) to label intermediate neural progenitors in the cerebral cortex (Kriegstein & Alvarez-Buylla, 2009). TUNEL staining shows that ZIKV infection leads to a significant increase in apoptotic cells in both Pax6- and Tbr2- positive NPCs (Fig. 4.S4A,B). However, we noticed that there is only a small fraction of TUNEL-positive NPCs (<2.5% for Pax6-positive NPCs; <1% for Tbr2-positive cells) in virally infected brains at E17.5. Therefore, we measured total Pax6- and Tbr2-positive cells and found that there is no significant difference between ZIKV- infected brains and controls (Fig. 4.S4C). Together, these results suggest that ZIKV causes cell cycle arrest and apoptosis, but there is no substantial depletion of the NPC pool in E17.5 infected brains.

**Figure 4.4. Abnormal vasculature and leaky BBB in ZIKV-infected brains.**



(A,C) Confocal micrographs of P3 (A) or P0 (C) coronal cortical sections stained with antibodies against PECAM-1 (green) after viral infection at E14.5. Hoechst stains nuclei (blue). Right panels are enlargements of the white boxed areas. Scale bars: 50  $\mu\text{m}$  (left panels in A); 20  $\mu\text{m}$  (right panels in A), 100  $\mu\text{m}$  (left panels in C) and 10  $\mu\text{m}$  (right panels in C). (B,D) Quantification of relative vessel density and diameter from the experiments shown in A and C. Measurements of vessel density and diameter in ZIKV-infected brain sections were normalized to that in controls. Error bars indicate s.e.m. of nine sections from three independent experiments. \* $P < 0.05$  (Student's t-test). (E,F) Confocal micrographs of coronal sections of P0 brains stained with antibodies against PECAM-1 (green) together with 10 kDa dextran tracer (red). Hoechst stains nuclei (blue). Scale bars: 50  $\mu\text{m}$ . Dextran tracer (10 kDa) revealed a leaky BBB (white arrowheads) in P0 brains after ZIKV infection at E14.5.

## ZIKV infection leads to abnormal vasculature and a leaky blood–brain barrier

### (BBB)

Brain calcification is a prominent fetal brain pathology associated with ZIKV infection in humans (Rita W. Driggers et al., 2016; Mlakar et al., 2016; Oliveira Melo et al., 2016). BBB dysfunction has been reported to cause calcification in neurons (Keller et al., 2013; Miklossy et al., 2005). Therefore, we examined the integrity of the vasculature in ZIKV-infected brains. We labeled blood vessels in the developing brain using antibodies against PECAM-1. Immunostaining results show that there is a significant increase in vessel density and vessel diameter in P3 virally infected cerebral cortex compared with controls (Fig. 4.4A,B). We also examined vessels at P0 and found a similar increase in vessel density and diameter (Fig. 4.4C,D). Thus, these results suggest that ZIKV infection results in abnormal vasculature in the developing brain.

The mouse BBB becomes functional at E15.5 (Ben-Zvi et al., 2014). Altered vasculature in ZIKV-infected brains prompted us to investigate whether the BBB is damaged after viral infection. To address this question, we performed a postnatal BBB permeability assay according to published methods (Ben-Zvi et al., 2014). Dextran tracer (10 kDa) was injected intracardially at P0 and antibodies against PECAM-1 subsequently used to visualize the blood vessels against the distribution of the dye. The tracer was confined to the capillaries in control brains (Fig. 4.4E) whereas ZIKV-infected brains showed obvious tracer leakage (Fig. 4.4F, white arrowheads) in the developing caudate. These results indicate that ZIKV alters vasculature integrity and results in a leaky BBB in the developing brain. Together, massive neuronal death and

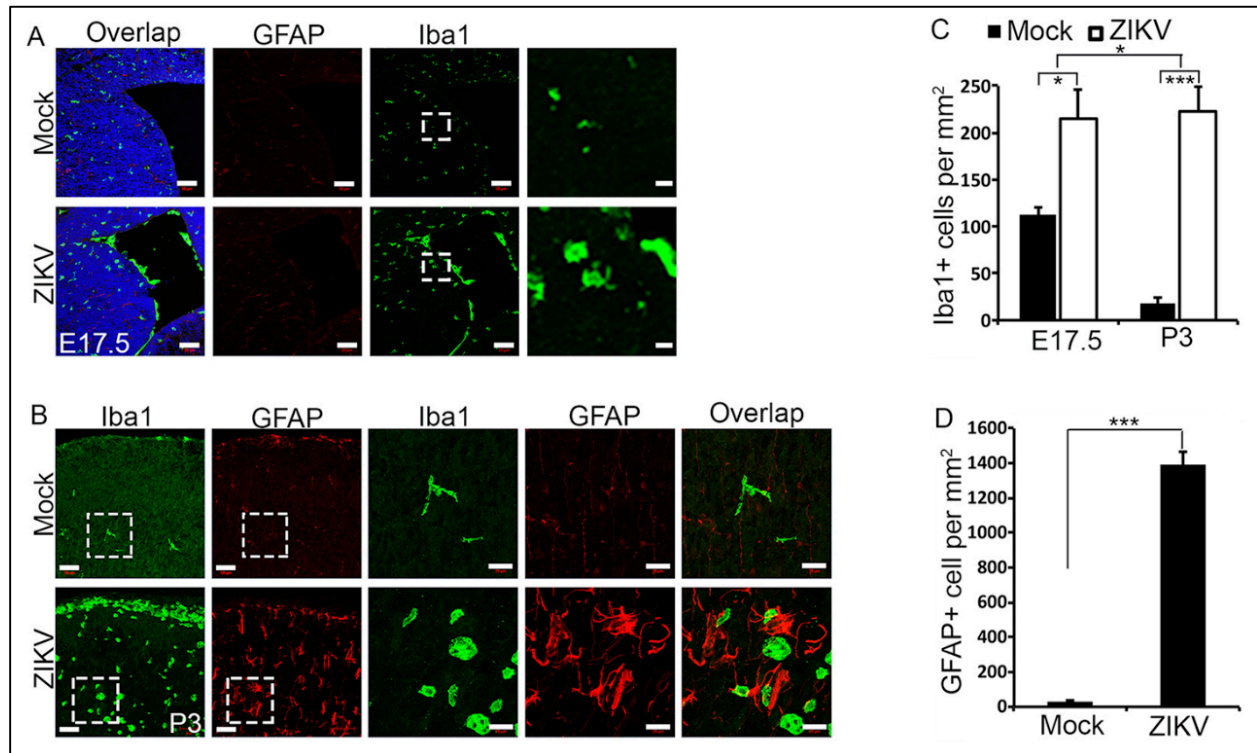
BBB leakage phenotypes suggest that ZIKV infection causes extensive damage in the developing brain.

#### ZIKV-infected brains exhibit extensive microglial activation and astrogliosis

Microglia are brain-resident innate immune cells that respond swiftly to viral infection by transforming into an activated state and performing their functions (Nayak, Roth, & McGavern, 2014). In their activated state, microglia will change from a ramified morphology to a rounded one, as well as increase in number. Using Iba1 as a marker of microglia, we found both morphological alterations and a significant increase in number of Iba1-positive cells as early as E17.5 in virally infected mouse brains in subcortical structures and ventricles (Fig. 4.5A,C), suggesting microglial activation 3 days post viral infection. P3 infected brains exhibited sustained microglial activation and morphological changes, with a drastic increase in Iba1-positive cells compared with controls (Fig. 4.5B,C), spread across the brain parenchyma. Importantly, there is a significant increase in Iba1-positive cells at P3 compared with E17.5 in virally infected brains (Fig. 4.5A-C), suggesting a continued and progressive increase in microglial activation after ZIKV infection.

Astrocytes are the most abundant cell type in the CNS and provide neuronal support by supplying nutrients, maintaining the chemical environment, and clearing neurotransmitters. Astrogliosis is the abnormal increase and change in morphology and behavior of astrocytes in the brain, typically in response to brain injury including viral infection (Sofroniew, 2009). To confirm that ZIKV infection induces brain damage, we examined the astrocyte population and morphology. Using GFAP staining to identify reactive astrocytes in the cortex at P3, we observed a significant increase in the number

**Figure 4.5. Extensive microglial activation and astrogliosis in ZIKV-infected brain.**



(A,B) Confocal micrographs of coronal sections of E17.5 (A) and P3 (B) brains stained with antibodies against Iba1 (green) or GFAP (red). Hoechst stains nuclei (blue). Right panels are enlargements of the regions outlined by white boxes in left panels. Scale bars: 50  $\mu\text{m}$  (left panels in A and B); 10  $\mu\text{m}$  (right panels in A) and 20  $\mu\text{m}$  (right panels in B). (C) Quantification of Iba1-positive cells per  $\text{mm}^2$  in a  $1.314 \times 10^5 \mu\text{m}^2$  boxed area of E17.5 cerebral cortex from the experiment shown in A, and a  $1.314 \times 10^5 \mu\text{m}^2$  boxed area of P3 cerebral cortex from the experiment shown in B. Error bars indicate s.e.m. of nine sections from three independent experiments. \* $P < 0.05$ , \*\*\* $P < 0.001$  (Student's t-test for comparison of mock- versus ZIKV- infected brains). Two-way ANOVA analysis detected a significant difference in the increase of Iba1-positive cells between E17.5 and P3 (\* $P < 0.05$ ). (D) Quantification of GFAP-positive cells in a  $1.314 \times 10^5 \mu\text{m}^2$  boxed area of P3 cerebral cortex from the experiment shown in B. Error bars indicate s.e.m. of nine sections from three independent experiments. \*\*\* $P < 0.001$  (Student's t-test).

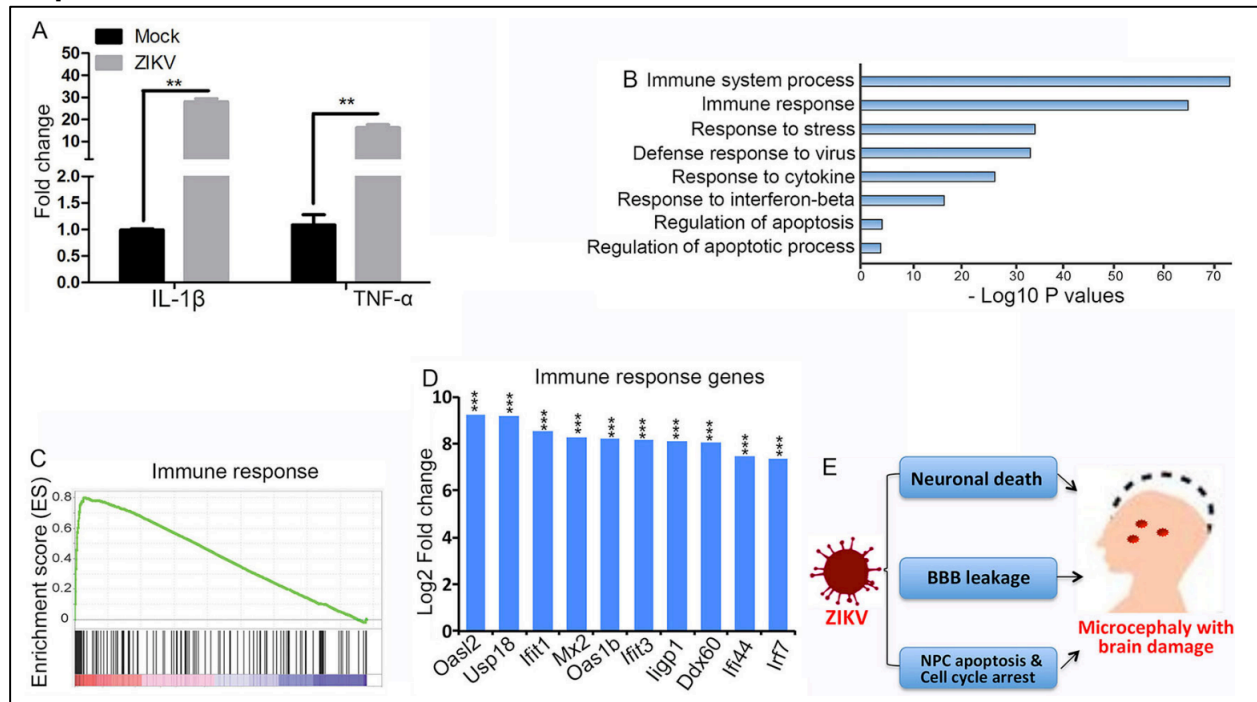
of astrocytes in ZIKV-infected brains (Fig. 4.5B,D), suggesting astrogliosis and brain injury in P3 brains. In healthy brains, GFAP is only expressed in the radial glia and fibrous astrocytes of the white matter, but strong GFAP expression in the cortex and changes in morphology indicate a change of protoplasmic astrocytes into reactive astrocytes (Fig. 4.5B). We did not detect significant changes in GFAP-positive cells at E17.5 (data not shown). Together, these results indicate that ZIKV infection results in progressive microglial activation and astrogliosis, further supporting the notion that ZIKV induces brain damage.

#### ZIKV induces dysregulation of genes involved in immune response

ZIKV triggers inflammation and an antiviral response in human skin fibroblasts, including the upregulation of interleukin-1 beta (IL-1 $\beta$ ; IL1B) (Hamel et al., 2015). It has been reported that IL-1 $\beta$  and tumor necrosis factor- $\alpha$  (TNF- $\alpha$ ) induce damages to the vasculature and neurons (Friedl et al., 2002; Lu, Wang, Yang, Yang, & Chen, 2005; Puhlmann et al., 2005; Takeuchi et al., 2006). Therefore, we hypothesize that NPCs will generate an immune and inflammation response after ZIKV infection. To test this hypothesis, we infected NPCs, isolated from developing brains, with ZIKV for 48 h followed by RT-PCR analyses. We found that expression of IL-1 $\beta$  and TNF- $\alpha$  was dramatically increased after viral infection (Fig. 4.6A), suggesting that ZIKV induced an immune response in the NPCs.

To improve our understanding of ZIKV-induced immune responses in the developing brain at genome-wide levels, we performed global transcriptome analyses (RNA-Seq) using RNAs isolated from E17.5 brains after viral infection at E14.5. A large number of differentially expressed genes after viral infection were identified with RNA-

**Figure 4.6. ZIKV induces dysregulation of genes involved in the immune response.**



(A) RT-PCR analysis of expression of IL-1 $\beta$  and TNF- $\alpha$  in NPCs. NPCs isolated from E14.5 developing brains were infected with ZIKV (multiplicity of infection: 5) followed by RNA isolation at 48 h post-infection. Error bars indicate s.e.m. of three independent experiments. \*\*P<0.01 (Student's t-test). (B) RNA-Seq analyses of E17.5 brains after ZIKV infection at E14.5. The dysregulated genes in ZIKV-infected brains compared with controls were subjected to GO analysis. (C) Gene set enrichment analysis (GSEA) reveals dysregulated genes in immune response in ZIKV-infected brains. x-axis represents the gene ranks in ordered immune response dataset. (D) RNA expression analyses of RNA-Seq data (Table S1 (Shao et al., 2016)) show that the top ten most significantly upregulated genes in infected brains are involved in immune response. \*\*\*P<0.001 (Student's t-test). (E) A diagram showing that ZIKV causes neuronal death, abnormal vasculature and BBB leakage, and cell cycle arrest and apoptosis of NPCs, resulting in postnatal microcephaly with brain damage.

Seq analysis (Table S1 (Shao et al., 2016)). We next performed Gene Ontology analyses with those genes for which expression was significantly altered after viral infection. Our results revealed a set of genes that are associated with the immune response and apoptosis pathways (Fig. 4.6B). Gene set enrichment analyses (GSEA) further show significant enrichments on both the immune system response and apoptosis pathways (Fig. 4.6C; data not shown). Most notably, the top ten most upregulated genes are associated with interferon response (Fig. 4.6D). Together, these results suggest that ZIKV infection triggers an aggressive immune response, which has the potential to cause exacerbation of brain damage by enhancing neuronal death and generating vascular abnormalities.

### Discussion

In this study, we have established a mouse model of fetal brain abnormalities associated with ZIKV, and provide a direct causative link between ZIKV and postnatal microcephaly in vivo. ZIKV triggers a strong immune response in the developing brain. In addition to disrupting NPCs, ZIKV infection leads to massive neuronal death and BBB leakage, resulting in postnatal microcephaly with extensive brain damage (Fig. 4.6E).

Studies from our mouse model provide novel insights into microcephaly associated with ZIKV infection during pregnancy. First, ZIKV infection is sufficient to cause postnatal microcephaly. Previous studies have all described embryonic lethality, whereas our ZIKV-infected pups survived after birth. Importantly, ZIKV-infected human fetuses can be born alive exhibiting microcephaly, which suggests that our postnatal microcephaly animal model is disease relevant. In addition to microcephaly, our

postnatal mouse model recapitulates major aspects of fetal brain abnormalities associated with ZIKV in humans, including extensive neuronal apoptosis and loss, axonal rarefaction, and reactive astrocyte and microglial cell accumulation (Rita W. Driggers et al., 2016; Mlakar et al., 2016; Oliveira Melo et al., 2016), which have not been described in previous animal models. Second, our data suggest that neuronal cell death contributes significantly to the microcephaly associated with ZIKV, consistent with the selective neuronal vulnerability to ZIKV observed in humans (Rita W. Driggers et al., 2016). Interestingly, these observations are in contrast with classic microcephaly conditions, in which NPC depletion is the major cause of the smaller brain phenotype based on studies from other animal models for microcephaly (Z. Chen et al., 2014; Gruber et al., 2011; Thornton & Woods, 2009). Our current studies cannot yet determine whether ZIKV directly infects terminally differentiated neurons, resulting in their death, or if ZIKV-infected NPCs differentiate into neurons followed by neuronal death. Future studies should address the relative contributions of neuronal death and reduced neuronal production due to defective NPCs in causing microcephaly. Another limitation of our studies is the lack of a control viral infection such as dengue virus, which would allow us to distinguish ZIKV-specific effects from general toxicity of viral infection. Although we observed consistent growth restriction and microcephaly from ZIKV-infected pups compared with controls (Fig. 4.1H, n=6), future studies should increase the numbers of mice analyzed in each experiment. Third, ZIKV-associated microcephaly is coupled with global growth restriction. It is intriguing that ZIKV intracerebral inoculation causes global growth restriction of mice. It is possible that local

brain infection of ZIKV can result in a global effect on growth restriction due to the inflammatory and antiviral immune responses of the embryo.

Our studies have uncovered that ZIKV causes BBB leakage in the developing brain, which could contribute to brain damage. Previous studies suggest that BBB deficiency leads to calcification in neurons (Keller et al., 2013), probably due to the formation of a nidus from plasma proteins accumulating in the parenchyma from a leaky BBB (Miklossy et al., 2005). We found altered vasculature and a leaky BBB in ZIKV-infected mouse brains. However, our multiple attempts failed to detect calcification in the ZIKV-infected brains, which could be due to the relatively short pregnancy period in mice compared with humans. Future studies should reveal whether BBB deficiency does indeed cause or contribute to brain calcification associated with ZIKV infection in humans. It will be of interest to determine what causes vascular abnormalities in ZIKV-infected brains, although inflammation associated with ZIKV infection is likely to play important roles (Friedl et al., 2002; Puhlmann et al., 2005). Future studies should also reveal potential detrimental effects of BBB leakage on NPCs and differentiated neurons.

We found that ZIKV causes extensive brain damage. Classical microcephaly is characterized by smaller brain size without other obvious neuronal and brain damage (Nigg & Stearns, 2011; Thornton & Woods, 2009). Previous studies examining ZIKV-induced microcephaly have focused on NPC behaviors and do not describe other negative contributions to brain development. Therefore, it remained unclear from the current literature whether animal models of ZIKV pathogenesis can be used to recapitulate brain abnormalities other than microcephaly. Our discovery of massive

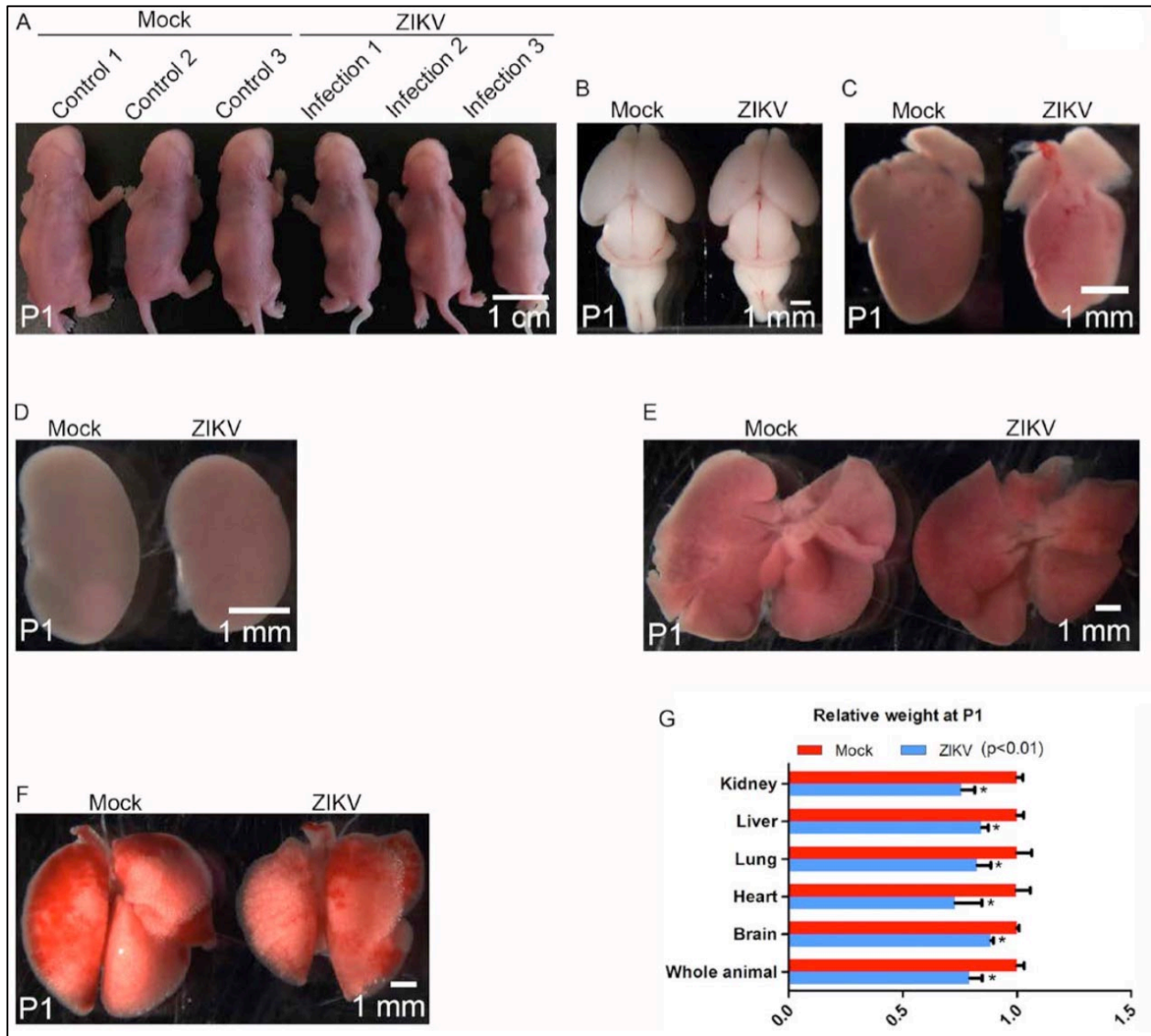
neuronal death, leaky BBB, and astrogliosis in ZIKV-infected brains is the first study to suggest that ZIKV causes extensive brain damage.

ZIKV has been detected in amniotic fluid, placental tissues, and fetal and newborn brains (Calvet et al., 2016; Rita W. Driggers et al., 2016; Mlakar et al., 2016; Noronha, Zanluca, Azevedo, Luz, & Santos, 2016), suggesting that ZIKV can cross the placenta and infect fetal brains. Furthermore, it has been reported that ZIKV can infect human placental macrophages and trophoblasts (Quicke et al., 2016). Mouse model studies suggest that ZIKV can infect and damage the placenta, and cause microcephaly and growth restriction (Cugola et al., 2016; Miner et al., 2016). Our intracerebral inoculation method bypasses the placenta and infects fetal brains directly. We acknowledge the limitations of our animal model in studying ZIKV disease mechanisms in early pregnancy, in particular in investigating if and how ZIKV crosses the placenta. However, the unique survival of our ZIKV-infected pups after birth due to a different virus dosage, infection methods and timing provides advantages for studying the wide spectrum of brain abnormalities associated with ZIKV infection.

### Acknowledgements

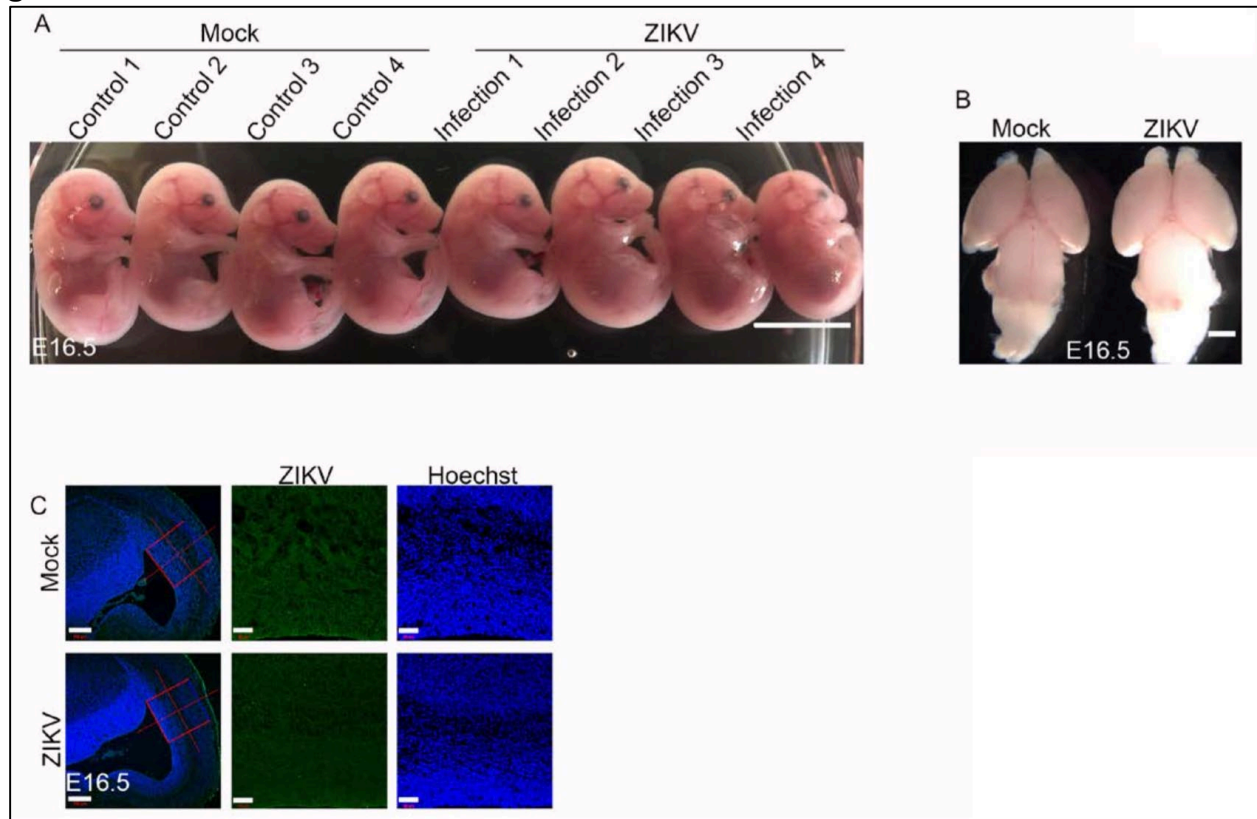
We thank Chen lab colleagues for stimulating discussions. Zika isolates were provided by the World Reference Center for Emerging Viruses and Arboviruses at UTMB.

**Supplemental Figure 4.S1. ZIKV infection results in microcephaly and growth restriction at P1.**



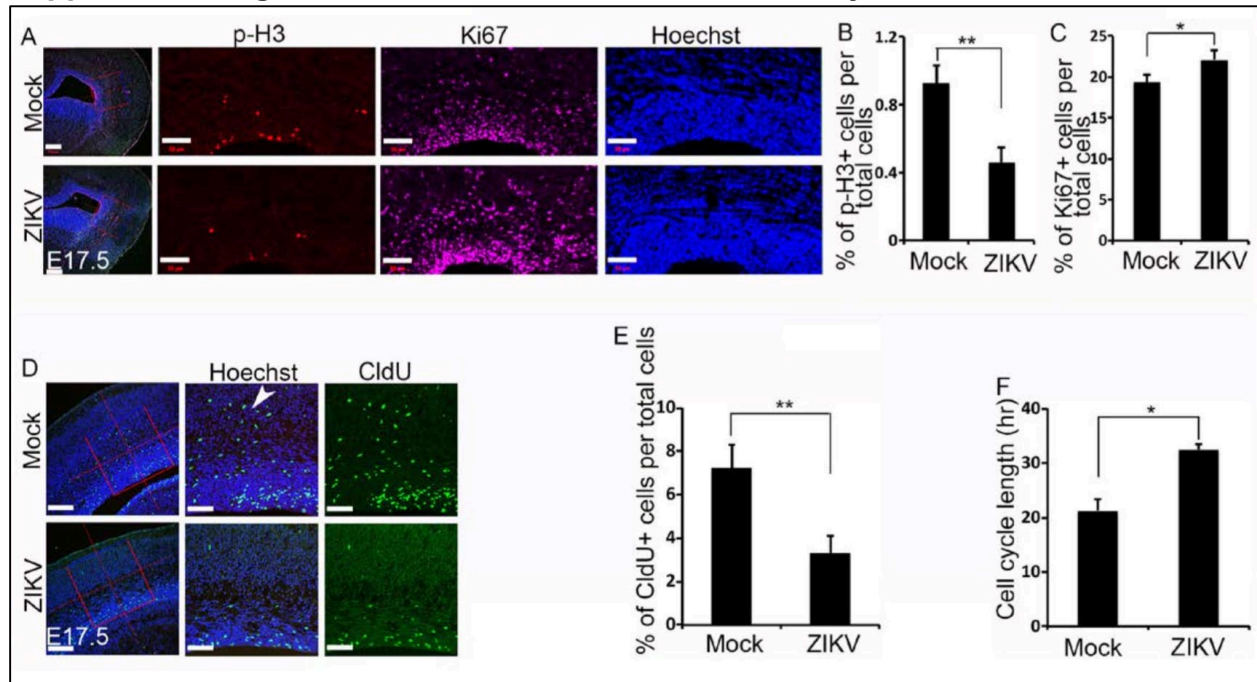
(A-F) Dorsal views of postnatal day 1 (P1) pups (A), brains (B), hearts (C), kidneys (D), livers (E), and lungs (F). Scale bar: 1 cm and 1 mm. ~ 1  $\mu$ l  $1.7 \times 10^6$  TCID<sub>50</sub>/mL ZIKV was injected into cerebral ventricles of embryonic day 14.5 (E14.5) brains followed by analyses at P1. (G) Relative weights of different organs from P1 control or ZIKV infected pups. Error bars indicate SEM of three independent experiments with one mock and one ZIKV infected brain in each experiment ( $p < 0.01$ , student's t-test).

**Supplemental Figure 4.S2. ZIKV infection does not cause microcephaly and growth restriction at E16.5.**



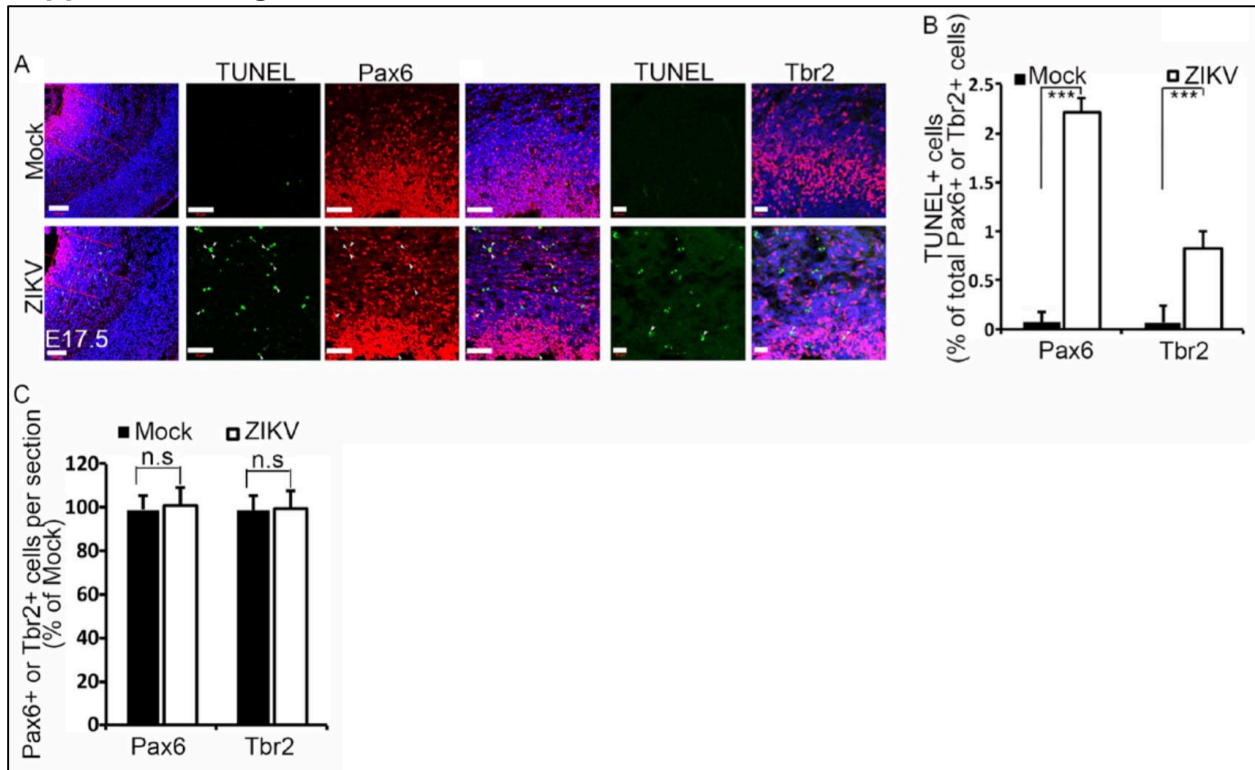
(A, B): Lateral views of E16.5 embryos (A) and dorsal views of brains (B). Scale bar: 1 cm and 1 mm.  $\sim 1 \text{ ul } 1.7 \times 10^6 \text{ TCID}_{50}/\text{mL}$  ZIKV was injected into the cerebral ventricles of embryonic day 14.5 (E14.5) brains followed by analyses at E16.5. (C) Confocal images of coronal sections from E16.5 brains stained with antibodies against Flavivirus group antigen (ZIKV, green). Hoechst stains nuclei (blue). Scale bar: 500  $\mu\text{m}$ .

**Supplemental Figure 4.S3. ZIKV infection leads to cell cycle arrest of NPCs.**



(A) Confocal micrographs of coronal sections stained with antibodies against p-H3 (red) and Ki67 (purple). Hoechst stains nuclei (blue). Right panels are enlargements of the ventricular regions in the red boxes in left panels. Scale bar: 200  $\mu\text{m}$  (left panels); 50  $\mu\text{m}$  (right panels). (B, C) Quantification of percentage of p-H3- (B) and Ki67- (C) positive cells per total cells in a  $7.492 \times 10^4 \mu\text{m}^2$  boxed area of E17.5 cerebral cortex from experiment A. Error bars indicate SEM of 9 sections from three independent experiments,  $**p < 0.01$  and  $*p < 0.05$  (Student's t-test). (D) Confocal micrographs of coronal sections stained with antibodies against CldU (green) after a 2 hr CldU pulse. Hoechst stains nuclei (blue). Right panels are enlargements of the regions outlined by red boxes in left panels. Scale bar: 200  $\mu\text{m}$  (left panels); 100  $\mu\text{m}$  (right panels). White arrowhead indicates cells outside the VZ/SVZ of cerebral cortex. (E) Quantification of percentage of CldU positive cells per total cells in a  $2.877 \times 10^5 \mu\text{m}^2$  boxed area of E17.5 cerebral cortex from experiment D. Error bars indicate SEM of 9 sections from three independent experiments,  $**p < 0.01$  (Student's t-test). (F) Quantification of cell cycle length of NPCs in the VZ/SVZ of E17.5 cerebral cortex. Pregnant mice were injected with CldU for 1.5 hrs followed by EdU injection for 0.5 hrs before brain dissection. Error bars indicate SEM of 9 sections from three independent experiments,  $*p < 0.05$  (Student's t-test).

**Supplemental Figure 4.S4. ZIKV causes minor cell death in NPCs.**



(A) TUNEL staining (green) reveals apoptotic cell death in Pax6-positive apical neural progenitors and Tbr2-positive intermediate neural progenitors. White arrowheads indicate TUNEL- and Pax6-double positive cells, and TUNEL- and Tbr2-double positive cells. Hoechst stains nuclei (blue). Right panels are enlargements of the regions outlined by red boxes in left panels. Scale bar: 100  $\mu$ m (left panels); 50  $\mu$ m (middle panels); 20  $\mu$ m (right panels). (B) Quantification of the percentage of TUNEL- positive cells out of total Pax6- or Tbr2-positive cells in experiments A. Error bars indicate SEM of 9 sections from three independent experiments, \*\*\*\* $p$  < 0.001 (Student's t-test). (C) Quantification of Pax6- or Tbr2- positive cells per section relative to Mock controls in experiments A. Error bars indicate SEM of 9 sections from three independent experiments, n.s represents not significant (Student's t-test).

## References

- Angevine, J. B., & Sidman, R. L. (1961). Autoradiographic study of cell migration during histogenesis of cerebral cortex in the mouse. *Nature*.  
<http://doi.org/10.1038/192766b0>
- Ben-Zvi, A., Lacoste, B., Kur, E., Andreone, B. J., Mayshar, Y., Yan, H., & Gu, C. (2014). Mfsd2a is critical for the formation and function of the blood-brain barrier. *Nature*. <http://doi.org/10.1038/nature13324>
- Brasil, P., Pereira, Jr., J. P., Raja Gabaglia, C., Damasceno, L., Wakimoto, M., Ribeiro Nogueira, R. M., ... Nielsen-Saines, K. (2016). Zika Virus Infection in Pregnant Women in Rio de Janeiro — Preliminary Report. *New England Journal of Medicine*.  
<http://doi.org/10.1056/NEJMoa1602412>
- Calvet, G., Aguiar, R. S., Melo, A. S. O., Sampaio, S. A., de Filippis, I., Fabri, A., ... de Filippis, A. M. B. (2016). Detection and sequencing of Zika virus from amniotic fluid of fetuses with microcephaly in Brazil: a case study. *The Lancet Infectious Diseases*. [http://doi.org/10.1016/S1473-3099\(16\)00095-5](http://doi.org/10.1016/S1473-3099(16)00095-5)
- Chen, J.-F., Zhang, Y., Wilde, J., Hansen, K. C., Lai, F., & Niswander, L. (2014). Microcephaly disease gene Wdr62 regulates mitotic progression of embryonic neural stem cells and brain size. *Nat Commun*, 5.  
<http://doi.org/10.1038/ncomms4885>
- Chen, Z., Jalabi, W., Hu, W., Park, H.-J., Gale, J. T., Kidd, G. J., ... Trapp, B. D. (2014). Microglial displacement of inhibitory synapses provides neuroprotection in the adult

- brain. *Nature Communications*, 5(July), 4486. <http://doi.org/10.1038/ncomms5486>
- Corbin, J. G., Nery, S., & Fishell, G. (2001). Telencephalic cells take a tangent: non-radial migration in the mammalian forebrain. *Nature Neuroscience*, 4 Suppl, 1177–82. <http://doi.org/10.1038/nn749>
- Cugola, F. R., Fernandes, I. R., Russo, F. B., Freitas, B. C., Dias, J. L. M., Guimarães, K. P., ... Beltrão-Braga, P. C. B. (2016). The Brazilian Zika virus strain causes birth defects in experimental models. *Nature*, 534(7606), 267–271. Retrieved from <http://dx.doi.org/10.1038/nature18296>
- Dang, J., Tiwari, S. K., Lichinchi, G., Qin, Y., Patil, V. S., Eroshkin, A. M., & Rana, T. M. (2016). Zika Virus Depletes Neural Progenitors in Human Cerebral Organoids through Activation of the Innate Immune Receptor TLR3. *Cell Stem Cell*, 19(2), 258–265. <http://doi.org/10.1016/j.stem.2016.04.014>
- Driggers, R. W., Ho, C.-Y., Korhonen, E. M., Kuivanen, S., Jääskeläinen, A. J., Smura, T., ... Vapalahti, O. (2016). Zika Virus Infection with Prolonged Maternal Viremia and Fetal Brain Abnormalities. *The New England Journal of Medicine*, NEJMoa1601824. <http://doi.org/10.1056/NEJMoa1601824>
- Driggers, R. W., Ho, C.-Y., Korhonen, E. M., Kuivanen, S., Jääskeläinen, A. J., Smura, T., ... Vapalahti, O. (2017). Zika Virus Infection With Prolonged Maternal Viremia and Fetal Brain Abnormalities. *Obstetric Anesthesia Digest*. <http://doi.org/10.1097/01.aoa.0000512046.09676.84>
- Friedl, J., Puhlmann, M., Bartlett, D. L., Libutti, S. K., Turner, E. N., Gnant, M. F. X., & Alexander, H. R. (2002). Induction of permeability across endothelial cell

monolayers by tumor necrosis factor (TNF) occurs via a tissue factor-dependent mechanism: relationship between the procoagulant and permeability effects of TNF. *Blood*.

Garcez, P. P., Loiola, E. C., Da Costa, R. M., Higa, L. M., Trindade, P., Delvecchio, R., ... Rehen, S. K. (2016). Zika virus: Zika virus impairs growth in human neurospheres and brain organoids. *Science*. <http://doi.org/10.1126/science.aaf6116>

Gruber, R., Zhou, Z., Sukchev, M., Joerss, T., Frappart, P. O., & Wang, Z. Q. (2011). MCPH1 regulates the neuroprogenitor division mode by coupling the centrosomal cycle with mitotic entry through the Chk1-Cdc25 pathway. *Nature Cell Biology*. <http://doi.org/10.1038/ncb2342>

Hamel, R., Dejarnac, O., Wichit, S., Ekchariyawat, P., Neyret, A., Luplertlop, N., ... Missé, D. (2015). Biology of Zika Virus Infection in Human Skin Cells. *Journal of Virology*. <http://doi.org/10.1128/JVI.00354-15>

Hevner, R. F., Shi, L., Justice, N., Hsueh, Y. P., Sheng, M., Smiga, S., ... Rubenstein, J. L. R. (2001). Tbr1 regulates differentiation of the preplate and layer 6. *Neuron*. [http://doi.org/10.1016/S0896-6273\(01\)00211-2](http://doi.org/10.1016/S0896-6273(01)00211-2)

Heymann, D. L., Hodgson, A., Sall, A. A., Freedman, D. O., Staples, J. E., Althabe, F., ... Menon, K. U. (2016). Zika virus and microcephaly: Why is this situation a PHEIC? *The Lancet*, 387(10020), 719–721. [http://doi.org/10.1016/S0140-6736\(16\)00320-2](http://doi.org/10.1016/S0140-6736(16)00320-2)

Keller, A., Westenberger, A., Sobrido, M. J., García-Murias, M., Domingo, A., Sears, R. L., ... Oliveira, J. R. M. (2013). Mutations in the gene encoding PDGF-B cause

brain calcifications in humans and mice. *Nature Genetics*.

<http://doi.org/10.1038/ng.2723>

Kriegstein, A., & Alvarez-Buylla, A. (2009). The Glial Nature of Embryonic and Adult Neural Stem Cells. *Annual Review of Neuroscience*, 32(1), 149–184.

<http://doi.org/10.1146/annurev.neuro.051508.135600>

Li, C., Xu, D., Ye, Q., Hong, S., Jiang, Y., Liu, X., ... Xu, Z. (2016). Zika Virus Disrupts Neural Progenitor Development and Leads to Microcephaly in Mice. *Cell Stem Cell*, 19(5), 672. <http://doi.org/10.1016/j.stem.2016.10.017>

Li, H., Saucedo-Cuevas, L., Regla-Nava, J. A., Chai, G., Sheets, N., Tang, W., ... Gleeson, J. G. (2016). Zika Virus Infects Neural Progenitors in the Adult Mouse Brain and Alters Proliferation. *Cell Stem Cell* (Vol. 19). Retrieved from

<http://www.sciencedirect.com/science/article/pii/S1934590916302521>

Lu, K.-T., Wang, Y.-W., Yang, J.-T., Yang, Y.-L., & Chen, H.-I. (2005). Effect of Interleukin-1 on Traumatic Brain Injury–Induced Damage to Hippocampal Neurons. *Journal of Neurotrauma*. <http://doi.org/10.1089/neu.2005.22.885>

Manzini, M. C., & Walsh, C. A. (2011). What disorders of cortical development tell us about the cortex: one plus one doesn't always make two. *Current Opinion in Genetics & Development*, 21(3), 333–339. <http://doi.org/10.1016/j.gde.2011.01.006>

Marín, O., & Rubenstein, J. L. R. (2003). CELL MIGRATION IN THE FOREBRAIN. *Annual Review of Neuroscience*, 26(1), 441–483.

<http://doi.org/10.1146/annurev.neuro.26.041002.131058>

- Marrs, C., Olson, G., Saade, G., Hankins, G., Wen, T., Patel, J., & Weaver, S. (2016). Zika Virus and Pregnancy: A Review of the Literature and Clinical Considerations. *American Journal of Perinatology*, 33(7), 625–639. <http://doi.org/10.1055/s-0036-1580089>
- Martynoga, B., Morrison, H., Price, D. J., & Mason, J. O. (2005). Foxg1 is required for specification of ventral telencephalon and region-specific regulation of dorsal telencephalic precursor proliferation and apoptosis. *Developmental Biology*, 283(1), 113–127. <http://doi.org/10.1016/j.ydbio.2005.04.005>
- Miklossy, J., Mackenzie, I. R., Dorovini-Zis, K., Calne, D. B., Wszolek, Z. K., Klegeris, A., & McGeer, P. L. (2005). Severe vascular disturbance in a case of familial brain calcinosis. *Acta Neuropathologica*, 109(6), 643–653. <http://doi.org/10.1007/s00401-005-1007-7>
- Miner, J. J., Cao, B., Govero, J., Smith, A. M., Fernandez, E., Cabrera, O. H., ... Diamond, M. S. (2016). Zika Virus Infection during Pregnancy in Mice Causes Placental Damage and Fetal Demise. *Cell*, 165(5), 1081–1091. <http://doi.org/10.1016/j.cell.2016.05.008>
- Mlakar, J. . J., Korva, M. M. . M., Tul, N. N. . N., Popović, M. M. ., Poljšak-Prijatelj, M. M. ., Mraz, J. J. . J., ... Avšič Županc, T. (2016). Zika Virus Associated with Microcephaly. *New England Journal of Medicine*, 374(10), 951–958. <http://doi.org/10.1056/NEJMoa1600651>
- Mullen, R. J., Buck, C. R., & Smith, A. M. (1992). NeuN, a neuronal specific nuclear protein in vertebrates. *Development*, 116(1), 201 LP-211. Retrieved from

<http://dev.biologists.org/content/116/1/201.abstract>

Nayak, D., Roth, T. L., & McGavern, D. B. (2014). Microglia Development and Function. *Annual Review of Immunology*, 32(1), 367–402. <http://doi.org/10.1146/annurev-immunol-032713-120240>

Nieto, M., Monuki, E. S., Tang, H., Imitola, J., Haubst, N., Khoury, S. J., ... Walsh, C. A. (2004). Expression of Cux-1 and Cux-2 in the subventricular zone and upper layers II–IV of the cerebral cortex. *Journal of Comparative Neurology*, 479(2), 168–180. <http://doi.org/10.1002/cne.20322>

Nigg, E. A., & Raff, J. W. (2009). Centrioles, Centrosomes, and Cilia in Health and Disease. *Cell*, 139(4), 663–678. <http://doi.org/10.1016/j.cell.2009.10.036>

Nigg, E. A., & Stearns, T. (2011). The centrosome cycle: Centriole biogenesis, duplication and inherent asymmetries. *Nature Cell Biology*, 13, 1154. Retrieved from <http://dx.doi.org/10.1038/ncb2345>

Noronha, L. de, Zanluca, C., Azevedo, M. L. V., Luz, K. G., & Santos, C. N. D. dos. (2016). Zika virus damages the human placental barrier and presents marked fetal neurotropism . *Memórias Do Instituto Oswaldo Cruz* . scielo .

Nowakowski, R. S., Lewin, S. B., & Miller, M. W. (1989). Bromodeoxyuridine immunohistochemical determination of the lengths of the cell cycle and the DNA-synthetic phase for an anatomically defined population. *Journal of Neurocytology*, 18(3), 311–318. <http://doi.org/10.1007/BF01190834>

Oliveira Melo, A. S., Malinger, G., Ximenes, R., Szejnfeld, P. O., Alves Sampaio, S., &

- Bispo de Filippis, A. M. (2016). Zika virus intrauterine infection causes fetal brain abnormality and microcephaly: tip of the iceberg? *Ultrasound in Obstetrics & Gynecology*, 47(1), 6–7. <http://doi.org/10.1002/uog.15831>
- Puhlmann, M., Weinreich, D. M., Farma, J. M., Carroll, N. M., Turner, E. M., & Alexander, H. R. (2005). Interleukin-1 $\beta$  induced vascular permeability is dependent on induction of endothelial Tissue Factor (TF) activity. *Journal of Translational Medicine*, 3(1), 37. <http://doi.org/10.1186/1479-5876-3-37>
- Qian, X., Nguyen, H. N., Song, M. M., Hadiono, C., Ogden, S. C., Hammack, C., ... Ming, G. L. (2016). Brain-Region-Specific Organoids Using Mini-bioreactors for Modeling ZIKV Exposure. *Cell*, 165(5), 1238–1254. <http://doi.org/10.1016/j.cell.2016.04.032>
- Quicke, K. M., Bowen, J. R., Johnson, E. L., McDonald, C. E., Ma, H., O'Neal, J. T., ... Suthar, M. S. (2016). Zika Virus Infects Human Placental Macrophages. *Cell Host and Microbe*, 20(1), 83–90. <http://doi.org/10.1016/j.chom.2016.05.015>
- Ramos da Silva, S., & Gao, S. J. (2016). Zika virus: An update on epidemiology, pathology, molecular biology, and animal model. *Journal of Medical Virology*. <http://doi.org/10.1002/jmv.24563>
- Saiz, J. C., Vázquez-Calvo, Á., Blázquez, A. B., Merino-Ramos, T., Escribano-Romero, E., & Martín-Acebes, M. A. (2016). Zika virus: The latest newcomer. *Frontiers in Microbiology*. <http://doi.org/10.3389/fmicb.2016.00496>
- Semple, B. D., Blomgren, K., Gimlin, K., Ferriero, D. M., & Noble-Haeusslein, L. J. (2013). Brain development in rodents and humans: Identifying benchmarks of

- maturation and vulnerability to injury across species. *Progress in Neurobiology*, 106, 1–16. <http://doi.org/10.1016/j.pneurobio.2013.04.001>
- Shao, Q., Herrlinger, S., Yang, S.-L., Lai, F., Moore, J. M. J. M., Brindley, M. A. M. A., & Chen, J.-F. J.-F. (2016). Zika virus infection disrupts neurovascular development and results in postnatal microcephaly with brain damage. *Development (Cambridge, England)*, 143(22), 4127–4136. <http://doi.org/10.1242/dev.143768>
- Siegenthaler, J. A., Tremper-Wells, B. A., & Miller, M. W. (2008). Foxg1 haploinsufficiency reduces the population of cortical intermediate progenitor cells: effect of increased p21 expression. *Cerebral Cortex*, 18(8), 1865–1875. <http://doi.org/10.1093/cercor/bhm209>
- Sofroniew, M. V. (2009). Molecular dissection of reactive astrogliosis and glial scar formation. *Trends in Neurosciences*, 32(12), 638–647. <http://doi.org/10.1016/j.tins.2009.08.002>
- Takeuchi, H., Jin, S., Wang, J., Zhang, G., Kawanokuchi, J., Kuno, R., ... Suzumura, A. (2006). Tumor necrosis factor- $\alpha$  induces neurotoxicity via glutamate release from hemichannels of activated microglia in an autocrine manner. *Journal of Biological Chemistry*, 281(30), 21362–21368. <http://doi.org/10.1074/jbc.M600504200>
- Tang, H., Hammack, C., Ogden, S. C., Wen, Z., Qian, X., Li, Y., ... Ming, G. L. (2016). Zika virus infects human cortical neural progenitors and attenuates their growth. *Cell Stem Cell*, 18(5), 587–590. <http://doi.org/10.1016/j.stem.2016.02.016>
- Thornton, G. K., & Woods, C. G. (2009). Primary microcephaly: do all roads lead to Rome? *Trends in Genetics*, 25(11), 501–510.

<http://doi.org/10.1016/j.tig.2009.09.011>

## CHAPTER 5

### THE AFRICAN ZIKA VIRUS MR-766 IS MORE VIRULENT AND CAUSES MORE SEVERE BRAIN DAMAGE THAN CURRENT ASIAN LINEAGE AND DENGUE VIRUS<sup>1</sup>

---

<sup>1</sup> Stephanie Herrlinger\*, Qiang Shao\*, Yanan Zhu, Mei Yang, Forrest Goodfellow, Xiao-Peng Qi, Fan Lai, Melinda A. Brindley, and Jian-Fu Chen. 2017. *Development*. 10.1242/dev.156752. \*co-first authorship. Reprinted here with permission of the publisher. URL: <http://dev.biologists.org/content/144/22/4114.long>

## Abstract

The Zika virus (ZIKV) has two lineages, Asian and African, and their impact on developing brains has not been compared. Dengue virus (DENV) is a close family member of ZIKV and co-circulates with ZIKV. Here, we performed intracerebral inoculation of embryonic mouse brains with dengue virus 2 (DENV2), and found that DENV2 is sufficient to cause smaller brain size due to increased cell death in neural progenitor cells (NPCs) and neurons. Compared with the currently circulating Asian lineage of ZIKV (MEX1-44), DENV2 grows slower, causes less neuronal death and fails to cause postnatal animal death. Surprisingly, our side-by-side comparison uncovered that the African ZIKV isolate (MR-766) is more potent at causing brain damage and postnatal lethality than MEX1-44. In comparison with MEX1-44, MR-766 grows faster in NPCs and in the developing brain, and causes more pronounced cell death in NPCs and neurons, resulting in more severe neuronal loss. Together, these results reveal that DENV2 is sufficient to cause smaller brain sizes, and suggest that the ZIKV African lineage is more toxic and causes more potent brain damage than the Asian lineage.

## Introduction

Zika virus (ZIKV) is an emerging Flaviviridae family member of significant public health concern. ZIKV infection during pregnancy causes severe congenital birth defects including microcephaly, fetal growth restriction, stillbirth, ocular disorders and CNS injury, among others (Brasil et al., 2016; Marrs et al., 2016; Ventura, Maia, Bravo-Filho, Góis, & Belfort, 2016). ZIKV has two major lineages: the Asian lineage and African lineage. The Asian lineage is currently circulating in North, Central and South America, and induces congenital brain disorders (Faria et al., 2016; Haddock et al., 2012; Hamel et al., 2016). Historically, there is no scientific documentation of ZIKV-associated birth defects in Africa, where the virus originated. It has been speculated that the African lineage of ZIKV evolved into a more virulent form as it traveled from Africa to South America. It is also possible that African countries have limited health programs and, as a result, did not document ZIKV-associated birth defects, or that infection with this lineage causes early embryonic lethality prior to virus detection (<http://time.com/4219240/zika-africa-origins-microcephaly-vaccine/>). Whereas these observations have raised the possibility that the historical African lineage is less virulent than the current Asian isolates associated with birth defects, experimental evidence supporting this hypothesis is lacking. Direct comparison of the impact of these lineages in the developing brain has not been performed.

Dengue virus (DENV) is a single positive-stranded RNA virus with four serotypes (DENV1-4). DENV and ZIKV belong to the same Flaviviridae family, and both viruses spread primarily through *Aedes* genus mosquitoes (Faria et al., 2016; Hamel et al., 2016). DENV is currently co-circulating with ZIKV in Brazil, the area most impacted by

the recent ZIKV outbreak (Marcio R.T. Nunes et al., 2014; Marcio Roberto Teixeira Nunes et al., 2012). Co-circulation and co-infection with different Flaviviridae family members is becoming a common phenomenon (Dupont-Rouzeyrol et al., 2015; Paniz-Mondolfi, Rodriguez-Morales, Blohm, Marquez, & Villamil-Gomez, 2016). DENV and ZIKV co-infection has also been identified in pregnant women, although pathological outcomes remain unknown so far (Villamil-Gómez et al., 2016). Recent studies showed a complex immunogenic crosstalk between ZIKV and DENV (Barba-Spaeth et al., 2016; Dejnirattisai et al., 2016; Priyamvada et al., 2016; Stettler et al., 2016; Swanstrom et al., 2016). Antibodies against E protein domain I/II (EDI/II) of ZIKV potentially enhanced DENV infection in vitro, and lethally enhanced DENV disease in mice (Stettler et al., 2016). These emerging data raise the concern of the potential detrimental effects of DENV on the developing brain. However, the consequence of DENV infection in the developing brain remains largely unknown.

To fill in these knowledge gaps, we have performed intracerebral inoculation of embryonic mouse brains. We found that DENV2 is sufficient to cause microcephaly through enhanced cell death in neural progenitor cells (NPCs) and neurons. To understand why DENV has not been linked with congenital brain disorders, we performed a side-by-side comparison. We found that DENV2 grows slower and causes minimal neuronal death, resulting in less severe microcephaly than the currently circulating ZIKV Asian lineage (MEX1-44). Importantly DENV2-infected pups exhibited no postnatal lethality. To directly compare ZIKV African strains and ZIKV Asian strains, we performed a side-by-side intracerebral inoculation of MEX1-44 (Asian lineage) and MR-766, a brain-adapted African lineage strain. Experimental results showed that MR-

766 is more potent in causing brain damage and postnatal mortality than MEX1-44. Our mechanistic studies suggest that MR-766 grows faster and causes much more NPC and neuronal death than MEX1-44.

## Materials and Methods

### Ethics statement

All animals were handled according to protocols approved by the Institutional Animal Care and Use Committee (IACUC) at the University of Georgia (UGA). All of the experiments related to ZIKV and DENV2 were conducted following protocols approved by the UGA Institutional Biosafety Committee.

### Viruses

DENV2, strain S16803 (GenBank GU289914), was isolated from a patient sample from Thailand in 1974 and passaged in C6/36 cells. The virus was passaged twice in Vero cells by the World Reference Center for Emerging Viruses and Arboviruses (WRCEVA) before mouse injections. ZIKV MEX1-44 was isolated in Chiapas, Mexico in January of 2016 from an infected *Aedes aegypti* mosquito. The virus was passaged by WRCEVA four times in Vero cells. We obtained this virus, with permission, through the University of Texas Medical Branch at Galveston (UTMB). We then amplified the stock an additional two passages in Vero cells, so the virus used in the experiments had been passaged six times in Vero cells from the time it was isolated from the mosquito. MR-766 is a Zika virus stock from the initial Zika virus isolation from

a sentinel rhesus monkey in 1947 from Uganda. The viral stock was passaged numerous times in mouse brain and Vero cell culture. Stock was provided by ATCC (ATCC VR-84). Designated tools and surfaces exposed to ZIKV or DENV2 were disinfected with 10% bleach to destroy remaining viral particles after use. All tissues used for histology were fixed in 4% PFA to inactivate the viruses for analysis.

#### Viral inoculation of embryonic brains

For timed pregnant mating, noon of the day after mating was considered embryonic day 0.5 (E0.5). Pregnant C57BL/6J or 129 mice with E14.5 embryos were treated with ketamine hydrochloride and xylazine to induce anesthesia.  $\sim 1 \mu\text{l}$   $3.4 \times 10^5$  TCID<sub>50</sub>/ml ZIKV (MEX-1-44 or MR766) or DENV2 (strain S16803) were injected into the lateral ventricles of E14.5 embryo brains. Control media was used as a sham injection. Injected embryos were placed back into pregnant dams and allowed to develop after surgery for varying periods of time according to the individual experiments.

#### Virus titration

Vero cells (African green monkey kidney epithelial cells) were obtained from ATCC. Vero cells were maintained in Dulbecco's modified Eagle's medium (DMEM) supplemented with penicillin/streptomycin and 10% fetal bovine serum (FBS) at 37°C with 5% CO<sub>2</sub>. ZIKV or DENV2 stocks were propagated on Vero cells after inoculating at a multiplicity of infection of 0.01 and harvesting supernatants at 96 h and 120 h post-infection. The viral titers for brains were determined as 50% tissue culture infectious doses (TCID<sub>50</sub>) on Vero cells. Briefly, brain tissues were homogenized in 10 volumes of

PBS and centrifuged at 3000 rpm for 10 min. The supernatant was serially diluted 10-fold in DMEM. A 100 µl aliquot of each diluted sample was added to 96-well plates containing a monolayer of Vero cells. Cells were cultured for 96-120 h at 37°C in a tissue culture incubator. Cytopathic effect (CPE) of endpoint dilutions was monitored.

#### Mouse brain phenotype analysis

Histological processing, TUNEL assay and immunohistochemical labeling of cryosections were performed as described previously (Chen et al., 2014) Coronal sections of the cerebral cortex from different stages of embryos were used as indicated in the figures and text. The primary antibodies used are listed in Table S1. The secondary antibodies used were Alexa 488 and Alexa 555 conjugated to specific IgG types (Invitrogen Molecular Probes). All the experiments were repeated at least three times, and representative images are shown in the individual figures.

#### EdU and CldU labeling study

After ZIKV or DENV2 inoculation of E14.5 brains, pregnant dams with E18.5 embryos were injected intraperitoneally with EdU (1mg/ml, Invitrogen, 100 µl per 100 g body weight) or CldU (10 mg/ml, Sigma, 100 µl for per 100 g body weight). The animals were sacrificed 45 min (for EdU) or 2 h (for CldU) after the injection. The brains were dissected and fixed in 4% paraformaldehyde (PFA) overnight. Subsequently, the brains were stored in 30% sucrose for 16 h and embedded in Tissue-Tek OCT Compound (Sakura). For EdU staining, cortical coronal sections were prepared for staining using

Click-iT plus EdU proliferation kit (Invitrogen). For CldU staining, cortical coronal sections were stained with antibody against CldU (Abcam, ab6326).

### Cell cycle length analysis

Cell cycle kinetics were determined using a dual labeling approach as described previously (Martynoga, Morrison, Price, & Mason, 2005; Shao et al., 2016). On embryonic day 18.5, the pregnant mouse was injected with CldU (10 mg/ml, Sigma, 100 ul for per 100 g body weight) at a time designated as T=0 h, such that all cells at S phase from the beginning of the experiment were labeled with CldU. At T=1.5 h, the pregnant mouse was injected with EdU (1 mg/ml, Invitrogen, 100 ul for per 100 g body weight) to label all cells in S-phase. The animal was killed at T=2 h and its embryos were collected immediately. Embryo sections were immunostained by an Anti-CldU antibody (Abcam, ab6326) and Click-iT EdU Alexa Fluor 555 imaging Kit (Life Technologies, C10338). Images were obtained on a Zeiss LSM 710 inverted confocal microscope. The length of S-phase ( $T_s$ ) and total length of cell cycle ( $T_c$ ) was determined based on the relative number of cells that incorporated CldU or EdU (Martynoga et al., 2005), or both. The ratio of the length of any one period of the cell cycle to that of another period is equal to the ratio of the number of cells in the first period to the number in the second period (Nowakowski, Lewin, & Miller, 1989). Thus, the length of S phase ( $T_s$ ) was calculated as the interval between both injections ( $T_i=1.5$  h) divided by the quotient of the density of CldU+EdU<sup>-</sup> cells (cells that were in but left S phase before EdU injection) and CldU+EdU<sup>+</sup> cells (cells remaining in S phase at the end of the experiment).  $T_i/T_s=L_{\text{cells}}/S_{\text{cells}}$  ( $T_i=1.5$ ;  $L_{\text{cells}}=\text{CldU+EdU}^-$ ;

Scells=CldU+EdU+). Using the same logic, the total cell cycle length can be calculated as:  $T_s/T_c = \text{Scells}/\text{Pcells}$  ( $T_c$ : total cell cycle length;  $\text{Pcells}$  is estimated by counting the total numbers of cells in the assessed area).

### In vitro infection and immunofluorescence

hNP1 Human Neural Progenitor Cells (ArunA Biomedical, derived from the WA09 human embryonic stem cells) were infected with MEX1-44, MR-766 or mock (cultured medium from Vero cells).  $1.8 \times 10^5$  cells seeded in four-well chamber slides were cultured for 24 h followed by virus infection (MOI=0.5, 1, 10, and 20). The infection conditions were 37°C for 2 or 6 h. Next, the inoculum was removed and cells were washed twice with DPBS (Hyclone) followed by fresh medium addition. After 72 h, cells were fixed with 4% paraformaldehyde for 10 min at room temperature. After blocking with 0.2% Triton X-100 and 10% goat serum in PBS, the cells were incubated with primary antibodies overnight at 4°C followed by incubation with secondary antibodies for 1 h at room temperature. Primary and secondary antibodies were diluted with 0.2% Triton X-100 and 2% BSA in PBS. Hoechst 33342 was added together with secondary antibodies at 1 µl/ml. The following antibodies were used: anti-Flavivirus group antigen antibody (mouse IgG2a, EMD Millipore, MAB10216; 1:1000), anti-active-caspase-3 (rabbit, BD 559565; 1:800), anti-Sox2 (rat IgG2a, BD14-9811; 1:1000), anti-mouse IgG2a Alexa Fluor 555, anti-rabbit Alexa Fluor 488 and anti-rat IgG2a Alexa Fluor 647 (Invitrogen). Images were acquired with a Zeiss 710 confocal microscope. ImageJ was used for analyzing data.

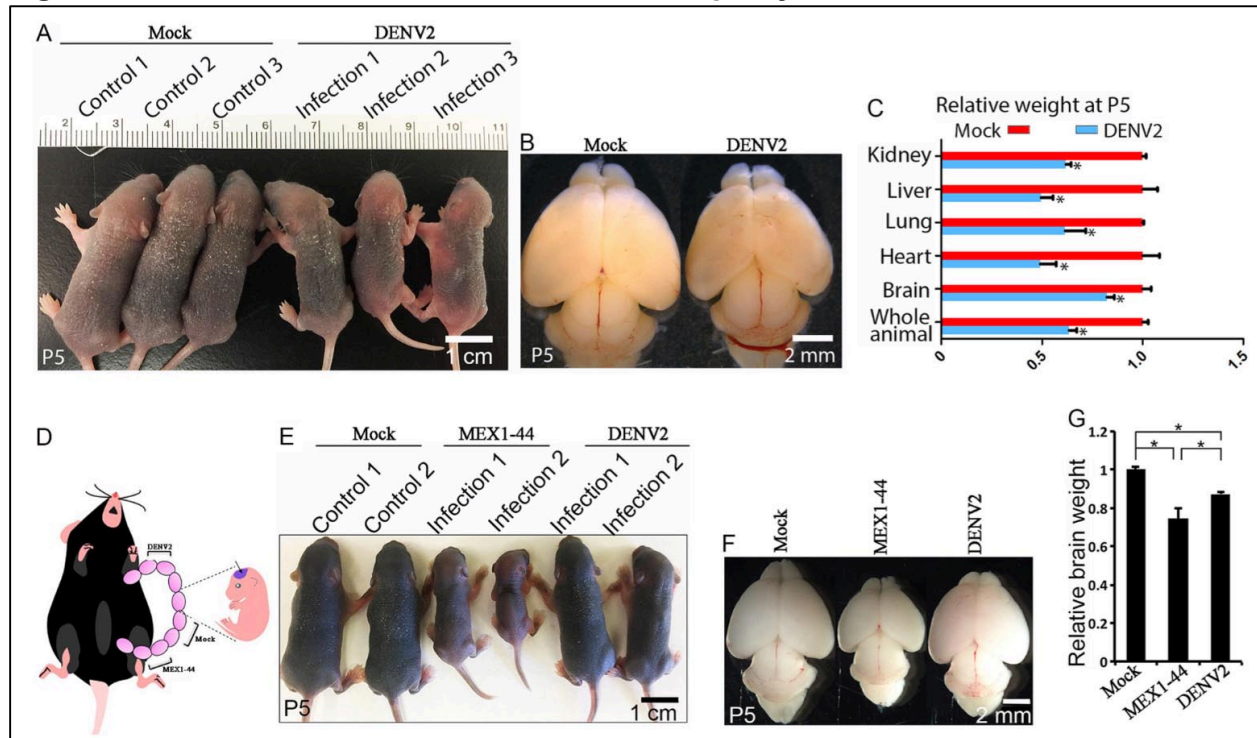
## Results

### DENV2 is sufficient to cause smaller brain sizes by inducing cell death in NPCs and neurons

To examine the effects of dengue virus (DENV) infection in the developing brain, we injected ~1  $\mu\text{l}$   $3.4 \times 10^5$  TCID<sub>50</sub>/ml DENV2 into the cerebral ventricles of embryonic day 14.5 (E14.5) mouse brains. DENV2, strain S16803 (GenBank GU289914), was isolated from a patient sample from Thailand in 1974 and passaged in C6/36 cells. The virus was passaged twice in Vero cells by the World Reference Center for Emerging Viruses and Arboviruses (WRCEVA) before mouse injections. Pups survived after DENV2 inoculation. At postnatal day 5 (P5), DENV2-infected pups were smaller and infected brain sizes were significantly reduced compared with controls (Fig. 5.1A-C). We dissected out different organs, including kidney, liver, lung and heart, and found that individual organ masses were also decreased (Fig. 5.1C). After inoculation of E14.5 brains, DENV2 starts to induce growth restriction and organ size reduction in P3 pups (Fig. 5.S1). These results suggest that DENV2 infection of embryonic brains is sufficient to cause growth restriction, including smaller brain sizes in mice.

Using antibodies against a Flavivirus group antigen, we detected extensive DENV2 in the cerebral cortex (Fig. 5.S2A). Massive neuronal death has been detected in the developing brain after ZIKV infection, so we considered whether the same could be true of DENV2 (Shao et al., 2016). To understand the causes of DENV2- induced microcephaly, we first examined neuronal survival. DENV2 infection caused a significant increase in caspase 3- and TUNEL- positive neurons in the cerebral cortex

**Figure 5.1. DENV2 causes less severe microcephaly than MEX1-44.**



(A) Dorsal views of postnatal day 5 (P5) pups.  $\sim 1 \mu\text{l}$   $3.4 \times 10^5$  TCID<sub>50</sub>/ml DENV2 was injected into cerebral ventricles of embryonic day 14.5 (E14.5) brains followed by analyses at P5. Scale bar: 1 cm. (B) Dorsal views of P5 brains after DENV2 intracerebral inoculation of E14.5 mouse brains. Scale bar: 2 mm. (C) Relative weights of different organs from control or DENV2-infected pups at P5. Error bars indicate the s.e.m. of six independent experiments (\* $P < 0.05$ , Student's t-test). (D) Experimental strategies of intracerebral inoculation of embryonic brains with mock, DENV2 or MEX1-44. (E) Dorsal views of postnatal day 5 (P5) pups.  $\sim 1 \mu\text{l}$   $3.4 \times 10^5$  TCID<sub>50</sub>/ml DENV2 or MEX1-44 were injected into E14.5 cerebral ventricles followed by analyses at P5. Scale bar: 1 cm. (F) Dorsal views of P5 brains. Scale bar: 2 mm. (G) P5 brain weights, relative to mock, from E14.5 intracerebral inoculation with vehicle (mock), DENV2 or MEX1-44. Error bars indicate the s.e.m. of six independent experiments. Two-way ANOVA analysis reveals a significant difference among different infections, \* $P < 0.05$ .

compared with controls (Fig. 5.S3A-C). DENV2 was able to infect NPCs labeled by Sox2 or nestin in the developing mouse brain (Fig. 5.S2B,C). ZIKV infection has been found to cause NPC apoptosis and cell cycle arrest, contributing to microcephaly in mice (Cugola et al., 2016; C. Li et al., 2016; Miner et al., 2016; Shao et al., 2016). Therefore, we examined NPCs in mice infected with DENV2 and found that this virus also resulted in NPC cell death (Fig. 5.S3D,E). Interestingly, there were no significant changes in CldU labeling and cyclin D1 staining in the ventricular/subventricular zone (VZ/SVZ) of mouse cortex after DENV2 infection (Fig. 5.S4). These results suggested that DENV2 infection did not interfere with NPC proliferation, which was further supported by p-H3 and Ki67 staining (Fig. 5.S5) and cell cycle length analysis in our subsequent studies (Fig. 5.3D). Together, these results suggest that DENV2 infection induces cell death in NPCs and neurons in the developing brain, resulting in a smaller brain size.

#### Asian lineage ZIKV causes more severe microcephaly than DENV2

Severe brain malformations have not been linked with DENV, whereas currently circulating ZIKV Asian lineage strains have been established to cause microcephaly and additional fetal brain abnormalities in mice (H. Li et al., 2016; Shao et al., 2016). We reasoned that DENV2 and ZIKV have different effects on the developing brain. To test this hypothesis, we performed a side-by-side comparison using DENV2 and MEX1-44. We injected Vero cell supernatant (mock),  $\sim 1 \mu\text{l}$   $3.4 \times 10^5$  TCID<sub>50</sub>/ml DENV2 or MEX1-44 into the cerebral ventricles of E14.5 brains (Fig. 5.1D). MEX1-44 infection resulted in a drastic reduction in body size at P5 (Fig. 5.1E, middle), whereas DENV2 caused a relatively mild reduction in body size (Fig. 5.1E, right). Whereas DENV2-infected brains

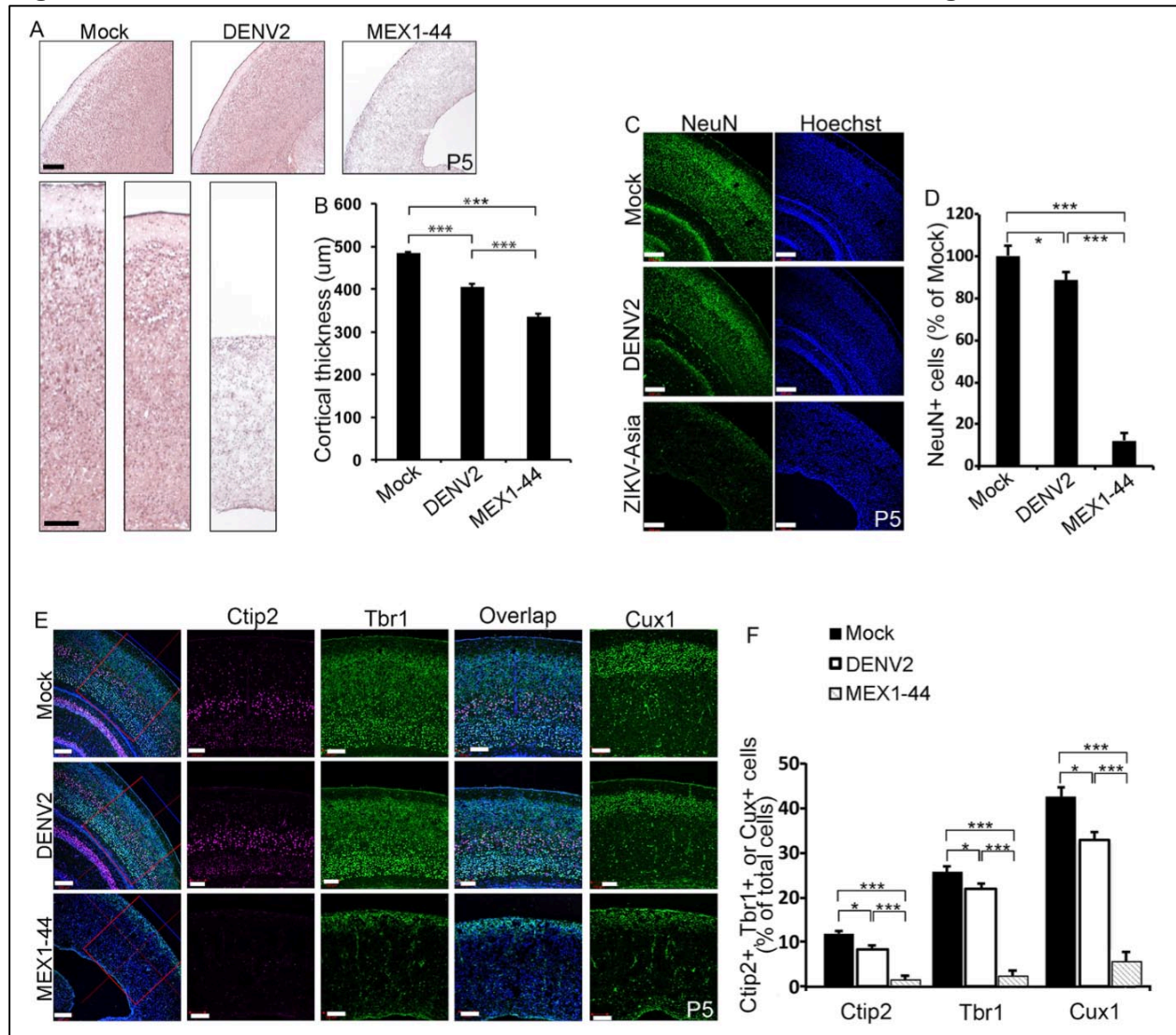
were slightly smaller and weighed less, MEX1-44 caused a substantial decrease in brain size and weight compared with controls (Fig. 5.1F,G). There was a significant difference in brain weight between DENV2- and MEX1-44-infected mice (Fig. 5.1G). Together, these results suggest that Asian lineage ZIKV causes more severe brain size reduction than DENV2 in the developing brain.

More neuron reduction and cortical thinning in Asian lineage ZIKV-infected brains compared with DENV2

To characterize virus-induced brain size reduction, we performed Hematoxylin and Eosin staining and found that the cortical radial thickness was significantly reduced in virally infected brains compared with mock-treated controls (Fig. 5.2A,B). MEX1-44 caused a more severe reduction in cortical thickness than DENV2 (Fig. 5.2A,B). Next, we quantified terminally differentiated neurons labeled by NeuN, a neuron-specific nuclear protein (Mullen, Buck, & Smith, 1992). DENV2 infection led to a slightly decreased number of neurons, whereas MEX1-44 caused a much more severe reduction in the number of neurons compared with controls (Fig. 5.2C,D). Together, these results suggest that ZIKV causes more neuron loss in the developing brain, resulting in more profound cortical thinning and microcephaly compared with DENV2.

The cerebral cortex consists of a six-layer structure generated through the 'inside-out' mechanism of corticogenesis. Although earlier-born neurons reside in the deeper layers, later-born neurons migrate through existing layers to form the more superficial layers (Angevine & Sidman, 1961; Marín & Rubenstein, 2003). To determine whether cortical lamination is impaired and which layer(s) of neurons may be affected in virally infected brains, we examined well-established layer markers. We used layer-

**Figure 5.2. MEX1-44 causes more neuron loss and cortical thinning than DENV2.**



(A) Coronal sections of P5 cerebral cortex stained with Hematoxylin and Eosin. Lower panels represent enlarged cerebral cortices from upper panels. Scale bars: 100 µm (upper panels); 50 µm (lower panels). (B) Quantification of cortical radial thickness from experiment in A. Error bars indicate s.e.m. of nine sections from three independent experiments. Two-way ANOVA revealed a significant difference among different infections,  $***P < 0.001$ . (C) Confocal imaging of P5 cerebral cortex stained with antibodies against NeuN (green). Hoechst stains nuclei (blue). Scale bars: 200 µm. (D) Quantification of the percentage of NeuN-positive cells out of total cells in virally infected cortices normalized to mock-treated controls. Error bars indicate s.e.m. of nine sections from three independent experiments. Two-way ANOVA revealed a significant difference among different infections,  $*P < 0.05$  and  $***P < 0.001$ . (E) Confocal microscope images of coronal sections from P5 cortex stained with antibodies against Ctip2 (purple), Tbr1 (green) and Cux1 (green). Hoechst stains nuclei (blue). The four rightmost panels are enlargements of the regions outlined by red boxes in left panels. Scale bars: 200 µm (left panels); 100 µm (right panels). (F) Quantification of the

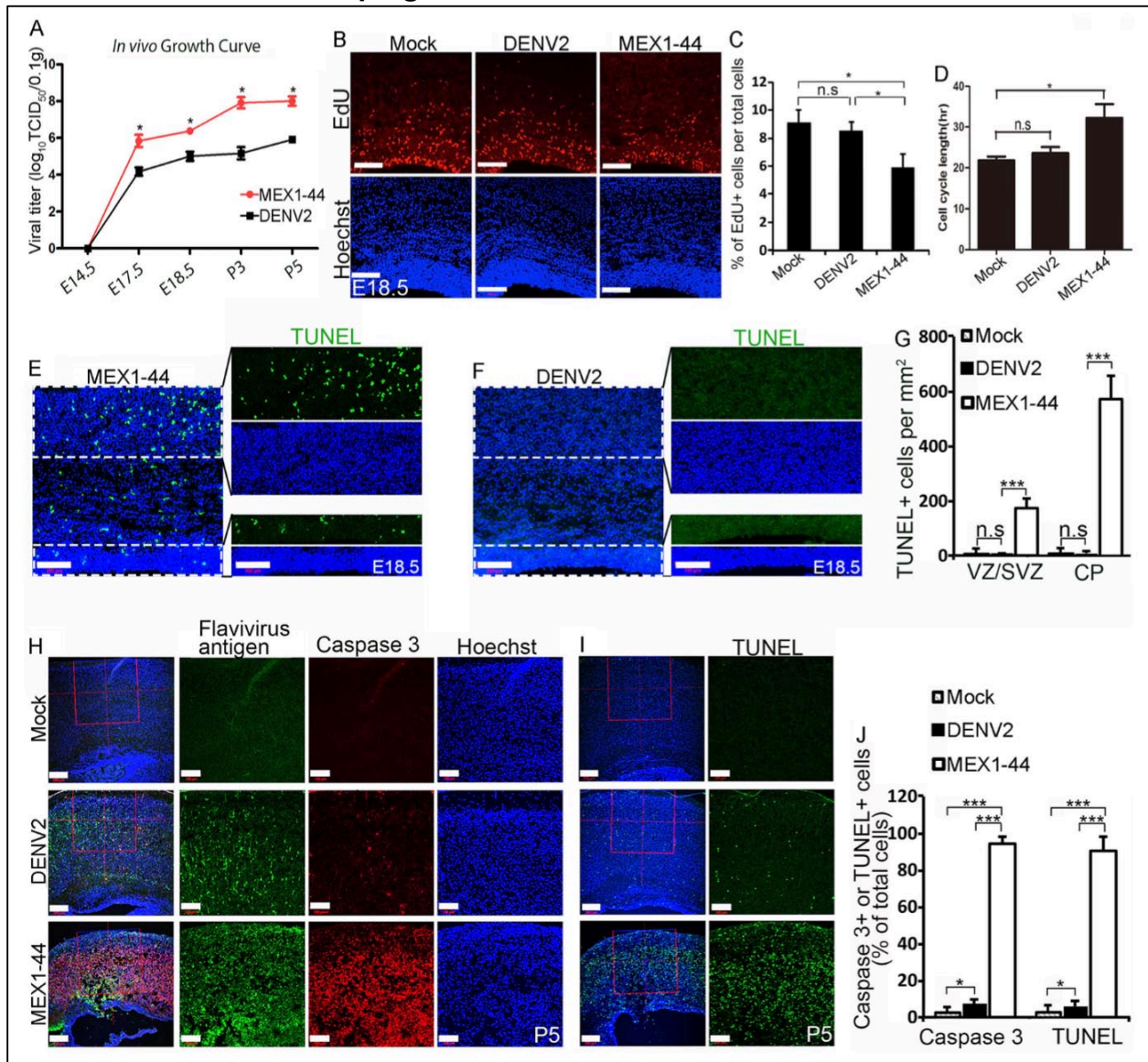
percentage of Ctip2-, Tbr1- and Cux1-positive cells out of total cells in the boxed areas of P5 cerebral cortex from experiment in E. Error bars indicate s.e.m. of nine sections from three independent experiments. Two-way ANOVA revealed a significant difference among different infections, \* $P < 0.05$  and \*\*\* $P < 0.001$ .

specific neuronal markers Tbr1 and Ctip2 to label layers V-VI, and Cux1 to label layers II-IV (Hevner et al., 2001; Nieto et al., 2004). DENV2 infection resulted in a significant decrease in total Tbr1-, Ctip2- and Cux1-labeled neurons compared with controls, but this decrease was far more severe after MEX1-44 infection (Fig. 5.2E,F). Layer organization appeared normal in both groups of virally infected brains (Fig. 5.2E). Together, these data suggest that MEX1-44 causes more severe neuronal loss in individual layers compared with DENV2, but neither virus dramatically disrupts layer organization in the developing cerebral cortex.

Asian lineage ZIKV causes more severe disruption of NPCs and neuronal death than DENV2 in the developing brain

To determine why MEX1-44 causes more severe microcephaly than DENV2, we performed a side-by-side comparison of the growth of these two viruses in the developing brain by measuring viral titers. Statistical analyses showed that DENV2 viral titer was significantly lower than that of MEX1-44 (Fig. 5.3A). Therefore, DENV2 grew less effectively in the developing brain compared with MEX1-44. We reasoned that viral growth itself is not sufficient to account for the substantial difference in microcephaly caused by these two viruses, given the extensive DENV2 infection in the developing brain at P5 (Fig. 5.S2A). As NPC disruption leads to microcephaly (Nigg & Raff, 2009; Thornton & Woods, 2009), we hypothesized that MEX1-44 is more potent in disrupting NPCs than DENV2. To test this hypothesis, we examined cell cycle progression and survival of NPCs. Compared with DENV2, MEX1-44 infection caused a reduced S-phase progression of NPCs, based on EdU labeling studies (Fig. 5.3B,C); and an increase in the percentage of p-Histone3 (p-H3)- and Ki67-positive cells in the

**Figure 5.3. MEX1-44 causes more severe disruption of NPCs and neuronal death than DENV2 in the developing brain.**



(A) In vivo growth analysis in the developing brain. Viral titers were determined in different stage brains using the TCID50 assay. Error bars indicate the s.e.m. of three independent measurements. ANOVA detected a significant increase in viral titer as development proceeded, \* $P < 0.05$ . (B) Confocal micrographs of E18.5 coronal sections with EdU-positive cells after a 45 min EdU pulse. Hoechst stains nuclei (blue). Scale bars: 100  $\mu m$ . (C) Quantification of the percentage of EdU-positive cells out of total cells in a  $1.76 \times 10^5 \mu m^2$  area from experiment in B. Error bars indicate s.e.m. of nine sections from three independent experiments. Two-way ANOVA revealed a significant difference between MEX1-44 and mock, as well as between MEX1-44 and DENV2, but no significant difference between mock and DENV2, \* $P < 0.05$ . (D) Quantification of cell cycle length of NPCs in the ventricular/subventricular zone (VZ/SVZ) of E18.5 cerebral cortex. Error bars indicate s.e.m. of nine sections from three independent experiments. Two-way ANOVA revealed a significant difference between MEX1-44 and mock, but no

significant difference between mock and DENV2, \*P<0.05. (E,F) TUNEL staining (green) revealed substantial apoptotic cell death in MEX1-44 (E)- but not DENV2 (F)- infected E18.5 cortex. Hoechst stains nuclei (blue). Scale bar: 100  $\mu\text{m}$ . (G) Quantification of the TUNEL-positive cells per  $\text{mm}^2$  from a  $4.76 \times 10^4 \mu\text{m}^2$  VZ/SVZ area or a  $1.14 \times 10^5 \mu\text{m}^2$  cortical plate (CP) area. Error bars indicate s.e.m. of nine sections from three independent experiments, \*\*\*P<0.001 (Student's t-test). (H) Confocal imaging of P5 cerebral cortex stained with antibodies against Flavivirus group antigen (labeling both DENV2 and MEX1-44, green) and cleaved caspase 3 (red). Hoechst stains nuclei (blue). Rightmost three panels are enlargements of the regions outlined by red boxes in the left panels. Scale bars: 200  $\mu\text{m}$  (left panels); 100  $\mu\text{m}$  (right panels). (I) TUNEL staining (green) of coronal sections of P5 cerebral cortex. Hoechst stains nuclei (blue). Right panels are enlargements of the regions outlined by red boxes in the left panels. Scale bars: 200  $\mu\text{m}$  (left panels); 100  $\mu\text{m}$  (right panels). (J) Quantification of the percentage of caspase 3 and TUNEL-positive cells out of total cells in a  $4.113 \times 10^5 \mu\text{m}^2$  boxed area in experiments in H and I. Two-way ANOVA revealed a significant difference between different viral infections, \*P<0.05 and \*\*\*P<0.001.

VZ/SVZ of the developing cortex (Fig. 5.S5). These results suggest that MEX1-44 caused cell cycle arrest to a significantly higher degree than DENV2, which was further supported by cell cycle length analyses (Fig. 5.3D). Next, we measured death of NPCs, as MEX1-44 is already known to induce apoptosis of NPCs (Shao et al., 2016). We did not detect apoptotic cells in the mock-treated controls, and TUNEL-positive cells were rarely found in the VZ/SVZ of DENV2-infected brains (Fig. 5.3F,G). In contrast, there was a substantial population of TUNEL-positive cells in the VZ/SVZ of MEX1-44-infected brains (Fig. 5.3E,G). Together, these results suggest that Asian lineage ZIKV (MEX1-44) causes a more potent infection, cell cycle arrest and cell death of NPCs than DENV2, resulting in more severe disruption of NPCs.

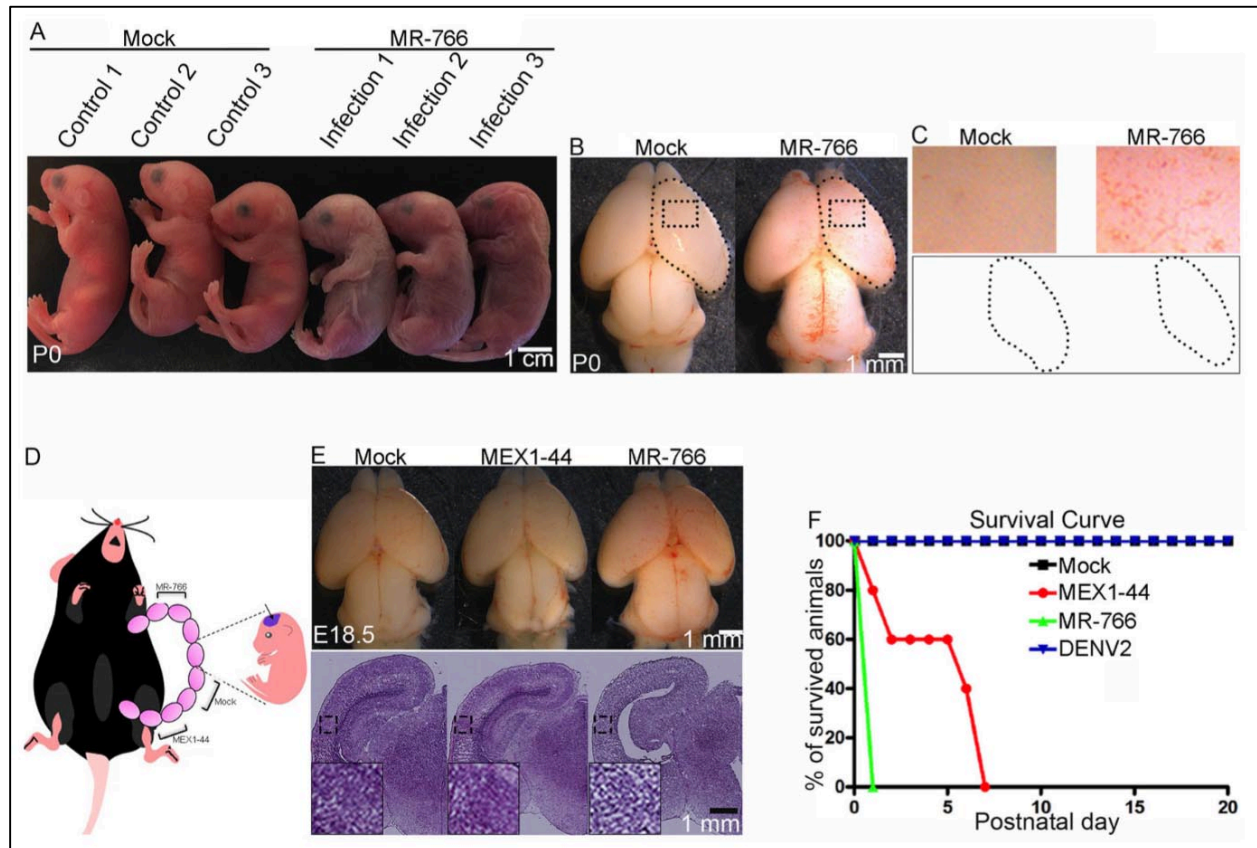
ZIKV (MEX1-44) infection leads to extensive neuronal death in the developing brain, which contributes to the microcephaly phenotype (Shao et al., 2016). Next, we compared neuronal death induced by MEX1-44 and DENV2. We examined the P5 cortical plate (CP) after intracerebral inoculation of E14.5 brains. Whereas cell death was rarely detected in mock-treated controls, MEX1-44 infection led to the massive neuronal death, reflected by strong caspase 3 and TUNEL staining (Fig. 5.3H,I). DENV2 also induced a significant increase in neuronal death, but to a much lesser degree than MEX1-44 (Fig. 5.3H-J). Together, these results suggest that Asian lineage ZIKV (MEX1-44) causes more pronounced apoptosis than DENV2, leading to more severe brain size reduction.

African lineage ZIKV (MR-766) causes more severe neuronal reduction, brain damage and postnatal mortality than Asian lineage ZIKV (MEX1-44)

Although there is no scientific documentation of MR-766-related birth defects, *in vitro* and *ex vivo* studies suggest that MR-766 causes cell cycle arrest and apoptosis of NPCs (Cugola et al., 2016; Simonin et al., 2016; Tang et al., 2016). To determine the effects of MR-766 infection in the developing brain, we performed intracerebral inoculation with  $\sim 1 \mu\text{l}$   $3.4 \times 10^5$  TCID<sub>50</sub>/ml virus per injection. Surprisingly, we were unable to recover postnatal pups alive; viral infection consistently led to lethality before or around birth (Fig. 5.4A). We dissected P0 virally infected brains and found a slightly reduced brain size with obvious vasculature abnormalities (Fig. 5.4B,C). MR-766-infected brains also exhibited severe edema, resulting in fragile brain tissues that could not be used for pathological analyses.

To directly compare the MR-766 and MEX1-44 ZIKV lineages, we performed a side-by-side analysis after intracerebral inoculation of E14.5 brains (Fig. 5.4D). We focused our analyses at stage E18.5 when living brain tissues can reliably be recovered. No obvious morphological differences were detected between infection groups. However, Hematoxylin and Eosin staining revealed that MR-766 caused cortical thinning with enlarged ventricles, which were not detected in the MEX1-44- or mock-treated brains (Fig. 5.4E). In addition, MR-766-infected brains exhibited an obvious defect in cortical structural integrity (Fig. 5.4E, insets), suggesting severe parenchymal cell loss. To directly compare the long-term consequence of viral infection, we performed animal survival analyses. Mock and DENV2-infected pups exhibited no postnatal lethality and survived for at least 2 months after birth, whereas MEX1-44-infected pups did not survive beyond P10, which is consistent with our previous publication (Shao et al., 2016). MR-766 infection resulted in early lethality around

**Figure 5.4. MR-766 causes more severe brain damage and postnatal death than MEX1-44.**



(A) Dorsal views of postnatal day 0 (P0) pups.  $\sim 1 \mu$ l  $3.4 \times 10^5$  TCID<sub>50</sub>/mL MR-766 was injected into cerebral ventricles of embryonic day 14.5 (E14.5) brains. Scale bar: 1 cm. (B) Dorsal views of P0 brains after intracerebral inoculation of E14.5 mouse brains with MR-766. Scale bar: 1 mm. Upper panels in C are enlargements of the regions with back dotted rectangles in B; lower panels in C represent a slightly reduced cortex surface after MR-766 infection. (D) Experimental strategies of intracerebral inoculation of embryonic brains with mock treatment, MEX1-44 or MR-766. (E) Dorsal view of E18.5 brain (upper panels).  $\sim 1 \mu$ l  $3.4 \times 10^5$  TCID<sub>50</sub>/ml MEX1-44 or MR-766 were injected into E14.5 cerebral ventricles followed by analyses at E18.5. Hematoxylin and Eosin staining revealed that MR-766 infection resulted in an enlarged ventricle and thinning radial cortex with substantial empty spaces (lower panels). Lower left panels represent enlarged areas from black dotted areas in the middle of the cortex. Scale bar: 1 mm. (F) Survival curves for control (mock), MEX1-44-, MR-766- and DENV2-infected pups.  $\sim 1 \mu$ l  $3.4 \times 10^5$  TCID<sub>50</sub>/ml MEX1-44, MR-766 or DENV2 were injected into cerebral ventricles of E14.5 brains. All the pups were monitored daily from postnatal day 0 to 20, and surviving DENV2-infected pups were observed until 2 months of age. The percentage of survival was calculated, and the survival curves represent three independent experiments (n=10).

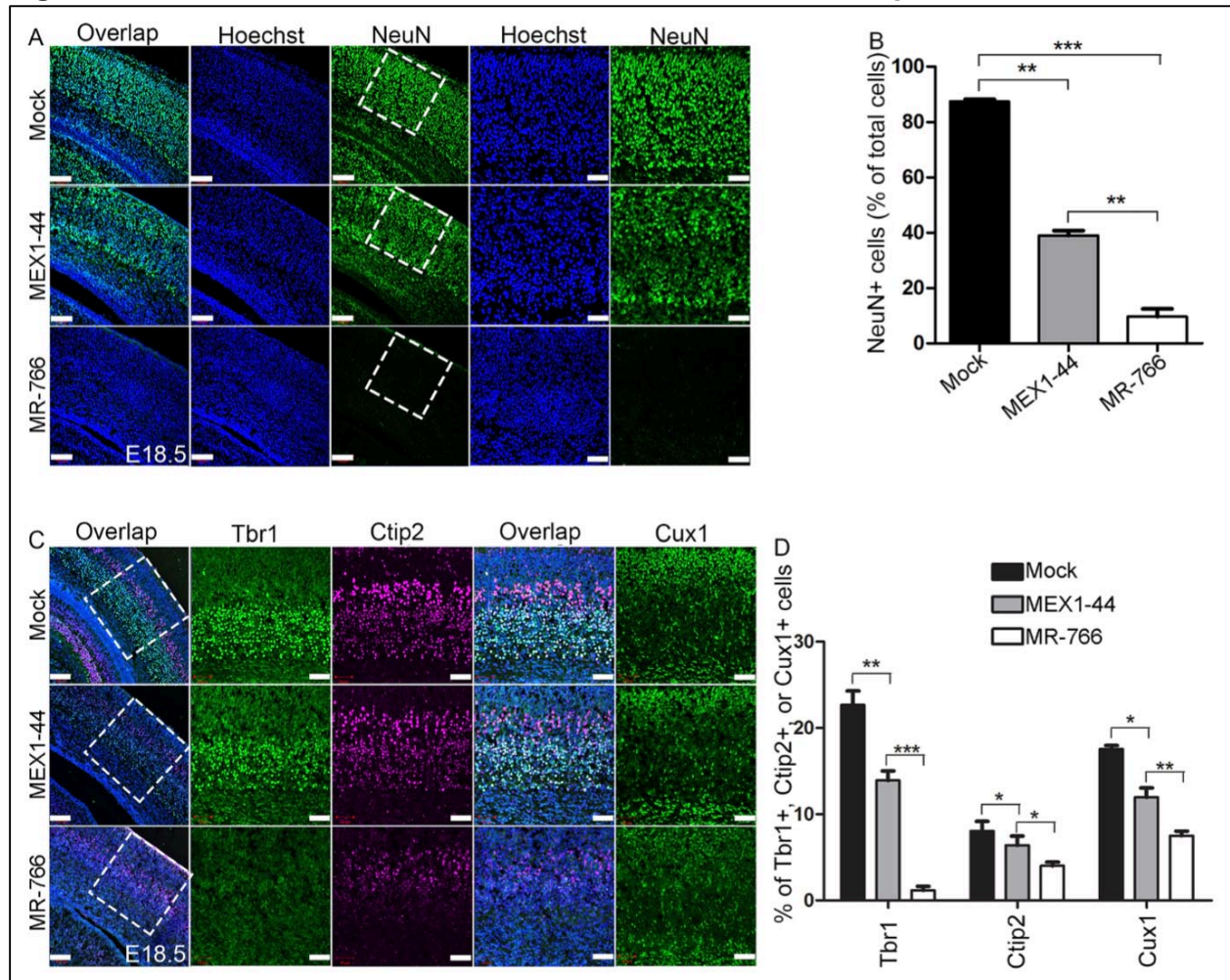
P0/P1 with 100% penetrance (Fig. 5.4F). Together, these results suggest that MR-766 causes more severe brain damage and postnatal mortality than MEX1-44 or DENV2.

Hematoxylin and Eosin staining results suggested that MR-766 infection led to substantial cell loss in the developing brain (Fig. 5.4E, inset). Next, we examined the neuronal population of the cortex using antibodies against NeuN (Mullen et al., 1992). Although both ZIKV strains caused a substantial reduction in neurons compared with controls, MR-766 infection resulted in a near elimination of the NeuN-positive cells by E18.5 (Fig. 5.5A,B). To investigate whether layer organization was disrupted by the viral infection, we examined layer markers as described above. We barely detected Tbr1-positive cells in MR-766-infected cerebral cortex at E18.5 (Fig. 5.5C,D). Compared with MEX1-44, MR-766 caused significantly larger decreases in total Tbr1-, Ctjp2- and Cux1-labeled neurons (Fig. 5.5C,D). Again, layer organization was not severely disrupted. Together, these data suggest that the African lineage ZIKV MR-766 causes more severe neuronal reduction than Asian lineage ZIKV MEX1-44.

African lineage ZIKV (MR-766) induces microglial activation and astrogliosis, and grows faster than Asian lineage ZIKV (MEX1-44)

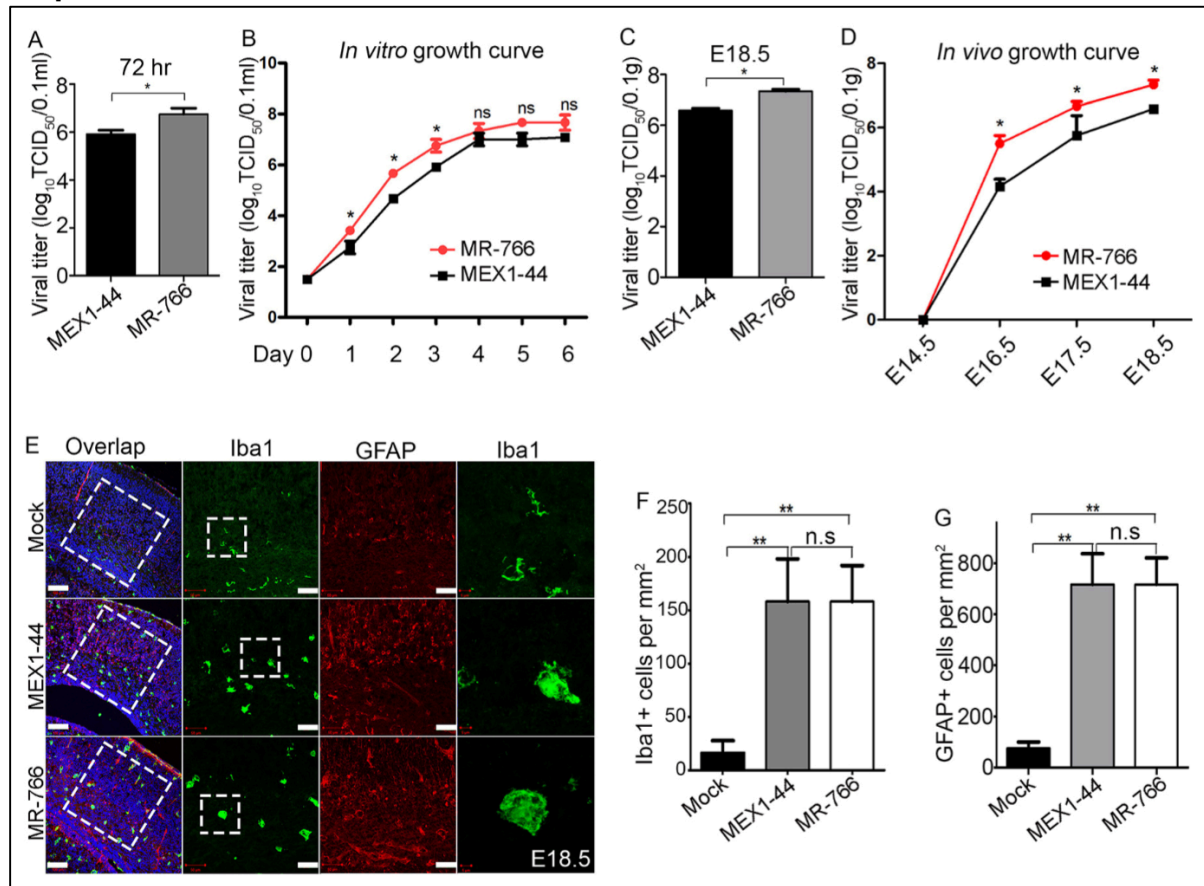
To understand the mechanisms underlying the differential virulence of MR-766 and MEX1-44, we examined their growth in vitro and in vivo. Viral titer measurement at 72 h post-infection of cultured human NPCs revealed that there was significantly more growth of MR-766 than of MEX1-44 (Fig. 5.6A). In vitro growth curve analyses showed that MR-766 grew faster than MEX1-44 from day 1 to day 3, although they exhibited similar viral titers from day 4 to day 6 (Fig. 5.6B), likely due to saturation. After intracerebral inoculation of E14.5 brains, we detected a higher viral titer of MR-766

**Figure 5.5. More neuron loss in MR-766 infected brains compared with MEX1-44.**



(A) Confocal imaging of E18.5 cerebral cortex stained with antibodies against NeuN (green). The two rightmost panels represent enlargements of areas outlined with white dotted boxes. Hoechst stains nuclei (blue). Scale bars: 100  $\mu\text{m}$  (left panels); 50  $\mu\text{m}$  (right panels). (B) Quantification of the percentage of NeuN-positive cells out of total cells within a  $4.0 \times 10^4 \mu\text{m}^2$  cortical plate areas in A. Error bars indicate s.e.m. of nine sections from three independent experiments. Two-way ANOVA revealed a significant difference among different infections,  $**P < 0.01$  and  $***P < 0.001$ . (C) Confocal microscope images of coronal sections from E18.5 cortex stained with antibodies against Ctip2 (purple), Tbr1 (green) and Cux1 (green). Hoechst stains nuclei (blue). Rightmost four panels are enlargements of the regions outlined by red boxes in the left panels. Scale bars: 100  $\mu\text{m}$  (left panels); 50  $\mu\text{m}$  (right panels). (D) Quantification of the percentage of Ctip2-, Tbr1- and Cux1-positive cells out of total cells in the boxed areas of E18.5 cerebral cortex from experiment in C. Error bars indicate s.e.m. of nine sections from three independent experiments. Two-way ANOVA revealed a significant difference among different infections,  $*P < 0.05$ ,  $**P < 0.01$  and  $***P < 0.001$ .

**Figure 5.6. MR-766 grows faster than MEX1-44 and triggers a similar immune response.**



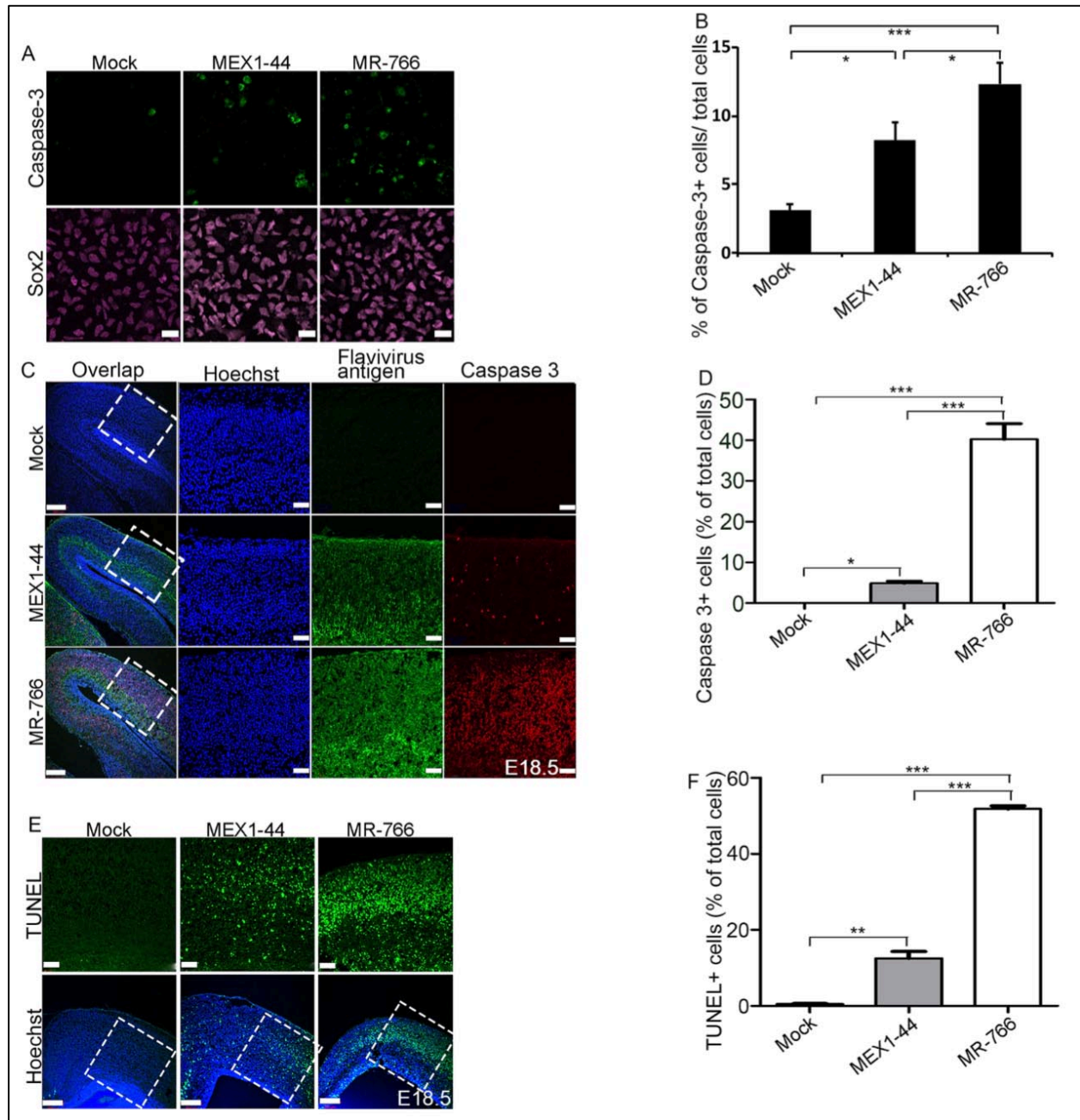
(A) Quantification of the viral titers at 72 h after MEX1-44 or MR-766 infection of human neural progenitor cells (hNPCs). Error bars indicate the s.e.m. of three independent measurements. \* $P < 0.05$  (Student's t-test). (B) In vitro growth analysis of viral infection in cultured hNPCs. Viral titers were determined on different days, as indicated using the TCID<sub>50</sub> assay. Error bars indicate the s.e.m. of three independent measurements. ANOVA revealed that MR-766 exhibited a higher rate of growth than MEX1-44 from post-infection day 1 to 3. \* $P < 0.05$ ; ns, not significant. (C) Quantification of the viral titers at E18.5 after MEX1-44 or MR-766 infection of E14.5 embryonic brains. Error bars indicate the s.e.m. of three independent measurements. \* $P < 0.05$  (Student's t-test). (D) In vivo growth analysis in the developing brain. Viral titers were determined at different stage brains using the TCID<sub>50</sub> assay. Error bars indicate the s.e.m. of three independent measurements. ANOVA detected a significant difference between the viral titers at each developmental stage, \* $P < 0.05$ . (E) Confocal micrographs of coronal sections of the E18.5 cerebral cortex stained with antibodies against GFAP (red) and Iba1 (green). Hoechst stains nuclei (blue). Scale bars: 100 μm (left); 50 μm (middle); 10 μm (right). Rightmost panels are enlargements of white dotted areas in the second panels. (F,G) Quantification of Iba1- or GFAP-positive cells per mm<sup>2</sup> area. Two-way ANOVA revealed a significant difference between ZIKV and control groups, but no significant difference was detected between MR-766 and MEX1-44. \*\* $P < 0.001$ ; ns, no significant difference.

relative to MEX1-44 in E18.5 brains (Fig. 5.6C). In vivo growth curve analyses showed that MR-766 amplified faster than MEX1-44 in the developing brains (Fig. 5.6D).

ZIKV infection triggers an innate immune response in the developing brain (Shao et al., 2016; Tang et al., 2016), which can restrict viral infection. However, ZIKV can also suppress the antiviral response of the host (Kumar et al., 2016). To determine whether MR-766 grows faster than MEX1-44 because it can more effectively dampen the host immune response, we examined virus-triggered immune response in the developing cortex. We used antibodies against Iba1 and GFAP to label microglia and astrocytes, respectively (Shao et al., 2016). Whereas both viruses induced microglial activation and astrogliosis (Fig. 5.6E), there was no significant difference in the percentages of Iba1- and GFAP-positive cells between two virally infected brains (Fig. 5.6E-G). These results suggest that differential host immune response may not be the major cause of the differences in brain damage induced by these two viruses.

African lineage ZIKV (MR-766) causes more aggravated cell death in NPCs and neurons than Asian lineage ZIKV (MEX1-44). ZIKV infection results in cell death of NPCs and neurons in the developing brain (Shao et al., 2016; Tang et al., 2016). To investigate why MR-766 caused more severe neuronal loss and brain damage than MEX1-44, we tested the hypothesis that MR-766 is more potent in causing death of NPCs and neurons than MEX1-44. We infected human NPCs and then performed cell death analyses, in which antibodies against Sox2 and caspase 3 were used to label NPCs and apoptotic cells, respectively (Fig. 5.7A). Statistical analysis showed that MR-766 infection resulted in a larger percentage of apoptotic NPCs compared with MEX1-

**Figure 5.7. MR-766 infection leads to more cell death in NPCs and neurons than MEX1-44.**



(A) Confocal imaging of human neural progenitor cells (hNPCs) stained with antibodies against Sox2 (purple) or caspase 3 (green). Scale bars: 20  $\mu$ m. (B) Quantification of the percentage of caspase 3-positive cells out of total hNPCs. Error bars indicate s.e.m. of results from three independent experiments. Two-way ANOVA revealed a significant difference between mock, MEX1-44 and MR-766 (\* $P$ <0.05, \*\*\* $P$ <0.001). (C) Confocal imaging of E18.5 cerebral cortex stained with antibodies against Flavivirus antigen (labeling MR-766 or MEX1-44, green) and caspase 3 (red). Hoechst stains nuclei (blue). Rightmost three panels are enlargements of the regions outlined by white dotted boxes in the left panels. Scale bars: 200  $\mu$ m (left panels); 50  $\mu$ m (right panels). (D)

Quantification of the percentage of caspase 3-positive cells out of total cells. Two-way ANOVA revealed a significant difference between different treatments, \* $P < 0.05$  and \*\*\* $P < 0.001$ . (E) TUNEL staining (green) on coronal sections of E18.5 brains. Hoechst stains nuclei (blue). Upper panels are enlargements of the regions outlined by white dotted boxes in lower panels. Scale bars: 50  $\mu\text{m}$  (upper panels); 200  $\mu\text{m}$  (lower panels). (F) Quantification of the percentage of TUNEL-positive cells out of total cells. Two-way ANOVA revealed a significant difference between different treatments, \*\* $P < 0.01$  and \*\*\* $P < 0.001$ .

44 (Fig. 5.7B). These results suggest that MR-766 is more potent in causing death of NPCs than MEX1-44 in vitro.

Next, we compared NPC and neuronal death induced by ZIKV in vivo. We examined E18.5 cerebral cortex after intracerebral inoculation of E14.5 embryonic brains. Whereas cell death was rarely detected in mock controls, MEX1-44 infection led to substantial cell death in both the VZ/SVZ and cortical plate, reflected by caspase 3 and TUNEL staining (Fig. 5.7C-F). Strikingly, MR-766 infection resulted in a much more dramatic increase in caspase 3- and TUNEL-positive cells in the developing brain compared with MEX1-44 (Fig. 5.7C-F). Together, these results suggest that MR-766 causes more pronounced death of NPCs and neurons than MEX1-44, which is likely why MR-766 infection causes more severe neuronal loss and brain damage.

### Discussion

In this work we found that DENV2 is sufficient to cause microcephaly due to increased cell death in neural progenitor cells (NPCs) and neurons. However, DENV2 infection has minimal detrimental effects on the developing brain and pups can ultimately survive embryonic infection. By performing side-by-side intracerebral inoculation, we discovered that the African lineage ZIKV (MR-766) causes more severe brain damage and postnatal lethality than currently circulating Asian lineage ZIKV (MEX1-44). MR-766 grows faster and causes more severe neuronal death in the developing brain, contributing to earlier lethality compared with MEX1-44.

The finding that African lineage ZIKV (MR-766) causes severe brain damage is supported by multiple analyses, including animal survival studies, in vitro and in vivo

viral growth assays, NPC and neuronal death assays, and cortical neuron number analyses. Based on studies using NPCs derived from human ES cells or iPS cells, it had remained unclear whether African lineage isolates exhibit a stronger detrimental effect on NPCs compared with Asian lineage isolates (Cugola et al., 2016; Simonin et al., 2016). It has been reported that MR-766 infection results in larger neurospheres than an Asian lineage isolate, which seemed to favor the hypothesis that African lineage ZIKV is less potent in damaging NPCs (Cugola et al., 2016). These observations are consistent with the fact that there is no scientific documentation of ZIKV-Africa-related birth defects. Here, our in vivo studies revealed that African lineage ZIKV (MR-766) is more virulent and causes more severe mortality and brain damage than currently circulating Asian lineage (MEX1-44). Because the MR-766 strain has been adapted to the mouse brain for many generations, our studies cannot yet draw a broad generalization that the African lineage of ZIKV is more virulent than the Asian lineage. However, using a low-passage, currently circulating African ZIKV strain, recent studies have reported that an African lineage isolate exhibited a higher infection rate and caused a higher degree of cell death in NPCs than an Asian lineage isolate (Simonin et al., 2016). In addition, studies by Shashank Tripathi et al. have reported that two African strains, the Senegal 1984 Strain DAKAR 41519 and Uganda 1947 Strain MR 766, have similar virulence and both cause more severe weight loss and mortality than Asian strains, including Puerto Rico 2015 (Strain PRVABC59), Cambodia 2010 (Strain FSS13025) and Malaysia 1966 (Strain P6- 740) (Tripathi et al., 2017). Our results focusing on the developing brain complement these studies, collectively suggesting that

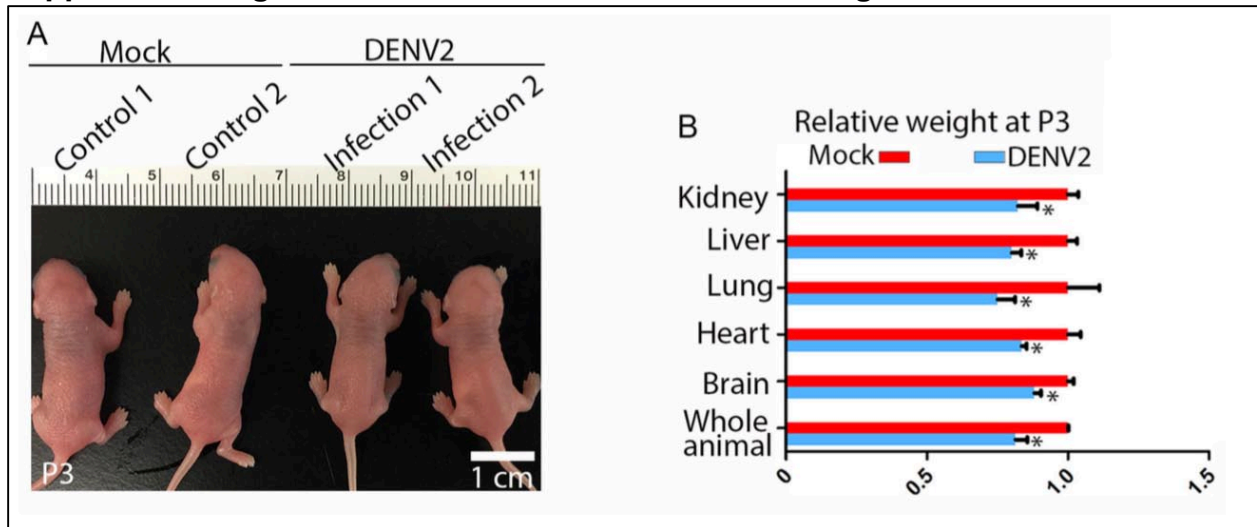
African lineage ZIKV is more virulent and causes more severe mortality and brain damage than the Asian lineage ZIKV.

Future studies should identify molecular mechanisms underlying this differential virulence between the African lineage and Asian lineage. It will be important to know whether African isolates are more effective in binding, entering or replicating in human NPCs, and whether they cause more pronounced cell cycle arrest of NPCs compared with Asian lineage isolates (C. Li et al., 2016; Shao et al., 2016). It has been reported that an Asian lineage isolate, but not MR-766, upregulates TP53 and viral response genes in human NPCs (Zhang et al., 2016). It will be informative to test whether the different virulence capacities of these two ZIKV strains are due to the differential induction of TP53 in the developing brain. Our functional studies of different ZIKV strains should provide a baseline for investigating how genetic changes in different ZIKV strains affect their pathogenesis in the developing brain. In the future, it will be important to use a reverse genetics systems for Asian and African Zika viruses to generate inter-lineage chimeric viruses followed by functional studies, which should facilitate the studies of ZIKV pathogenesis in the developing brain (Atieh, Baronti, de Lamballerie, & Nougairède, 2016; Gadea et al., 2016).

We found that DENV2 infection is sufficient to cause microcephaly and global growth restriction. DENV2 infects human and mouse NPCs, which is consistent with previous publications in hNPCs (Garcez et al., 2016). DENV2 infection causes a significant increase in cell death in NPCs and neurons, resulting in smaller brain sizes. Interestingly, microcephaly in DENV2-infected pups was accompanied by global growth restriction, which was also observed in ZIKV (MEX1-44)-infected pups (Shao et al.,

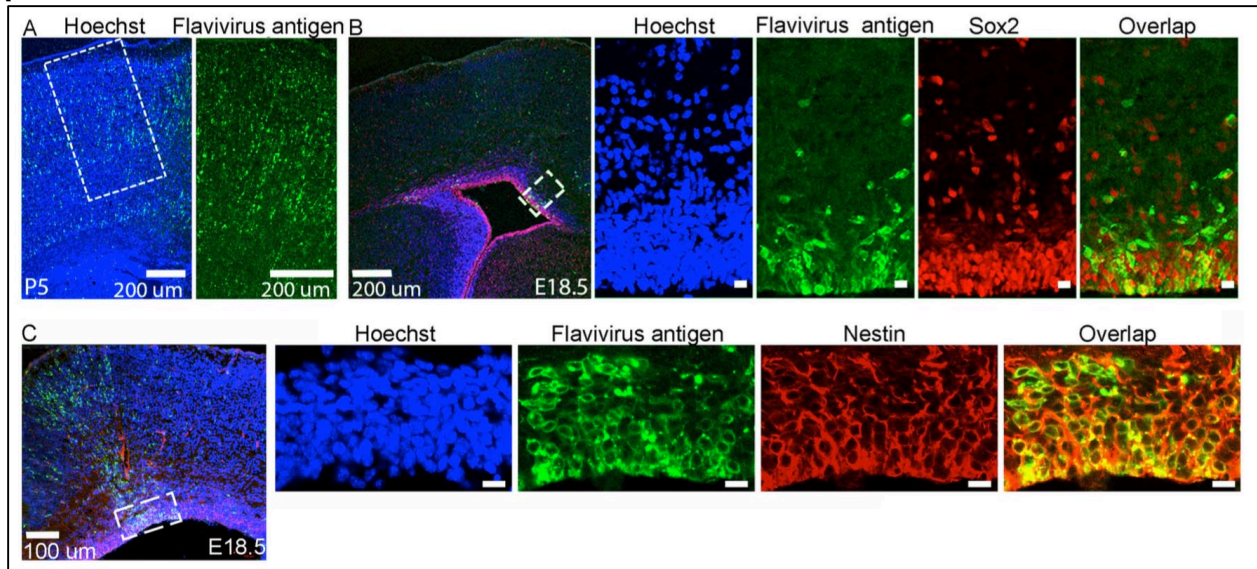
2016). In addition to its specific damage to the brain, intracerebral inoculation of viruses could have an adverse impact on global growth due to inflammation and the immune response of the fetus during development. Our results suggest that DENV2 is intrinsically less potent in damaging the developing brain than ZIKV; however, our studies cannot rule out any long-term potential neurological deficiencies in these DENV2- infected pups. It has been reported that antibodies against E protein domain I/II (EDI/II) of ZIKV lethally enhanced DENV disease in mice (Stettler et al., 2016). Future studies should determine whether immunity to ZIKV could exacerbate brain damage derived from DENV infection.

**Supplemental Figure 5.S1. DENV2 is sufficient to cause growth restriction at P3.**



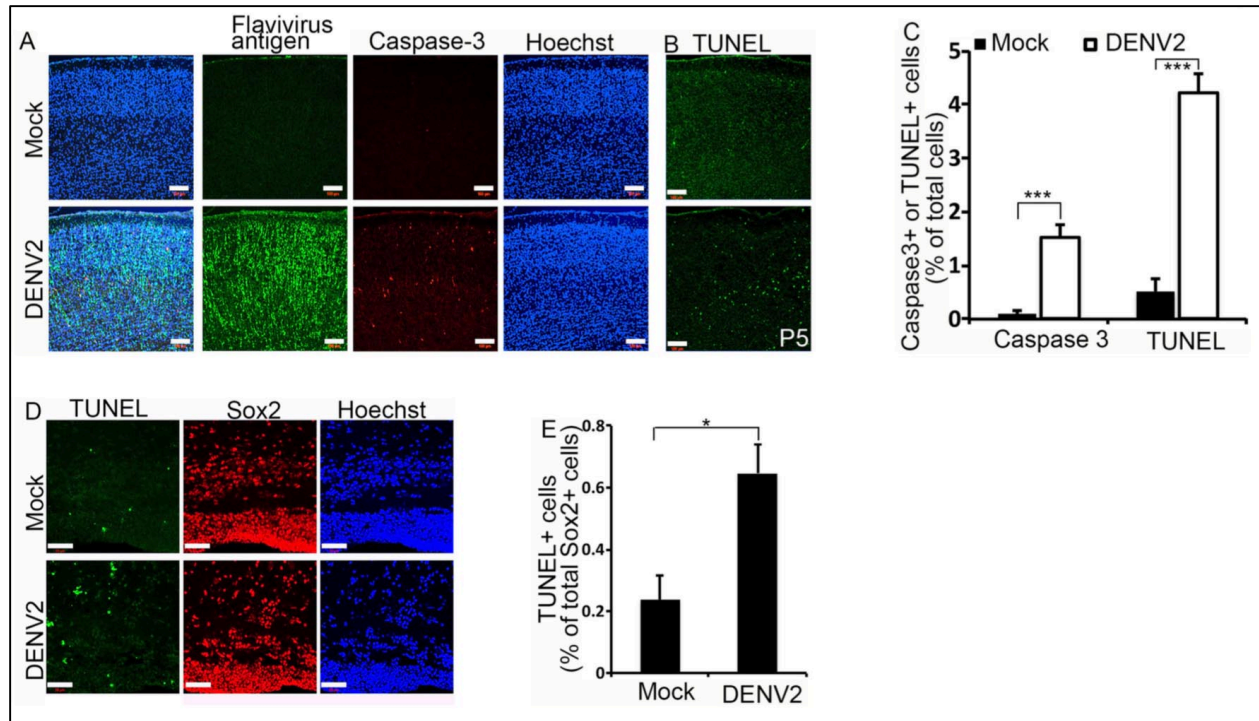
(A) Dorsal views of P3 mouse pups after mock or DENV2 intracerebral inoculation of the brain at E14.5. Scale bar: 1 cm. (B) Relative weights of different organs from control and DENV2 infected pups at P3. Error bars indicate the SEM of four independent experiments, \* $p < 0.05$  (Student's t-test).

**Supplemental Figure 5.S2. DENV2 infection has minimal impact on NPC proliferation.**



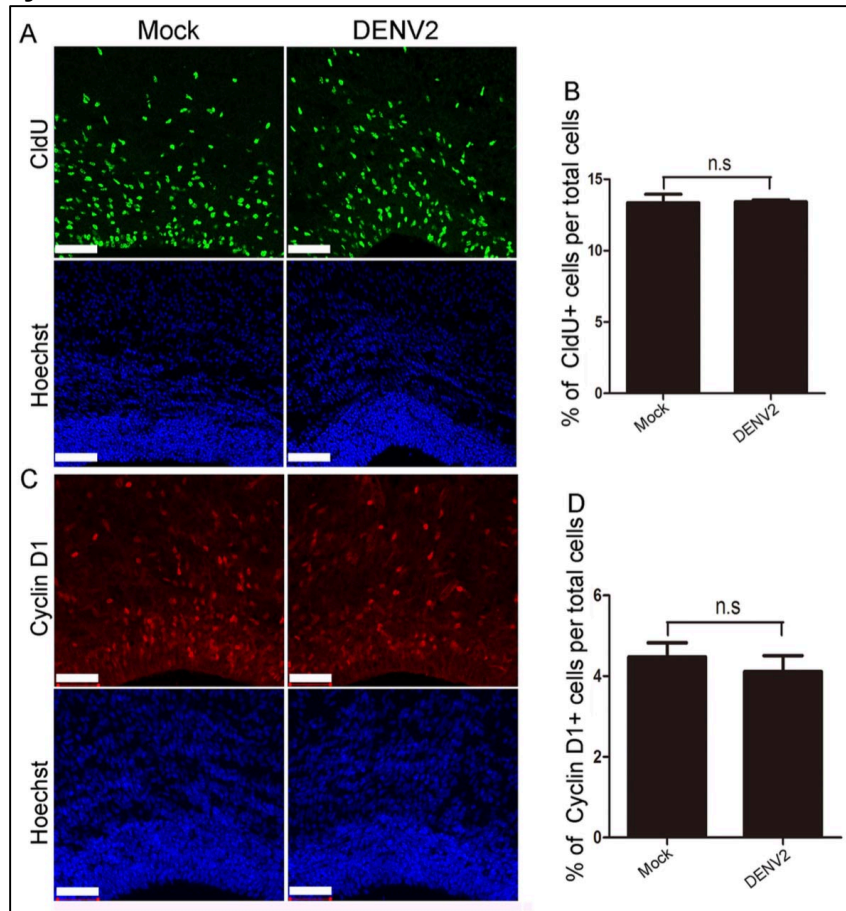
(A) Confocal imaging of E18.5 cerebral cortex stained with antibodies against CldU (green) after 2hr CldU pulse. Hoechst stains nuclei (blue). Scale bar: 100  $\mu\text{m}$ . (B) Quantification of the percentage of CldU-positive cells out of total cells in DENV2-infected cortices normalized to controls. Error bars indicate SEM of 9 sections from three independent experiments. Student's t-test revealed no significant difference between mock and DENV2-infected groups. (C) Confocal imaging of E18.5 cerebral cortex stained with antibodies against Cyclin D1 (red). Hoechst stains nuclei (blue). Scale bar: 100  $\mu\text{m}$ . (D) Quantification of the percentage of Cyclin D1-positive cells out of total cells in DENV2-infected cortices normalized to controls. Error bars indicate SEM of 9 sections from three independent experiments. Student's t-test revealed no significant difference between mock and DENV2-infected groups.

**Supplemental Figure 5.S3. DENV2 infection leads to increased cell death in neurons and NPCs.**



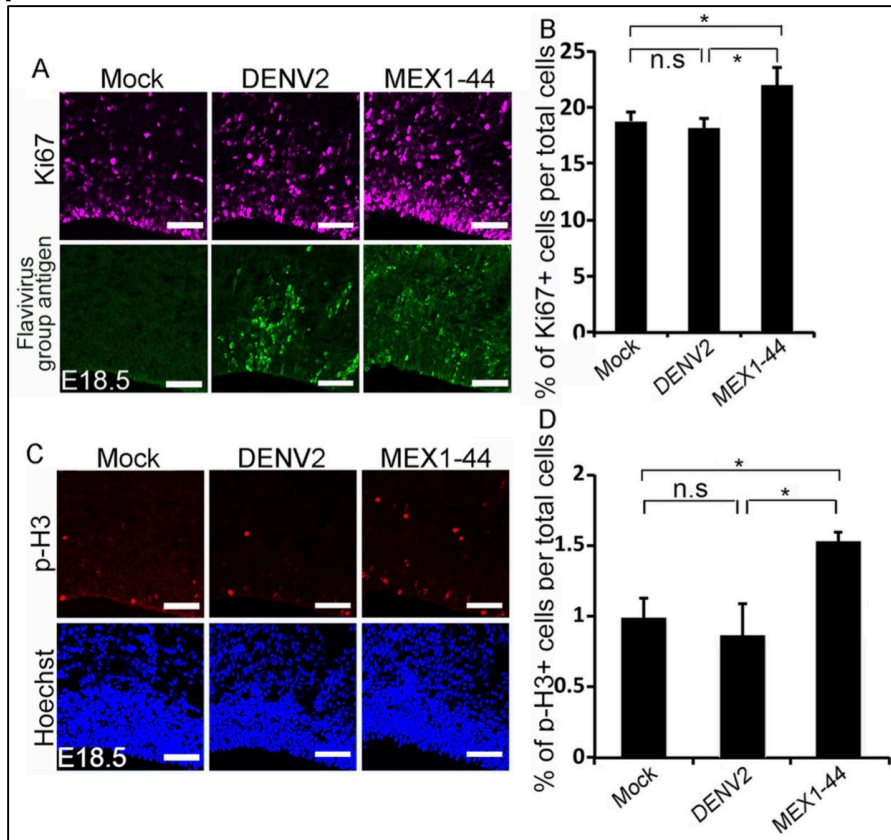
(A) Confocal imaging of P5 cerebral cortex stained with antibodies against Flavivirus group antigen (labeling DENV2, green) and cleaved Caspase 3 (red). Hoechst stains nuclei (blue). Scale bar: 100  $\mu$ m. (B) TUNEL staining (green) reveals an increase in cell death in DENV2-infected cortices compared to controls. Hoechst stains nuclei (blue). Scale bar: 100  $\mu$ m. (C) Quantification of the percentage of Caspase-3 or TUNEL-positive cells out of total cells in DENV2-infected cortices normalized to controls. Error bars indicate SEM of 9 sections from three independent experiments, \*\*\* $p$  < 0.001 (Student's t-test). (D) TUNEL staining (green) reveals apoptotic cell death in Sox2-positive neural progenitor cells (NPCs) (red). Hoechst stains nuclei (blue). Scale bar: 50  $\mu$ m. (E) Quantification of the percentage of TUNEL- and Sox2-double positive cells out of total Sox2-positive cells in D. Error bars indicate SEM of 9 sections from three independent experiments, \* $p$  < 0.05 (Student's t-test).

**Supplemental Figure 5.S4. MEX1-44, but not DENV2, infection causes NPC cell cycle arrest.**



(A) Confocal imaging of E18.5 cerebral cortex stained with antibodies against Ki67 (labeling proliferating cells, far red) and Flavivirus group antigen (labeling DENV2 and MEX1-44, green). Hoechst stains nuclei (blue). Scale bar: 100  $\mu$ m. (B) Quantification of the percentage of Ki67-positive cells out of total cells. Error bars indicate SEM of 9 sections from three independent experiments. Two-way ANOVA revealed a significant difference between MEX1-44 and mock, and between MEX1-44 and DENV2, but no significant difference between mock and DENV2,  $*p < 0.05$ . (C) Confocal imaging of E18.5 cerebral cortex stained with antibodies against p-Histone3 (labeling mitotic cells, red). Hoechst stains nuclei (blue). Scale bar: 100  $\mu$ m. (D) Quantification of the percentage of p-Histone3-positive cells out of total cells in DENV2/MEX1-44 infected cortices normalized to mock. Error bars indicate SEM of 9 sections from three independent experiments, Two-way ANOVA revealed a significant difference between MEX1-44 and mock, and between MEX1-44 and DENV2, but no significant difference between mock and DENV2,  $*p < 0.05$ .

**Supplemental Figure 5.S5. DENV2 infects NPCs and is detected in the cortical plate.**



(A) Confocal imaging of E18.5 cortex after DENV2 inoculation of E14.5 brains stained with antibodies against Sox2 (red), and Flavivirus group antigen (green). Hoechst stains nuclei (blue). Scale bar: 200  $\mu$ m (left panel), 10  $\mu$ m (right panels). (B) Confocal imaging of P5 cortex after DENV2 inoculation of E14.5 brains stained with antibodies against Flavivirus group antigen (green). Hoechst stains nuclei (blue). Scale bar: 200  $\mu$ m. (C) Confocal imaging of E18.5 cortex after DENV2 inoculation of E14.5 brains stained with antibodies against Nestin (red), and Flavivirus group antigen (green). Hoechst stains nuclei (blue). Scale bars: 100  $\mu$ m (left panel), 10  $\mu$ m (right panels).

## References

- Angevine, J. B., & Sidman, R. L. (1961). Autoradiographic study of cell migration during histogenesis of cerebral cortex in the mouse. *Nature*.  
<http://doi.org/10.1038/192766b0>
- Atieh, T., Baronti, C., de Lamballerie, X., & Nougairède, A. (2016). Simple reverse genetics systems for Asian and African Zika viruses. *Scientific Reports*, 6, 39384. Retrieved from <http://dx.doi.org/10.1038/srep39384>
- Barba-Spaeth, G., Dejnirattisai, W., Rouvinski, A., Vaney, M.-C., Medits, I., Sharma, A., ... Rey, F. A. (2016). Structural basis of potent Zika–dengue virus antibody cross-neutralization. *Nature*, 1–23. <http://doi.org/10.1038/nature18938>
- Brasil, P., Pereira, Jr., J. P., Raja Gabaglia, C., Damasceno, L., Wakimoto, M., Ribeiro Nogueira, R. M., ... Nielsen-Saines, K. (2016). Zika Virus Infection in Pregnant Women in Rio de Janeiro — Preliminary Report. *New England Journal of Medicine*. <http://doi.org/10.1056/NEJMoa1602412>
- Chen, J.-F., Zhang, Y., Wilde, J., Hansen, K. C., Lai, F., & Niswander, L. (2014). Microcephaly disease gene Wdr62 regulates mitotic progression of embryonic neural stem cells and brain size. *Nat Commun*, 5. <http://doi.org/10.1038/ncomms4885>
- Cugola, F. R., Fernandes, I. R., Russo, F. B., Freitas, B. C., Dias, J. L. M., Guimarães, K. P., ... Beltrão-Braga, P. C. B. (2016). The Brazilian Zika virus strain causes birth defects in experimental models. *Nature*, 534(7606), 267–271. Retrieved from

<http://dx.doi.org/10.1038/nature18296>

Dejnirattisai, W., Supasa, P., Wongwiwat, W., Rouvinski, A., Barba-spaeth, G., Duangchinda, T., ... Screaton, G. R. (2016). Dengue virus sero-cross-reactivity drives antibody-dependent enhancement of infection with Zika virus, (June), 1–8. <http://doi.org/10.1038/ni.3515.NATURE>

Dupont-Rouzeyrol, M., O'Connor, O., Calvez, E., Daures, M., John, M., Grangeon, J.-P., & Gourinat, A.-C. (2015). Co-infection with Zika and dengue viruses in 2 patients, New Caledonia, 2014.(LETTERS)(Report)(Letter to the editor). *Emerging Infectious Diseases*, 21(2), 381. <http://doi.org/10.3201/eid2102.141553>

Faria, N. R., Do Socorro Da Silva Azevedo, R., Kraemer, M. U. G., Souza, R., Cunha, M. S., Hill, S. C., ... Vasconcelos, P. F. C. (2016). Zika virus in the Americas: Early epidemiological and genetic findings. *Science*, 352(6283), 345–349. <http://doi.org/10.1126/science.aaf5036>

Gadea, G., Bos, S., Krejbich-Trotot, P., Clain, E., Viranaicken, W., El-Kalamouni, C., ... Desprès, P. (2016). A robust method for the rapid generation of recombinant Zika virus expressing the GFP reporter gene. *Virology*, 497, 157–162. <http://doi.org/https://doi.org/10.1016/j.virol.2016.07.015>

Garcez, P. P., Loiola, E. C., Da Costa, R. M., Higa, L. M., Trindade, P., Delvecchio, R., ... Rehen, S. K. (2016). Zika virus: Zika virus impairs growth in human neurospheres and brain organoids. *Science*. <http://doi.org/10.1126/science.aaf6116>

Haddow, A. D., Schuh, A. J., Yasuda, C. Y., Kasper, M. R., Heang, V., Huy, R., ... Weaver, S. C. (2012). Genetic characterization of Zika virus strains: Geographic

expansion of the asian lineage. *PLoS Neglected Tropical Diseases*, 6(2).

<http://doi.org/10.1371/journal.pntd.0001477>

Hamel, R., Liégeois, F., Wichit, S., Pompon, J., Diop, F., Talignani, L., ... Missé, D.

(2016). Zika virus: epidemiology, clinical features and host-virus interactions.

*Microbes and Infection*, 18(7), 441–449.

<http://doi.org/https://doi.org/10.1016/j.micinf.2016.03.009>

Hevner, R. F., Shi, L., Justice, N., Hsueh, Y. P., Sheng, M., Smiga, S., ... Rubenstein, J.

L. R. (2001). Tbr1 regulates differentiation of the preplate and layer 6. *Neuron*.

[http://doi.org/10.1016/S0896-6273\(01\)00211-2](http://doi.org/10.1016/S0896-6273(01)00211-2)

Kumar, A., Hou, S., Airo, A. M., Limonta, D., Mancinelli, V., Branton, W., ... Hobman, T.

C. (2016). Zika virus inhibits type-I interferon production and downstream signaling.

*EMBO Reports*, 17(12), 1766 LP-1775. Retrieved from

<http://embor.embopress.org/content/17/12/1766.abstract>

Li, C., Xu, D., Ye, Q., Hong, S., Jiang, Y., Liu, X., ... Xu, Z. (2016). Zika Virus Disrupts

Neural Progenitor Development and Leads to Microcephaly in Mice. *Cell Stem Cell*,

19(5), 672. <http://doi.org/10.1016/j.stem.2016.10.017>

Li, H., Saucedo-Cuevas, L., Regla-Nava, J. A., Chai, G., Sheets, N., Tang, W., ...

Gleeson, J. G. (2016). Zika Virus Infects Neural Progenitors in the Adult Mouse

Brain and Alters Proliferation. *Cell Stem Cell* (Vol. 19). Retrieved from

<http://www.sciencedirect.com/science/article/pii/S1934590916302521>

Marín, O., & Rubenstein, J. L. R. (2003). CELL MIGRATION IN THE FOREBRAIN.

*Annual Review of Neuroscience*, 26(1), 441–483.

<http://doi.org/10.1146/annurev.neuro.26.041002.131058>

Marrs, C., Olson, G., Saade, G., Hankins, G., Wen, T., Patel, J., & Weaver, S. (2016).

Zika Virus and Pregnancy: A Review of the Literature and Clinical Considerations. *American Journal of Perinatology*, 33(7), 625–639. <http://doi.org/10.1055/s-0036-1580089>

Martynoga, B., Morrison, H., Price, D. J., & Mason, J. O. (2005). Foxg1 is required for

specification of ventral telencephalon and region-specific regulation of dorsal telencephalic precursor proliferation and apoptosis. *Developmental Biology*, 283(1), 113–127. <http://doi.org/10.1016/j.ydbio.2005.04.005>

Miner, J. J., Cao, B., Govero, J., Smith, A. M., Fernandez, E., Cabrera, O. H., ...

Diamond, M. S. (2016). Zika Virus Infection during Pregnancy in Mice Causes Placental Damage and Fetal Demise. *Cell*, 165(5), 1081–1091. <http://doi.org/10.1016/j.cell.2016.05.008>

Mullen, R. J., Buck, C. R., & Smith, A. M. (1992). NeuN, a neuronal specific nuclear

protein in vertebrates. *Development*, 116(1), 201 LP-211. Retrieved from <http://dev.biologists.org/content/116/1/201.abstract>

Nieto, M., Monuki, E. S., Tang, H., Imitola, J., Haubst, N., Khoury, S. J., ... Walsh, C. A.

(2004). Expression of Cux-1 and Cux-2 in the subventricular zone and upper layers II–IV of the cerebral cortex. *Journal of Comparative Neurology*, 479(2), 168–180. <http://doi.org/10.1002/cne.20322>

Nigg, E. A., & Raff, J. W. (2009). Centrioles, Centrosomes, and Cilia in Health and

Disease. *Cell*, 139(4), 663–678. <http://doi.org/10.1016/j.cell.2009.10.036>

- Nowakowski, R. S., Lewin, S. B., & Miller, M. W. (1989). Bromodeoxyuridine immunohistochemical determination of the lengths of the cell cycle and the DNA-synthetic phase for an anatomically defined population. *Journal of Neurocytology*, 18(3), 311–318. <http://doi.org/10.1007/BF01190834>
- Nunes, M. R. T., Faria, N. R., Vasconcelos, H. B., Medeiros, D. B. de A., de Lima, C. P. S., Carvalho, V. L., ... Vasconcelos, P. F. da C. (2012). Phylogeography of dengue virus serotype 4, Brazil, 2010-2011. *Emerging Infectious Diseases*, 18(11), 1858–1864. <http://doi.org/10.3201/eid1811.120217>
- Nunes, M. R. T., Palacios, G., Faria, N. R., Sousa, E. C., Pantoja, J. A., Rodrigues, S. G., ... Lipkin, W. I. (2014). Air Travel Is Associated with Intracontinental Spread of Dengue Virus Serotypes 1-3 in Brazil. *PLoS Neglected Tropical Diseases*, 8(4). <http://doi.org/10.1371/journal.pntd.0002769>
- Paniz-Mondolfi, A. E., Rodriguez-Morales, A. J., Blohm, G., Marquez, M., & Villamil-Gomez, W. E. (2016). ChikDenMaZika Syndrome: The challenge of diagnosing arboviral infections in the midst of concurrent epidemics. *Annals of Clinical Microbiology and Antimicrobials*, 15(1), 1–4. <http://doi.org/10.1186/s12941-016-0157-x>
- Priyamvada, L., Quicke, K. M., Hudson, W. H., Onlamoon, N., Sewatanon, J., Edupuganti, S., ... Wrammert, J. (2016). Human antibody responses after dengue virus infection are highly cross-reactive to Zika virus. *Proceedings of the National Academy of Sciences*, 113(28), 7852–7857. <http://doi.org/10.1073/pnas.1607931113>

- Shao, Q., Herrlinger, S., Yang, S.-L., Lai, F., Moore, J. M. J. M., Brindley, M. A. M. A., & Chen, J.-F. J.-F. (2016). Zika virus infection disrupts neurovascular development and results in postnatal microcephaly with brain damage. *Development (Cambridge, England)*, *143*(22), 4127–4136. <http://doi.org/10.1242/dev.143768>
- Simonin, Y., Loustalot, F., Desmetz, C., Foulongne, V., Constant, O., Fournier-Wirth, C., ... Salinas, S. (2016). Zika Virus Strains Potentially Display Different Infectious Profiles in Human Neural Cells. *EBioMedicine*, *12*, 161–169. <http://doi.org/10.1016/j.ebiom.2016.09.020>
- Stettler, K., Beltramello, M., Espinosa, D. A., Graham, V., Cassotta, A., Bianchi, S., ... Sallusto, FedericaCorti, D. (2016). Specificity, cross-reactivity and function of antibodies elucidated by Zika virus infection. *Science*, *353*(6296), 247–252. <http://doi.org/10.1126/science.aad8728>
- Swanstrom, J. A., Plante, J. A., Plante, K. S., Young, E. F., MCGowan, E., Gallichotte, E. N., ... Heise, M. T. (2016). Isolated from Dengue Patients Are Protective against Zika Virus. *MBio*, *7*(4), 1–8. <http://doi.org/10.1128/mBio.01123-16>.Editor
- Tang, H., Hammack, C., Ogden, S. C., Wen, Z., Qian, X., Li, Y., ... Ming, G. L. (2016). Zika virus infects human cortical neural progenitors and attenuates their growth. *Cell Stem Cell*, *18*(5), 587–590. <http://doi.org/10.1016/j.stem.2016.02.016>
- Thornton, G. K., & Woods, C. G. (2009). Primary microcephaly: do all roads lead to Rome? *Trends in Genetics*, *25*(11), 501–510. <http://doi.org/10.1016/j.tig.2009.09.011>
- Tripathi, S., Balasubramaniam, V. R. M. T., Brown, J. A., Mena, I., Grant, A., Bardina, S.

V., ... García-Sastre, A. (2017). A novel Zika virus mouse model reveals strain specific differences in virus pathogenesis and host inflammatory immune responses. *PLoS Pathogens*, 13(3), 1–19.  
<http://doi.org/10.1371/journal.ppat.1006258>

Ventura, C. V., Maia, M., Bravo-Filho, V., Góis, A. L., & Belfort, R. (2016). Zika virus in Brazil and macular atrophy in a child with microcephaly. *The Lancet*, 387(10015), 228. [http://doi.org/10.1016/S0140-6736\(16\)00006-4](http://doi.org/10.1016/S0140-6736(16)00006-4)

Villamil-Gómez, W. E., Rodríguez-Morales, A. J., Uribe-García, A. M., González-Arismendy, E., Castellanos, J. E., Calvo, E. P., ... Musso, D. (2016). Zika, dengue, and chikungunya co-infection in a pregnant woman from Colombia. *International Journal of Infectious Diseases*, 51, 135–138.  
<http://doi.org/10.1016/j.ijid.2016.07.017>

Zhang, N., Zhang, N., Qin, C. F., Liu, X., Shi, L., & Xu, Z. (2016). Zika Virus Disrupts Neural Progenitor Development and Leads to Microcephaly in Mice. *Cell Stem Cell*.  
<http://doi.org/10.1016/j.stem.2016.04.017>

## CHAPTER 6

### DISCUSSION AND FUTURE DIRECTIONS

#### 5.1 The Role of Lin28 in Neurodevelopment

##### 5.1.1 Summary of Findings

The studies performed in **Chapter 2** have outlined several major novel contributions to the field of neurodevelopment. Our group previously showed that loss of Lin28A can cause microcephaly in mice (Yang et al., 2015). In this dissertation work, I have shown that the RNA-binding protein Lin28A/B is required for neural tube closure and that loss of their function causes cranial NTDs (Fig. 2.1). Mutant *Lin28a/b* neural tube NPCs exhibit reduced proliferation and precocious differentiation (Fig. 2.2) likely contributing to NTDs. Interestingly, inadequate maintenance of cell proliferation is associated with contributing to cranial NTDs in particular (Copp, 2005) suggesting that cell proliferation regulation is especially important in this region. Combining a mouse model of reduced protein synthesis (*Rpl24<sup>Bst/+</sup>*) (Barna et al., 2008; Signer, Magee, Salic, & Morrison, 2014) with *Lin28a<sup>-/-</sup>* mutants demonstrated that Lin28 is required to promote protein synthesis in brain development (Fig. 2.3). Conversely, dampening protein synthesis in embryos ectopically overexpressing Lin28A in the developing neocortex can rescue Lin28A-overexpression induced macrocephaly (Fig. 2.4) suggesting that protein synthesis is carefully regulated in part by Lin28 during cortical development. Polysome sequencing data helped us identify biological mechanisms that Lin28 may promote at the protein synthesis level, in particular ribosome biogenesis and cell cycle progression

(Fig. 2.5). In confirmation, many target genes identified within these biological mechanisms were found to be reduced in protein abundance despite showing no significant change at the total mRNA level in *Lin28a/b* mutant neocortices (Fig. 2.5-6). Additionally, nucleoli size was found to be regulated by Lin28 activity in NPCs, which is an indicator for ribosome biogenesis activity, suggesting that Lin28 can indeed drive ribosome biogenesis activity (Fig. 2.6).

Overall, these studies have identified NPC-specific roles of post-transcriptional Lin28 function not previously described. Equally important, these studies have contributed to the growing knowledge of the dynamic and careful regulation of protein synthesis during development.

#### *5.1.2 Remaining questions and considerations*

Our studies described Lin28A nucleoli localization in NPCs and demonstrated evidence supporting Lin28 regulation of nucleolar size and therefore ribosome biogenesis output; however, this does not necessarily completely elucidate this nucleolar mechanism (Fig. 2.6). There are two possible ways that Lin28 is functioning in this location: through let-7 dependent and let-7 independent functions. It has been reported that monomethylation of Lin28A via SET7/9 promotes Lin28A nucleolar localization and inhibits pre-let-7 biogenesis in hES cells (Kim et al., 2014), while Lin28 NPC nucleolar localization remains unexplored. The nucleolus is also the site where ribosome and ribonucleoprotein complex assembly begins, and it is possible that Lin28 assembles with the ribosome prior to maturation and nucleolar exit of ribosomes in NPCs (Derenzini et al., 2000). These mechanisms could be tested more directly by

isolating nucleoli and pulling down Lin28-bound complexes to identify Lin28A-binding partners specific to its nucleolar localization and function in WT NPCs.

While loss of Lin28A/B function in neurodevelopment results in NTDs, it does not necessarily follow that loss of its function in NPCs caused the observed embryonic lethality in *Lin28a/b* mutants; on rare occasions a fetus may survive through birth with anencephaly (despite dying of complications later on), and there are surgical techniques that correct or ameliorate problems arising from other NTDs such as spina bifida as the patients survive birth (Adzick, Sutton, Crombleholme, & Flake, 1998; Baird & Sadovnick, 1984; Lanzieri et al., 2017). Our embryos experience embryonic lethality at post-implantation from E12.5 and never survive gestation (Fig. 2.1). It is suggested that embryonic lethality of mouse embryos at these stages is frequently caused by inadequate implantation or trophoblast development and cardiovascular insufficiency (Papaioannou & Behringer, 2012). Lin28 is expressed in mouse trophoblasts, and shRNA knockdown of Lin28 in human trophoblasts was shown to exhibit precocious differentiation *in vitro* (Seabrook et al., 2013). It is therefore likely that Lin28 (and potentially protein synthesis regulation) plays a critical role in implantation during pregnancy.

Some evidence from our studies indicated that loss of Lin28A/B may have resulted in a posteriorization of the neural tube. Posterior hox gene transcript abundance was increased in hindbrain samples isolated for PolySeq experiments, including *Hoxd9*, *Hoxa6*, and *Hoxb7*, all of which exhibited at least a 2.5-fold increase (Fig. 2.5H). *Lin28a/b* mutants exhibit reduced tail length and potentially reduced total neural tube length (Fig. 2.1C) which may also suggest atypical A/P patterning

(Yamaguchi, 2001). Neurulation finishes when primary neurulation and secondary neurulation sites join in the posterior neural tube (Harrington, Hong, & Brewster, 2009), generating a transitional zone where junctional neurulation takes place, where elements of primary and secondary neurulation take place in the same anterior/posterior (A/P) plane (Dady, Havis, Escriou, Catala, & Duband, 2014). Evidence of junctional neurulation was sometimes observed in inappropriately anterior neural tube sections in *Lin28a/b* mutants, although this data was not quantified. To address whether *Lin28a/b* mutants are posteriorized, in-situ hybridization studies could be performed to confirm whether typically posterior hox genes and A/P gradients are inappropriately shifted anteriorly, combined with more rigorous morphological and cellular characterization of junctional neurulation. If true, this would implicate an additional role of Lin28A/B in not just specifically promoting NPC proliferation, but a specific role in possibly maintaining anterior NPC fates.

## **5.2 Zika Virus Impact on Neurodevelopment**

### *5.2.1 Summary of Findings*

Our data and others have confirmed that ZIKV can indeed cause microcephaly (C. Li et al., 2016; H. Li et al., 2016; Shao et al., 2016; Souza et al., 2016) and does so in part through the disruption of NPC behaviors (Dang et al., 2016; Souza et al., 2016), among other damages. We have described a rodent model for studying Zika virus-induced microcephaly and found that the Zika virus is causal for microcephaly and other extensive brain damage (**Chapter 3, Chapter 4**). This model more accurately portrays

human Zika virus-associated microcephaly in that the infected pups survive postnatally, uniquely allowing us to examine brain developmental stages similar to the third trimester in humans (Semple, Blomgren, Gimlin, Ferriero, & Noble-Haeusslein, 2013). In addition to causing microcephaly, Zika virus infection also causes global growth restriction, neuronal loss, axonal rarefaction, astrogliosis, microglial activation, and corpus callosum diminishment, mimicking phenotypes seen in affected humans (**Chapter 4**) (Driggers et al., 2017; Mlakar et al., 2016) (Fig. 4.1-3). In particular, this work has identified a striking vasculature dysfunction in developing brains exposed to the Zika virus. Blood vessels develop at a higher concentration in the affected brains, are abnormally dilated, and leak their contents into the brain, demonstrating a defective blood-brain-barrier (BBB) (Fig. 4.4). These results together demonstrate the dramatic negative impact that the Zika virus has on the developing brain, and has provided us the preliminary observations to ask new questions about flaviviruses and their causal role in neurodevelopmental defects.

To directly ask whether the Zika virus has evolved to become more virulent and capable of causing neurodevelopmental disorders, we compared two isolates of the Zika virus from the older African lineage and the more recent Asian lineage in side-by-side intracerebral inoculation studies in **Chapter 5**. We surprisingly found that despite the African lineage never previously being associated with causing birth defects, the African lineage isolate (MR-766) exhibited more aggressive virulence (Fig. 5.6) and neuronal cell loss and damage (Fig. 5.4-5) than the Asian lineage isolate (MEX1-44) in mice, ultimately resulting in embryonic lethality of E14.5 infected embryos (Fig. 5.4) (Shao et al., 2017) prior to birth. These results suggest that the Zika virus has

potentially evolved to become less virulent and damaging, allowing infected fetuses to survive gestation when they previously may not have.

We also addressed whether a co-circulating and closely related arbovirus, the Dengue virus, could be a contributing factor in causing neurodevelopmental defects in Zika virus infected individuals. Side-by-side comparison studies with the Dengue virus (serotype 2, DENV2) and the Zika virus in our rodent model using intracerebral embryonic brain inoculation (**Chapter 5**) (Shao et al., 2017) allowed us to examine DENV2-specific contributions alongside Zika virus-inoculated embryos. In these studies, we show that the Dengue virus is indeed capable of infecting NPCs and induce massive gliosis, causing a mild reduction in cortical thickness, and pups survive postnatally (Fig. 5.1-3). These data suggest that Dengue virus fetal infection may indeed contribute to causing neurodevelopmental defects, albeit more subtly than the Zika virus, if present in the brain as it develops.

### *5.2.2 Remaining questions*

While the Zika virus outbreak in 2015 resulted in a 10-fold increase in microcephaly in affected areas, Zika virus infection during pregnancy does not guarantee that a child will result with this condition. 4% of ZIKV infected American mothers resulted in children with microcephaly (Cragan et al., 2017; Mlakar et al., 2016) while the rate of microcephaly associated birth defects in Brazil is estimated up to 13% in infected mothers, in less affluent areas in particular (Jaenisch, Rosenberger, Brito, & Brady, 2017), indicating that other factors likely work in concert with Zika virus in infected individuals that result in microcephaly. In both cases, it is clear that ZIKV infection alone does not guarantee birth defects in the fetuses of infected mothers. This

illustrates the multifactorial aspect of microcephaly and it is thus important for the field to continue to identify these compounding risk factors. For example, a new study from Brazil has identified a potential genetic vulnerability in mothers infected with the Zika virus to cause microcephaly with genetic variations in adenylate cyclase genes (Rossi, Faucz, & Melo, 2018).

Another looming question remains regarding individuals infected with Zika virus during gestation that do not exhibit obvious defects at birth. The only metric in a microcephaly diagnosis is a head circumference two standard deviations below the mean, leaving less obvious perturbations to brain development and connectivity undetected until functional problems arise later on in development (Woods, 2004). It has been shown that immune activation in pregnant mothers has the capacity to cause behavioral abnormalities in humans and mice (Atladóttir et al., 2010; Patterson, 2009; Shin Yim et al., 2017). Future research directions should examine reduced concentration or later-stage models of Zika virus inoculation in brain development, such as utilizing neonatal infection to mimic third trimester infection (Chapter 3) (Semple et al., 2013), to discover whether milder cases of Zika virus infection during brain development can cause behavioral abnormalities and inform potentially affected individuals and the field.

Our protocol (**Chapter 3**) describes a method of inoculating ZIKV intraventricularly to circumvent disabling the antiviral response of the murine model in the adult; however, this route of injection does not completely model the typical route of infection. Blood-born adult stage infection has been described in the mouse previously but requires the use of the interferon (IFN) regulatory factor (IRF) transcription factors IRF-3, -5, -7 triple

knockout strain or the SJL mouse line (Lazear et al., 2016; Miner et al., 2016). Despite this, our major findings that neurovascular development is disrupted in Zika virus-infected brains has recently been verified in IFN mice injected intraperitoneally (Garcez et al., 2018) as well as our strain-specific observations in human cell lines (Goodfellow et al., 2018), reinforcing the validity of the biological observations from our model.

### **5.3 Conclusions**

This work has addressed mechanisms underlying two major types of neurodevelopmental disruption: neural tube defects and microcephaly. These studies have highlighted the complexity of the roles of genetic and environmental factors on neurodevelopment, as well as their multimodality. While many questions still remain, these contributions will hopefully inspire further investigation into the post-transcriptional regulation of NPCs and other developmental cell types, and instruct future investigations into arbovirus impact and other environmental stressors in neurodevelopment.

## 5.4 References

- Adzick, N. S., Sutton, L. N., Crombleholme, T. M., & Flake, A. W. (1998). Successful fetal surgery for spina bifida. *Lancet*, 352(9141), 1675–1676. Retrieved from <http://proxy-remote.galib.uga.edu/login?url=http://search.ebscohost.com/login.aspx?direct=true&db=bth&AN=1318527&site=eds-live>
- Atladóttir, H. Ó., Thorsen, P., Østergaard, L., Schendel, D. E., Lemcke, S., Abdallah, M., & Parner, E. T. (2010). Maternal infection requiring hospitalization during pregnancy and autism spectrum disorders. *Journal of Autism and Developmental Disorders*, 40(12), 1423–1430. <http://doi.org/10.1007/s10803-010-1006-y>
- Baird, P. A., & Sadovnick, A. D. (1984). Survival in Infants with Anencephaly. *Clinical Pediatrics*, 23(5), 268–271. <http://doi.org/10.1177/000992288402300505>
- Barna, M., Pusic, A., Zollo, O., Costa, M., Kondrashov, N., Rego, E., ... Ruggero, D. (2008). Suppression of Myc oncogenic activity by ribosomal protein haploinsufficiency. *Nature*, 456, 971. Retrieved from <http://dx.doi.org/10.1038/nature07449>
- Copp, A. J. (2005). Neurulation in the cranial region--normal and abnormal. *Journal of Anatomy*, 207(5), 623–635. <http://doi.org/10.1111/j.1469-7580.2005.00476.x>
- Cragan, J. D., Mai, C. T., Petersen, E. E., Liberman, R. F., Forestieri, N. E., Stevens, A. C., ... Honein, M. A. (2017). Baseline Prevalence of Birth Defects Associated with Congenital Zika Virus. *Morbidity and Mortality Weekly Report*, 66(8), 219–220. <http://doi.org/10.15585/mmwr.mm6608a4>

- Dady, A., Havis, E., Escriou, V., Catala, M., & Duband, J.-L. (2014). Junctional Neurulation: A Unique Developmental Program Shaping a Discrete Region of the Spinal Cord Highly Susceptible to Neural Tube Defects. *Journal of Neuroscience*, 34(39), 13208–13221. <http://doi.org/10.1523/JNEUROSCI.1850-14.2014>
- Dang, J., Tiwari, S. K., Lichinchi, G., Qin, Y., Patil, V. S., Eroshkin, A. M., & Rana, T. M. (2016). Zika Virus Depletes Neural Progenitors in Human Cerebral Organoids through Activation of the Innate Immune Receptor TLR3. *Cell Stem Cell*, 19(2), 258–265. <http://doi.org/10.1016/j.stem.2016.04.014>
- Derenzini, M., Trerè, D., Pession, A., Govoni, M., Sirri, V., & Chieco, P. (2000). Nucleolar size indicates the rapidity of cell proliferation in cancer tissues. *Journal of Pathology*, 191(2), 181–186. [http://doi.org/10.1002/\(SICI\)1096-9896\(200006\)191:2<181::AID-PATH607>3.0.CO;2-V](http://doi.org/10.1002/(SICI)1096-9896(200006)191:2<181::AID-PATH607>3.0.CO;2-V)
- Driggers, R. W., Ho, C.-Y., Korhonen, E. M., Kuivanen, S., Jääskeläinen, A. J., Smura, T., ... Vapalahti, O. (2017). Zika Virus Infection With Prolonged Maternal Viremia and Fetal Brain Abnormalities. *Obstetric Anesthesia Digest*. <http://doi.org/10.1097/01.aoa.0000512046.09676.84>
- Garcez, P. P., Stolp, H. B., Sravanam, S., Christoff, R. R., Ferreira, J. C. C. G., Dias, A. A., ... Molnár, Z. (2018). Zika virus impairs the development of blood vessels in a mouse model of congenital infection. *Scientific Reports*, 8(1), 12774. <http://doi.org/10.1038/s41598-018-31149-3>
- Goodfellow, F., Willard, K., Wu, X., Scoville, S., Stice, S., Brindley, M., ... Brindley, M. A. (2018). Strain-Dependent Consequences of Zika Virus Infection and Differential

Impact on Neural Development. *Viruses* 2018, Vol. 10, Page 550, 10(10), 550.

<http://doi.org/10.3390/V10100550>

Harrington, M. J., Hong, E., & Brewster, R. (2009). Comparative analysis of neurulation: First impressions do not count. *Molecular Reproduction and Development*, 76(10), 954–965. <http://doi.org/10.1002/mrd.21085>

Jaenisch, T., Rosenberger, D., Brito, C., & Brady, O. (2017). Risk of microcephaly after Zika virus infection in Brazil , 2015 to 2016, 95(3), 191–198.

Kim, S.-K., Lee, H., Han, K., Kim, S. C., Choi, Y., Park, S.-W., ... Lee, D. (2014). SET7/9 Methylation of the Pluripotency Factor LIN28A Is a Nucleolar Localization Mechanism that Blocks let-7 Biogenesis in Human ESCs. *Cell Stem Cell*, 15(6), 735–749. <http://doi.org/10.1016/j.stem.2014.10.016>

Lanzieri, T. M., Leung, J., Caviness, A. C., Chung, W., Flores, M., Blum, P., ... Demmler-Harrison, G. (2017). Long-term outcomes of children with symptomatic congenital cytomegalovirus disease. *Journal of Perinatology: Official Journal Of The California Perinatal Association*. <http://doi.org/10.1038/jp.2017.41>

Lazear, H. M. M., Govero, J., Smith, A. M. M., Platt, D. J. J., Fernandez, E., Miner, J. J. J., & Diamond, M. S. S. (2016). A Mouse Model of Zika Virus Pathogenesis. *Cell Host and Microbe*, 19(5), 720–730. <http://doi.org/10.1016/j.chom.2016.03.010>

Li, C., Xu, D., Ye, Q., Hong, S., Jiang, Y., Liu, X., ... Xu, Z. (2016). Zika Virus Disrupts Neural Progenitor Development and Leads to Microcephaly in Mice. *Cell Stem Cell*, 19(5), 672. <http://doi.org/10.1016/j.stem.2016.10.017>

- Li, H., Saucedo-Cuevas, L., Regla-Nava, J. A., Chai, G., Sheets, N., Tang, W., ... Gleeson, J. G. (2016). *Zika Virus Infects Neural Progenitors in the Adult Mouse Brain and Alters Proliferation*. *Cell Stem Cell* (Vol. 19). Retrieved from <http://www.sciencedirect.com/science/article/pii/S1934590916302521>
- Miner, J. J., Cao, B., Govero, J., Smith, A. M., Fernandez, E., Cabrera, O. H., ... Diamond, M. S. (2016). Zika Virus Infection during Pregnancy in Mice Causes Placental Damage and Fetal Demise. *Cell*, *165*(5), 1081–1091. <http://doi.org/10.1016/j.cell.2016.05.008>
- Mlakar, J. . J., Korva, M. M. . M., Tul, N. N. . N., Popović, M. M. ., Poljšak-Prijatelj, M. M. ., Mraz, J. J. . J., ... Avšič Županc, T. (2016). Zika Virus Associated with Microcephaly. *New England Journal of Medicine*, *374*(10), 951–958. <http://doi.org/10.1056/NEJMoa1600651>
- Papaioannou, V., & Behringer, R. (2012). Early embryonic lethality in genetically engineered mice: diagnosis and phenotypic analysis. *Veterinary Pathology*, *49*(1), 64–70. <http://doi.org/10.1021/nl061786n.Core-Shell>
- Patterson, P. H. (2009). Immune involvement in schizophrenia and autism: Etiology, pathology and animal models. *Behavioural Brain Research*, *204*(2), 313–321. <http://doi.org/https://doi.org/10.1016/j.bbr.2008.12.016>
- Rossi, Á. D., Faucz, F. R., & Melo, A. (2018). Variations in maternal adenylate cyclase genes are associated with congenital Zika syndrome in a cohort from, 1–16. <http://doi.org/10.1111/joim.12829>
- Seabrook, J. L., Cantlon, J. D., Cooney, A. J., McWhorter, E. E., Fromme, B. A.,

- Bouma, G. J., ... Winger, Q. A. (2013). Role of LIN28A in Mouse and Human Trophoblast Cell Differentiation1. *Biology of Reproduction*, 89(4), 1–13,1–95,95. Retrieved from <http://dx.doi.org/10.1095/biolreprod.113.109868>
- Semple, B. D., Blomgren, K., Gimlin, K., Ferriero, D. M., & Noble-Haeusslein, L. J. (2013). Brain development in rodents and humans: Identifying benchmarks of maturation and vulnerability to injury across species. *Progress in Neurobiology*, 106, 1–16. <http://doi.org/10.1016/j.pneurobio.2013.04.001>
- Shao, Q., Herrlinger, S., Yang, S.-L., Lai, F., Moore, J. M. J. M., Brindley, M. A. M. A., & Chen, J.-F. J.-F. (2016). Zika virus infection disrupts neurovascular development and results in postnatal microcephaly with brain damage. *Development (Cambridge, England)*, 143(22), 4127–4136. <http://doi.org/10.1242/dev.143768>
- Shao, Q., Herrlinger, S., Zhu, Y.-N., Yang, M., Goodfellow, F., Stice, S. L. S. L., ... Chen, J.-F. J.-F. (2017). The African Zika virus MR-766 is more virulent and causes more severe brain damage than current Asian lineage and Dengue virus. *Development*, 144(22). <http://doi.org/10.1242/dev.156752>
- Shin Yim, Y., Park, A., Berrios, J., Lafourcade, M., Pascual, L. M., Soares, N., ... Choi, G. B. (2017). Reversing behavioural abnormalities in mice exposed to maternal inflammation. *Nature*, 549(7673), 482–487. <http://doi.org/10.1038/nature23909>
- Signer, R. A. J., Magee, J. A., Salic, A., & Morrison, S. J. (2014). Haematopoietic stem cells require a highly regulated protein synthesis rate. *Nature*, 508(7498), 49–54. <http://doi.org/10.1038/nature13035>
- Souza, B. S. F., Sampaio, G. L. A., Pereira, C. S., Campos, G. S., Sardi, S. I., Freitas,

- L. A. R., ... Soares, M. B. P. (2016). Zika virus infection induces mitosis abnormalities and apoptotic cell death of human neural progenitor cells. *Scientific Reports*, 6(November), 39775. <http://doi.org/10.1038/srep39775>
- Woods, C. G. (2004). Human microcephaly. *Current Opinion in Neurobiology*, 14, 112–117. <http://doi.org/10.1016/j.conb.2004.01.003>
- Yamaguchi, T. P. (2001). Heads or tails: Wnts and anterior-posterior patterning. *Current Biology*, 11(17), 713–724. [http://doi.org/10.1016/S0960-9822\(01\)00417-1](http://doi.org/10.1016/S0960-9822(01)00417-1)
- Yang, M., Yang, S.-L., Herrlinger, S., Liang, C., Dzieciatkowska, M., Hansen, K. C., ... Chen, J.-F. (2015). Lin28 promotes the proliferative capacity of neural progenitor cells in brain development. *Development*, 142(9), 1616–1627. <http://doi.org/10.1242/dev.120543>